RICE UNIVERSITY

Nanocars: Towards Photoactive, Directionally-Controlled Surface Rolling Molecules

by

Jason Matthew Guerrero

A THESIS SUBMITTED
IN PARTIAL FULFILLMENT OF THE
REQUIREMENTS FOR THE DEGREE

Doctor of Philosophy

APPROVED, THESIS COMMITTEE:

James M. Tour
Chao Professor of Chemistry

Paul S. Engel
Professor of Chemistry

Kevin F. Kelly
Assistant Professor of Electrical and
Computer Engineering

HOUSTON, TX

JUNE 2009

For my beautiful wife Leticia and my wonderful son Jason Jr.

Abstract

***Nanocars*: Towards Photoactive, Directionally-Controlled Surface Rolling Molecules**

by

Jason Matthew Guerrero

Described in this thesis are efforts to advance our understanding of single molecule machines through the synthesis and study of an array of nanovehicles. In the first chapter, nanoscale transport is explored through the synthesis and solution-based studies of a photoactive, metal-ion-chelating nanocar. Utilizing an appended photoactive dipyridylethylene moiety as a metal chelating unit, it is expected that this molecule, upon photoirradiation, will form a strong bidentate ligand for carrying metal ions along surfaces. Following this, in the second chapter, directional control and propulsion are explored through the synthesis of motorized nanocars. Studies towards a dual-motored nanocar as well as the synthesis of an ultra-fast motorized nanocar are described. The third chapter covers our efforts to complement previous STM studies, where single molecule fluorescence spectroscopy is used for imaging and mechanistic elucidation of translational movement of fluorescently-tagged nanovehicles. The synthetic routes towards these molecules are covered, as well. In chapters 4 and 5, various nanovehicles are synthesized using contrasting approaches. In chapter 4, self-assembly methods mirroring those used in biological construction are used to produce nanocars and nanotrains. Moieties of 2-pyridones and terpyridyl groups were used for self-assembling via hydrogen bonding and metal complex formation, respectively. Traditional organic

synthesis is used to build carborane-wheeled nanovehicles in chapter 5. These molecules are expected to move in predetermined patterns on atomically smooth surfaces, depending on their specific configuration of axles and wheels. Finally, in chapter 6, nanocomponentry is explored through the synthesis and studies of molecular devices such as azobenzene-fullerene switches and fullerene-oligo(phenylene ethynylene) molecular wires. The presence of fullerenes and oligo(phenylene ethynylene)s (OPEs) in azobenzene derivatives was found to have a large effect on the photoisomerization behavior of the molecules. Lastly, a series of fullerene-terminated oligo(phenylene ethynylene) (OPEs) molecular wires have been synthesized as potential molecular electronic devices. Electronic properties such as the energy levels and the distribution of HOMOs and LUMOs of fullerene-terminated OPEs have been calculated using ab initio method at the B3LYP/6-31G(d) level.

Acknowledgements

Albert Einstein once said "If we knew what it was we were doing, it would not be called research, would it?" I could not agree more. When I first began my research career as a graduate student, I had no idea what I was doing in the lab. I recall often wondering how these people training me in the lab, who were a mere few years ahead of me, could know so much and possess such skill. Now I am in the same position they once were, with several years of synthetic organic training and knowledge under my belt, as well as a laundry list of experiences I have had along the way. I now know that those very skills I was once so in awe of are merely the tip of the iceberg in what makes the whole of a scientist. Over the years I have had the incredible privilege to work with and for some of the most talented people I have ever met and learn about what some of those things are. From being trained as a first year graduate student all the way to the culmination of my work at Rice, I have continued to be in awe of the people around me. I owe much of who I am and what I have done to you.

First and foremost, I must thank God for all that he has given me. Thank you, Lord, for all that you have blessed me with. I know that without you I am nothing, and I would have nothing. There are many times in my life where one small difference, one small occurrence, could have changed everything for the worse. At times my faith has wavered, but I know that I have always been able to seek you in my darkest hour, and you have continuously carried me through. I thank you for all the blessings and affording me the opportunities you have given me.

I thank Dr. Tour for all of his patience, support, guidance and critiques that have given me strength and made me a better person and researcher. I know I am stronger

because of the lessons you have taught me. I owe much to you. I thank you for taking me in when you didn't have to. I thank you for your prayers regarding some of the personal issues in my life. You helped me to have strength when at times I was very down and scared, and when I thought I may not make it through.

I have many other people from Rice to thank. I would like to thank Dr. Dustin James especially. Your professionalism and attitude have always been awe-inspiring for me. Thank you for all of your advice, your helpful review of my material, and your kindness. Thank you to Dr. Victor Behar. I greatly appreciate your giving me the opportunity to work in your laboratory and allowing me to learn. Thank you to our wonderful collaborators. Dr. Stephan Link and Saumyakanti Katua, thank you for your excellent work on our fluorescence project as well as your advice and input into our project. To my committee members, Dr. Kevin Kelly, thank you very much for your collaboration over the years, your wonderful STM work, and your helpful insight. Thank you to my other committee member, Dr. Paul Engel. I very much enjoyed taking your classes and it was a real delight to learn from you. You have been an excellent teacher and source of information. Dr. Larry Alemany, thank you very much for all of your NMR work on our molecules. Thank you to all of the support staff at Rice. Without your contributions, nearly everything would come to a screeching halt. My labmates through the years, Dr. Chad Stearman, thank you for your training and advice. I have continued to use both throughout my graduate career. Dr. David Abmayr, thank you for your friendship. I enjoyed working alongside you for the short time we had. Thank you to my nanocar co-workers Dr. Jean-Francios Morin, Dr. Yasuhiro Shirai, and Dr. Takashi Sasaki for all of your camaraderie, help and introducing me to the nanocar project. Thank

you to Dr. Guillaume Vives, who has been a great co-worker and mentor to me. I greatly appreciate all of your help late in my graduate career. I believe you will make a wonderful professor, and your students will be very lucky to have you. I also feel fortunate to call you my friend and look forward to your future successes. I have come to know many other friends in the Tour group. Dr. Condell Doyle, Dr. B. Katherine Price, Amanda Higginbotham and Ashley Leonard, you have all been wonderful people to know and share friendship with. You each are very talented and special, and every one of you deserves the very best. To the postdocs Dr. Meng Lu, Dr. Tao He, Dr. Jacob Berlin and Dr. Dmitri Kosynkin, thank you for your input into my projects and your advice and friendship. Jacob, thanks for being the only other person I have to talk baseball with! Finally, I owe a huge thanks to my great friend David Corley. You have been an incredible friend and comrade both in the lab and out. I will forever remember our late nights in the lab fueled by insane amounts of caffeine, and then coming back in super early! Looking back, I have to say that it was quite fun. You are so very talented and intelligent; I know you have great things ahead of you. I feel lucky to call you both a co-worker and friend.

To my family, thank you all. To the woman who has loved me all my life, my mother Sheila, words cannot express my thanks to you. Your spirit, kindness and advice have given me untold strength throughout my life. For the 20+ years that I have been in school, you have always believed in me, you never once waivered. I thank you for that. I thank you for your love and support. Only now am I able to fully appreciate how special of a person you are, for being a single mother all those years and still providing for me. You are amazing and I love you with all my heart. To my stepfather, Larry Stonecipher,

thank you for your love and life lessons. You instilled in me a wonderful work ethic that has served me well. I am proud to call you "dad". To my grandparents, Antonio and Mary Ann Guerrero, I thank you both so very much for caring for me and teaching me about the Lord, as well as being incredible role models in my life and pushing me to go to school. Without you both I do not know where I would be. Thank you grandma, I know that you are looking down on me from heaven and watching over me. To my aunt Nettie, thank you for being such a wonderful person to me. Your care will forever be remembered. Thank you for helping with the baby while I finished my thesis. To my new family, those who I am now proud to call both family members and friends since marrying Leticia, thank you. Alma and Matias, thank you both for your generosity and support. I am forever grateful. Jose, I look forward to our future tee times!

I have saved my greatest personal thank you for last. To my lovely wife Leticia and my beautiful son Jason Jr. Lety, you and Jaybird are my reason for living. All that I have done and all of the school I have completed is for you. All that I will ever accomplish in the future will be with you. Thank you, Lety for everything. You have been my best friend, my love, my strength and spirit for so long now. We have been through a lot, and you have kept me going when I thought it impossible. You are a wonderful wife and mother. Thank you for giving me the gifts of your love and our son. To my Jaybird, I love you with all of my heart. The moment I laid eyes on you I knew that there was nothing I would not do for you. I look forward to seeing the man you will become, and I hope that all that I have accomplished will give you a better life than I had.

To all listed and all that are not, I dedicate my thesis to you. Thank you for being a part of this chapter of my life. I look forward to beginning a new one and seeing you there.

Table of Contents

Title Page i

Abstract iii

Acknowledgements v

Table of contents x

Preface xv

List of symbols and abbreviations xxiii

Chapter 1

Photomodulated Transport 1

1.1 Towards a Surface-Rolling and Photo-Activated Metal Carrier: The Nanobackhoe 2

Introduction 3

Results and Discussion 5

Conclusion 16

Experimental Section 17

References and Notes 27

Supporting Information for Chapter 1 30

Chapter 2

Towards Increased Rotational Speed of Light-Powered Motorized Single Molecule Nanocars 61

2.1 Design and Synthesis of Dual-Motored and Ultra-Fast Nanocars 62
Introduction 63
Results and Discussion 65
Conclusion 73
Experimental Section 74
References and Notes 82

Supporting Information for Chapter 2 87

Chapter 3

Synthesis and Studies of Fluorescently-Tagged Nanomachines 99

3.1 Micrometer-Scale Translation and Monitoring of Individual Nanocars on Glass 100
Introduction 101
Results and Discussion 103
Conclusion 114
Experimental Section 115
References and Notes 117

3.2 Synthesis of Fluorescent Dye-Tagged Nanomachines for Single Molecule Fluorescence Spectroscopy 120

Introduction 121
Results and Discussion 124
Conclusion 131
Experimental Section 132
References and Notes 140

Supporting Information for Chapter 3.1 144
Supporting Information for Chapter 3.2 148

Chapter 4

Construction of Nanovehicles through Self-Assembly 170

4.1 Towards an Assembly Line: Self-Assembling Nanocars 171
Introduction 172
Results and Discussion 175
Conclusion 183
Experimental Section 183
References and Notes 184

4.2 Nanotrains and Self-Assembled 2D Arrays Built from Carboranes Linked by Hydrogen Bonding of Dipyridones 189
Introduction 190
Results and Discussion 192
Conclusion 199
Experimental Section 199
References and Notes 200

Chapter 5

Carborane-Wheeled Nanocars 207

5.1 Synthetic Routes toward Carborane-Wheeled Nanocars 208

Introduction 209

Results and Discussion 211

Conclusion 223

Experimental Section 223

References and Notes 229

Supporting Information for Chapter 5 232

Chapter 6

Fullerene-Based Nanodevices 241

6.1 Synthesis and Photoisomerization of Fullerene- and OPE-Azobenzene Derivatives 242

Introduction 243

Results and Discussion 246

Conclusion 258

Experimental Section 259

References and Notes 263

6.2 Fullerene Terminated Molecular Wires 268

Introduction 269

Results and Discussion 270

Conclusion 286

Experimental Section 287

References and Notes 296

Supporting Information for Chapter 6.1 300
Supporting Information for Chapter 6.2 307

Nanocars: Towards Photoactive, Directionally-Controlled Surface Rolling Molecules

Preface

By Jason M. Guerrero

Science and engineering on the nanoscale offers novel possibilities for the design and synthesis of functional materials. Performing electronic and mechanical operations with specifically designed molecules presents the ultimate limit of miniaturization and has a profound impact on many fields ranging from molecular computing to medicine. The quest for functional molecular devices[1] has stimulated the design and synthesis of a variety of organic compounds such as motors,[2] rotors,[3] barrows,[4] scissors,[5] turnstiles,[6] elevators,[7] shuttles,[8] and nanovehicles[9] that resemble macroscopic machinery. This quest is driven by the impetus to miniaturize machinery in scientific, medical and technological disciplines as the most advanced current fabrication methods, the ''top-down'' approach to miniaturization (such as that used in the semiconductor industry) nears its limits in scaling.[10] The strategy used in the top-down approach is to shrink, and shrink again, a macroscopic entity using photolithography and the related techniques[11] to reach an equivalent micro- or nano-scopic entity. It is thought that the inherent limitations of this strategy will lead to a dead end in the next few years. For instance, silicon's band structure disappears when silicon layers are just a few atoms thick.[10] Photolithography and other related techniques, also used for microelectromechanical systems (MEMS) fabrication, are limited by the wavelengths at which they operate.

On the other hand, the "bottom-up" approach consists of building functional micro- or nano-scopic entities from the most basic organic building blocks. We need only to look at the life around us to see that this approach, inspired by what natural systems[12] are using, holds promise to develop new molecular devices. Biology uses thermodynamically controlled methods such as self-assembly and enzymatically controlled assembling routes such as bond scission and replacement that result in the precise positioning of molecular-sized entities for the construction of higher order structures. Adapting these approaches into the non-natural arena of organic synthesis, many of the initial molecular machines synthesized by chemists were made to work and to be studied as ensembles in solution, and their processes were readily studied using the abundant solution-phase analytical tools available. While these initial studies provided a cornerstone for future nanomachine development, to realize the successful execution of tasks used in common fabrication, and in a few cases, to mimic the tasks undertaken in biological systems, the deposition and study of molecule-sized machines on a surface is a crucial step. Thus, there has been a paradigm shift toward the development of surface-based molecular machines. Accordingly, a few types of surface-mounted molecular machines including altitudinal [13] and azimuthal [14] rotors, cyclodextrin necklaces, [15] molecular muscles, [16] and molecular shuttles [17] have been prepared and assembled on surfaces. Macroscopic effects have also been reported, such as the rotation of a micrometric glass rod on a liquid crystal film doped with a unidirectional light-powered molecular motor [18] and the millimeter-length directional transport of a diiodomethane drop across a surface using photoresponsive molecular shuttles.[17] These studies successfully demonstrated the effectiveness of such machines and the ability to exploit

changes in their configurational populations using external stimuli to carry out a specified task.

Despite these exciting results, the manipulation of nano-sized entities still represents one of the most difficult challenges for nanoscience. Various nanomanipulators have recently been developed for inclusion into microscopy setups and are often able to address entities that are only 1-2 nm in size.[19] However, these probes must be precisely positioned and are able to address only one of these entities at a time. Furthermore, control of these materials using a tool that is 8-9 orders of magnitude greater in size presents an obvious drawback in terms of efficiency. To overcome this hurdle, once again we need to look no further than nature. More exactly, if we examine the manner in which biology performs transportation and construction, we find that objects are manipulated and organized by molecular machines of comparable size, usually within 1-3 orders of magnitude. For example, small molecules such as oxygen, amino acids and short protein chains are transported by diffusion or by proteins or vesicles via gross fields of influence, diffusion and Brownian motion, and are placed in specific locations by enzymes via molecular recognition, to build higher order structures or carry out important tasks. Larger systems are transported by motor proteins such as dynein, kinesin and myosin, which all move, powered by chemical reactions, in a directionally-controlled fashion along a track such as an actin filament or microtubule. As an ensemble, these molecular machines can move organelles, vesicles, and, when enough of these proteins are present, even neurons and muscles. Concomitantly, the nanoscientist is faced with the challenge of controlling differing internal modes of operation including rotation of specific bonds for movement, directional control, molecular recognition, etc.,

within a single molecule. We are then posed with the following question: What design platform is a chemist able to manipulate, using traditional organic synthesis, for the inclusion of multiple components to build functional nanomachines?

Primary attempts to address some of the hurdles associated with controlling single molecule machines resulted in various groups reporting the synthesis of landers,[20] wheelbarrows,[21] nanowalkers,[22] and poly-aromatic systems[23] for the purpose of investigating their behavior on surfaces. These systems, however, only display a single internal mode of operation, carrying out only one task. Further expanding on this idea, our group has combined various nanocomponentry with molecular axles containing fullerene, *p*-carborane or organometallic wheels to construct a number of nanovehicles designed for directed motion and transport along atomically flat surfaces.[9] Due to their obvious resemblance to macroscopic vehicles, we have termed these single molecule machines "nanocars". These nanocars synthesized in our laboratory are each calculated to be approximately 3 × 4 nm in size, and can be produced on the ~30 mg scale (~10^{18} nanocars) using small laboratory reaction flasks, or more nanocars than the number of automobiles made in the history of the world (which is <10^8 automobiles). It would take 30 nanocars, side by side, to span the 90 nm width of a small line in the most advanced logic chip being made today.[10] To conceptualize the possibilities of controlling such a vast number of molecular machines, by contrast, the concerted movement of ~10^{12} myosin motor proteins which are, on average, 45 times larger than a nanocar, are responsible for a typical muscle fiber contraction.[24] Therefore, it is the inspiration by nature and the resultant possibilities to mimic its capability that drive us to continue our quest to develop functional, surface-active molecular machines. Initial proof-of-concept

experiments have shown, using STM, the directed movement of fullerene-wheeled nanocars on atomically-flat Au(111) surfaces upon thermal and electrostatic activation.[25] However, our project is still in its embryonic stages, and we are only now learning to construct and manipulate these devices with some degree of efficiency.

Therefore, building upon our initial results, described in this thesis are efforts to advance our understanding of single molecule machines through the synthesis and study of an array of nanovehicles. In the first chapter, nanoscale transport is explored through the synthesis and solution-based studies of a photoactive, metal-ion-chelating nanocar. Following this, in the second chapter, directional control and propulsion are explored through the synthesis of motorized nanocars. The third chapter covers our efforts to complement previous STM studies, where single molecule fluorescence spectroscopy is used for imaging and mechanistic elucidation of translational movement of fluorescently-tagged nanovehicles. Their synthesis is covered, as well. In chapters 4 and 5, various nanovehicles are synthesized using contrasting approaches. In chapter 4, self-assembly methods mirroring those used in biological construction are used to produce nanocars and nanotrains. Traditional organic synthesis is used to build carborane-wheeled nanovehicles in chapter 5. Finally, in chapter 6, nanocomponentry is explored through the synthesis and studies of molecular devices such as azobenzene-fullerene switches and fullerene-oligo(phenylene ethynylene) molecular wires.

References

(1) (a) Balzani, V.; Venturi, M.; Credi, A. *Molecular Devices and Machines: Concepts and Perspectives for the Nanoworld*; Wiley-VCH: Weinheim, 2008. (b) Leigh, D. A.; Zerbetto, F.; Kay, E. R. *Angew. Chem. Int. Ed.* **2007**, *46*, 72-191. (c) Kottas, G. S.; Clarke, L. I.; Horinek, D.; Michl, J. *Chem. Rev.* **2005**, *105*, 1281-1376. (d) Rapenne, G. *Org. Biomol. Chem.* **2005**, *3*, 1165-1169.

(2) (a) Kelly, T. R.; De Silva, H.; Silva, R. A. *Nature* **1999**, *401*, 150-152. (b) Koumura, N.; Zijistra, R. W. J.; Van Delden, R. A.; Harada, N.; Feringa, B. L. *Nature* **1999**, *401*, 152-155. (c) Leigh, D. A.; Wong, J. K. Y.; Dehez, F.; Zerbetto, F. *Nature* **2003**, *424*, 174-179. (d) Balzani, V.; Clemente-Leon, M.; Credi, A.; Ferrer, B.; Venturi, M.; Flood, A. H.; Stoddart, J. F. *Proc. Natl. Acad. Sci. U. S. A.* **2006**, *103*, 1178-1183. (e) Carella, A.; Rapenne, G.; Launay, J. P. *New J. Chem.* **2005**, *29*, 288-290.

(3) (a) Kottas, G. S. ; Clarke, L. I.; Horinek, D.; Michl, J. *Chem. Rev.*, **2005**, *105*, 1281-1376. (b) Jian, H.; Tour, J. M. *J. Org. Chem.*, **2003**, *68*, 5091-5103.

(4) (a) Jimenez-Bueno, G.; Rapenne, G. *Tetrahedron Lett.* **2003**, *44*, 6261-6263. (b) Rapenne, G.; Jimenez-Bueno, G. *Tetrahedron* **2007**, *63*, 7018-7026.

(5) Muraoka, T.; Kinbara, K.; Aida, T. *Nature* **2006**, *440*, 512-515.

(6) Bedard, T. C.; Moore, J. S. *J. Am. Chem. Soc.* **1995**, *117*, 10662-10671.

(7) Badjic, J. D.; Balzani, V.; Credi, A.; Silvi, S.; Stoddart, J. F. *Science* **2004**, *303*, 1845-1849.

(8) (a) Armaroli, N.; Balzani, V.; Collin, J. P.; Gavina, P.; Sauvage, J. P.; Ventura, B. *J. Am. Chem. Soc.* **1999**, *121*, 4397-4408. (b) Brouwer, A. M.; Frochot, C.; Gatti, F. G.;

Leigh, D. A.; Mottier, L.; Paolucci, F.; Roffia, S.; Wurpel, G. W. H. *Science* **2001**, *291*, 2124-2128.

(9) (a) Shirai, Y.; Morin, J.-F.; Sasaki, T.; Guerrero, J. M.; Tour, J. M. *Chem. Soc. Rev.* **2006**, *35*, 1043-1055. (b) Vives, G.; Tour, J. M. *Acc. Chem. Res.* **2009**, in press.

(10) (a) James, D. K.; Tour, J. M. *Aldrichimica Acta*, **2006**, *39*, 47-56. (b) James, D. K.; Tour, J. M., *Top. Curr. Chem.*, **2005**, *257*, 33-62.

(11) a.) Kawata, S.; Sun, H.-B.; Tanaka, T.; Takada, K. *Nature*, **2001**, *412*, 697. b.) B. Li, H. Yu, A. Sharon and X. Zhang, *Appl. Phys. Lett.*, **2004**, *85*, 2426-2428.

(12) (a) Alberts, B. *Cell* **1998**, *92*, 291-294. (b) Kinbara, K.; Aida, T. *Chem. Rev.* **2005**, *105*, 1377-1400.

(13) Zheng, X.; Mulcahy, M. E.; Horinek, D.; Galeotti, F.; Magnera, T. F.; Michl, J. *J. Am. Chem. Soc.* **2004**, *126*, 4540-4542.

(14) Jian, H.; Tour, J. M. *J. Org. Chem.* **2003**, *68*, 5091-5103.

(15) Shigekawa, H.; Miyake, K.; Sumaoka, J.; Harada, A.; Komiyama, M. *J. Am. Chem. Soc.* **2000**, *122*, 5411-5412.

(16) Liu, Y.; Flood, A. H.; Bonvallet, P. A.; Vignon, S. A.; Northrop, B. H.; Tseng, H.-R.; Jeppesen, J. O.; Huang, T. J.; Brough, B.; Baller, M.; Magonov, S.; Solares, S. D.; Goddard, W. A.; Ho, C.-M.; Stoddart, J. F. *J. Am. Chem. Soc.* **2005**, *127*, 9745-9759.

(17) Berna, J.; Leigh, D. A.; Lubomska, M.; Mendoza, S. M.; Perez, E. M.; Rudolf, P.; Teobaldi, G.; Zerbetto, F. *Nat. Mater.* **2005**, *4*, 704-710.

(18) Eelkema, R.; Pollard, M. M.; Vicario, J.; Katsonis, N.; Ramon, B. S.; Bastiaansen, C. W. M.; Broer, D. J.; Feringa, B. L. *Nature* **2006**, *440*, 163.

(19) (a) Kaegi, R.; Holzer, L. *Atmos. Environ.* **2003**, *37*, 4353-4359. (b) Culpepper, M. L.; Anderson, G. *Prec. Eng.* **2004**, *28*, 469–482. (c) Yang. T.; Holzer, L.; Kaegi, R.; Winnefield, F.; Keller, B. *Ultramicroscopy* **2007**, *107*, 1068-1077.

(20) Rosei, F.; Schunack, M.; Jiang, P.; Gourdon, A.; Legsgaard, E.; Stensgaard, I.; Joachim, C.; Besenbacher, F. *Science* **2002**, *296*, 328-331.

(21) Grill, L.; Rieder, K.-H.; Moresco, F.; Jimenez-Bueno, G.; Wang, C.; Rapenne, G.; Joachim, C. *Surf. Sci.* **2005**, *584*, L153-L158.

(22) Kwon, K.-Y.; Wong, K. L.; Pawin, G.; Bartels, L.; Stolbov, S.; Rahman, T. S. *Phys. Rev. Lett.* **2005**, *95*, 166101-166104.

(23) (a) Gimzewski, J. K.; Joachim, C.; Schlittler, R. R.; Langlais, V.; Tang, H.; Johannsen, I. *Science* **1998**, *281*, 531-533. (b) Gross, L.; Rieder, K. –H.; Moresco, F.; Stojkovic, S. M.; Gourdon, A.; Joachim, C. *Nat. Mater.* **2005**, *4*, 892-895.

(24) Molloy, J. *Biophys. J.* **2005**, *89*, 1-2.

(25) Shirai, Y.; Osgood, A. J.; Zhao, Y.; Kelly, K. F.; Tour, J. M. *Nano Lett.* **2005**, *5*, 2330-2334.

List of Symbols and Abbreviations

A	Amps
Å	Angstrom
Ac	acetyl
AFM	atomic force microscopy
$AgBF_4$	silver tetrafluoroborate
AgF	silver fluoride
$AgNO_3$	silver nitrate
AM-1	Austin Model-1
Ar	aryl, argon
aq.	aqueous
$BF_3{\cdot}OEt_2$	borontrifluoride diethyletherate
bp	boiling point
br	broad (spectral)
t-Bu	*tert*-butyl

n-Bu	normal-butyl
CaH_2	calcium hydride
calcd	calculated
CH_3	methyl
C_4H_9Br	1-bromobutane
$CHCl_3$	chloroform
CH_2Cl_2	dichloromethane
CH_3CN	acetonitrile
cm	centimeters(s)
cm^{-1}	inverse centimeter(s) or wavenumbers
CPK	Corey-Pauling-Koltun
CS_2	carbon disulfide
CuBr	copper bromide
CuI	copper iodide
d	day(s), doublet (spectral)
dd	doublet of doublet (spectral)

DMF	*N*,*N*'-dimethylformamide
DMSO	dimethylsulfoxide
DSC	differential scanning calorimetry
E_g	band gap
Et	ethyl
equiv	equivalent
Et_2O	diethyl ether
EtOAc	ethyl acetate
Et_3N	triethylamine
eV	electron volt
FTIR	fourier transform infrared
g	gram(s)
h	hour(s)
HCHO	formaldehyde
HNO_3	nitric acid
HOMO	highest occupied molecular orbital

HOPG	highly ordered pyrolytic graphite
HRMS	high-resolution mass spectrum
H_2O	water
H_2SO_4	sulfuric acid
Hz	Hertz
I_t	tunneling current
IPES	inverse photoelectron spectroscopy
i-Pr_2NH	diisopropylamine
IR	infrared
J	coupling constant (spectral)
K	degrees in Kelvin
kcal	kilocalorie
KBr	potassium bromide
K_2CO_3	potassium carbonate
L	Liter(s)
LHMDS	lithium hexamethyl disilazide

LUMO	lowest unoccupied molecular orbital
m	meter(s), milli, multiplet (spectral)
mp	melting point
M	moles per liter
MALDI	matrix-assisted laser desorption ionization
MALDI-TOF	matrix-assisted laser desorption ionization – time-of-flight
MeI	methyl iodide
MeOH	methanol
$MgSO_4$	magnesium sulfate
MHz	megahertz
min	minute(s)
mol	mole(s)
MS	mass spectrometry, material studio (software)
MW	molecular weight
N_2	nitrogen
$NaBH_4$	sodium borohydride

NaH	sodium hydride
$NaHCO_3$	sodium bicarbonate
NaI	sodium iodide
NaOH	sodium hydroxide
NBS	*N*-bromosuccinimide
NH_4Cl	ammonium chloride
nm	nanometer
NMR	nuclear magnetic resonance
NO_2	nitro
OPE	oligo(phenylene ethynylene)
p	*para*
p	pico
Pd/Cu	$Pd(PPh_3)_2Cl_2$/CuI Sonogashira coupling condition
$Pd(PhCN)_2Cl_2$	palladium(II) bis(benzonitrile) dichloride
$Pd(PPh_3)_2Cl_2$	palladium(II) bis(triphenylphosphino)dichloride
$Pd(OAc)_2$	palladium(II) acetate

Ph	phenyl
$P(OMe)_3$	trimethylphosphite
PPh_3	triphenylphosphine
$HP(^tBu)_3BF_4$	tri-*tert*-butyl phosphonium tetrafluoroborate
ppm	parts per million (spectral)
PSS	photostationary state
q	quartet (spectral)
s	second(s), single (spectral)
SAM	self-assembled monolayer
STM	scanning tunneling microscopy
t	triplet (spectral)
T_c	crystallization temperature
TBAF	tetrabutylammonium fluoride
TBAH	tetrabutylammonium hydride
t-BuONO	*tert*-butylnitrite
TEA	triethylamine

TEM	transmission electron microscopy
TESP	tapping-mode etched silicon probe
TFA	trifluoroacetic acid
TGA	thermo gravimetric analysis
THF	tetrahydrofuran
TIPSA	triisopropylsilyl acetylene
TIPS	triisopropylsilyl
TLC	thin layer chromatography
TMS	trimethylsilyl, tetramethylsilane (spectral)
TMSA	trimethylsilyl acetylene
TMSCl	trimethylsilyl chloride
TRITC	tetramethylrhodamineisothiocyanate
UHV	ultra high vacuum
UPS	ultraviolet photoelectron spectroscopy
UV	ultraviolet
V	Volt

V_b	bias voltage
vis	visible (light)
°C	degrees Celsius
Δ_{abs}	change in absorption
δ	chemical shift in parts per million downfield from TMS
μ	micro, dipole moment
λ	wavelength

Chapter 1

Photomodulated Transport

1.1

Initial Studies Towards a Surface Rolling Photoactivated Metal Ion Carrier: The Nanobackhoe

Introduction

Spurred by the ever-increasing interest directed towards bottom-up construction, the current thrust of much physical and biological science research is to address the eventual need for molecular machinery.[1] In order for nanomachines to mimic the everyday tasks carried out by their macroscopic counterparts, some of the more difficult hurdles associated with molecular machine production must be addressed.[2] To help provide insight into the development of future nanomachines, particularly methods for controlled propulsion, communication, transport and directionality, our group has taken interest in the combination and assembly of molecular axles, wheels and interchangeable componentry (particularly photo- and electro-active moieties) into surface-rolling nanovehicles.[3,4]

In recent years, many advances have been made in the design, synthesis and testing of photoactive moieties for inclusion into molecular machines.[5,6] While these molecules have proven to be quite successful in carrying out translational motion in solution and on surfaces,[7] as it is usually reversible and almost always associated with a large change in geometric structure, little work has been done in the area of light-induced transportation of nanomaterials. Rather than using photoisomerization as a direct tool for propulsion and thus translational motion, we report the synthesis of a new nanocar bearing a photoactive dipyridylethylene[8] (DPE) unit for the controlled acquisition of metal ions,[9] as shown in Figure 1. Studies of its photoactive behavior as a free ligand and when complexed to a metal, taking advantage of the DPE's two discrete binding

modalities when isomerized from *trans* (weaker, monodentate chelation) to *cis* (stronger, bidentate chelation) are also described.

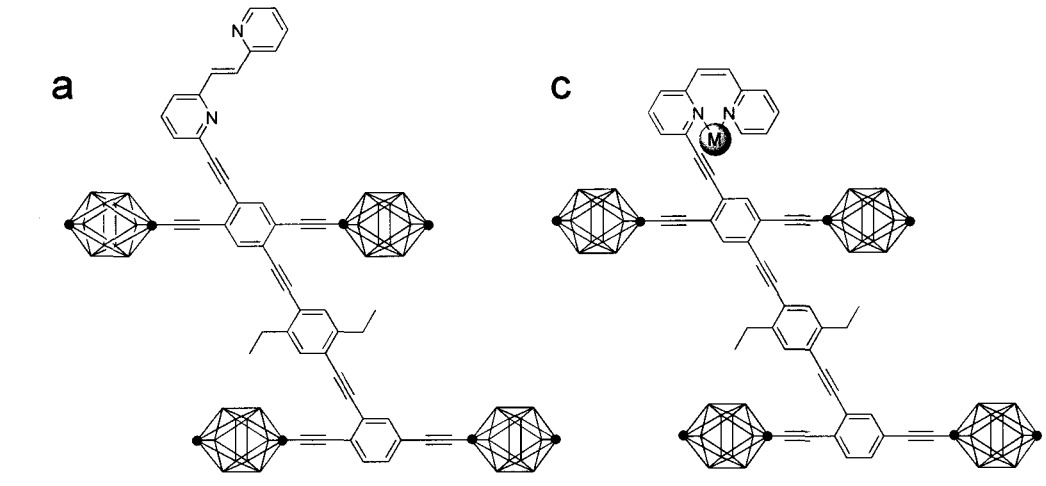

Figure 1. Structure of nanobackhoe **1** in *trans* (a,b) and complexed *cis* (c,d) and its geometry optimized in each case (b, d) with MS Modeling 4.0. M = $Cu(CH_3CN)_2^+$

Design and Synthesis of Nanobackhoe 1. The orientation of the dipyridylethylene moiety relative to the nanocar is designed to be sterically demanding to prevent the chelation of a single metal center to more than one nanobackhoe. As shown in

Figure 1, in the absence of a surface, upon isomerization to the *cis* form of the dipyridylethylene claw, the minimal energy conformation, as calculated by molecular modeling[10] of the complexed nanobackhoe, places the metal center in a seven-membered ring with the metal atom above the nanocar. Additionally, the alkynyl moiety of the dipyridylethylene claw portion allows free rotation[3b] before and after isomerization, thereby increasing the possibility of metal release to a surface or other receiving agent. Due to the unsymmetrical nature of the molecule, it was necessary to combine two different halves of the car in a convergent manner, one bearing an axle which has been used in previous syntheses and a second, differentially-substituted axle bearing the aforementioned DPE claw.

Results and Discussion

To selectively obtain the *trans* form of the claw with a pendant bromide for subsequent Sonogashira coupling, a Horner-Wadsworth-Emmons olefination[11] (Scheme 1) of commercially available α-picoline and 6-bromopyridine-2-carboxaldehyde was performed using α-picoline and diethylchlorophosphate to form the in situ deprotonated Arbuzov-type product. Immediate condensation onto the aldehyde provided olefin **2** with greater than 99:1 E:Z selectivity (as determined by ^{1}H NMR). Sonogashira coupling of trimethylsilylacetylene (TMSA) to the aryl bromide at 60 °C afforded TMS-alkyne **3**.

Scheme 1. Synthesis of dipyridylethylene claw

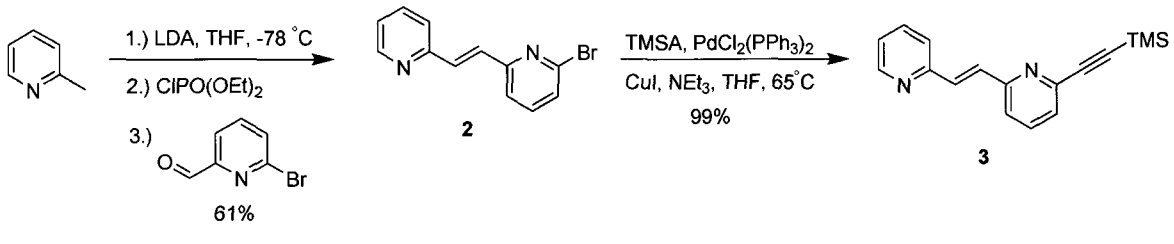

The claw-bearing axle was then synthesized beginning with previously described **4**[4d] (Scheme 2) undergoing desilyl bromination using $AgNO_3$ and NBS in acetone[12] to provide the dialkynyl bromide, which was immediately reacted with with a cuprated *p*-carborane species to introduce wheels, giving diiodide axle **5**. To arrive at the lower half of the backhoe, TMS alkyne **3** was deprotected and reacted immediately with diiodide axle **5** in a statistical Sonogashira coupling to give the desired claw axle **6** in 24 % yield.

Scheme 2. Synthesis of claw-bearing axle

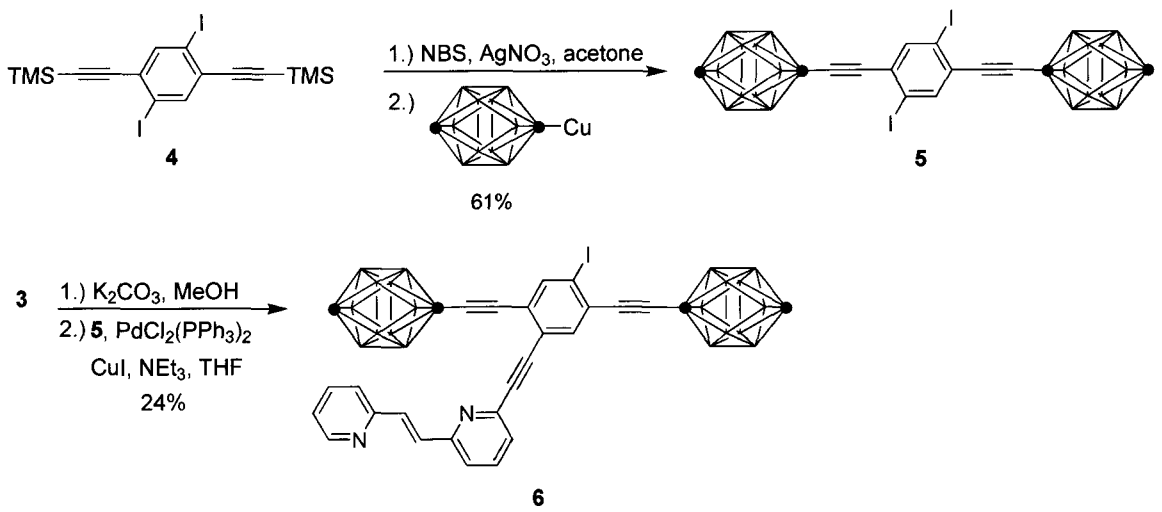

The second half of the molecule includes the inner chassis of the nanobackhoe bearing a central dialkylated benzene ring for increased solubility. Following known procedures, 1,4-diiodo-2,5-diethylbenzene (**7**) (Scheme 3) was synthesized in two steps from commercially available 4-ethylacetophenone.[13] To ease chromatographic separation by adding a highly polar group, a statistical Sonogashira coupling of 2-methyl-3-butyne-2-ol to diiodide **7** gave the monoalkyne **8** in 77% yield. For stability reasons,[14] triisopropylsilyl-protected acetylene (TIPSA) was chosen to couple to the monoiodide, subsequently providing the protected inner chassis **9**. For deprotection, **9** was subjected to sodium hydroxide in refluxing toluene[15] to give the differentially substituted inner chassis **10**. Pd-catalyzed coupling to previously reported iodide axle **11**[4a] followed by TBAF deprotection gave the free alkyne half-backhoe **12**. A final Sonogashira coupling of the terminal alkyne to claw axle **6** was performed to provide nanobackhoe **1** in 61% yield.

Scheme 3. Completion of nanobackhoe

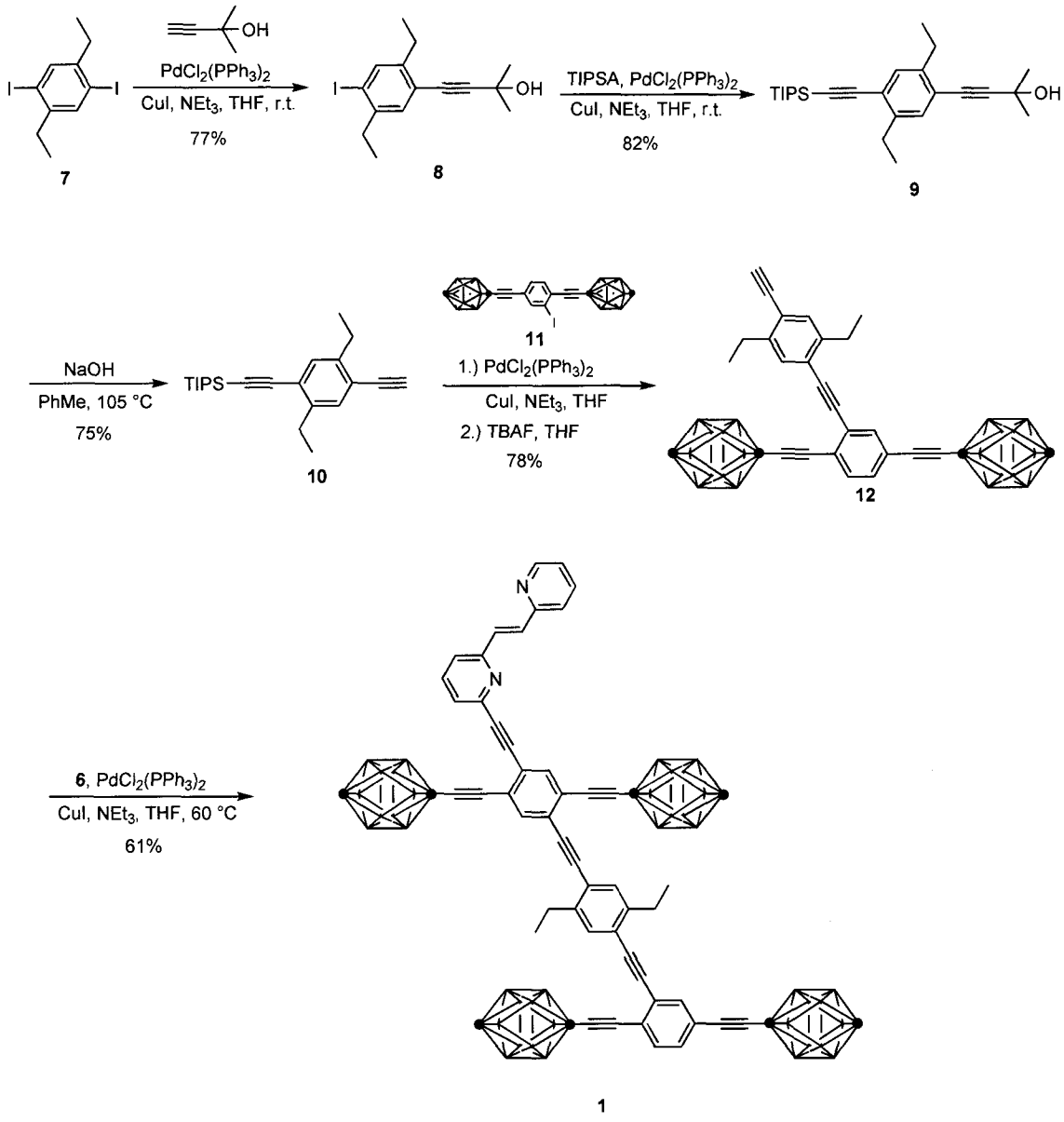

Photoinitiated Isomerization and Chelation. To determine the optimal conditions for both photoisomerization and chelation, *trans* **3** was irradiated under a variety of conditions and studied by both NMR and UV/Vis spectroscopy (Figures 2 and 3). Irradiation at the λ_{max} of **3** (313 nm) for extended periods of time yielded a significant amount of byproducts in addition to the desired *cis* isomer, evidenced by the appearance of ^{1}H resonances not corresponding to either isomer. In an effort to avoid the

aforementioned unwanted side reactions, investigation of various wavelengths and irradiation times led to a final protocol of pulsed irradiations at 365 nm of compound **3,** performed at 15 min intervals over the course of several hours. It was interesting to note that irradiation slightly off of the λ_{max} led to more efficient conversion of *trans* **3** to *cis* **3**. It was found that 365 nm and 313 nm wavelengths give clean conversion as long as the process involves long pulsed irradiations, with irradiation at 313 nm consisting of 5 min intervals.

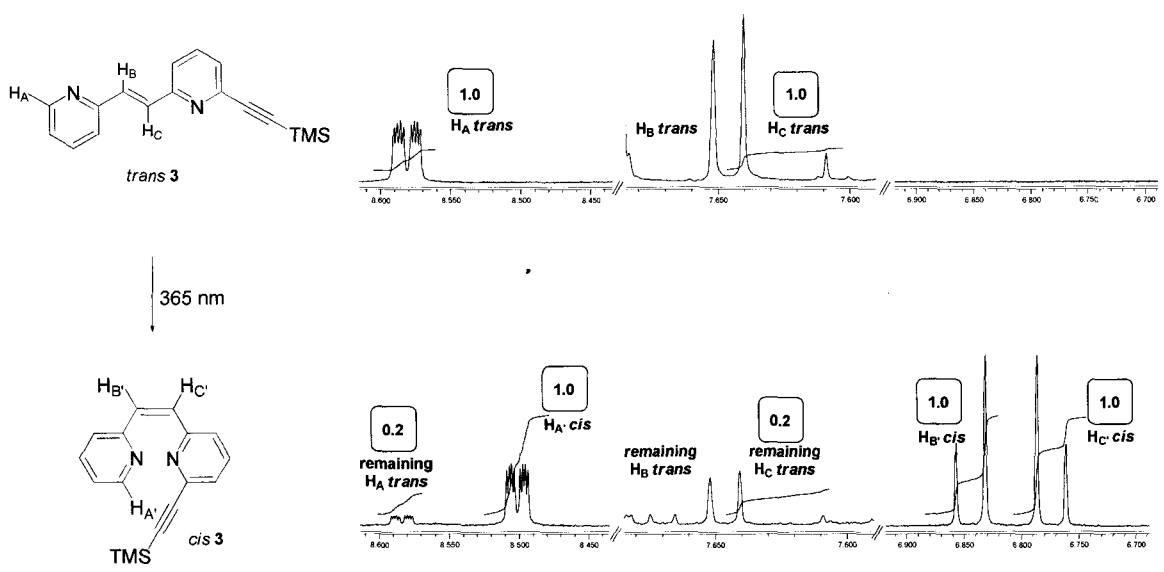

Figure 2. Spectral monitoring of *trans*-to-*cis* isomerization of **3** by ^{1}H NMR. Both the pyridyl 6' and alkene resonances can be monitored. The pyridyl and alkene protons are explicitly shown and labeled for clarity. Relative integration values are shown in the boxes. The *trans*-alkenyl coupling constant is 16 Hz. The *cis*-alkenyl coupling constant is 13 Hz. Note that the H_B *trans* alkene signal overlaps with an adjacent aryl signal, rendering its integration value inaccurate.

In addition to monitoring by ^{1}H NMR, the isomerization process can also be followed by UV/Vis (Figure 3). Significant decrease in the λ_{max} occurring at ~330 nm can be observed. As before, pulsed irradiation was performed on a dilute sample to avoid decomposition.

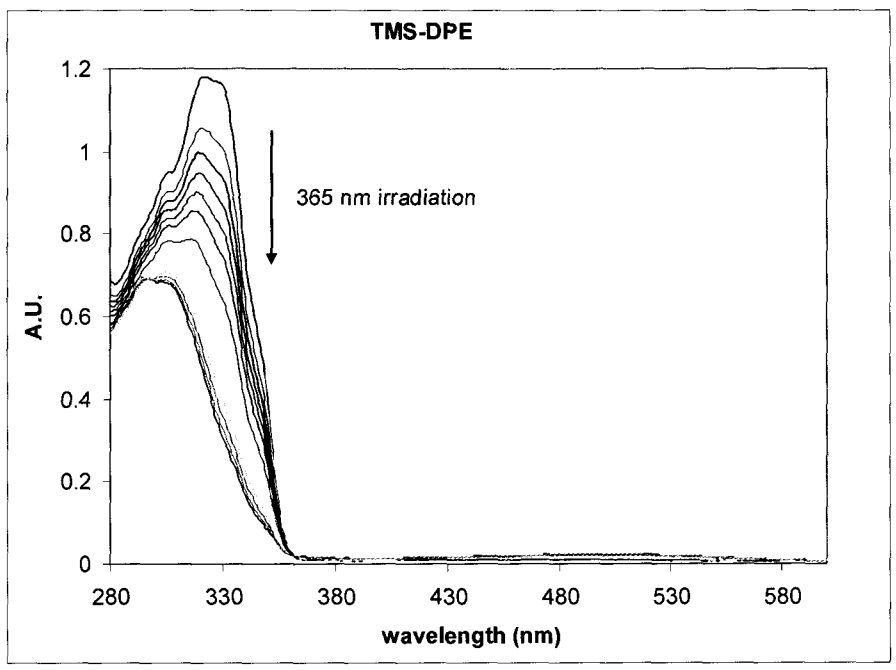

Figure 3. UV/Vis monitoring of the photoinduced isomerization from *trans* **3** to *cis* **3.**

Upon verification of suitable conditions for isomerization of **3**, irradiation was then performed on *trans* nanobackhoe **1**. ^{1}H NMR behavior similar to that of compound **3** could be noted. The *cis* alkene resonances coalesce in the parent compound. Therefore, integration of the monitored *cis* alkene peak results in a value representing both alkene protons. Due to the increased number of aryl signals and their overlap with those of the *trans* alkene, their integration is not a useful diagnostic.

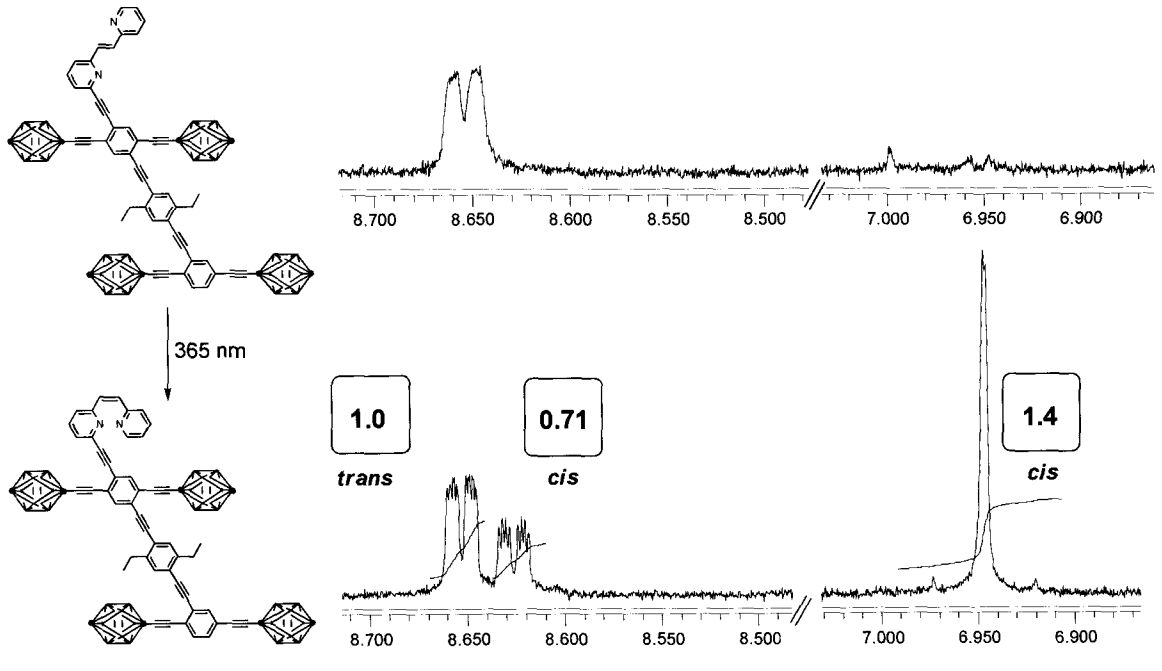

Figure 4. Photoisomerization of nanobackhoe **1**. Note that both cis alkene protons coalesce into a single signal. The slight outer signals adjacent to the cis alkene correspond to a slight AB quartet.

As in compound **3**, the photoactive behavior of nanobackhoe **1** could also be monitored using UV/Vis. As can be seen in the UV/Vis spectrum (Figure 5), the backhoe exhibits a very broad λ_{max} occurring in the range between 330-400 nm. Irradiation using 365 nm resulted in a concomitant decrease in the maximum absorption consistent with formation of the *cis* isomer.

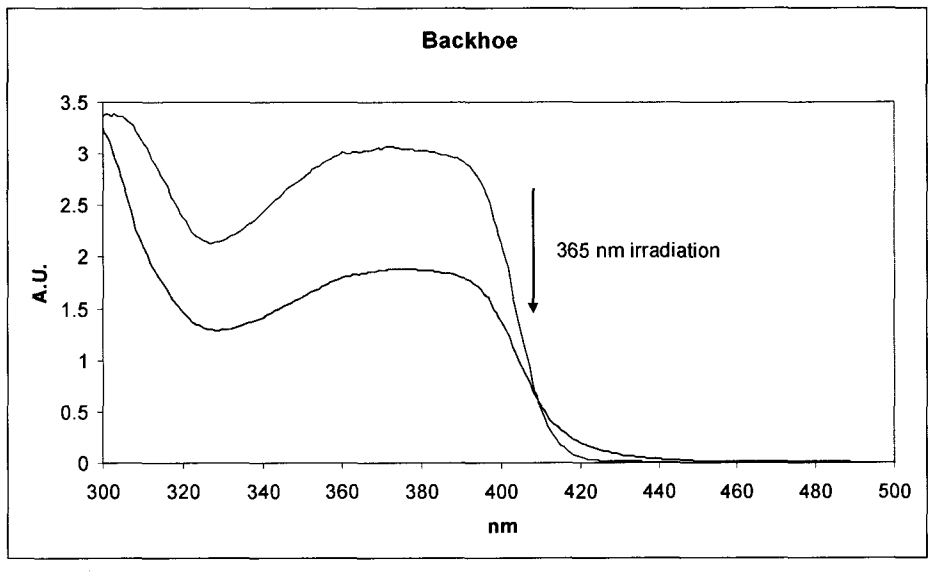

Figure 5. UV/Vis monitoring of the photoisomerization of *trans* nanobackhoe **1** to *cis* nanobackhoe **1**.

The photoattenuative metal ion chelation ability of both model compound **3** and nanobackhoe **1** was also investigated using ^{1}H NMR. Unfortunately, a lack of metal-to-ligand charge transfer (MLCT) peaks in the UV/Vis spectra of **1** and **3** outside of the range of their respective π systems (> 400 nm, > 365 nm) precluded the use of UV/Vis as a diagnostic tool for chelation. The NMR behavior is shown in Figure 6 for compound **3**. The initial spectrum represents a pure solution of **3**. Upon adding 1 equivalent of $Cu(CH_3CN)_4PF_6$,[16] a significant amount of peak broadening occurs in some aryl resonances. To ascertain which resonances experience this broadening, 2D NMR was performed on a solution of compound **3**. It was thus confirmed that the peaks exhibiting the most broadening correspond to the free pyridyl ring (distal from the alkyne). Interestingly, the behavior of the *cis* alkene resonances of chelated *cis* **3** is similar to that

of the nanobackhoe **1** post-irradiation, where a coalescence of both alkenes occurs. In this case, no AB-quartet is observed.

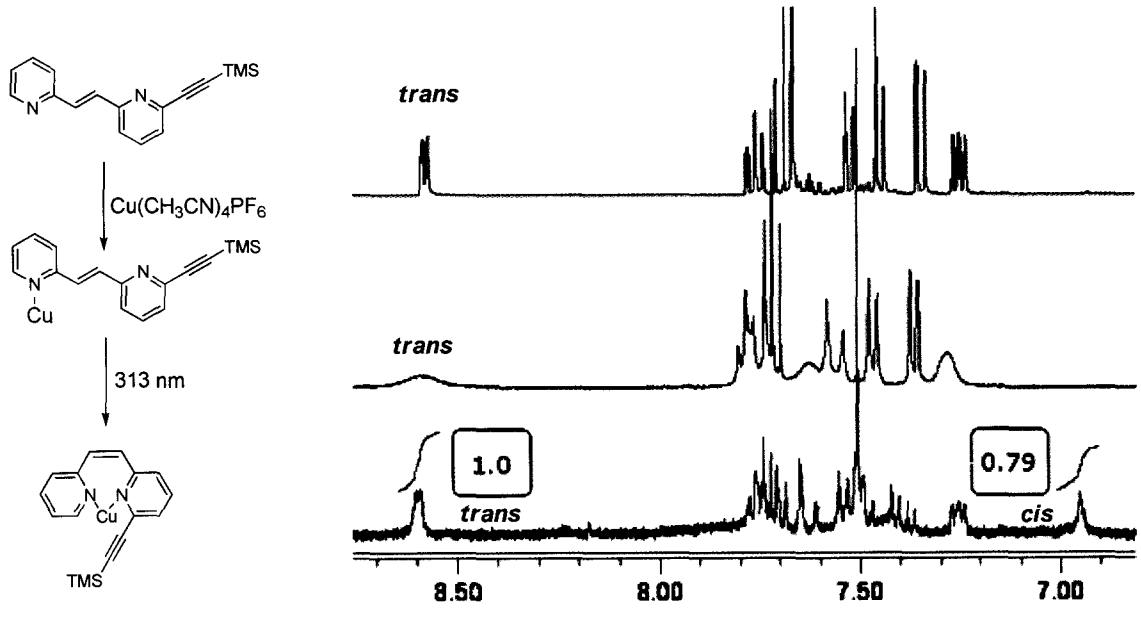

Figure 6. NMR monitoring of photoattenuated chelation. From the top down, 100% *trans* solution of **3**, followed by addition of 1 equiv. of $Cu(CH_3CN)_4PF_6$. Note the significant peak broadening of the aryl protons on the chelated pyridine. The bottom spectrum is post-irradiation at the photostationary state (PSS) in the presence of copper. In the case of the monodentate complex, Cu = $Cu(CH_3CN)_3^+$ and in the bidentate complex, Cu = $Cu(CH_3CN)_2^+$.

With a method for chelation and isomerization in hand, the experiments were attempted with nanobackhoe **1**. As in model compound **3**, significant peak broadening occured in the aryl region upon addition of 1 equiv. of Cu. Additionally, the pyridyl 6' ^1H (the most downfield resonance) experiences an upfield shift, encroaching into the region

where the *cis* pyridyl resonance appears. Upon irradiation at 365 nm, ^{1}H NMR indicates formation of the *cis* isomer. However, the *cis* alkene peaks are severely broadened to the point where analysis is difficult. Therefore, monitoring of the process must be done by observation of the pyridyl 6' ^{1}H *trans*-to-*cis* process.

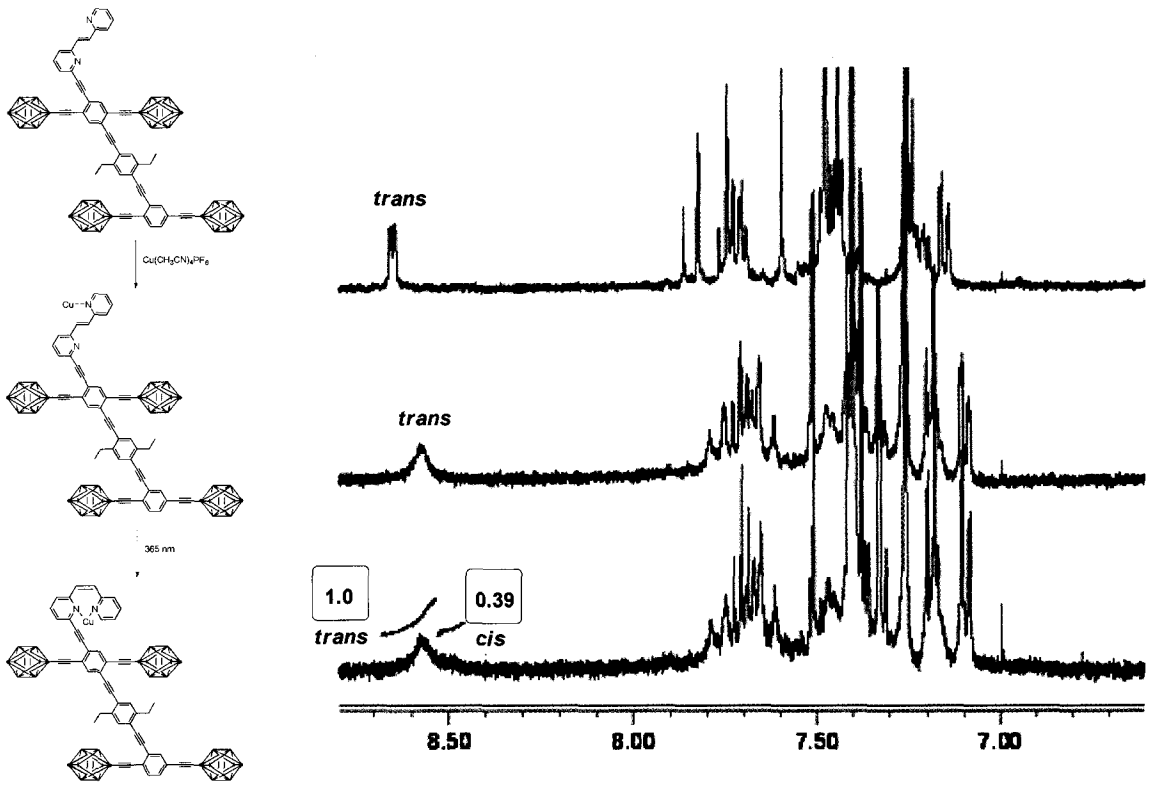

Figure 7. From top-to-bottom, a 100% trans solution of nanobackhoe **1**, followed by addition of 1 equiv. of $Cu(CH_3CN)_4PF_6$. The bottom trace is after irradiation to the PSS. The monochelated Cu = $Cu(CH_3CN)_3^+$ while the dichelated Cu = $Cu(CH_3CN)_2^+$.

The unisomerized combinations of both **1** and **3** yielded a monodentate chelation complex where the pyridyl ring distal from the alkyne serves as a ligand with the metal center. Upon irradiation, a bidentate complex was formed (the "picking up" process), as

evidenced by a shift and broadening of *cis* pyridyl and alkene proton resonances. A collapse of the alkene resonances from doublets to a singlet was also observed, which is in direct support of the modeled cyclic configuration.

Attempted Claw Opening for Metal Ion Release. To switch back to the weaker, monodentate chelating form (thereby affording the opportunity for release), the back-irradiation process, *cis*-to-*trans* was attempted by using 254 nm light on the model compound **3** after the PSS had been reached (approx. 80% cis), as described by Zhu and co-workers.[9c] As the processes were quite facile to observe by UV/Vis, this was the method of choice for determination of switching efficiency. Presumably, upon irradiation of *cis* **3**, the UV/Vis trace should begin to return to the original *trans* **3** spectrum. However, as shown in Figure 8, upon short pulsed irradiations at 254 nm, the solution of *cis* **3** began to form products not identified as *cis* or *trans* **3**. Monitoring of this process via ^{1}H NMR also revealed signals that could not be identified as *cis* or *trans*. Despite this, it is possible that the *cis*-to-*trans* isomerization behavior of the DPE-based nanobackhoe on a surface may prove to be more efficient as has been shown on copper-based self-assembled monolayers (SAMs).[9d]

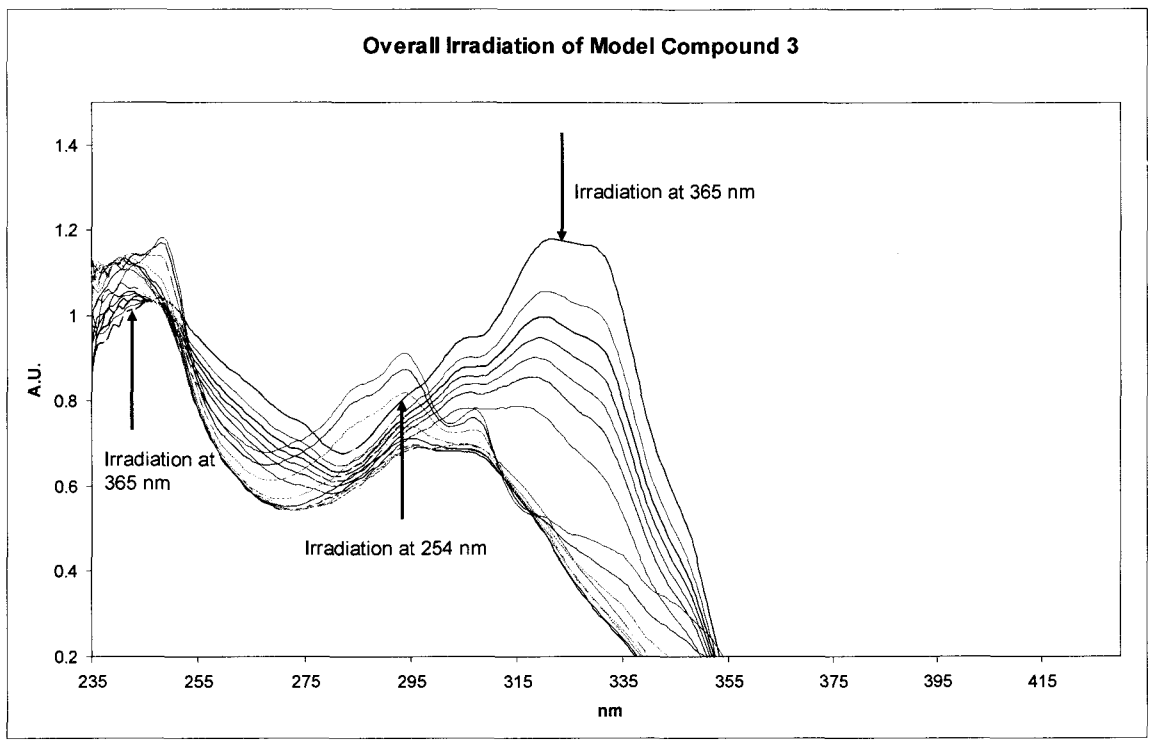

Figure 8. Overall irradiation of the bare ligand **3**. Appearance of λ_{max} at 254 nm after 365 nm irradiation. Attempted back-irradiation of **3** using 254 nm light resulted in the appearance of a λ_{max} at 295 nm that does not correspond to starting *trans* **3**.

Conclusion

In summary, we have synthesized a new nanocar with the capability to selectively uptake metals when directed by light as an external stimulus. Irradiation of the *trans* isomer of both the model compound **3** and the nanobackhoe **1** at 365 nm provides a bidentate ligand with the capability to complex metals for eventual transport and rational placement. While the photoactive grasping of metal ions by the nanobackhoe has so far proven to be an irreversible process, we consider the successful synthesis and proof-of-concept controlled uptake of copper to be a large step towards the development of

nanoscale construction agents. Furthermore, the structural integrity of the nanobackhoe may be compromised after proper uptake and placement of its cargo as a method for release. Studies to determine the backhoe's ability to transfer the metal ions to receiving agents and its behavior on surfaces are planned.

Experimental Section

General Methods. All reactions were performed under an atmosphere of nitrogen unless stated otherwise. Compounds **4**,[4d] **7**[13] and **11**[4a] were prepared according to literature procedures. $Cu(CH_3CN)_4PF_6$ was purchased from Strem and Sigma Aldrich chemicals and recrystallized from acetonitrile prior to use.[16] Reagent grade diethyl ether and THF were distilled from sodium benzophenone ketyl. Diisopropylamine, triethylamine (TEA) and CH_2Cl_2 were distilled over CaH_2. TBAF (1.0 M solution in THF) and *n*-BuLi (2.5 M in hexanes) were obtained from Sigma-Aldrich and used as received. Flash column chromatography was performed using 230–400 mesh silica gel from EM Science. Thin layer chromatography was performed using glassplates precoated with silica gel 40 F254 purchased from EM Science. NMR experiments were conducted on 400 and 500 MHz Bruker instruments. MS measurements were performed at the University of South Carolina Mass Spectrometry facility or the Rice University Mass Spectrometry facility. NMR and UV–vis spectroscopy irradiation experiments were performed in deoxygenated solutions at ~1.7 mM (NMR) or 4~17 μM (UV–vis) using a 100 W Hg arc light source (EFOS ActicureA4000 UV light source/curing system) with appropriate wavelength Hg line filters (Andover) and band-pass filters. The light intensity

after passing through the filters was monitored with a radiant power meter (Oriel). Typical light intensity for NMR and UV/Vis experiments was 1.0 mW/cm^2. The isomerization reactions were done while stirring or in 15 min intervals with intermittent sonication to avoid decomposition of the DPE moiety. The rate of the thermal isomerization for all experiments was slow enough to allow the determination of the photoisomerization yields at the PSS without significant change using normal NMR and UV–vis operations (measured within 1-3 min after reaching the PSS). Compounds were named using Chemdraw Ultra 11.0.

General Procedure for the Coupling of a Terminal Alkyne with an Aryl Halide Using a Palladium-Catalyzed Cross-Coupling (Sonogashira) Protocol. To an oven-dried round-bottom flask equipped with a magnetic stir bar were added the aryl halide, the terminal alkyne, $PdCl_2(PPh_3)_2$ (ca. 2 mol % per aryl halide), and CuI (ca. 4 mol % per aryl halide). A solvent system of TEA, THF, or both was added depending on the substrates. Upon completion, the reaction was quenched with a saturated solution of NH_4Cl. The organic layer was then diluted with hexanes, diethyl ether, or CH_2Cl_2 and washed with water or saturated NH_4Cl (1×). The combined aqueous layers were extracted with hexanes, diethyl ether, or CH_2Cl_2 (2×). The combined organic layers were dried over $MgSO_4$ and filtered, and the solvent was removed from the filtrate in vacuo to afford the crude product, which was purified by column chromatography (silica gel). Eluents and other slight modifications are described below for each compound.

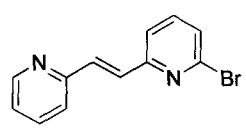

(*E*)-2-bromo-6-(2-(pyridin-2-yl)vinyl)pyridine 2. A solution of LDA was prepared by adding *n*-BuLi (4.39 mL, 12.3 mmol) dropwise to a stirred solution of diisopropylamine (1.76 mL, 12.3 mmol) in THF (51 mL) at -78 °C. The solution was stirred for 30 min, followed by dropwise addition of 2-picoline (0.5 g, 5.6 mmol). The bright orange solution was allowed to stir for 20 min at -55 °C, followed by addition of diethylchlorophosphate (0.810 mL, 5.61 mmol) upon which the solution immediately darkened. The cooling bath was removed for 10 min, and then replaced and the reaction was cooled back to -78 °C. A solution of 6-bromopyridine-2-carboxaldehyde (0.800 g, 4.30 mmol) in THF (10 mL) was then transferred via cannula into the reaction and the mixture was allowed to warm to room temperature overnight. The reaction was quenched by addition of a saturated solution of NH_4Cl (50 mL). The organics were extracted with Et_2O (100 mL), washed with water (3 × 100 mL), dried over $MgSO_4$, and the solvent was removed *in vacuo*. Purification via column chromatography (1:1 EtOAc:hexanes) yielded 680 mg (61%) of analytically pure *trans*-**2** as a white solid. FTIR (drop cast) 3049, 1584, 1564, 1542, 1470, 1436, 1406, 1116, 980 cm^{-1}; ^1H NMR ($CDCl_3$, 400 MHz) δ 8.64 (d, J = 4.0 Hz, 1H), 7.74 (d, J = 15 Hz, 1H), 7.69 (td, J_1 = 1.8 Hz, J_2 = 7.7 Hz, 1H), 7.61 (d, J = 15 Hz, 1H), 7.52 (t, J = 7.6 Hz, 1H), 7.43 (dt, J_1 = 8.0 Hz, J_2 = 1.0 Hz, 1H), 7.35 (td, J_1 = 7.8 Hz, J_2 = 0.8 Hz, 1H), 7.22-7.19 (m, 1H) ; ^{13}C NMR ($CDCl_3$, 100 MHz) δ 156.5, 154.7, 150.0, 142.4, 139.1, 136.9, 133.5, 130.1, 126.9, 123.9, 123.2, 122.2; HRMS *m/z* calcd for $C_{12}H_9BrN_2$ 261.0027, found 261.0031 (M^+).

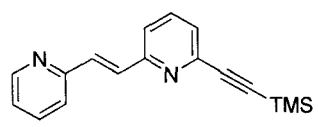

(*E*)-2-(2-(pyridin-2-yl)vinyl)-6-((trimethylsilyl)ethynyl)pyridine 3. See the general procedure for Sonogashira protocol. *Note: The reaction was run in an aluminum foil-wrapped screw-cap tube to discourage cis isomer formation.* The reagents used were **2** (0.261g, 1.00 mmol), TMSA (1.3 mL, 3.00 mmol), $PdCl_2(PPh_3)_2$ (0.007g, 0.001 mmol), CuI (0.015 g, 0.007 mmol), TEA (1.1 mL), and THF (8 mL). The reaction was heated to 65 °C and allowed to stir 1 h. The reaction was quenched via addition of an aqueous saturated solution of NH_4Cl (20 mL). The organics were extracted with CH_2Cl_2 (40 mL), washed with 1×10^{-3} M EDTA (10 mL), dried over $MgSO_4$, and the solvents were removed by rotary evaporation. The material was then purified via elution through a short silica gel plug (1:3 EtOAc:hexanes) to yield 0.275 g (99%) of **3** as an off-white solid. FTIR (drop cast) 2959, 1585, 1564, 1470,1442, 1384, 1250, 1123, 1084 cm^{-1}; ^1H NMR ($CDCl_3$:CD_3CN (1:1), 500 MHz) δ 8.60 (ddd, J_1 = 4.8 Hz, J_2 = 1.8 Hz, J_3 = 0.86 Hz, 1H), 7.74 (ddd, J_1 = 7.7 Hz, J_2 = 7.7 Hz, J_3 = 1.8 Hz, 1H), 7.71 (dd, J_1 = 7.8 Hz, J_2 = 7.8 Hz, 1H), 7.68 and 7.65 AB quartet (J = 15.8 Hz), 7.51(ddd, J_1 = 7.8 Hz, J_2 = 1.0 Hz, J_3 = 1.0 Hz, 1H), 7.47 (dd, J_1 = 7.9 Hz, J_2 = 0.97 Hz, 1H), 7.37 (dt, J_1 = 7.7 Hz, J_2 = 0.99 Hz, 1H), 7.36 (dd, J_1 = 7.7 Hz, J_2 = 0.99 Hz, 1H), 7.24 (ddd, J_1 = 7.5 Hz, J_2 = 4.8 Hz, J_3 = 1.1 Hz, 1H), 0.290 (s, 9H) ; ^{13}C NMR ($CDCl_3$:CD_3CN (1:1), 125 MHz) δ 155.8, 155.1, 150.2, 143.2, 137.6, 137.3, 133.0, 131.5, 123.8, 123.5, 123.1, 126.9, 104.5, 94.6, -0.232; HRMS *m/z* calcd for $C_{17}H_{18}N_2Si$ 278.1239, found 278.1240 (M^+).

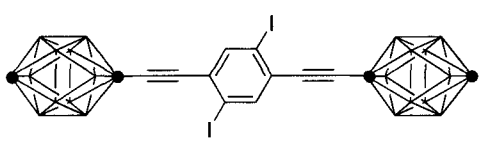

Compound 5. To a 100 mL round bottom flask was added **4** (1.00 g, 1.91 mmol), $AgNO_3$ (0.100 g, 0.573 mmol), NBS (0.714 g, 4.01 mmol) and acetone (50 mL). The reaction was allowed to stir for 2 h in the dark (covered with aluminum foil), and then poured into H_2O (100 mL). The resulting white precipitate was filtered and dried by rotary evaporation. *Note: The alkynyl bromide decomposes over time to a yellow solid, releasing HBr. Care should be taken when handling the compound.* Then, to a flame-dried 50 mL 3-neck flask with stir bar was added p-carborane (0.302 g, 2.10 mmol) and freshly distilled THF (15 mL) under nitrogen. The reaction was then cooled to -78 °C, upon which *n*-BuLi (0.880 mL, 2.20 mmol) was added dropwise to yield a thick milky solution. The cooling bath was then removed and the reaction was allowed to stir for 30 min upon which the solution became transparent. The cooling bath was then replaced, and the reaction again cooled to -78 °C. CuBr (0.395 g, 2.75 mmol) was added, and the reaction was again allowed to stir for 30 min at room temperature until the solution was dark green/brown in color. The alkynyl bromide (0.535 g, 1.00 mmol) was then added all at once, and the reaction was allowed to stir overnight. The reaction was quenched by addition of two drops of H_2O, then poured through a short silica gel plug and eluted with hexanes. Removal of solvent by rotary evaporation and purification via column chromatography (100 % hexanes) yielded 0.440 g (61%, 2 steps) of **5** as a white solid. FTIR (drop cast) 2613, 1463, 1384, 1123, 1084, 1064, 1047 cm^{-1}; ^1H NMR ($CDCl_3$, 400 MHz) δ 7.63 (s, 2H), 3.34-1.47 (br m, 22H); ^{13}C NMR ($CDCl_3$, 100 MHz) δ 141.7, 129.9, 99.6, 91.8, 79.2, 68.9, 61.0; HRMS *m/z* calcd for $C_{14}H_{24}B_{20}I_2$ 663.1949, found 663.1944 (M^+).

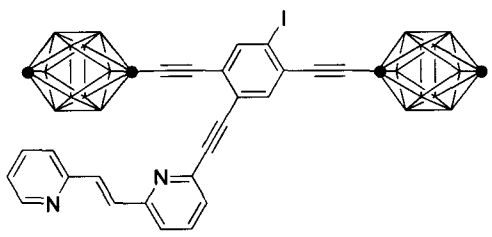

Compound 6. In a 100 mL round bottom flask, compound **3** (0.275 g, 0.99 mmol) was dissolved in CH_2Cl_2 (50 mL) and MeOH (20 mL). K_2CO_3 (0.500 g, 3.8 mmol) was added, and the reaction was allowed to stir 3 h, after which H_2O (100 mL) was added and the organics separated. After drying over $MgSO_4$, the solvent was removed by rotary evaporation to yield the intermediate alkyne, which was immediately subjected to the general Sonogashira protocol. *Note: The reaction was run in an aluminum foil-wrapped sealed tube to discourage cis isomer formation.* The reagents used were the deprotected alkyne (0.031g, 0.178 mmol), **5** (0.160 g, 0.298 mmol), $PdCl_2(PPh_3)_2$ (0.007g, 0.012 mmol), CuI (0.008 g, 0.023 mmol), TEA (0.335 mL), and THF (3.50 mL). The reaction was heated to 65 °C and allowed to stir overnight. The reaction was quenched via addition of an aqueous saturated solution of NH_4Cl (20 mL). The organics were extracted with CH_2Cl_2 (40 mL), washed with 1×10^{-3} M EDTA (10 mL), dried over $MgSO_4$, and the solvents were removed by rotary evaporation. The molecule was then purified via column chromatography (1:4 EtOAc:hexanes) to yield 0.032 g (24%, 2 steps) of **6** as an off-white solid. FTIR (drop cast) 3060, 2923, 2613, 1584, 1574, 1543, 1434, 1406, 1384, 1147, 1119 cm^{-1}; ^1H NMR ($CDCl_3$, 400 MHz) δ 8.64 (d, J = 4.0 Hz, 1H), 7.86 – 7.71 (m, 5 H), 7.55 – 7.36 (m, 4 H), 7.23 – 7.20 (m, 2 H), 3.30-1.57 (br, 22H); ^{13}C NMR ($CDCl_3$, 100 MHz) δ 171.2, 161.2, 155.6, 155.1, 155.0, 149.9, 149.0, 142.6, 141. 8, 137.5, 137.2, 136.8, 136.77, 136.71, 136.67, 135.6, 133.1, 132.0, 131.6, 131.3, 131.0, 129.8, 129.1, 128.6, 126.4, 125.3, 123.6, 123.3, 122.8, 122.76,

122.2, 120.9, 101.2, 100.3, 92.6,92.5, 91.9, 81.7, 91.1, 80.8, 76.0, 69.0, 64.4, 60.8, 60.6, 53.5, 36.7, 29.7, 24.7, 23.4, 21.1, 14.2, 8.0; HRMS *m/z* calcd for $C_{28}H_{33}B_{20}IN_2$ 742.3759, found 742.3759 (M^+).

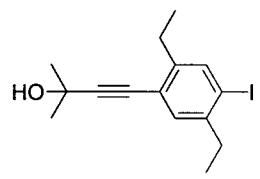

4-(2,5-diethyl-4-iodophenyl)-2-methylbut-3-yn-2-ol 8. See the general procedure for Sonogashira protocol. The reagents used were 2,5-diethyl-1,4-diiodobenzene **7** (2.50g, 6.48 mmol), 2-methyl-3-butyne-2-ol (0.400 mL, 3.89 mmol), $PdCl_2(PPh_3)_2$ (0.181g, 0.257 mmol), CuI (0.098 g, 0.514 mmol), TEA (7.3 mL), and THF (92 mL). The reaction was allowed to stir overnight and quenched via addition of an aqueous saturated solution of NH_4Cl (100 mL). The organics were extracted with CH_2Cl_2 (100 mL), dried over $MgSO_4$, and the solvents were removed by rotary evaporation. The material was then purified via column chromatography (3:7 EtOAc:hexanes) to yield 1.03 g (77%) of **8** as light-yellow oil. FTIR (KBr) 3350, 2967, 2930, 2870, 1477, 1456, 1380, 1264, 1206, 1164, 1061, 997, 962, 930, 890, 874 cm^{-1}; ^1H NMR ($CDCl_3$, 400 MHz) δ 7.64 (s, 1H), 7.21 (s, 1H), 2.66 (m, 4H), 1.63 (s, 6H), 1.19 (m, 6H); ^{13}C NMR ($CDCl_3$, 100 MHz) δ 145.5, 144.0, 138.9, 131.8, 122.3, 101.0, 98.3, 80.5, 66.0, 33.7, 31.7, 27.0, 14.7, 14.6; HRMS *m/z* calcd for $C_{15}H_{19}IO$ 342.0481, found 342.0471 (M^+).

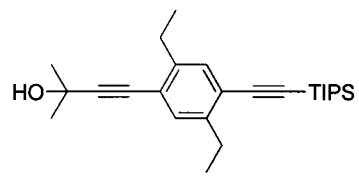

4-(2,5-diethyl-4-((triisopropylsilyl)ethynyl)phenyl)-2-methylbut-3-yn-2-ol 9. See the general procedure for Sonogashira protocol. The reagents used were **8** (1.03 g, 3.01 mmol), TIPSA (0.742 mL, 3.3 mmol), $PdCl_2(PPh_3)_2$ (0.019g, 0.027 mmol), CuI (0.010 g, 0.053 mmol), TEA (3.4 mL), and THF (43 mL). The reaction was allowed to stir overnight and quenched via addition of an aqueous saturated solution of NH_4Cl (100 mL). The organics were extracted with CH_2Cl_2 (100 mL), dried over $MgSO_4$, and the solvents were removed by rotary evaporation. The material was then purified via a short silica gel plug (1:1 EtOAc:Hexanes) to yield 0.910 g (82%) of **9** as light-red oil. FTIR (KBr) 3337, 2962, 2941, 2891, 2865, 2146, 1490, 1460, 1463, 1222, 1163, 896, 883 cm^{-1}; ^1H NMR ($CDCl_3$, 400 MHz) δ 7.27 (s, 1H), 7.22 (s, 1H), 2.73 (m, 4H), 2.07 (s, 1H), 1.63 (s, 6H), 1.22 (m, 6H), 1.13 (s, 21H); ^{13}C NMR ($CDCl_3$, 100 MHz) δ 144.0, 143.5, 132.3, 131.8, 122.9, 122.0, 105.5, 98.5, 95.5, 81.0, 65.9, 31.7, 27.5, 27.3, 18.9, 15.1, 14.8, 11.5; HRMS *m/z* calcd for $C_{26}H_{40}OSi$ 396.2848, found 396.2853 (M^+).

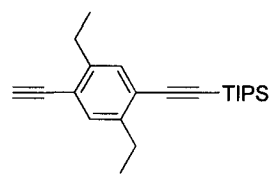

((2,5-diethyl-4-ethynylphenyl)ethynyl)triisopropylsilane 10. To a 100 mL round bottom flask with stir bar was added **9** (0.397 g, 1.00 mmol), NaOH (0.160 g, 4.00 mmol) and dry toluene (30 mL). The reaction was then fitted with a reflux condenser and heated at reflux overnight under nitrogen. H_2O (40 mL) was added, followed by CH_2Cl_2 (50 mL). The organics were separated, dried over $MgSO_4$, and the solvent removed by rotary evaporation. The resulting oil was purified via a short silica gel plug (100 % hexanes) to yield 0.212 g (75%) of **10** as a dark red oil. FTIR (KBr) 2961, 2941, 2890,

2865, 2147, 1488, 1462, 1062, 995, 882 cm^{-1}; ^1H NMR ($CDCl_3$, 400 MHz) δ 7.32 (s, 1H), 7.31 (s, 1H), 3.30 (s, 1H), 2.77 (quintet, J = 7.6 Hz, 4H), 1.25 (t, J = 7.6 Hz, 6H), 1.16 (s, 21H); ^{13}C NMR ($CDCl_3$, 100 MHz) δ 143.9, 143.8, 132.3, 132.1, 123.3, 121.3, 105.2, 95.6, 82.3, 81.5, 76.7, 27.3, 27.0, 18.7, 14.9, 14.8, 11.4; HRMS *m/z* calcd for $C_{23}H_{34}Si$ 338.2430, found 338.2428 (M^+).

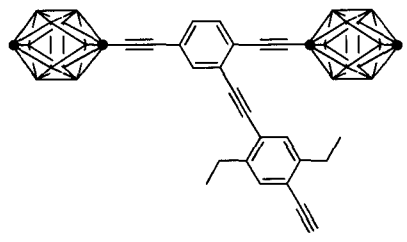

Compound 12. See the general procedure for Sonogashira protocol. The reagents used were **11** (0.090 g, 0.167 mmol), **10** (0.056 g, 0.167 mmol), $PdCl_2(PPh_3)_2$ (0.010g, 0.014 mmol), CuI (0.010 g, 0.053 mmol), TEA (4 mL), and THF (8 mL). The reaction was allowed to stir overnight and quenched via addition of an aqueous saturated solution of NH_4Cl (10 mL). The organics were extracted with CH_2Cl_2 (30 mL), washed with 1×10^{-3} M EDTA, dried over $MgSO_4$, and the solvents removed *in vacuo*. The resulting solid was run through a short silica gel plug, yielding a white solid. The solid was then dissolved in 10 mL CH_2Cl_2, and TBAF (2 mL) was added. The mixture was stirred for 20 min, followed by addition of silica gel. The solvent was removed from the resulting slurry, and the silica gel-product mixture loaded on to a dry-packed silica gel column (100 % hexanes), yielding 0.077 g (78%) of **12** as a white solid. FTIR (KBr) 2609, 1493, 1061, 888, 825 cm^{-1}; ^1H NMR ($CDCl_3$, 400 MHz) δ 7.42 (d, 1H), 7.38 (d, J = 1.0 Hz, 1H), 7.37 (s, 1H), 7.23 (d, J = 8.0 Hz, 1H), 7.14 (dd, J_1 = 8.0 Hz, J_2 = 1 Hz, 1H), 3.34 (s, 1H), 3.30-1.57 (br, 22H) 1.30 (m, 9H); ^{13}C NMR ($CDCl_3$, 100 MHz) δ 144.3, 143.6, 135.2,

132.6, 132.4, 131.2, 126.7, 124.0, 122.6, 122.2, 122.1, 93.2, 91.1, 82.5, 82.0, 60.6, 53.7, 27.2, 15.0, 14.9; HRMS *m/z* calcd for $C_{28}H_{38}B_{20}$ 591.4965, found 591.4977 (M^+).

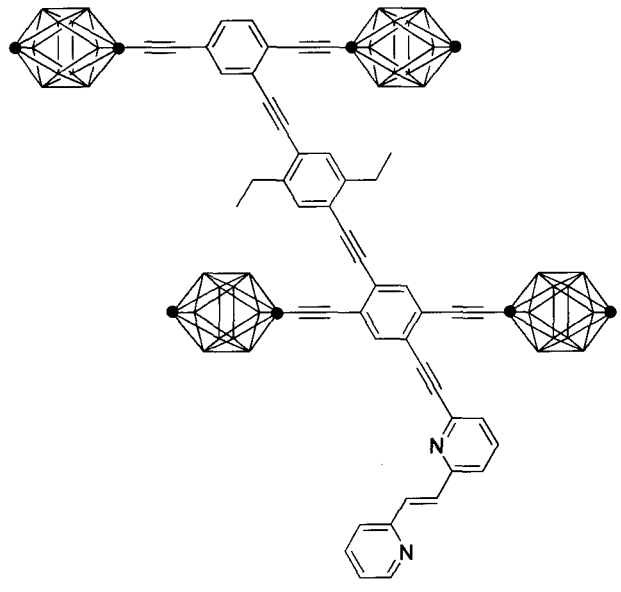

Backhoe 1. See the general procedure for Sonogashira protocol. *Note: The reaction was run in an aluminum foil-wrapped screw-cap tube to discourage cis isomer formation.* The reagents used were **14** (0.011 g, 0.018 mmol), **8** (0.013 g, 0.018 mmol), $PdCl_2(PPh_3)_2$ (0.010g, 0.014 mmol), CuI (0.010 g, 0.053 mmol), TEA (4 mL), and THF (8 mL). The reaction was allowed to stir overnight at 60 °C in a sealed tube and quenched via addition of an aqueous saturated solution of NH_4Cl (10 mL). The organics were extracted with CH_2Cl_2 (30 mL), washed with 1×10^{-3} M EDTA, dried over $MgSO_4$, and the solvents removed by rotary evaporation. The resulting solid was purified via column chromatography (1:4 EtOAc:hexanes) to yield 0.013 g (61%) of **1** as a fluorescent green solid. FTIR (drop cast) 2925, 2853, 2614, 2365, 1455, 1384, 1062 cm^{-1}; ^1H NMR ($CDCl_3$, 400 MHz) δ 8.67 (d, J = 4.0 Hz, 1H), 7.86 (d, J = 15 Hz, 1H), 7.79 – 7.71 (m, 3H), 7.61 (s, 1H), 7.55 – 7.42 (m, 7H), 7.25 - 7.21 (m, 2H), 7.17 (dd, J_1 = 15 Hz, J_2 = 4 Hz, 1H),

3.3 – 1.5 (br, 48 H, includes four benzylic protons), 1.40 (t, J = 8Hz, 6H); ^{13}C NMR ($CDCl_3$, 100 MHz) δ 155.6, 154.9, 149.7, 143.7, 143.6, 142.7, 136.8, 136.4, 135.3, 135.0, 132.8, 132.4, 132.1,132.0, 131.1, 131.0, 126.5, 126.4, 126.3, 124.8, 124.4, 123.9, 123.6, 123.0, 122.9, 122.7, 122.2, 95.1, 94.8, 93.2, 91.6, 91.4, 91.3, 91.1, 87.9, 85.4, 69.1, 60.6, 60.4, 29.7, 27.1, 14.8; DI *m/z* calcd for $C_{56}H_{70}B_{40}N_2$ 1205, found 1205 (M^+).

References and Notes

(1) (a) Balzani, V; Credi, A; Venturi, M *Molecular Devices and Machines: A Journey into the Nano World*; Wiley-VCH: Weinheim, Germany, 2003. (b) Ozin, G.; Manners, I.; Fournier-Bidoz, S.; Arsenault, A. *Adv. Mater.* **2005**, *17*, 3011-3018. (c) Balzani, V. *Small* **2005**, *1*, 278-283.

(2) Balzani, V; Credi, A; Raymo, F. M.; Stoddart, J. F. *Angew. Chem., Int. Ed.* **2000**, *39,* 3348-3391

(3) (a) Shirai, Y.; Osgood, A. J.; Zhao, Y.; Kelly, K. F.; Tour, J. M. *Nano Lett.* **2005**, *5*, 2330-2334. (b) Shirai, Y.; Osgood, A. J.; Zhao, Y.; Yao, Y.; Saudan, L.; Yang, H.; Yu-Hung, C.; Sasaki, T.; Morin, J.-F.; Guerrero, J. M.; Kelly, K. F.; Tour, J. T. *J. Am. Chem. Soc.* **2006**, *128*, 4854-4864. (c) Shirai, Y.; Morin, J.-F.; Sasaki, T.; Guerrero, J. M.; Tour, J. M. *Chem. Soc. Rev.* **2006**, *35*, 1043-1055.

(4) (a) Morin, J.-F.; Shirai, Y.; Tour, J. M. *Org. Lett.* **2006**, *8*, 1713-1716. (b) Sasaki, T.; Tour, J. M. *Tetrahedron Lett.* **2007**, *48*, 5821-5824. (c) Sasaki, T.; Morin, J.-F.; Lu, M.; Tour, J. M. *Tetrahedron Lett.* **2007**, *48*, 5817-5820. (d) Morin, J.-F.; Sasaki, T.; Shirai,

Y.; Guerrero, J. M.; Tour, J. M. *J. Org. Chem.* **2007**, *72*, 9481-9490. (e) Sasaki, T.; Tour, J. M. *Org. Lett.* **2008,** *10*, 897-900.

(5). (a) Kelly, T. R.; De Silva, H.; Silva, R. A. *Nature* **1999**, *401*, 150-152. (b) Koumura, N.; Geertsma, E. M.; Meetsma, A.; Feringa, B. L. *J. Am. Chem. Soc.* **2000**, *122*, 12005-12006. (c) Feringa, B. L. *Nature* **2005**, *437*, 1337-1340. (d) Klok, M.; Boyle, N.; Pryce, M. T.; Meetsma, A.; Browne, W. R.; Feringa, B. L. *J. Am. Chem. Soc.* **2008**, *130*, 10484-10485.

(6) (a) Saha, S.; Johansson, E.; Flood, A. H.; Tseng, H.-R.; Zink, J. I.; Stoddart, J. F. *Chem. Eur. J.* **2005**, *11*, 6846-6958. (b) Saha, S.; Stoddart, J. F. *Chem. Soc. Rev.* **2007**, *36*, 77-92. (c) Credi, A.; Venturi, M. *Cent. Eur. J. Chem.* **2008**, *6*, 325-329.

(7) (a) Hagen, S.; Leyssner, F.; Nandi, D.; Wolf, M.; Tegeder, P. *Chem. Phys. Lett.* **2007**, *444*, 85-90. (b) Schmidt, P. M. ; Horn, K.; Dil, J. H.; Kampen, T. U. *Surf. Sci.* **2007**, *601*, 1775-1780. (c) Sasaki, T.; Tour, J. M. *Org. Lett.* **2008**, *10*, 897-900. (d) Alemani, M.; Selvanathan, S.; Ample, F.; Peters, M. V.; Rieder, K.–H.; Moresco, F.; Joachim, C.; Hecht, S.; Grill, L. *J. Phys. Chem. C* **2008**, *112*, 10509-10514.

(8) (a) Brierley, M.; Geary, W. J. *J. Chem Soc. A* **1968**, *9*, 2130-2133. (b) Lee, Y. J.; Whitten, D. G.; Pedersen, L. *J. Am. Chem. Soc.* **1971**, *93*, 6330-6332. (c) Whitten, D. G.; Lee, Y. J. *J. Am. Chem. Soc.* **1972**, *94*, 9142-9148. (d) Vansant, J.; Smets, G. *J. Org. Chem.* **1980**, *45*, 1557-1565.

(9). (a) Bayer, E.; Witte, E. G. *J. Coord. Chem.* **1977**, *7*, 13-22. (b) Willner, I.; Marx-Tibbon, S.; Cohen, S.; Eichen, Y.; Kaftori, M. *J. Phys. Org. Chem.* **1997**, *10*, 435-444. (c) Yam, V. W.-W.; Yang, Y.; Zhang, J.; Chu, B. W.-K. ; Zhu, N. *Organometallics* **2001**, *20*,

4911-4918. (d) Cooper, C. G. F.; MacDonald, J. C.; Soto, E.; McGimpsey, W. G. *J. Am. Chem. Soc.* **2004**, *126*, 1032-1033.

(10) The molecules were modeled using SPARTAN X at the semi-empirical level, and a perspective model was made using the forecite modeling option in MS Modeling 4.0.

(11) Kawano, T. ; Kato, T. ; Du, C.-X. ; Ueda, I. *Tetrahedron Lett.* **2002**, *43*, 6697-6700.

(12) Kim, S.; Kim, S.; Lee, T.; Ko, H.; Kim, D. *Org. Lett.* **2004**, *6*, 3601-3604.

(13) Kosynkin, D.; Tour, J. M. *Org. Lett.* **2001**, *3*, 993-995.

(14) The harsh conditions needed for removal of the carbinol protecting group can often remove trimethylsilyl protecting groups as well.

(15) Pourjavadi, A.; Marandi, G. B. *J. Chem. Res., Synop.* **2002**, *11*, 552-555.

(16) Kubas, G. J. *Inorg. Synth.* **1990**, *28*, 68-70.

Supporting Information for Chapter 1.1

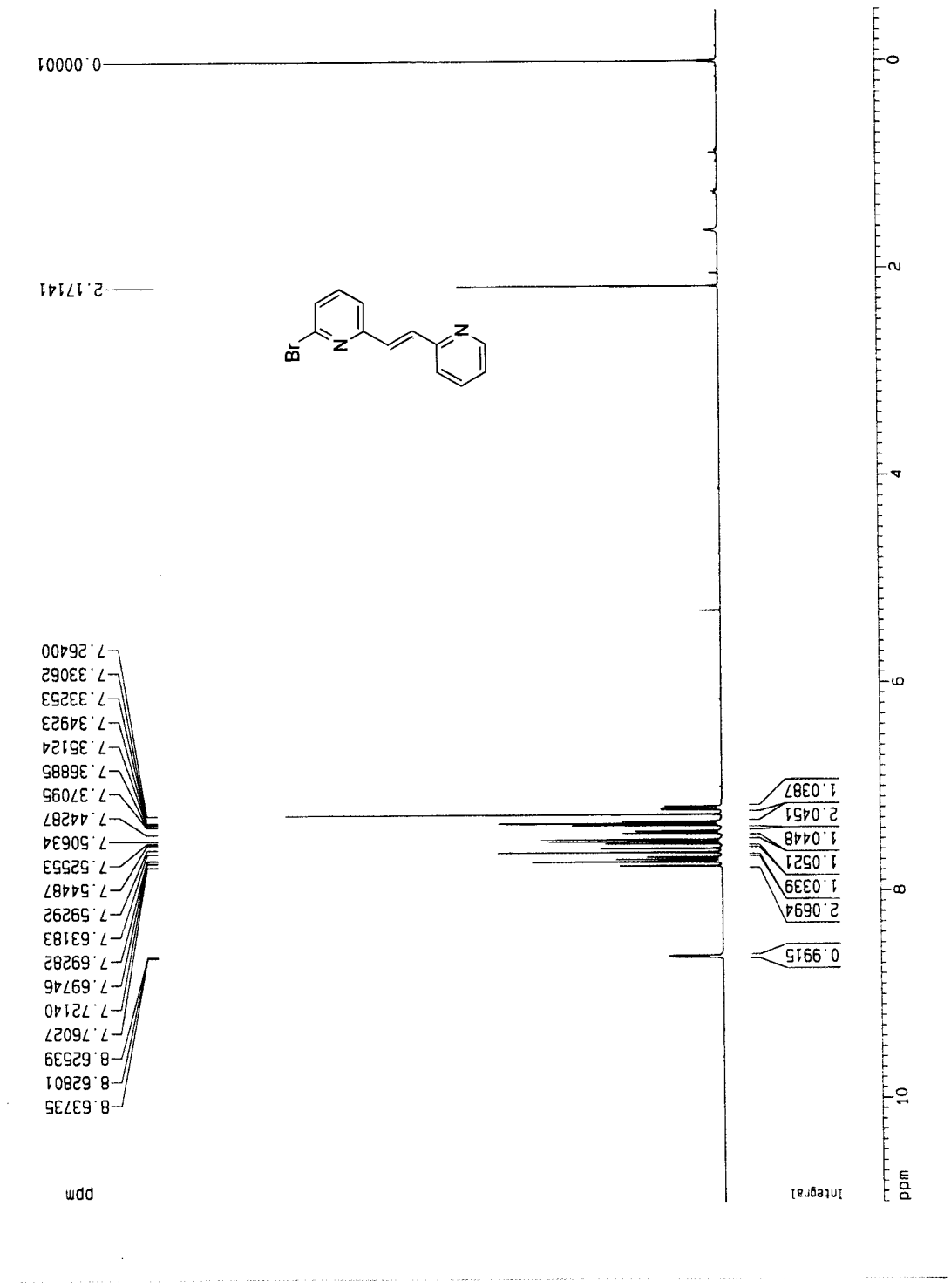

Figure S-1.1-1. ^{1}H NMR Spectrum of Compound **2**.

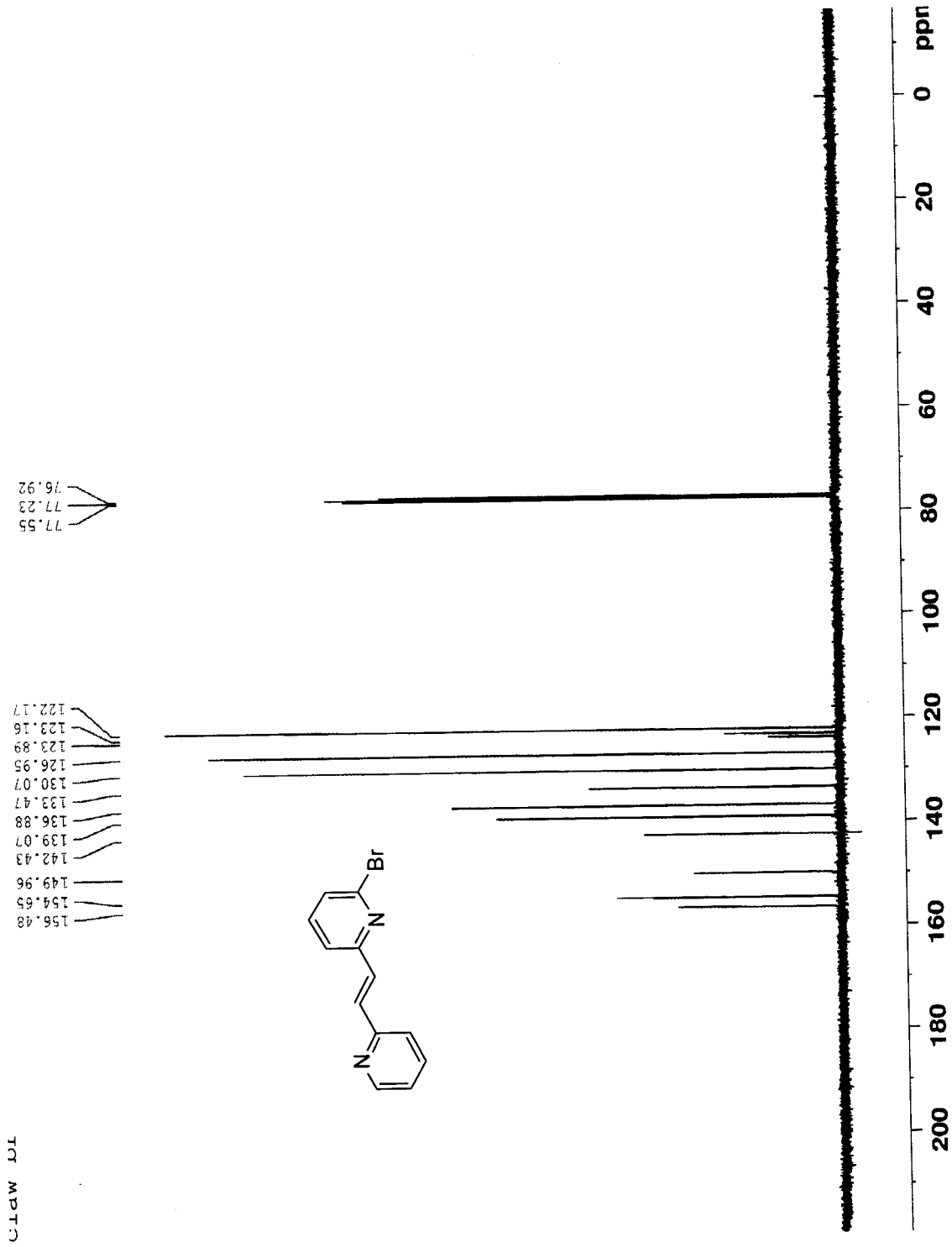

Figure S-1.1-2. ^{13}C NMR Spectrum of Compound **2**.

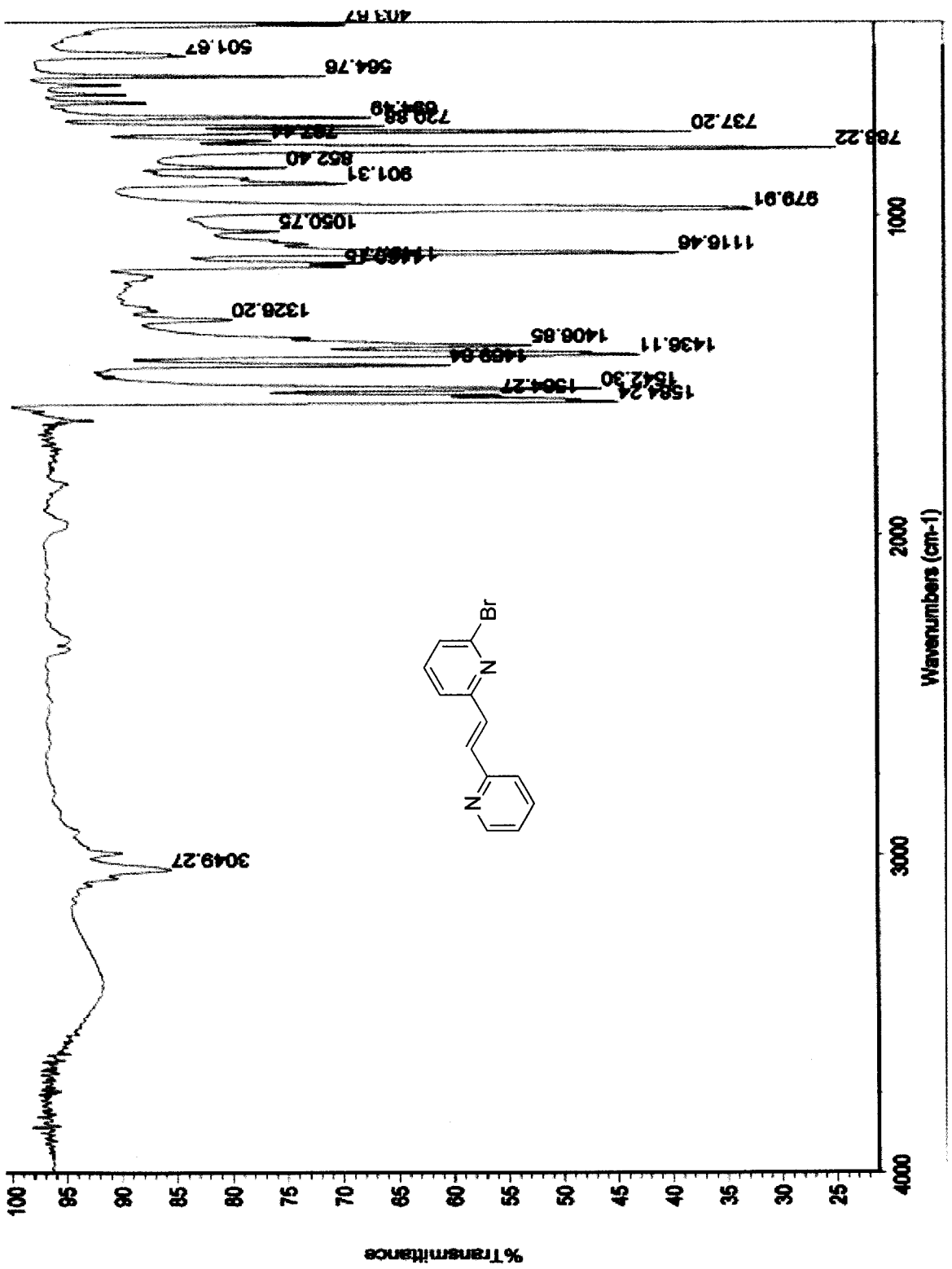

Figure S-1.1-3. IR Spectrum of Compound **2**.

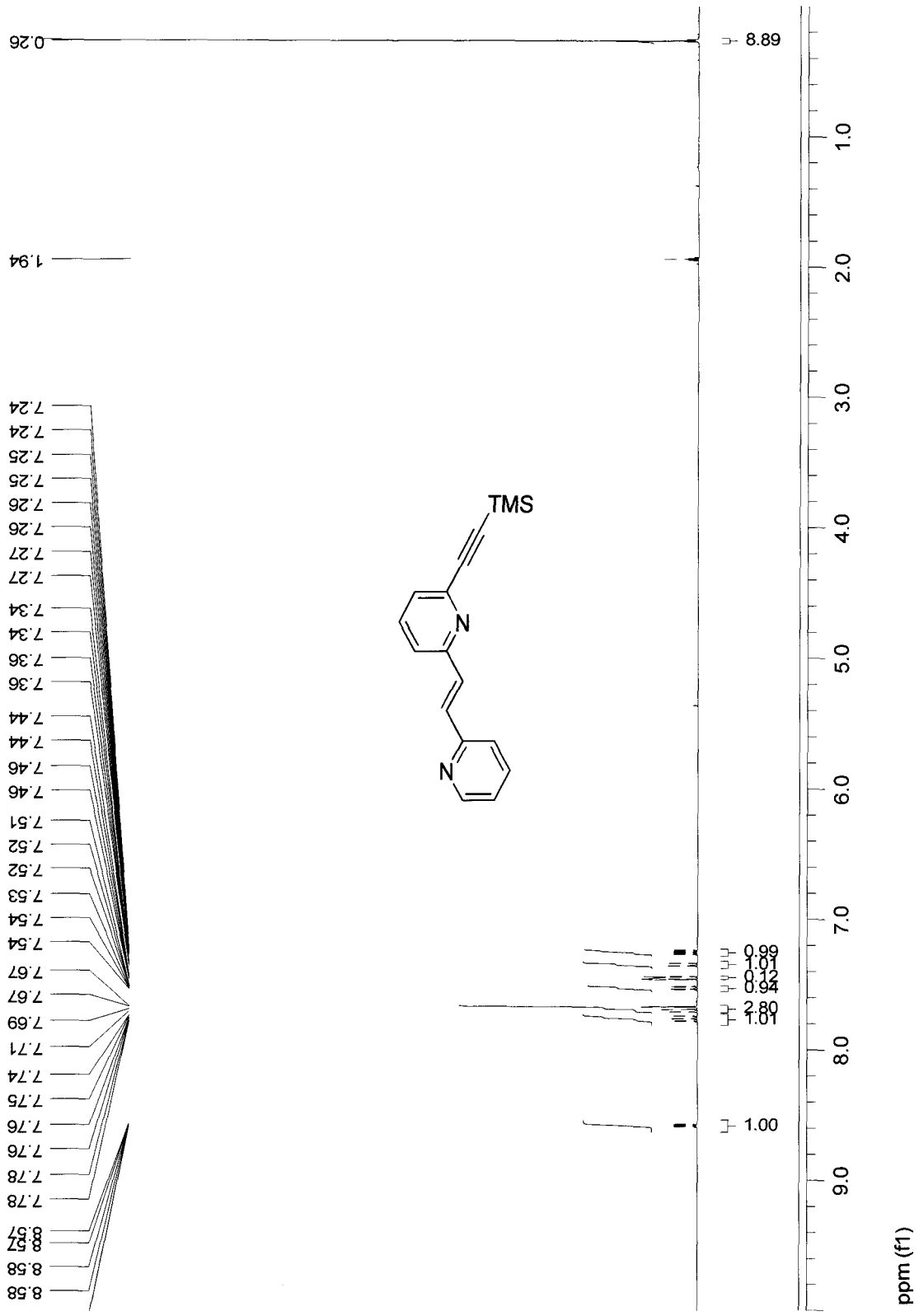

Figure S-1.1-4. ^{1}H NMR Spectrum of Compound **3**.

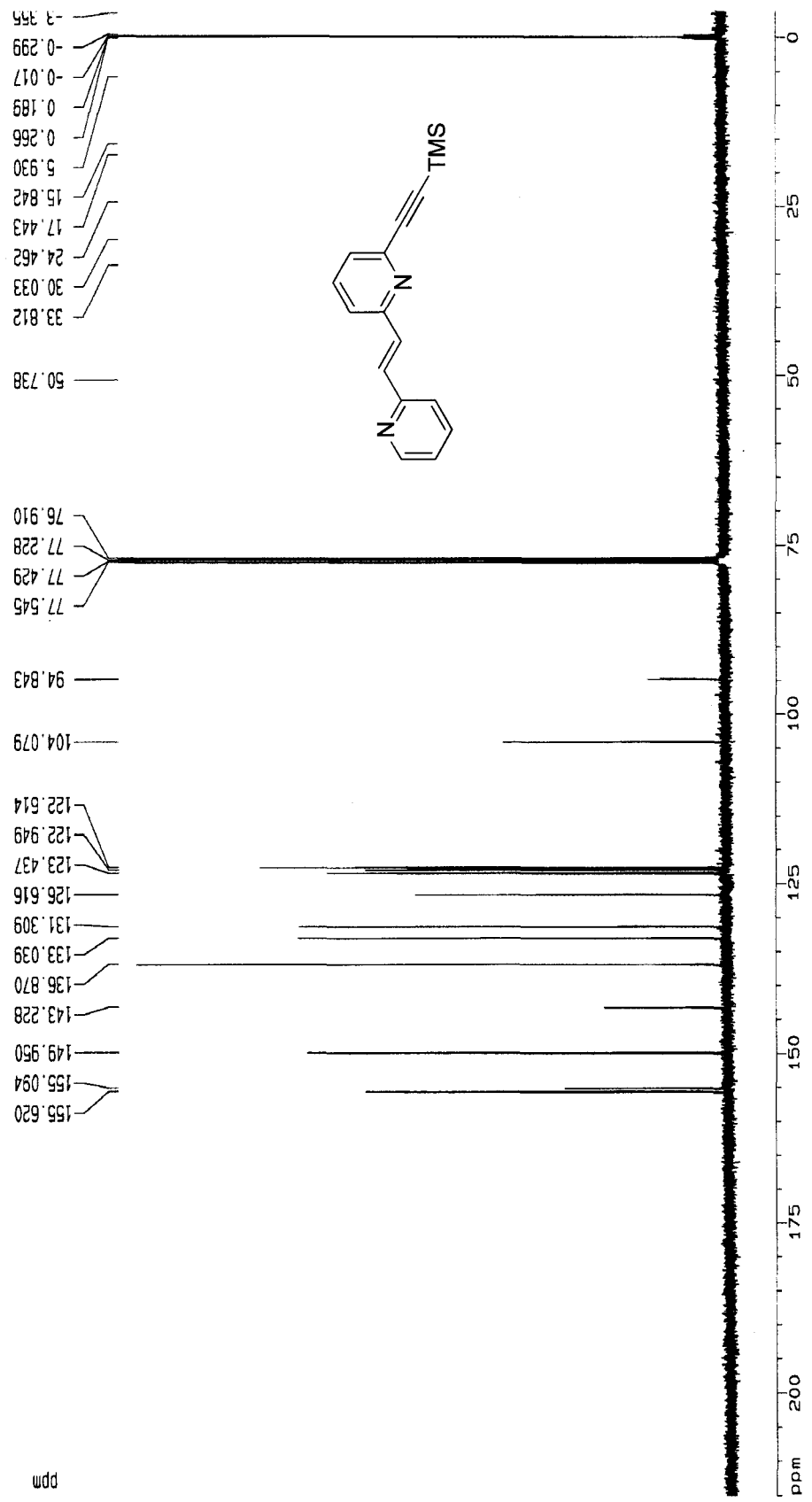

Figure S-1.1-5. ^{13}C NMR Spectrum of Compound **3**.

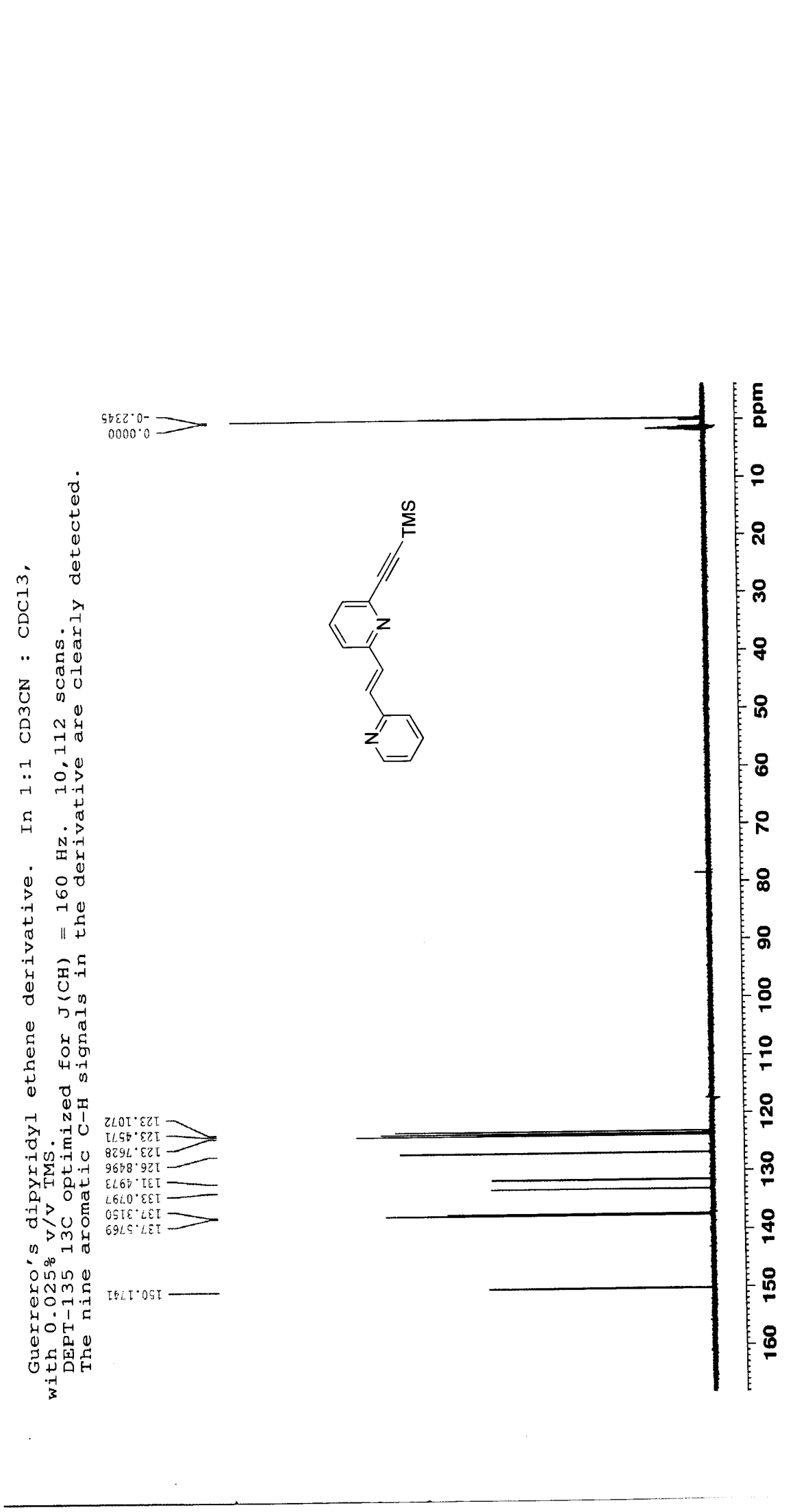

Figure S-1.1-6. ^{13}C DEPT-135 NMR Spectrum of Compound **3**.

Guerrero's dipyridyl ethene derivative. In 1:1 CD3CN : CDCl3, with 0.025% v/v TMS.
COSY. 1024 increments, 4 scans/increment.
Set of 4 coupled spins in aromatic ring: 8.603, 7.744, 7.512, and 7.242 ppm.
Set of 3 coupled spins in the other aromatic ring: 7.714, 7.472, and 7.366 ppm.
Pair of coupled spins: the ethene AB quartet with peaks at 7.704, 7.673, 7.662, and 7.630 ppm.
1D proton spectrum shown above and to the left.

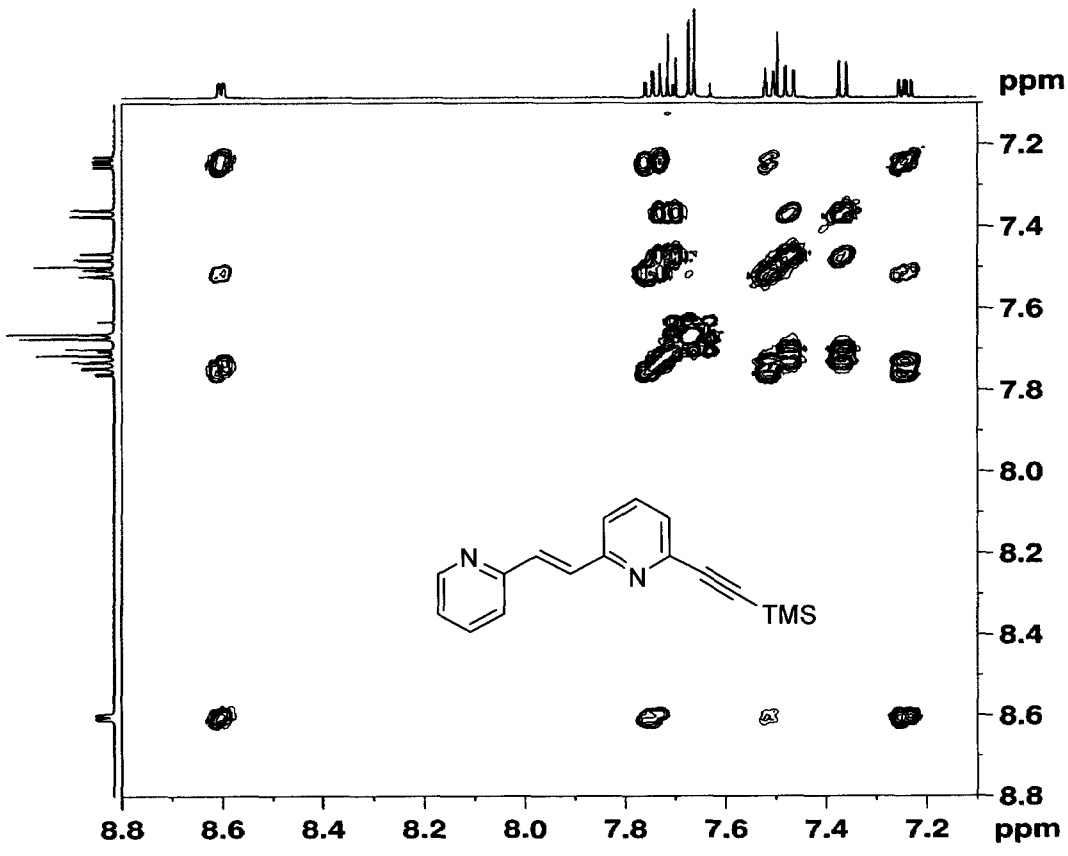

Figure S-1.1-7. ^{1}H-^{1}H COSY NMR Spectrum of Compound **3**.

Guerrero's dipyridyl ethene derivative. In 1:1 CDCl3 : CD3CN with 0.025% v/v TMS.
1H-13C HMBC. 2048 increments (for digital resolution = 0.08 ppm in the 13C dimension in order to resolve long-range correlations). 48 scans/increment. Optimized for 1J(CH) = 140 Hz and

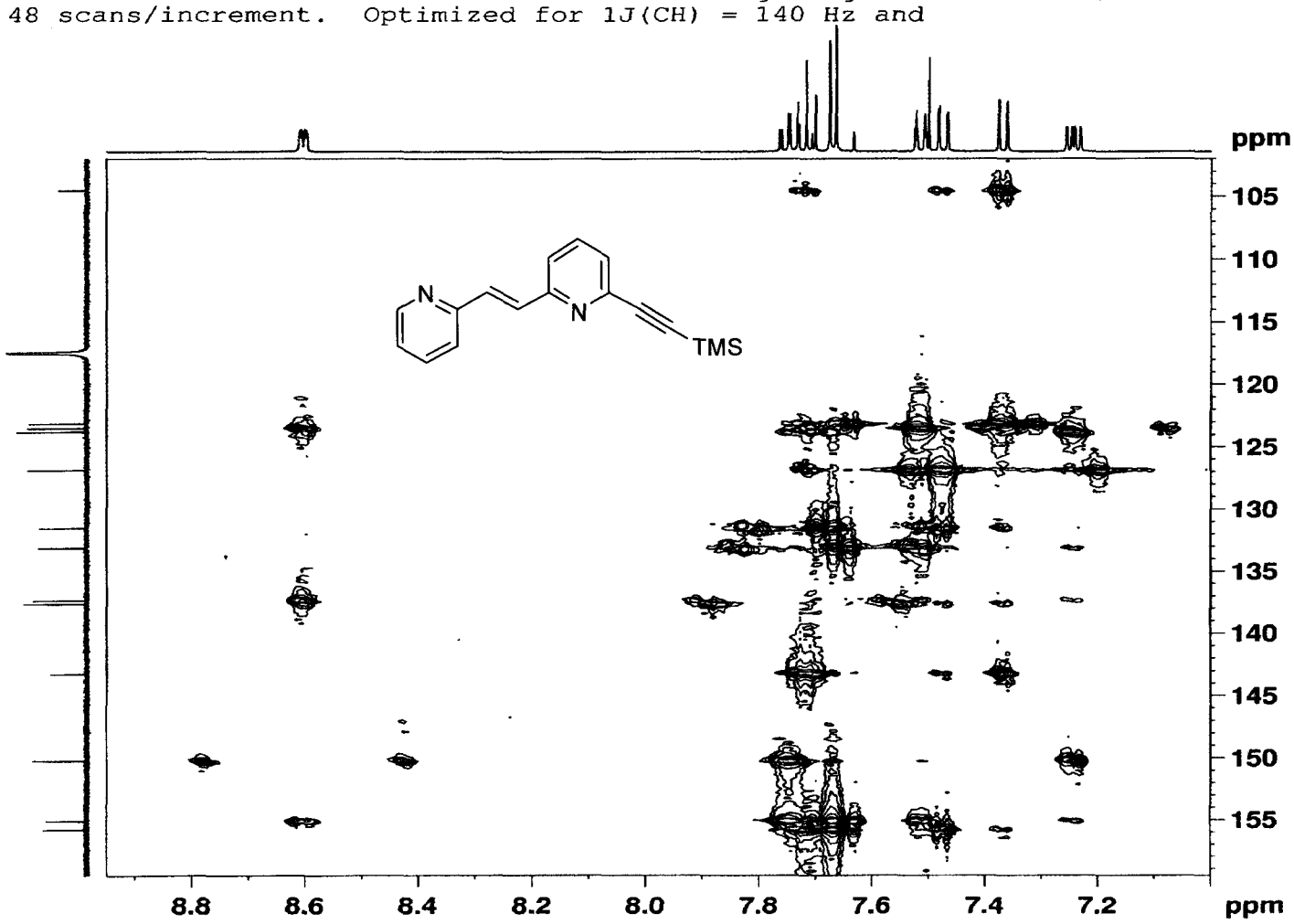

Figure S-1.1-8. ^{1}H-^{13}C HMBC NMR Spectrum of Compound **3**.

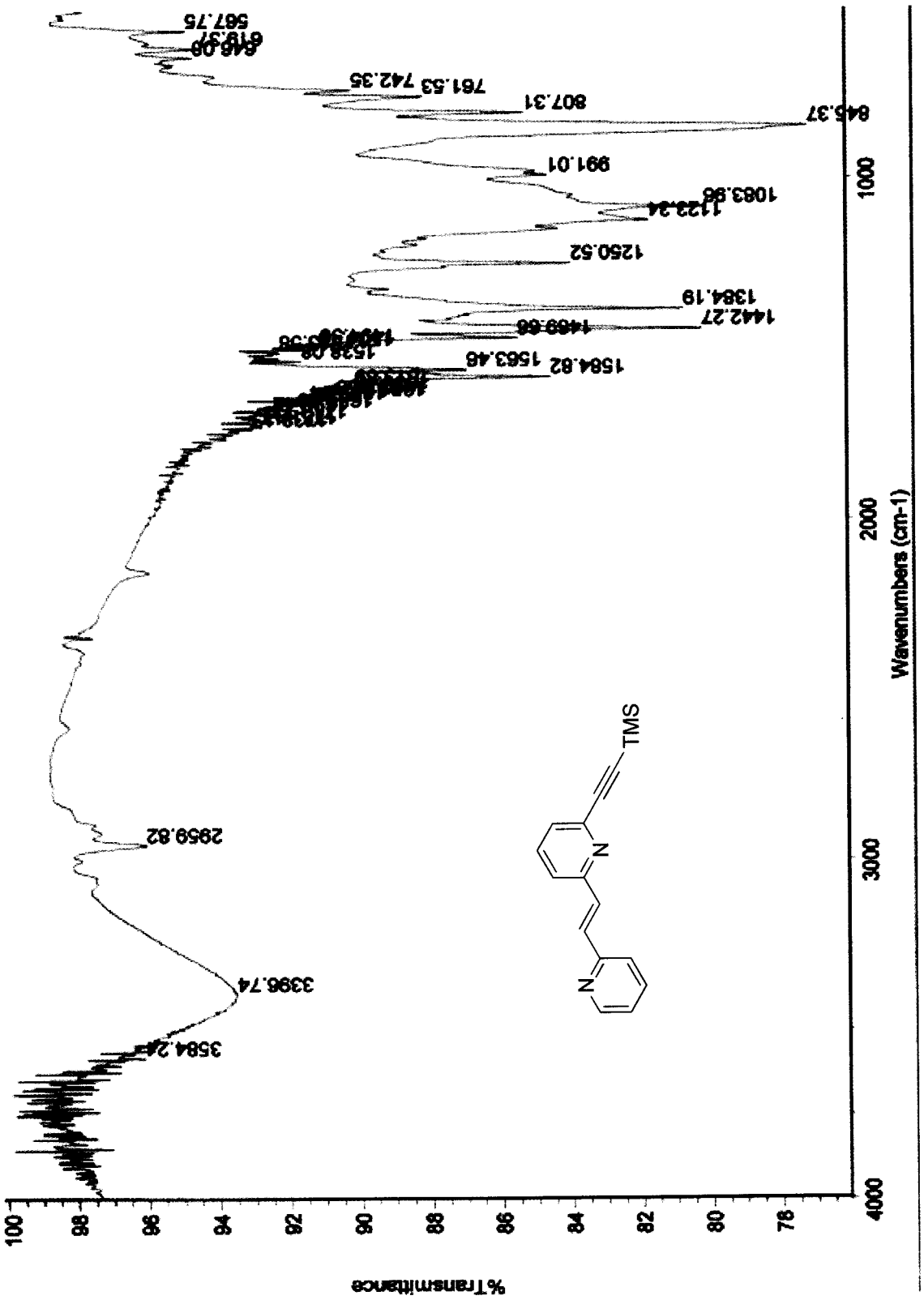

Figure S-1.1-9. IR Spectrum of Compound **3**.

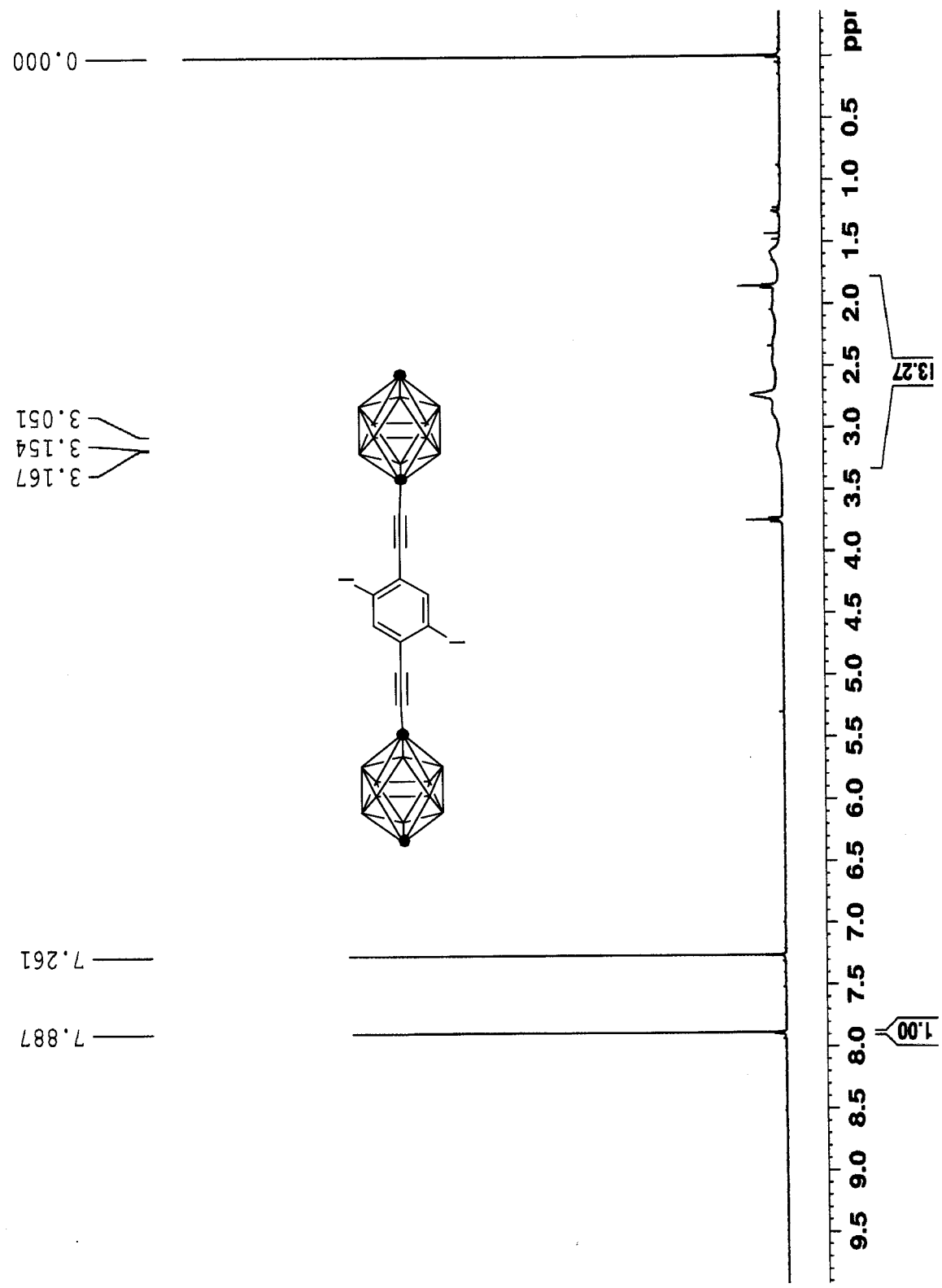

Figure S-1.1-10. ^{1}H NMR Spectrum of Compound **5**.

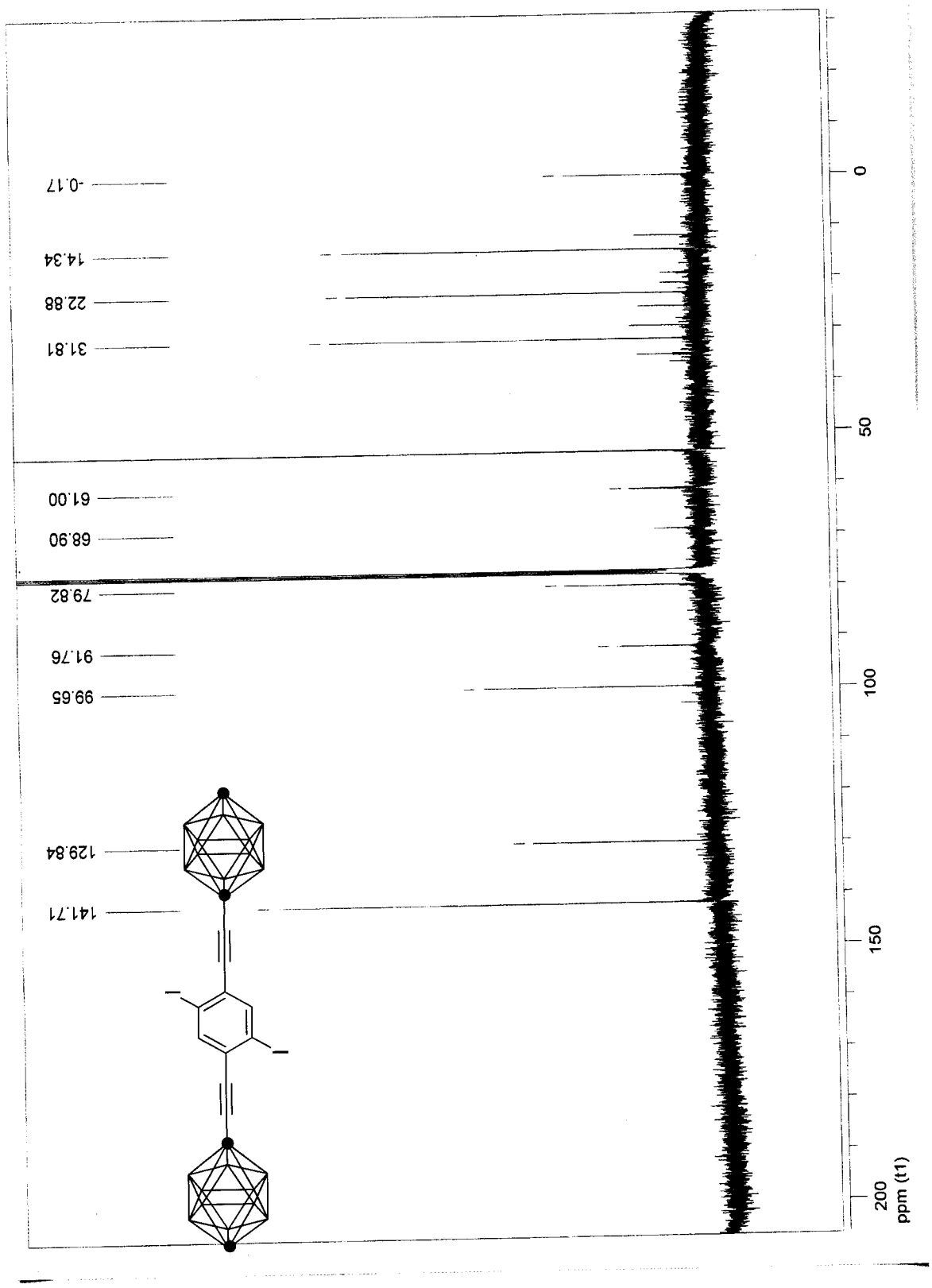

Figure S-1.1-11. ^{13}C NMR Spectrum of Compound **5**.

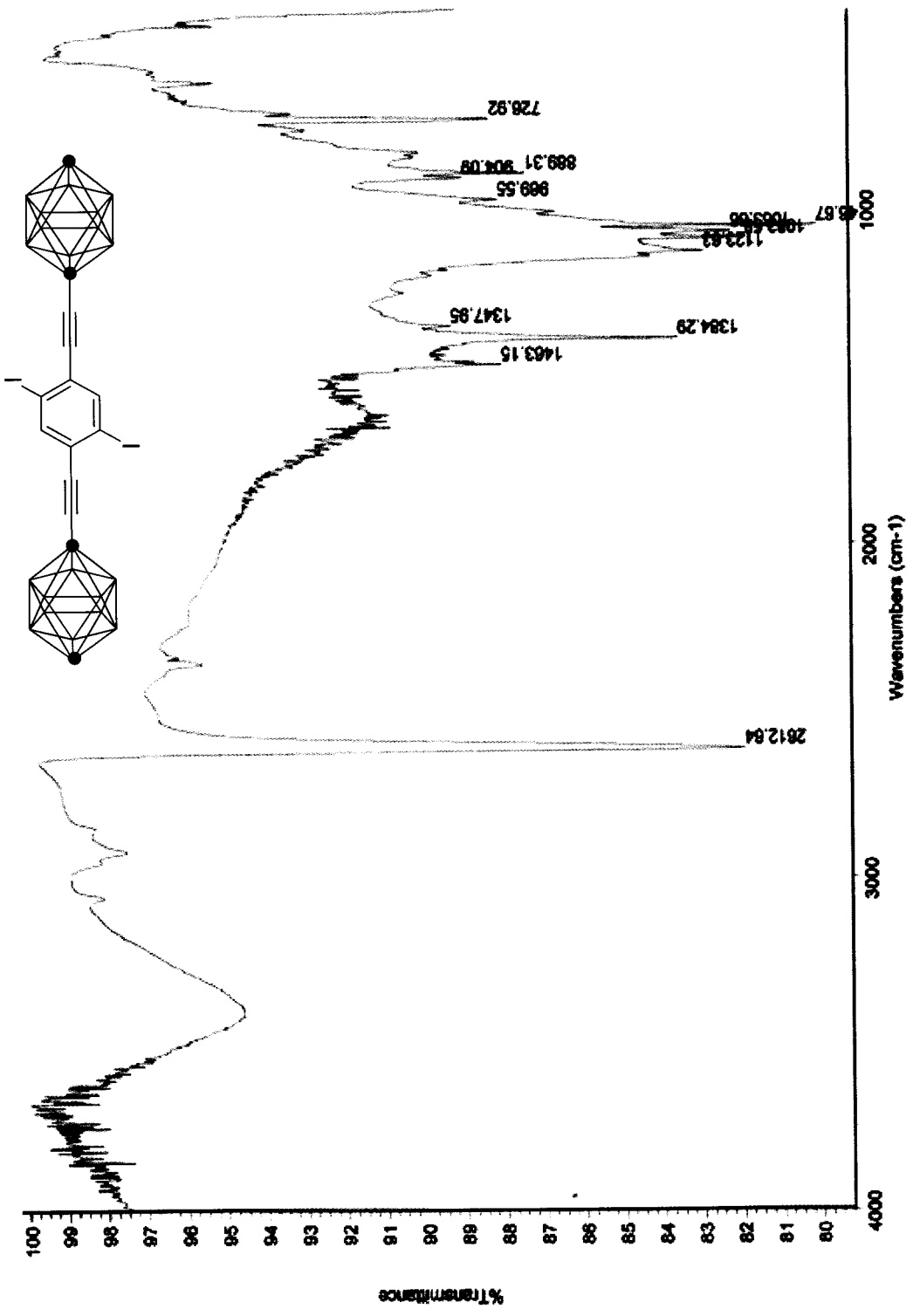

Figure S-1.1-12. IR Spectrum of Compound **5**.

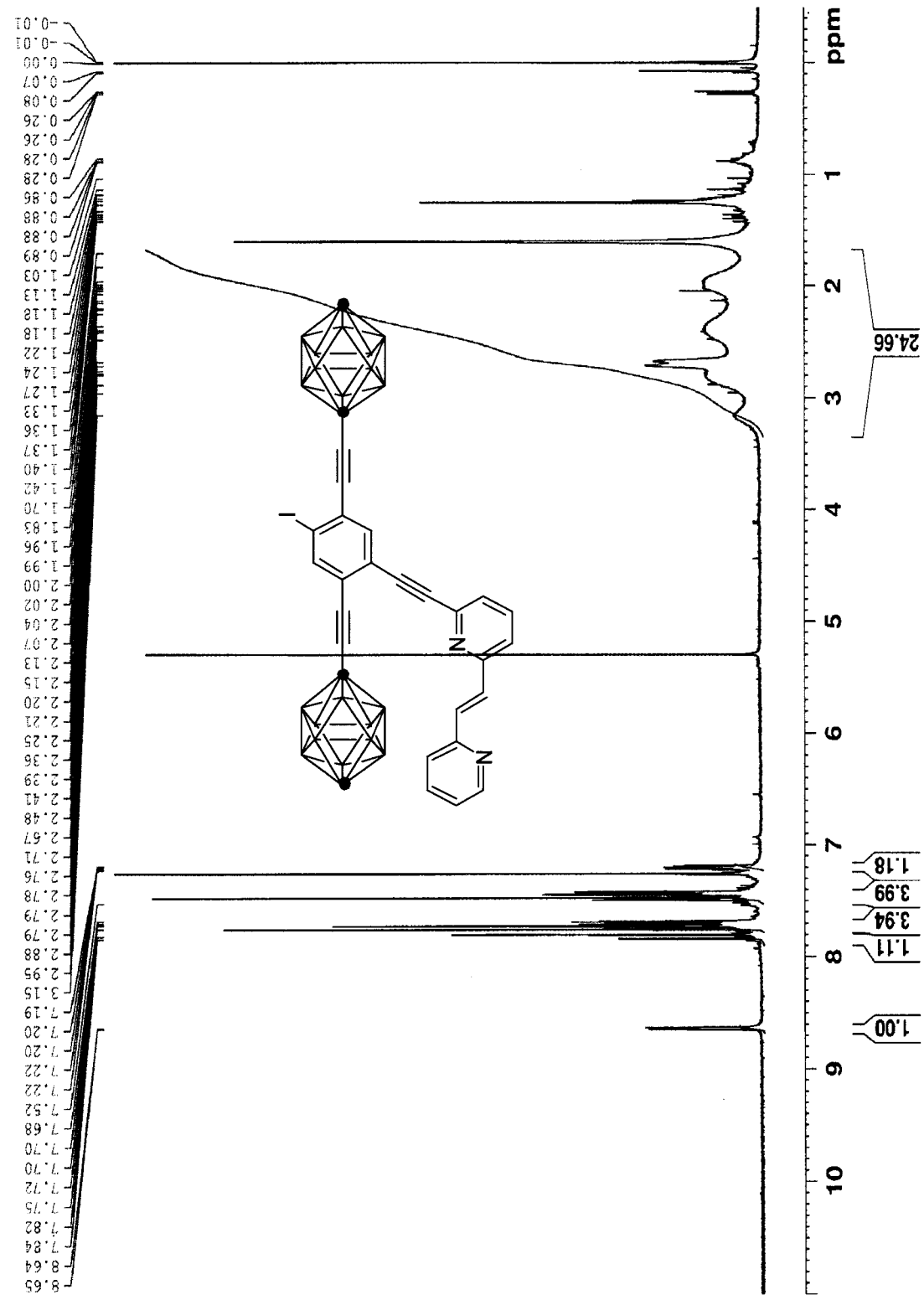

Figure S-1.1-13. ^{1}H NMR Spectrum of Compound **6**.

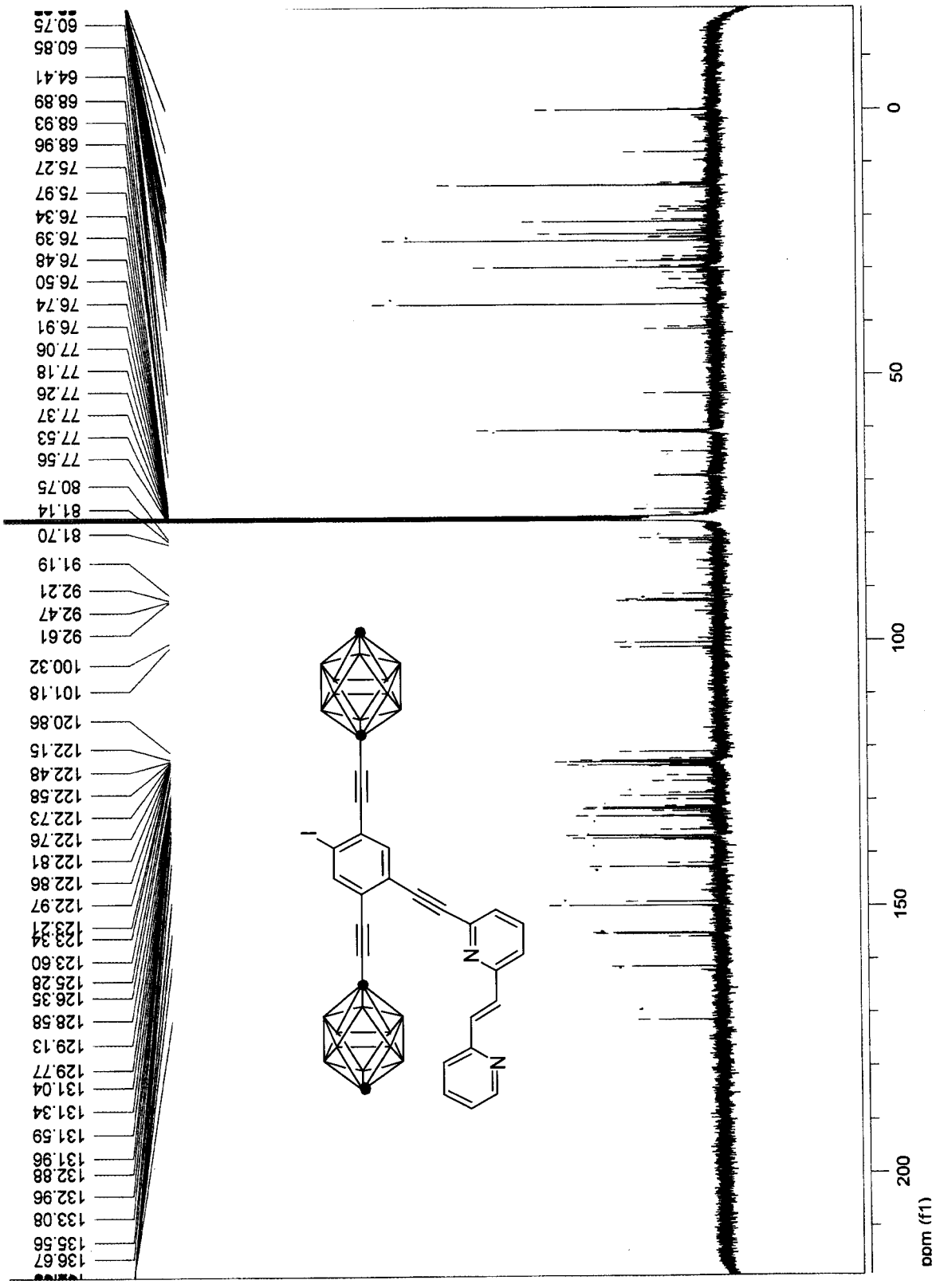

Figure S-1.1-14. ^{13}C NMR Spectrum of Compound **6**.

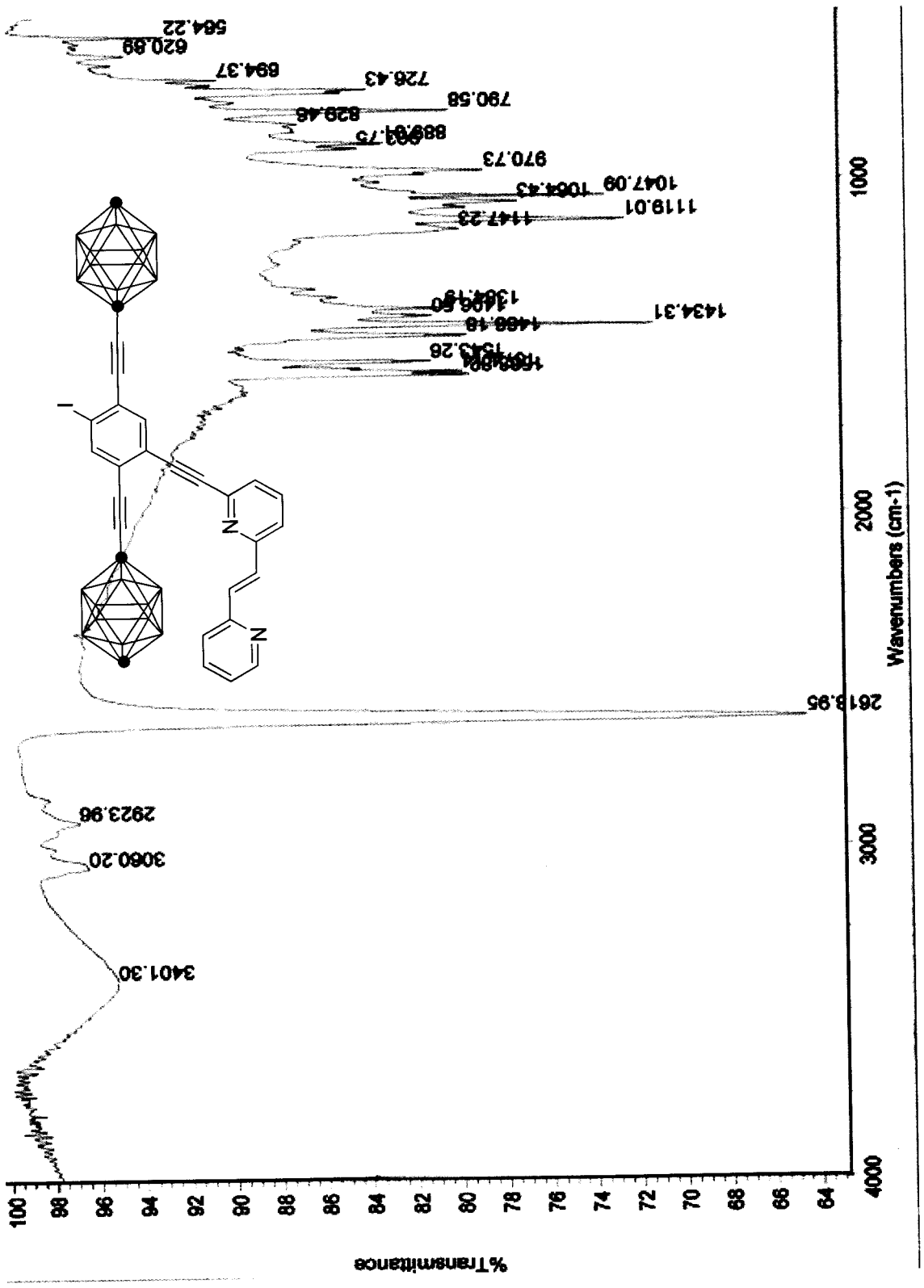

Figure S-1.1-15. IR Spectrum of Compound **6**.

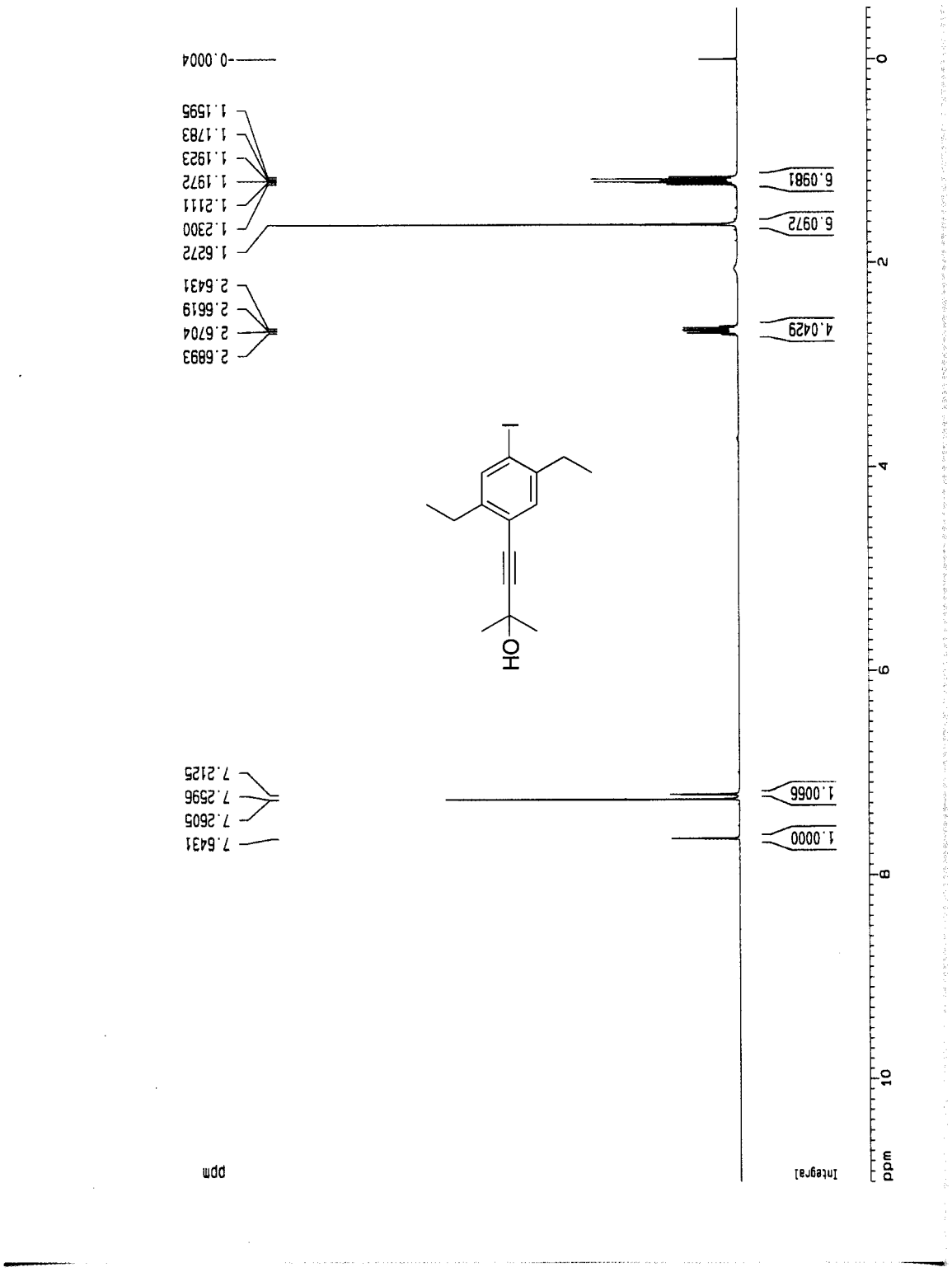

Figure S-1.1-16. ^{1}H NMR Spectrum of Compound **8**.

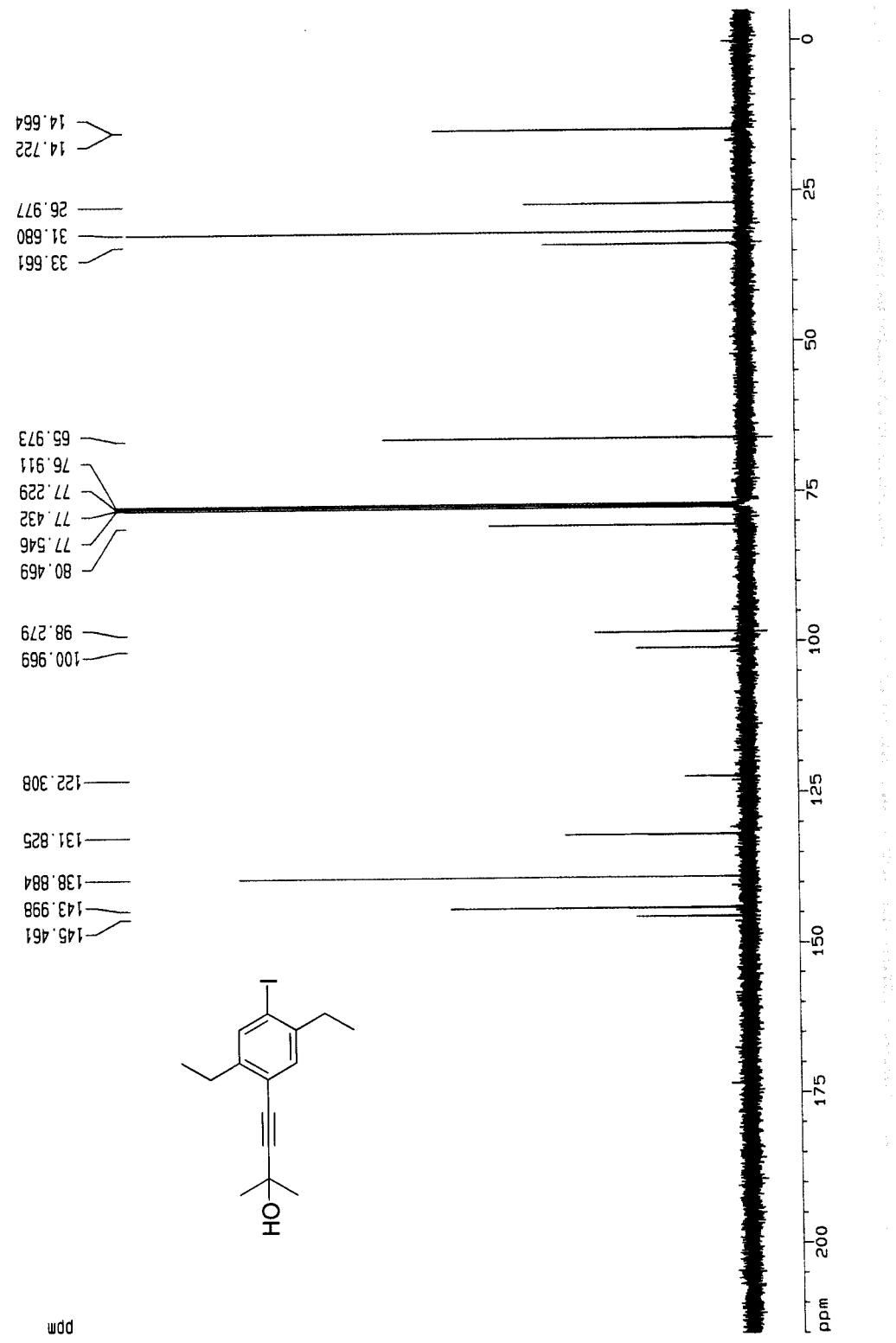

Figure S-1.1-17. ^{13}C NMR Spectrum of Compound **8**.

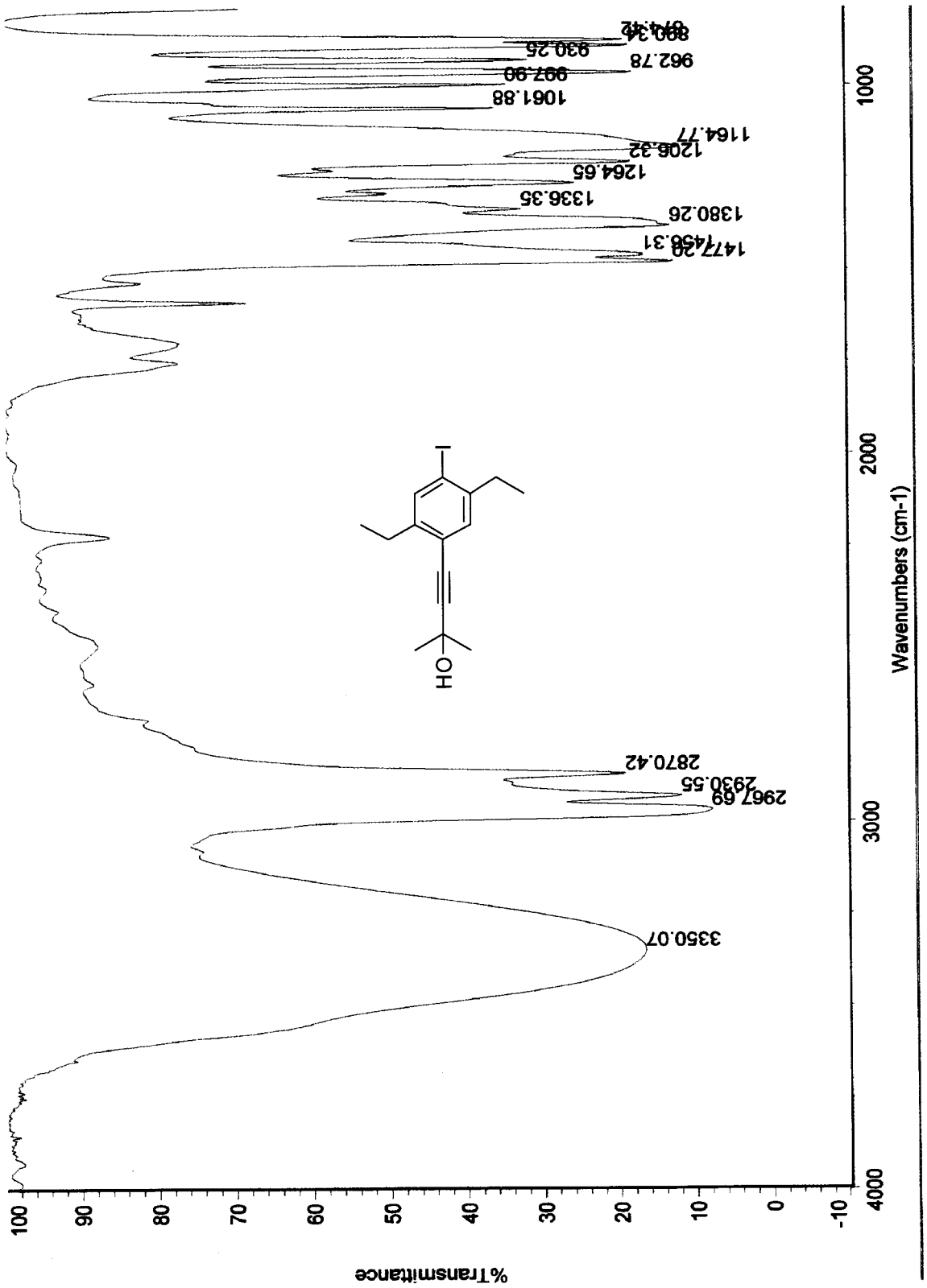

Figure S-1.1-18. IR Spectrum of Compound **8**.

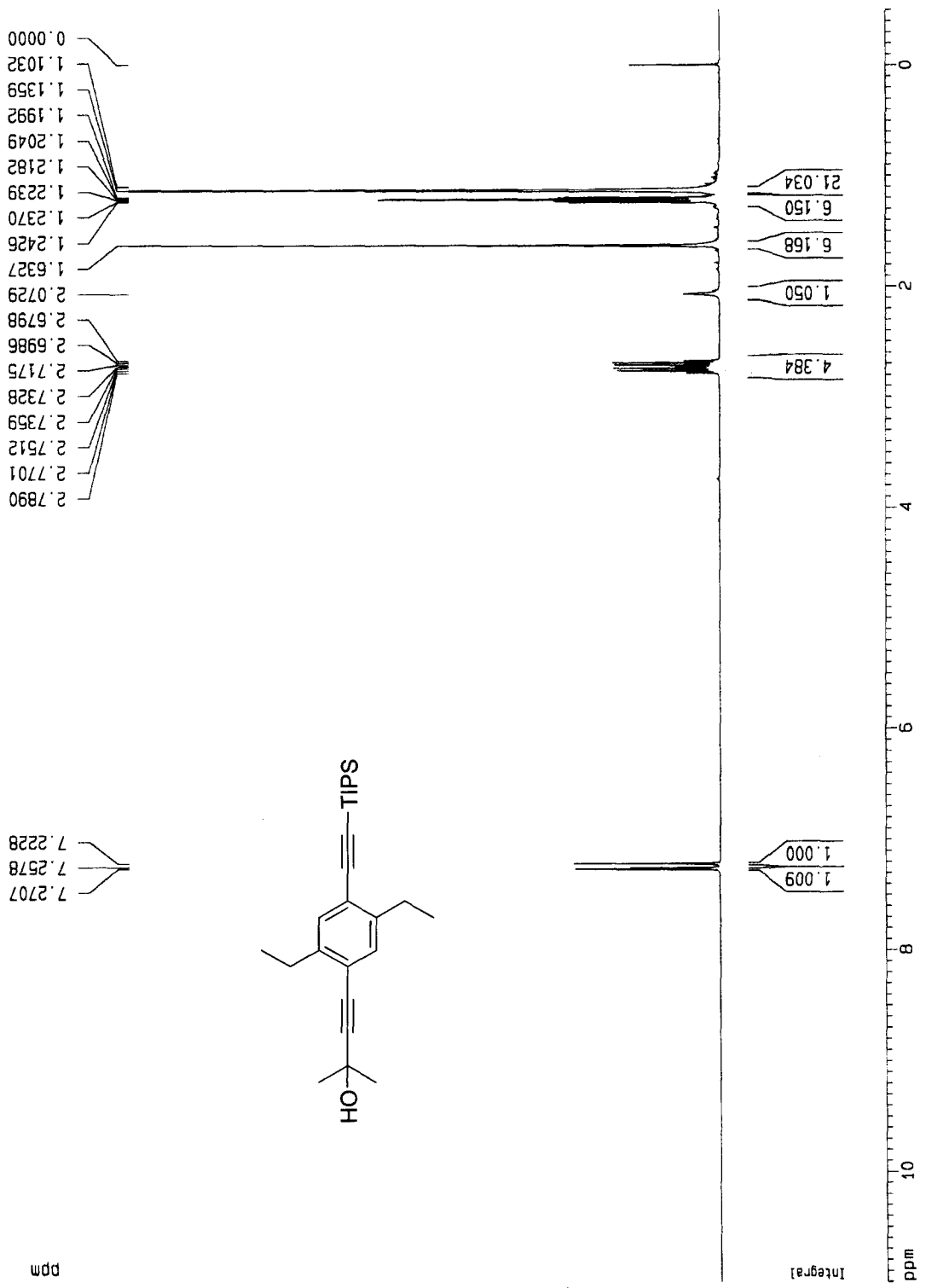

Figure S-1.1-19. ^{1}H NMR Spectrum of Compound **9**.

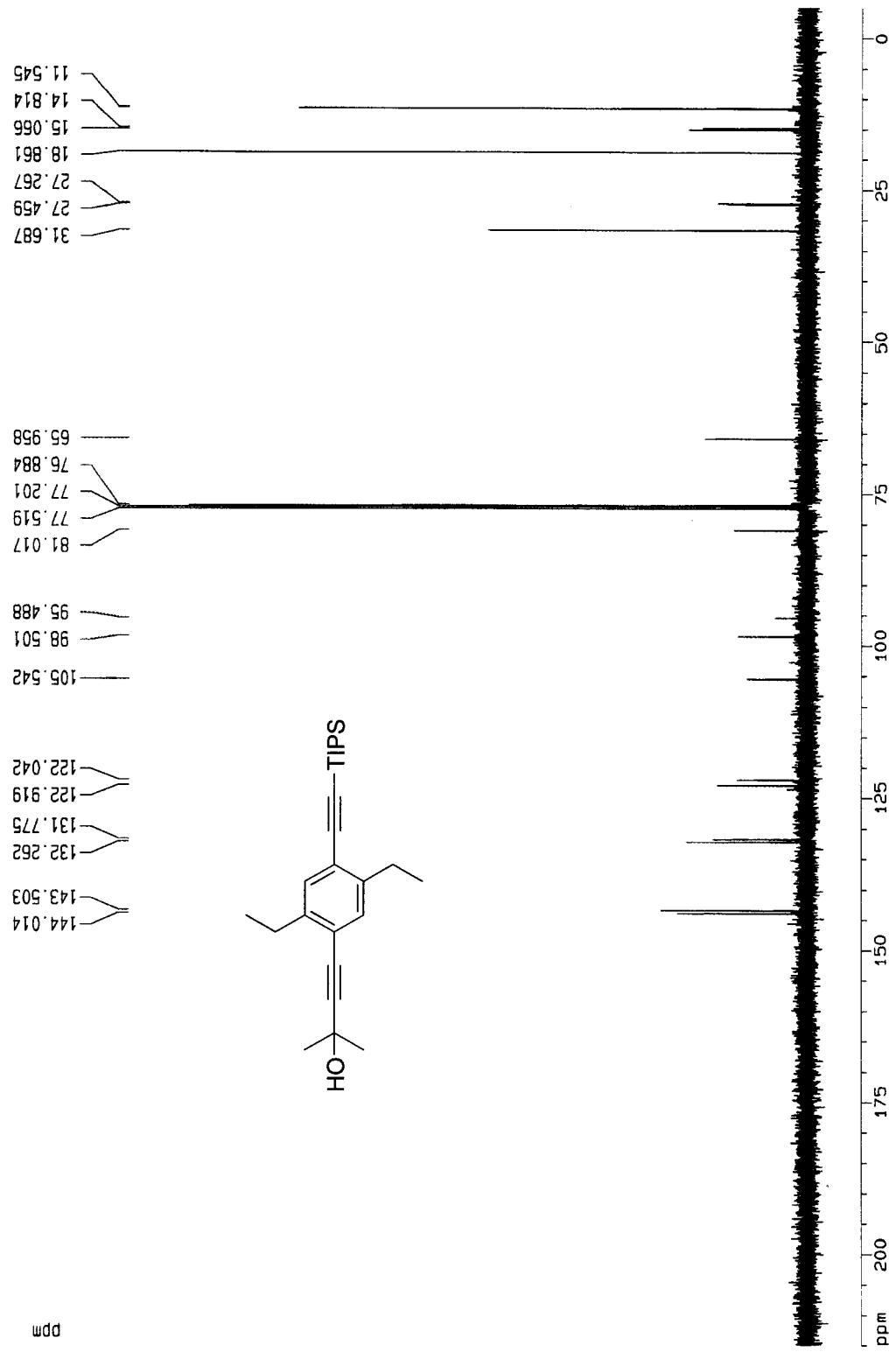

Figure S-1.1-20. ^{13}C NMR Spectrum of Compound **9**.

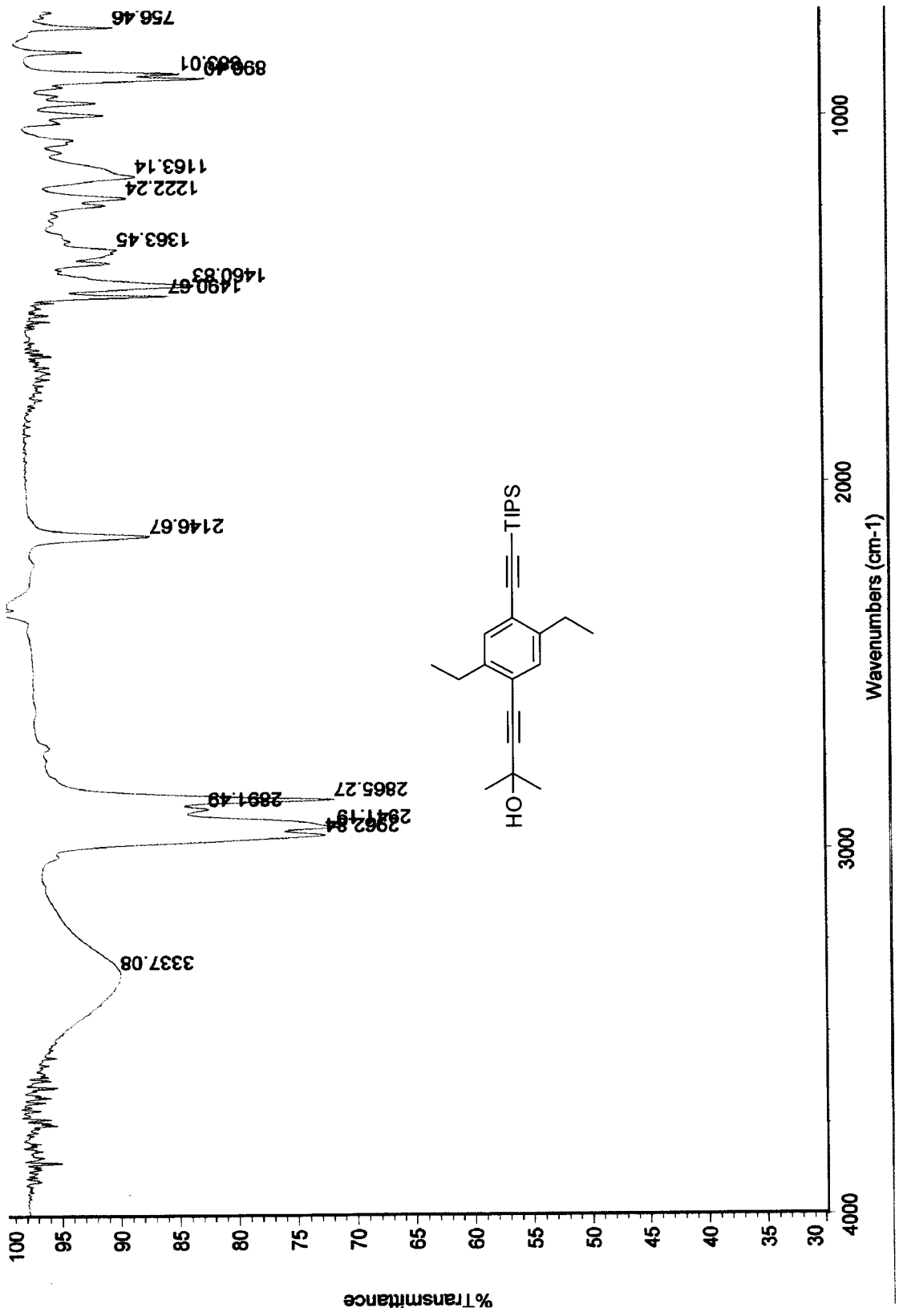

Figure S-1.1-21. IR Spectrum of Compound **9**.

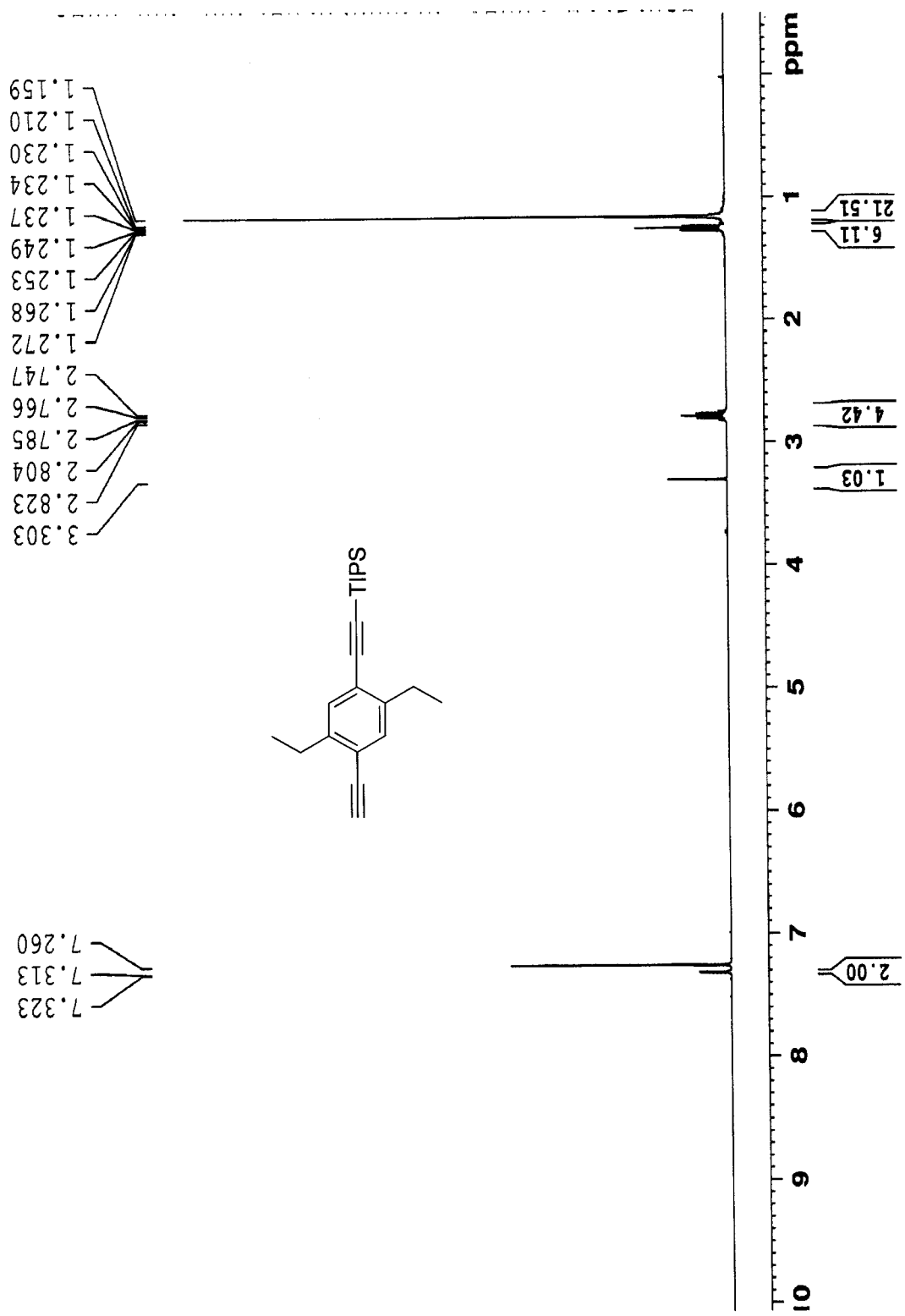

Figure S-1.1-22. ^{1}H NMR Spectrum of Compound **10**.

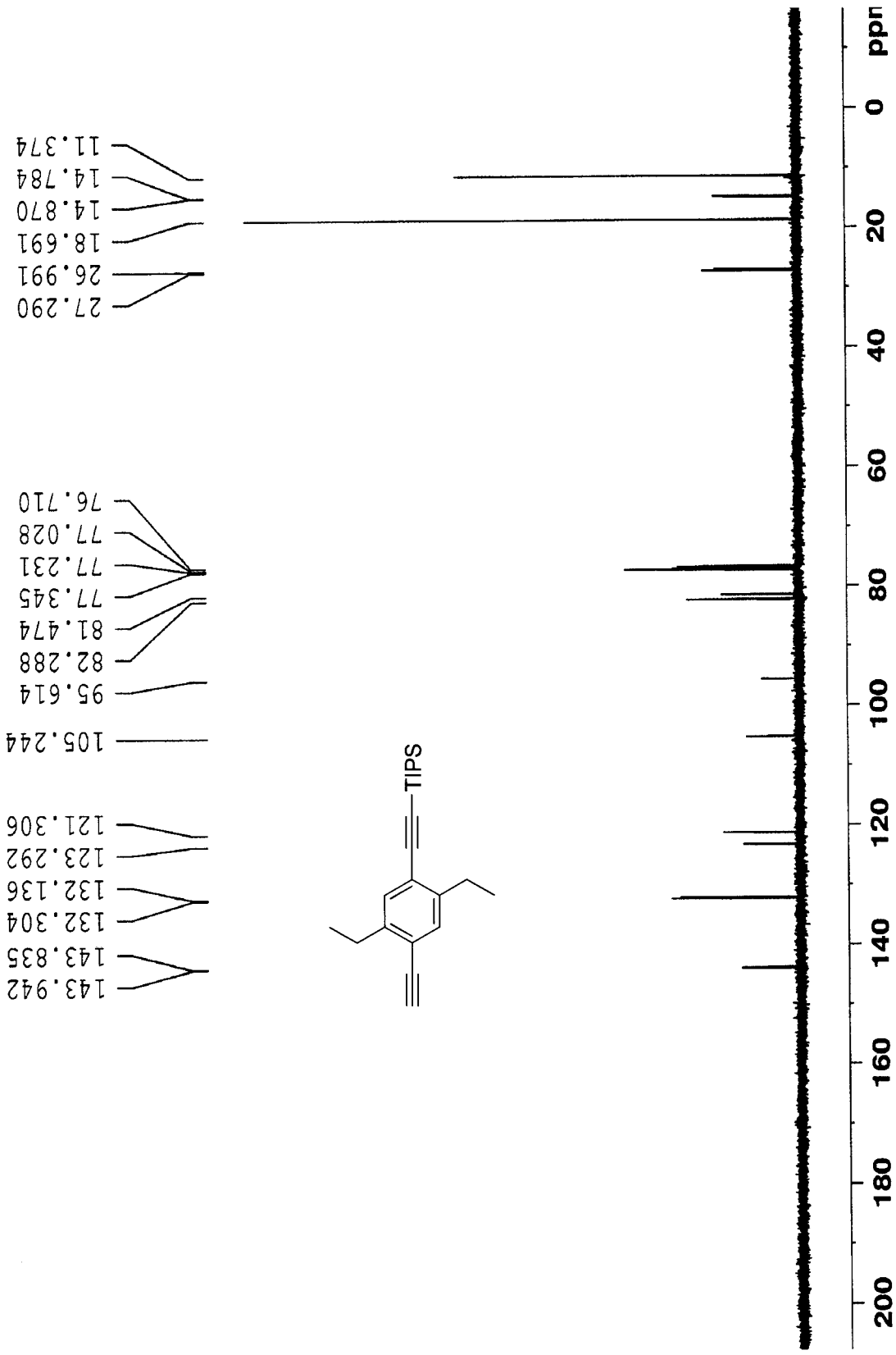

Figure S-1.1-23. ^{13}C NMR Spectrum of Compound **10**.

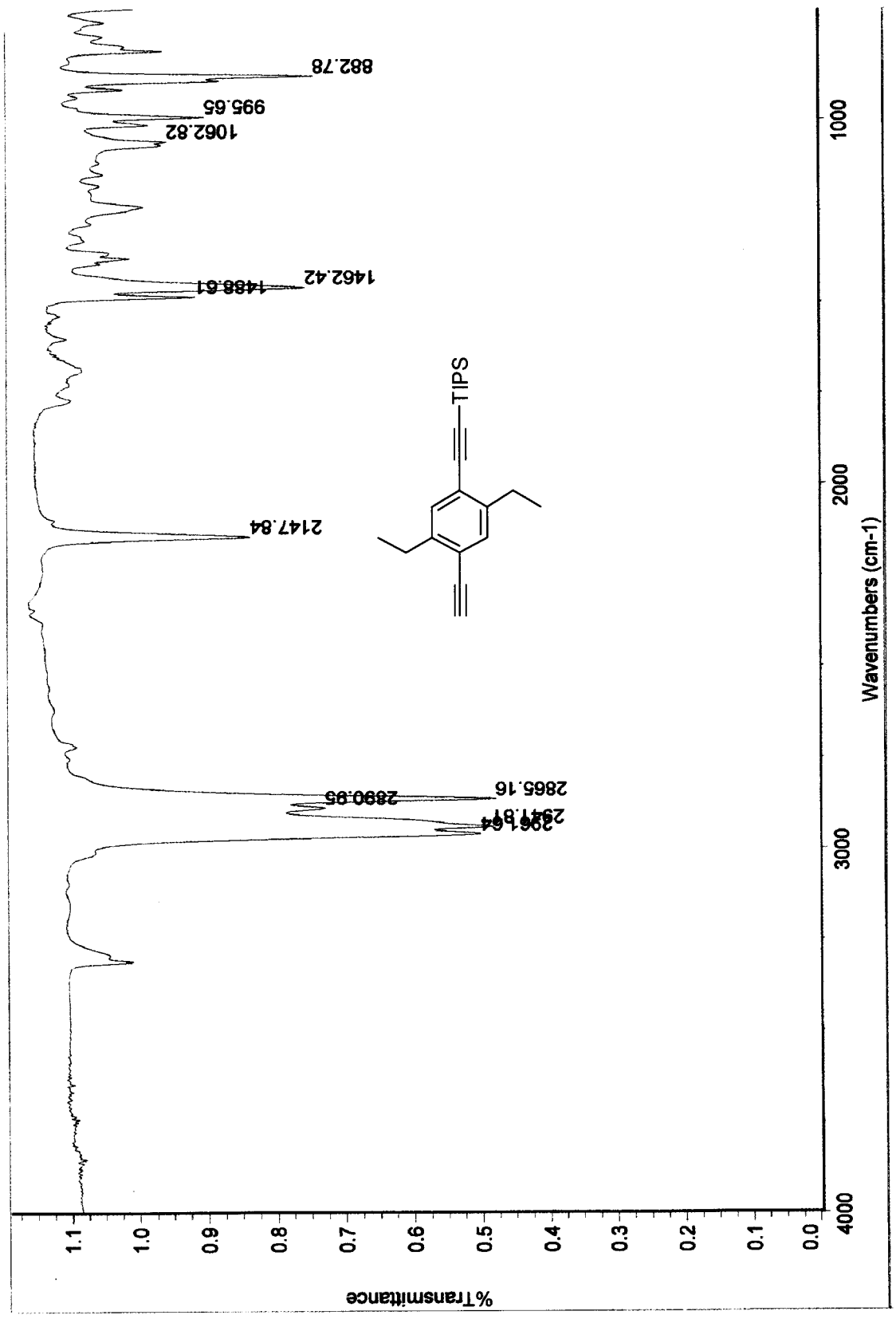

Figure S-1.24. IR Spectrum of Compound **10**.

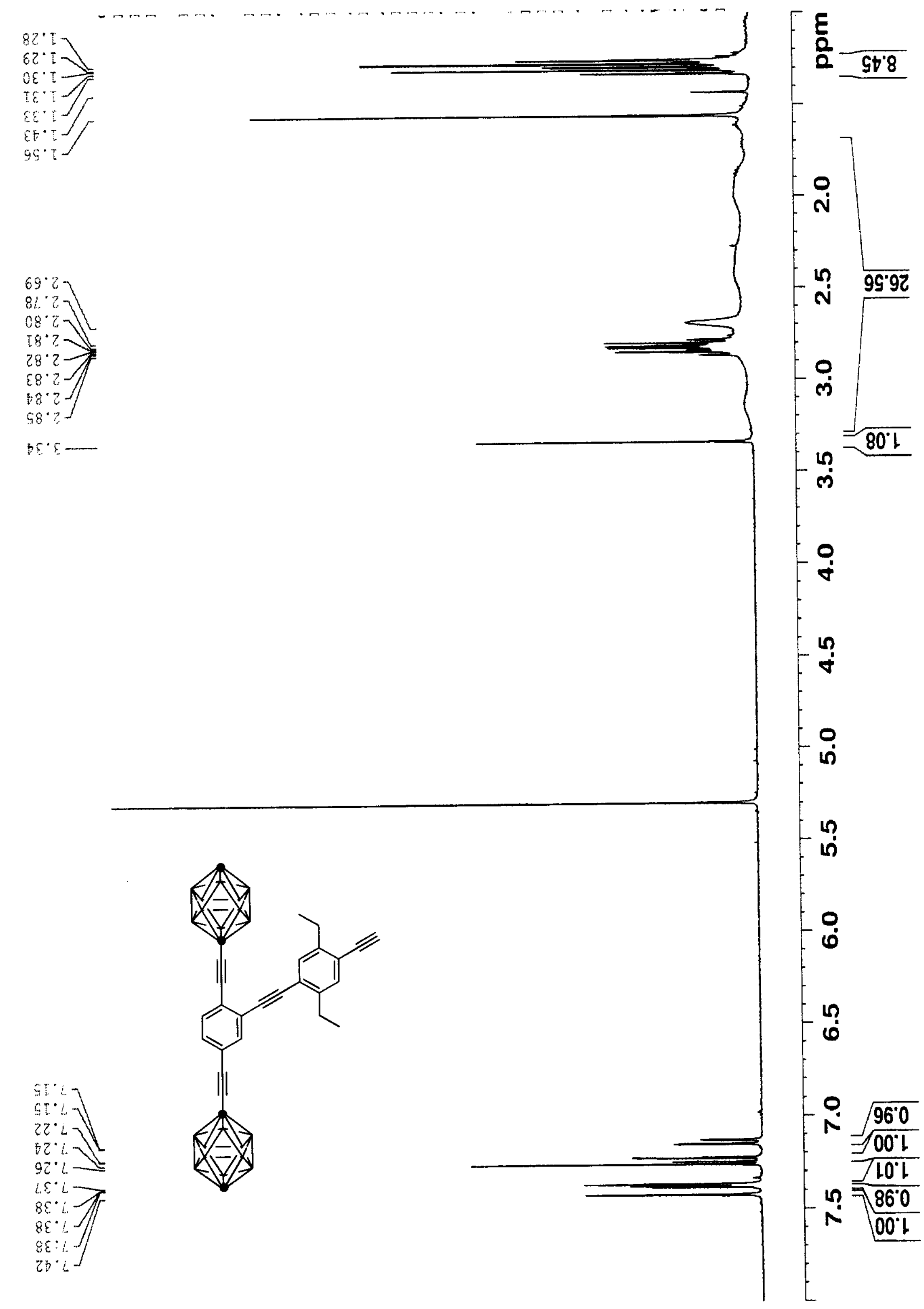

Figure S-1.1-25. ^{1}H NMR Spectrum of Compound **12**.

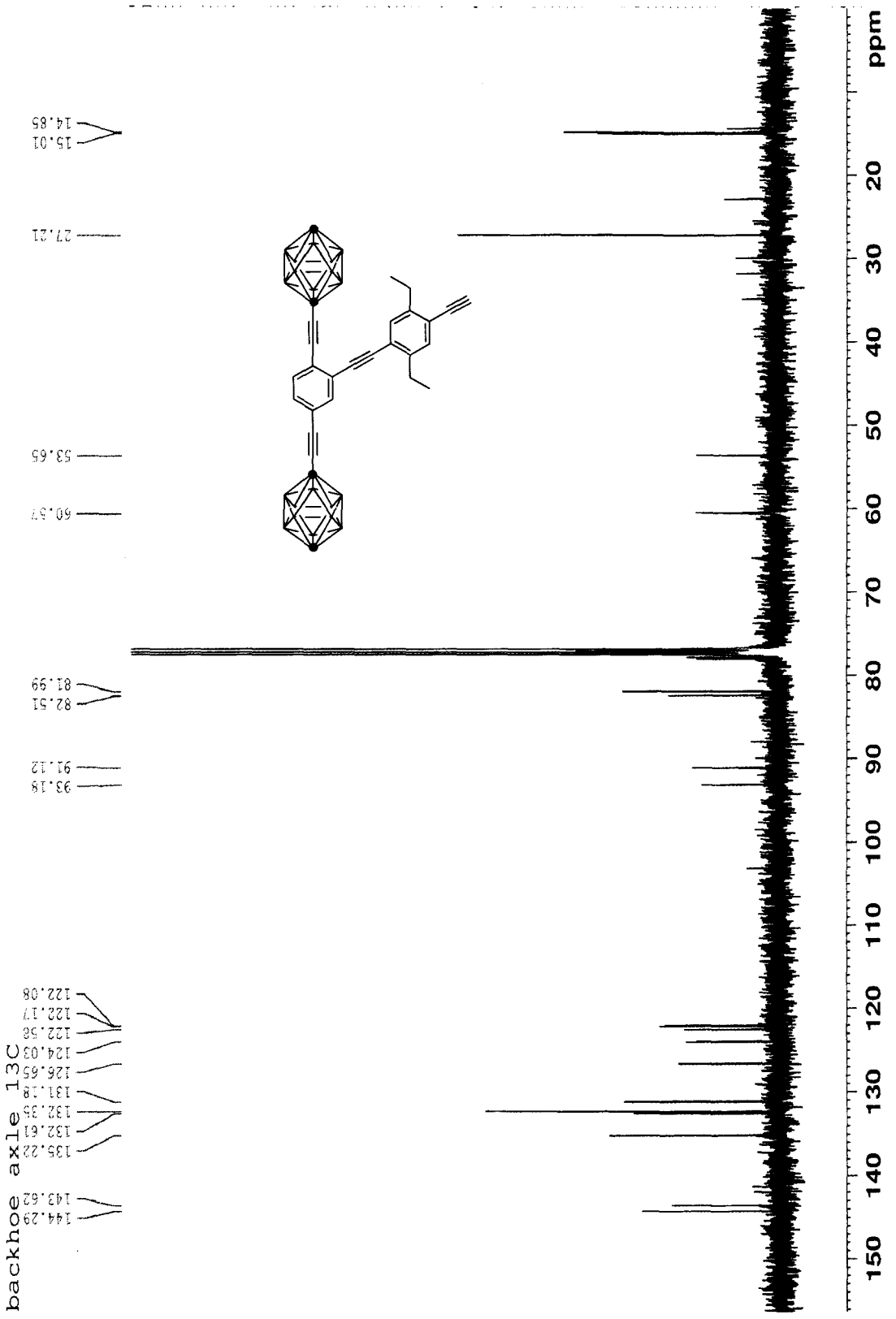

Figure S-1.1-26. ^{13}C NMR Spectrum of Compound **12**.

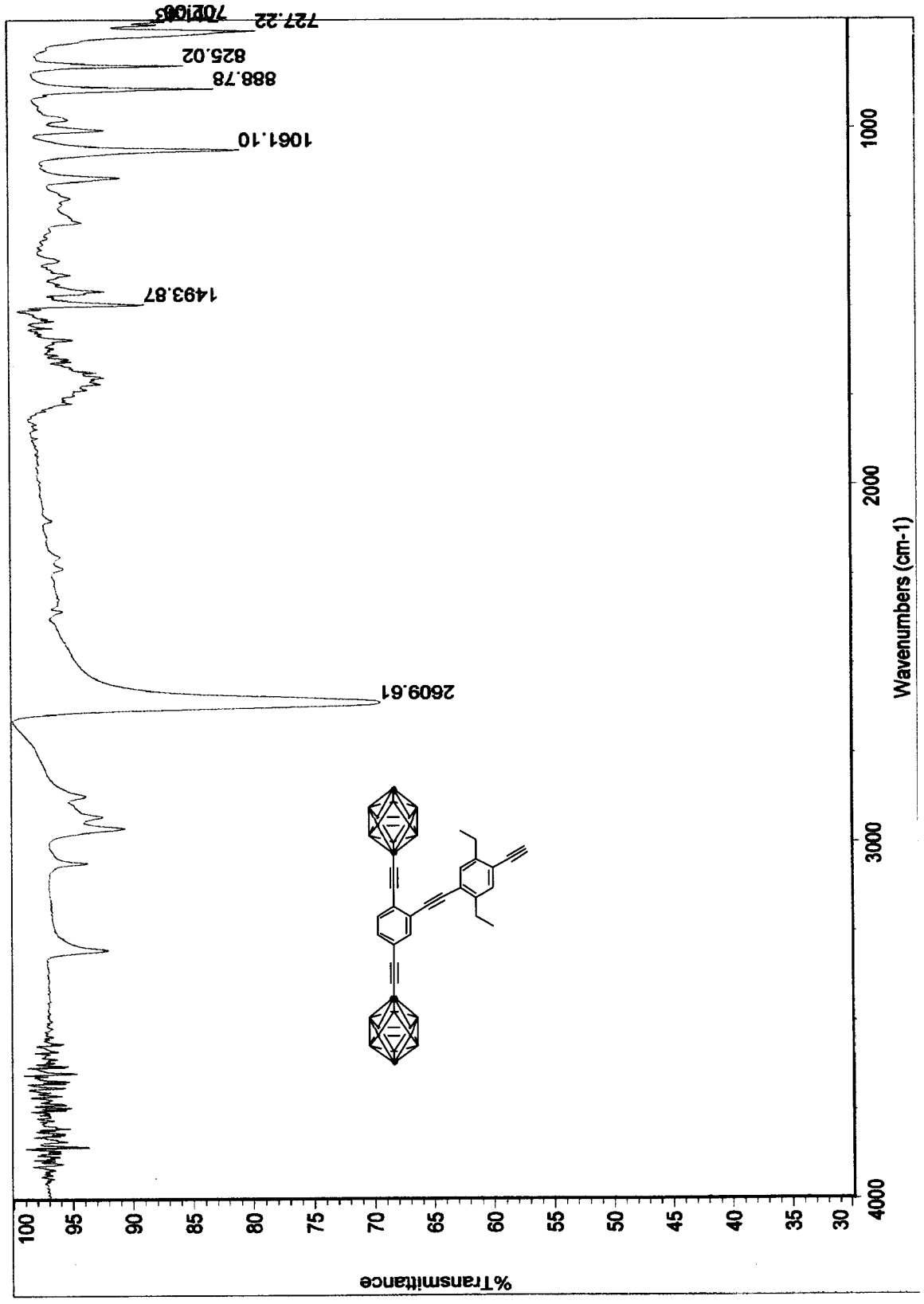

Figure S-1.1-27. IR Spectrum of Compound **12**.

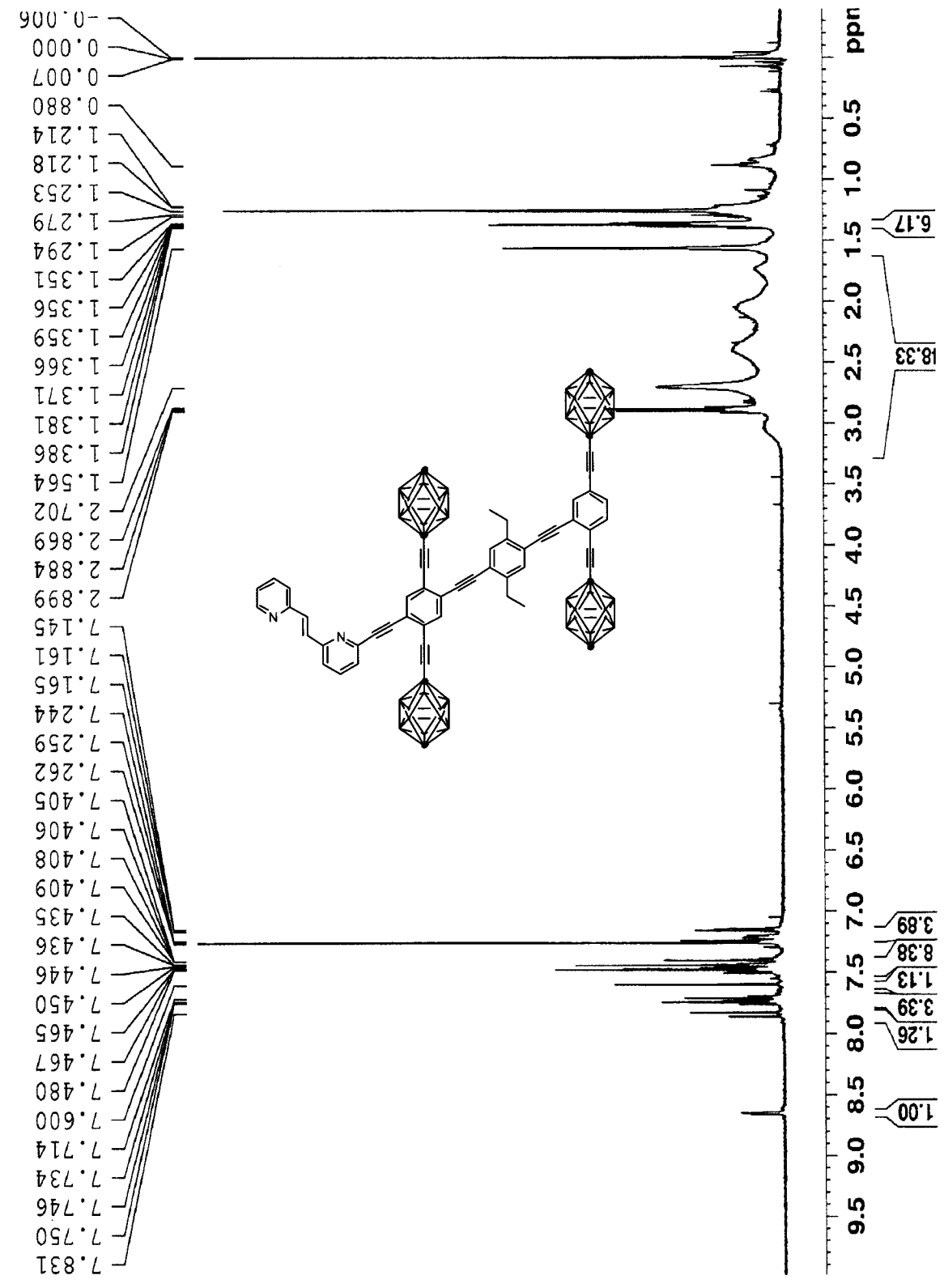

Figure S-1.1-28. ^{1}H NMR Spectrum of Nanobackhoe **1**.

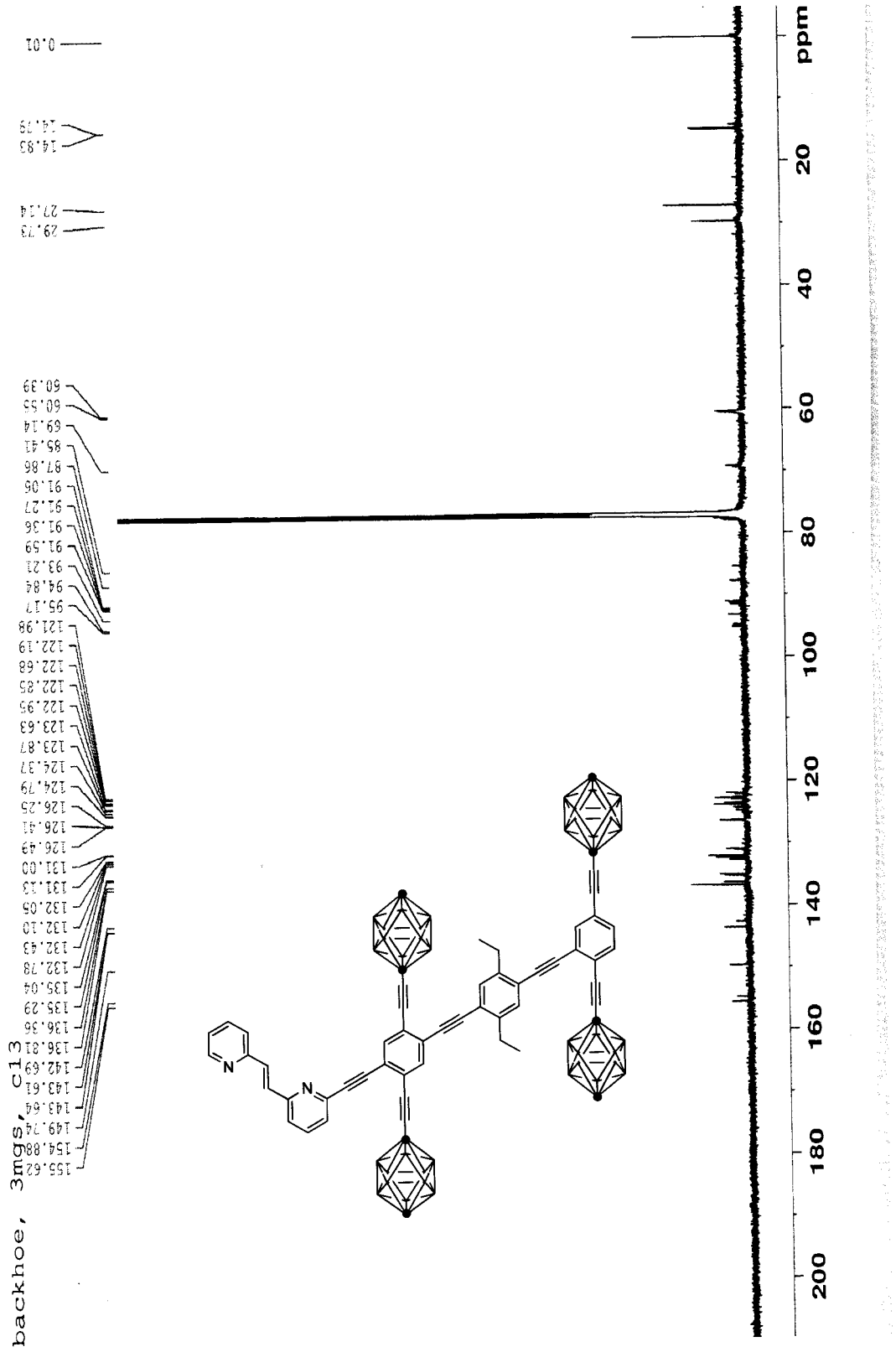

Figure S-1.1-29. ^{13}C NMR Spectrum of Nanobackhoe **1**.

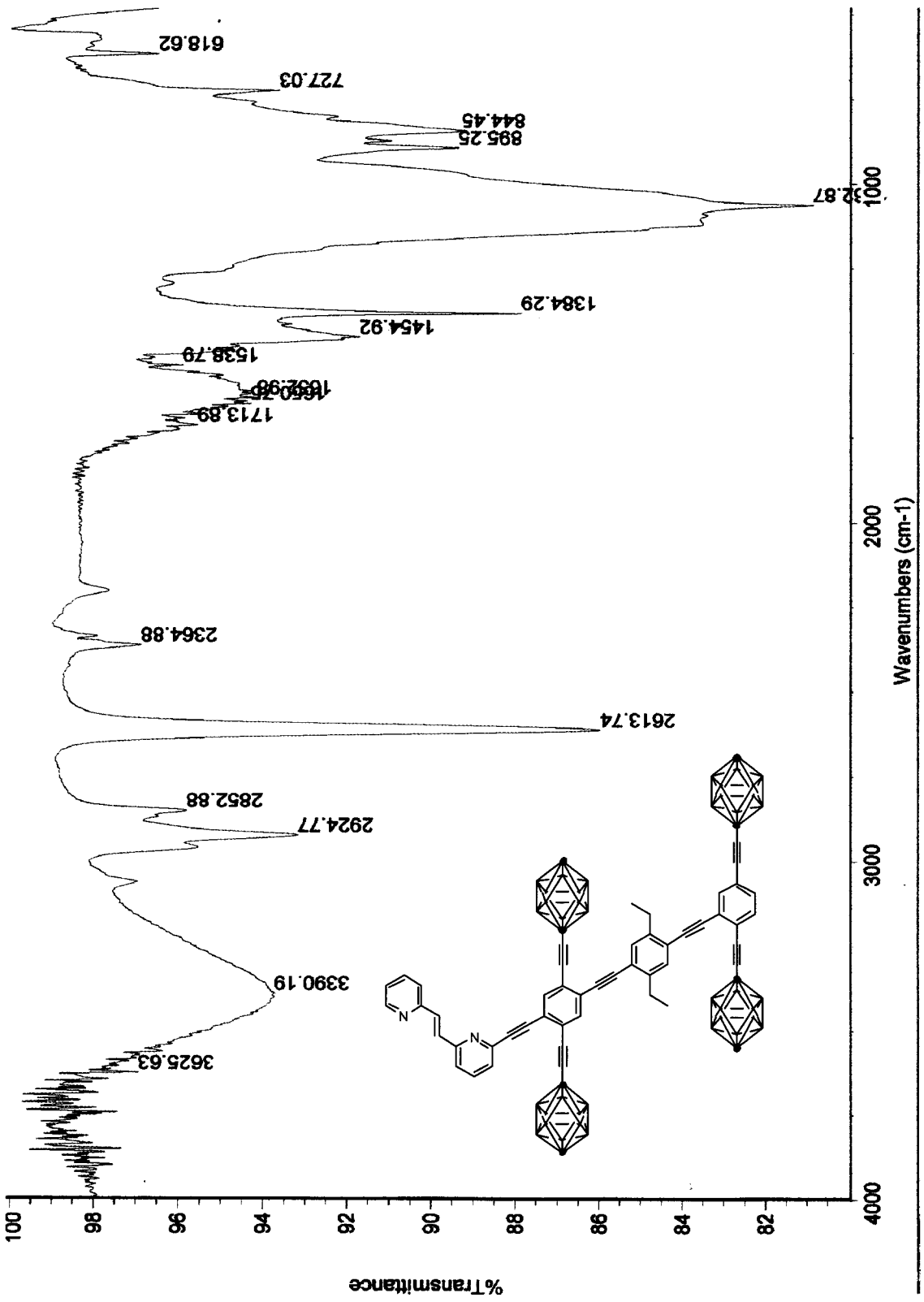

Figure S-1.1-30. IR Spectrum of Nanobackhoe **1**.

Chapter 2

Towards Increased Rotational Speed of Light-Powered Motorized Single Molecule Nanocars

2.1

Design and Synthesis of Dual-Motored and Ultra-Fast Nanocars

Introduction

Directing motion of single molecules using external stimuli is one of the most intriguing features necessary for the eventual implementation of nanomachinery into real-world applications.[1] Consequently, many groundbreaking and creative molecular devices, such as electroactive rotors,[2] shuttles,[3] DNA motors[4] and unidirectional motors,[1,5] have been developed for this endeavor. Our corresponding efforts have resulted in the development of nanocars: single molecules bearing molecular axles and wheels that are able to serve as a test-bed for developing surface-based tasks such as directed motion, transport and construction of molecular assemblies.[6]

Employing scanning tunneling microscopy (STM), we successfully observed controlled motion of fullerene-wheeled nanocars. Due to a combination of molecular design, the high symmetry of fullerenes (I_h, icosahedral) and the strength of their interaction with the gold surface, thermally and electrically induced (by the STM tip) motion occurred orthogonal to the axles of the nanocar.[7] As proof-of-concept, these initial experiments have led us to further pursue directional propulsion using light as an external stimulus.[8] Coincidentally, we have shown that the photoexcited states of unidirectional molecular motors and azobenzene molecular switches undergo rapid intra- and intermolecular quenching by fullerenes, effectively rendering them inactive in solution.[8,9] To this end, after screening various candidates for molecular wheels, we arrived at nanocar structure **1**, as the symmetry (D_{5h} point group) and non-photoquenching nature of *p*-carboranes, make them an attractive alternative to fullerenes.

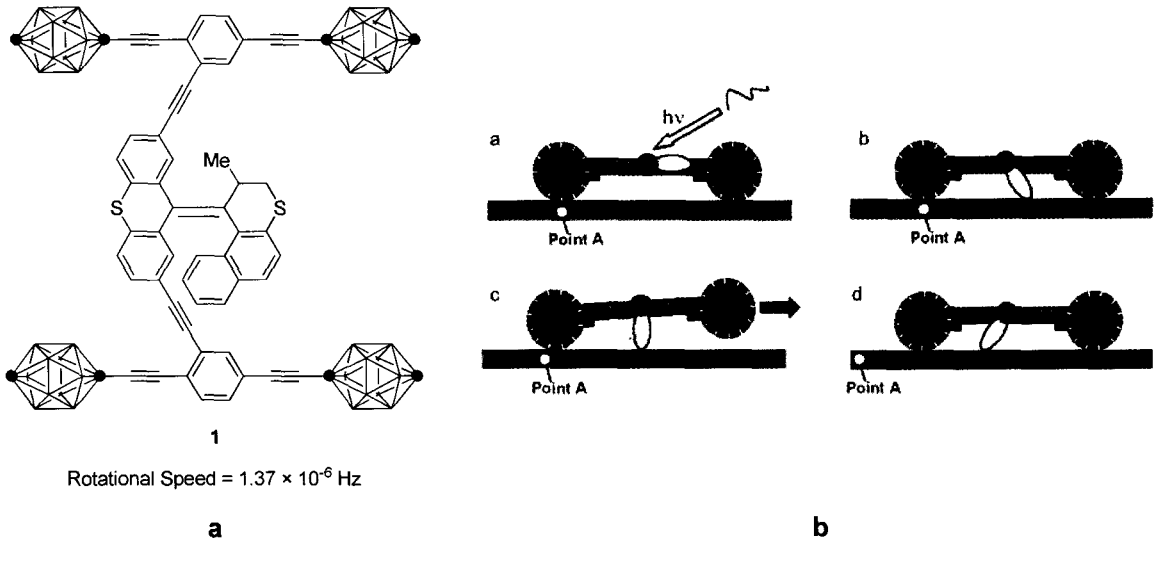

Figure 1. (a) The structure and rotational speed of the original motorized nanocar 1 and (b) its proposed mechanism of motion. The *p*-carborane wheels have BH at every intersection except at the left and right vertices which represent C and CH positions, *ipso* and *para*, respectively, relative to the alkynes. Image adapted from Ref. 8.

Indeed, upon completion of the motorized prototype using *p*-carborane wheels and a light-powered unidirectional Feringa motor,[10] we demonstrated the rotational movement of the nanocar's motor in solution at elevated temperature.[8] Although the *p*-carborane wheels proved to be very useful for construction and motorization, early STM studies of carborane-wheeled nanovehicles have indicated that the relatively weak carborane-gold interaction leads to rapid non-directionally controllable motion at ambient temperature.[11] To stifle this non-rotating wheel motion in an effort to obtain fine rotational control, a variety of approaches may be necessary, including imaging atop a self-assembled alkanethiol monolayer, using a surface with greater interaction with carboranes and/or imaging at lower temperatures.[12] Furthermore, imaging using other microscopy methods where non-conductive substrates such as glass or mica are compatible may be necessary.

Exacerbating this issue, solution-based kinetic data of the original motorized nanocar indicate that the unstable form of the molecular motor persists for 101 h at room temperature.[8] Upon photoirradiation, isomerization to the unstable form occurs on the femtosecond timescale, making the rate-limiting step for a 180° rotation the thermal decay from this unstable state to a relaxed, stable state of the motor, termed a thermal helical inversion.[13] As two thermal helix inversions are necessary for one full rotation, we determined that the original motorized nanocar **1** has a rotation rate of 1.37×10^{-6} Hz, or one rotation every 202 h under ambient conditions. Only at a higher operating temperature of 65 °C does the motor begin to exhibit a much more manageable 1.8 rotations per hour. While such stability is a boon for room temperature spectroscopic determination of kinetic data, room- and low-temperature imaging would be unnecessarily time-consuming and impractical. To overcome this hurdle, we report herein a bifurcated approach towards increasing the speed of motorized nanocars through the utilization of two distinct types of motors recently reported by Feringa and co-workers.[14] The resultant motorized nanocars should display increased rotational speeds sufficient for imaging under a wide range of conditions.

Results and Discussion

Molecular Design of Doubly-Motorized Nanocars. In 2006, Feringa and co-workers described the synthesis of four new light-powered molecular motors.[14a] It was reported that bulky substituents on the cyclopentane moiety cause an increase in double-bond length of the bridging alkene (the axis of rotation), giving rise to greater single-

bond character. In addition, the steric interaction of the aryl units as they move past one another is decreased, a result of decreasing the size of the bridging cycloalkane. These two structural modifications result in motors with increased rotational speed, up to 87 Hz at room temperature.

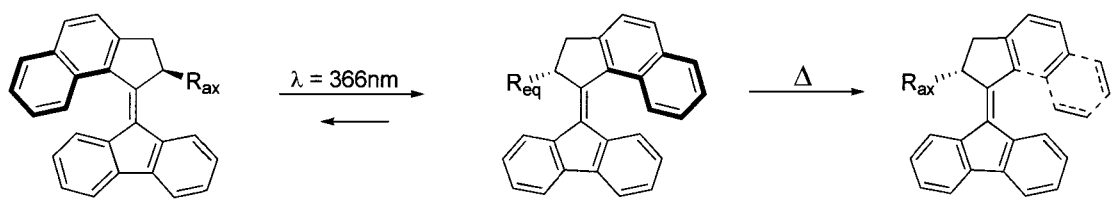

stable unstable stable

R	k^o (s^{-1})	$t^{1/2}$ (s)	RPH	RPS	DBL (Å)
Ph	1.18×10^{-3}	587	3.24	.0009	1.3753
Me	3.64×10^{-3}	190	10.8	.003	1.3775
^{i}Pr	7.32×10^{-3}	95	18	.005	1.3800
^{t}Bu	1.21×10^{2}	5.74×10^{-3}	313200	87	1.3859

Figure 2. Fluorene-based molecular motors developed by Feringa. Note the increased rotational speed (RPS) as the substituent (R) has greater steric demand. k^o represents the rate constant. $t^{1/2}$ represents the half-life of the unstable form at room temperature, RPH = rotations per hour, RPS = rotations per second, DBL = double bond length (given in angstroms). Figure adapted from reference 15a.

To construct a motorized nanocar using a design similar to the fluorene-based molecular motors, the extension of fluorenone into indenofluorenedione (Figure 3) was necessary to obtain axles with parallel orientation and limit any possible steric interaction of the motor with the axles. In addition, the presence of two ketone moieties allows the

inclusion of two motors, which may effectively double the number of "power strokes" along a surface. Thus, when R = *t*-butyl, the doubly-motorized nanocar may exhibit up to 174 rotations per second.

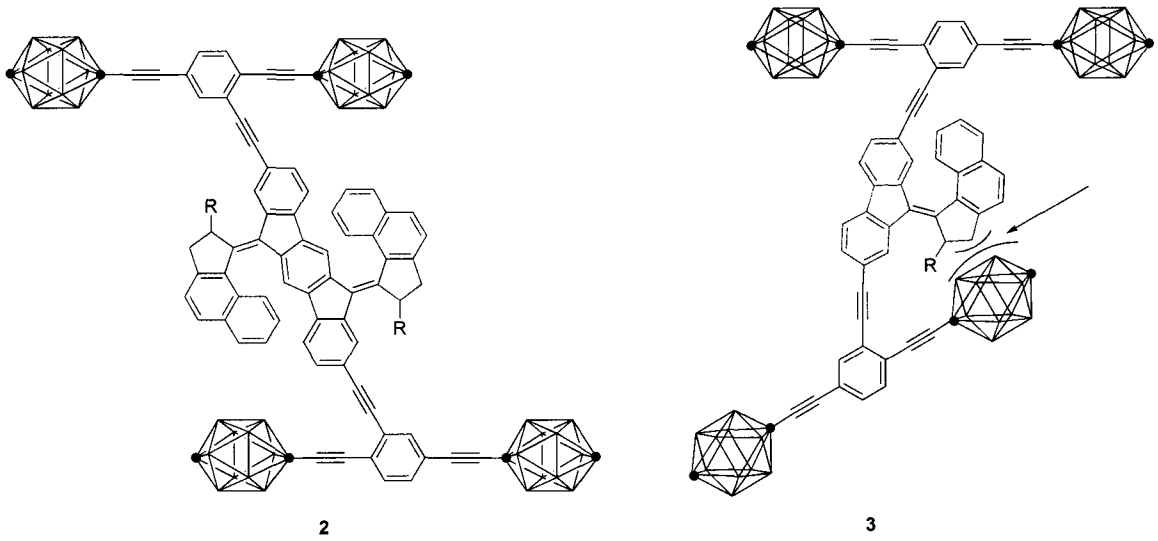

2 3

Figure 3. Structures of indenofluorene-based dual motor nanocar **2** and the nanocar resulting from use of fluorene as a stator, nanocar **3**. Indenofluorene is colored red, the rotors in blue and fluorene in green. Note the steric interaction of the motor and axle in nanocar **3**.

Synthesis. The synthesis of the rotor portions of the motorized nanocar, a slight variation of the reported sequence by Feringa and co-workers,[14a] is shown in Scheme 1. The *t*-butyl rotor's purpose for construction was to be included into the doubly-motorized nanocar, while the methyl rotor was constructed for use in later nanocars (*vide infra*). To construct the rotors, the appropriate enolate was formed using lithium hexamethyldisilazide at -78 °C, followed by alkylation using 2-bromomethylnaphthalene. The purifications at this point were quite difficult, thus the crude mixtures were taken

through hydrolysis, resulting in acids **4**, which were easier to purify and led to an increased overall yield in the case of the methyl-substituted version. Formation of the acyl chloride using thionyl chloride in refluxing dichloromethane followed by an aluminum trichloride-induced Friedel-Crafts intramolecular acylation yielded ketones **5**.

To prepare for the key motor formation step, a Staudinger-type diazo-thioketone coupling,[15] the rotors were appropriately substituted at their ketonic positions. Due to the high steric demand of the *t*-butyl-substituted ketone, only one approach can be taken, where the rotor bears the thioketone coupling partner. Conversely, both routes have been reported with the methyl version,[14a] where the rotor may serve as either the thioketone or diazo coupling moiety. Thus, *t*-butyl ketone **5a** was thionated using phosphorous pentasulfide in hot toluene to form thioketone **6**. Methyl ketone **5b** was heated in hydrazine monohydrate, yielding hydrazone **7** (the thioketone proved to be difficult to isolate in pure form). To fully realize the diazo coupling partner, **7** was oxidized using active manganese dioxide in dichloromethane to form azo **8**, which was taken directly on to the motor formation step.

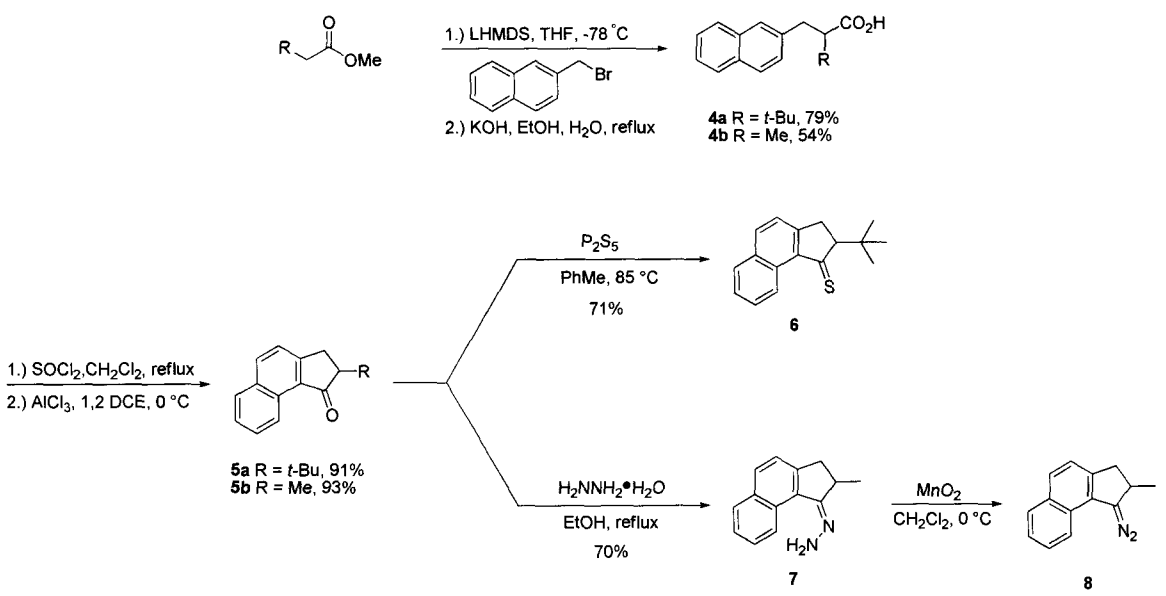

Scheme 1. Synthesis of rotor portions for motorized nanocars.

To arrive at the double-stator indenofluorenedione chassis with pendant bromides for eventual axle attachment, as shown in Scheme 2, a Suzuki coupling of 1,4-diiodo-2,5-xylene (**9**)[16] with 4-bromobenzeneboronic acid provided substituted terphenyl **10**.[16] Oxidation of the *p*-dimethyl moiety to the dicarboxylic acid, followed by immediate Freidel-Crafts intramolecular acylation using concentrated sulfuric acid at elevated temperature provided dibromo-indenofluorenedione **11**.[16]

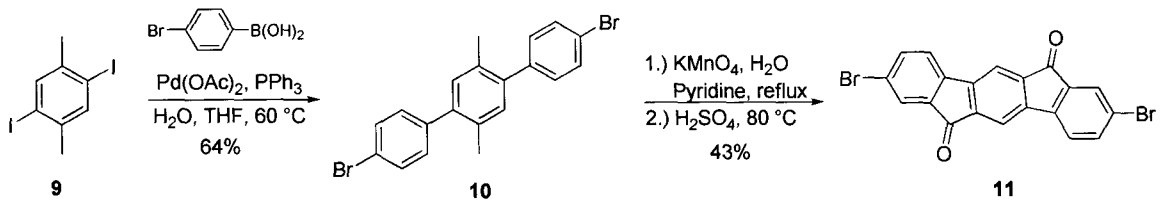

Scheme 2. Synthesis of stator chassis of dual motor nanocar.

In an effort to realize the double-diazo coupling partner for motor formation, insoluble diketone **11** was both (1) derivatized directly to a dihydrazone by refluxing in hydrazine monohydrate and ethanol to produce **12** and (2) coupled to solubilizing triisopropylsilylacetylene (TIPSA) at the bromide positions to produce **13** for subsequent derivatization. However, attempts to form a soluble dihydrazone from **13** using hydrazine monohydrate under various conditions resulted in complete alkyne reduction, precluding the use of **13** as a parent compound for double diazo formation.

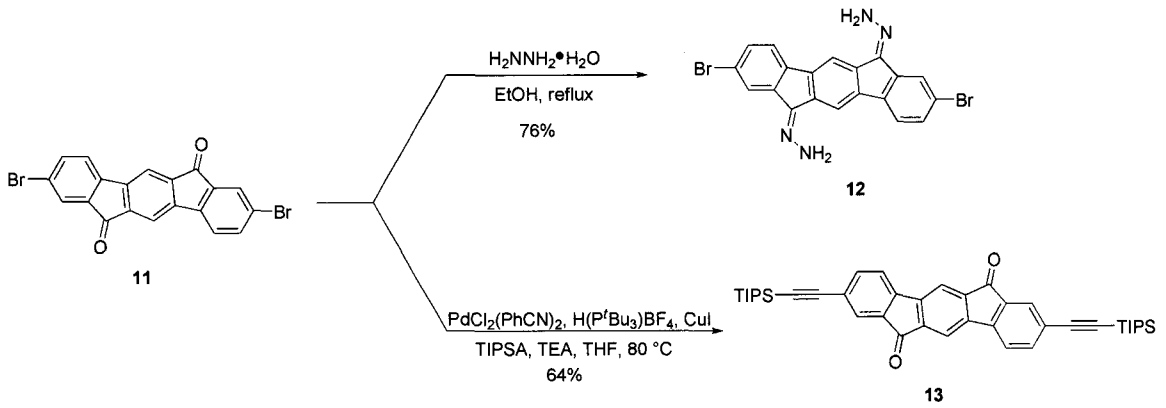

Scheme 3. Synthesis of dihydrazone and soluble diketone stators.

As shown in Scheme 4, likely a result of the poor solubility of **12**, formation of bis(diazo) **14** using bis(trifluoroacetoxy)iodobenzene in DMF, a homogeneous reagent for the oxidation of hydrazones to diazo species,[17] was unsuccessful. Heterogeneous oxidation reagents such as Ag_2O, HgO and MnO_2 also proved to be ineffectual, thereby negating the strategy to react the inner chassis with thioketone **6**.

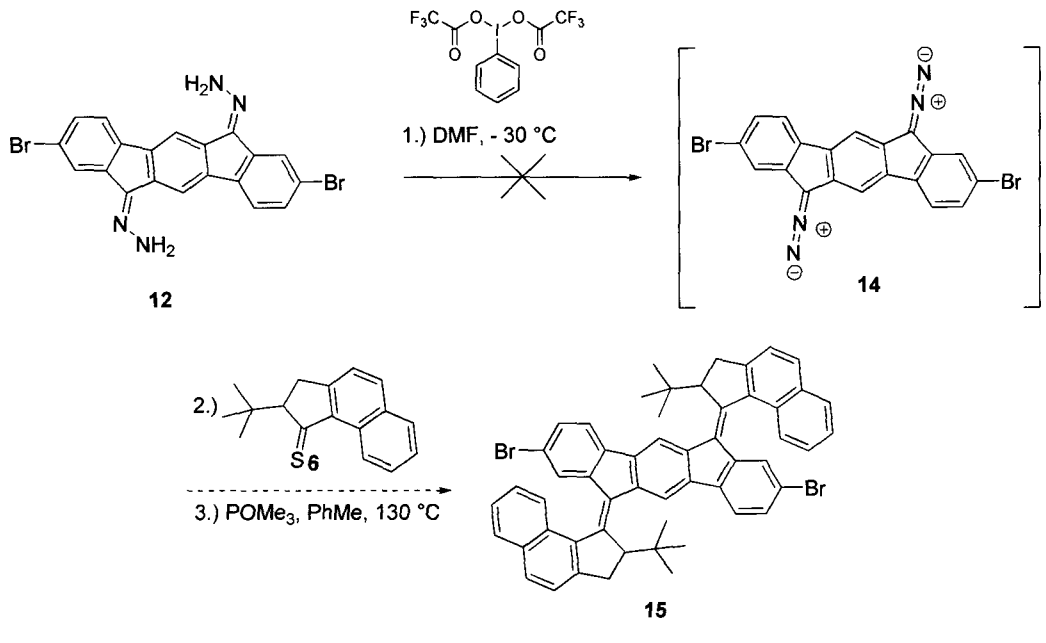

Scheme 4. Unsuccessful approach towards formation of dimotor **15** via dihydrazone **12**.

Due to the lower rotation speed of the methyl-substituted version versus a *t*-butyl (18 rotations per hour vs. 87 rotations per second), the approach to couple the methyl-substituted diazo **8** to a dithioketone double stator was not attempted.

Molecular Design of Ultra-Fast Motorized Nanocar. In 2008, Feringa and co-workers reported the combination of two previously-reported motor halves, a thioxanthenone stator unit and cyclopentane-naphthalene rotor **5b**, a combination which was shown to increase rotation speed into the MHz regime at room temperature.[14b] Inclusion of this motor into a nanocar (Figure 4), while only a slight change in structure from the original motorized nanocar **1**, should exhibit a 10^{12}-fold increase in rotational speed, affording the capability to study light-powered molecular motion of carborane-wheeled nanomachines at both ambient and reduced temperatures.

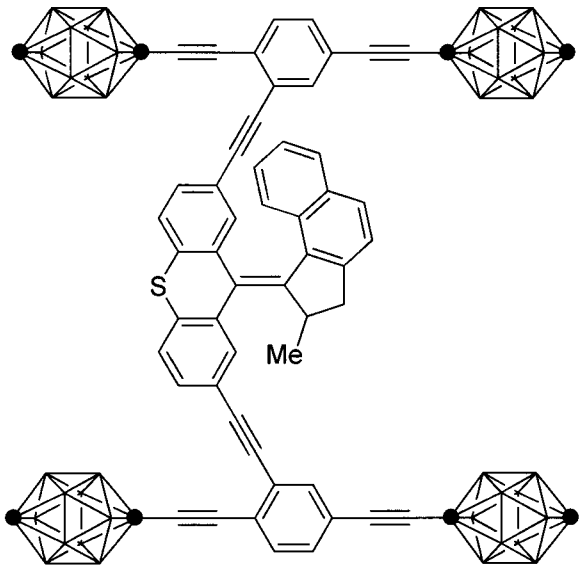

Figure 4. Structure of ultra-fast motorized nanocar **16**.

Synthesis. The synthesis of the ultra-fast motorized nanocar is presented in Schemes 5 and 6. The coupling agents used for the motor synthesis, 2,6-dibromo-thioxanthene-thione **17** and diazo **8**, were constructed using known procedures.[8,14] To carry out the Staudinger-type diazo-thioketone coupling, the thioketone **17** was added to a stirred solution of diazo **8**, freshly prepared by oxidation of the hydrazone using MnO_2 in dichloromethane. The resulting intermediate episulfide was immediately reduced using trimethylphosphite in toluene in a screw-cap tube at 130 °C to form dibrominated molecular motor **18**.

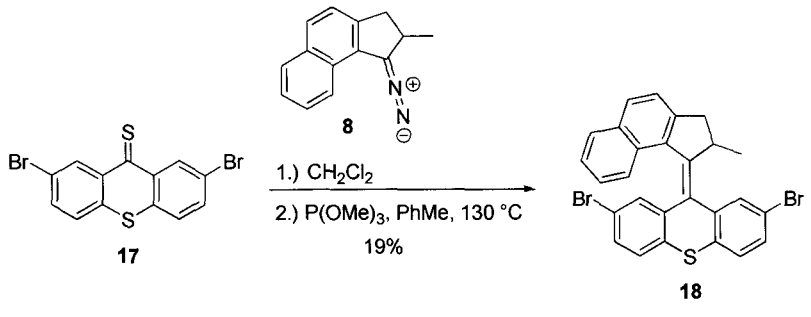

Scheme 5. Synthesis of dibrominated MHz rotational speed molecular motor.

Due to the sterically-hindered and electronically-deactivated nature of the the aryl bromides in motor **18**, alkynylated axle **19**[18] was coupled to molecular motor **18** under Sonogashira conditions using a Fu catalyst system[19] at elevated temperature, giving motorized nanocar **16** in 15 % yield.

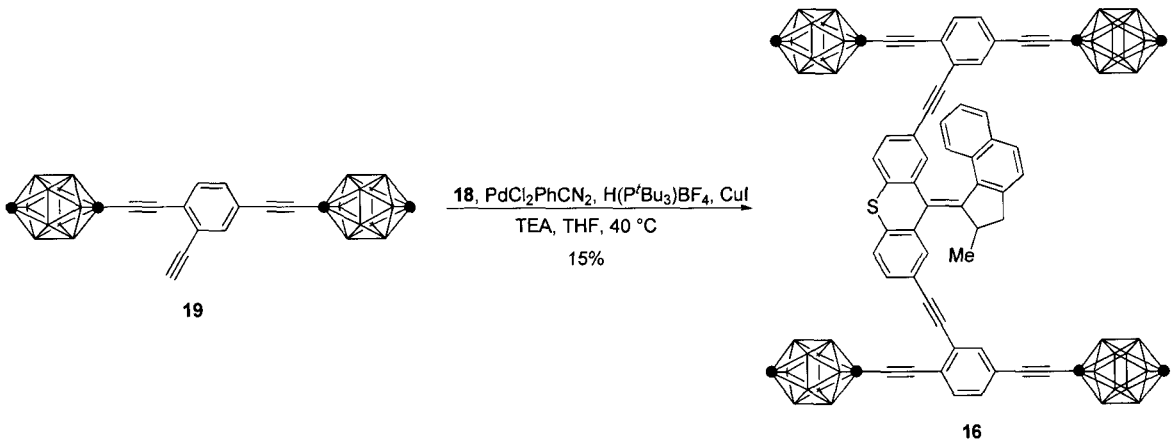

Scheme 6. Completion of synthesis of motorized nanocar **19**.

Conclusions

Studies toward the design and synthesis of two distinct types of motorized nanocars are reported. Indenofluorene-based dual motored nanocars **2** proved to be

difficult to synthesize. The key step, motor formation, was the limiting step in realizing the completion of this class of nanocar. Moreover, the scarcity of literature precedence for multiple oxidations of molecules such as **12** is a testament to the difficulty associated with the construction of such a system (as of this writing, no one has reported such a transformation). On the other hand, construction of nanocars **2** using the opposing method where the TIPS-alkynylated indenofluorenedione is dithionated seems promising, as similar transformations have been reported on substrates containing multiple ketone positions. In addition, oxidations of hydrazones such as **7** have been demonstrated both here and in the literature. It may be possible to explore other diazo coupling partners in the future to construct other doubly-motored nanocars with fast rotation speeds.

Conversely, the synthesis of ultra-fast nanocar **16** was a relatively straightforward process, although the key Staudinger-type diazo-thioketone coupling proceeded in relatively low yield. Although the overall molecular structure represents a slight variance from the original motorized nanocar **1**, we expect a 10^{12}-fold increase in rotation rate in solution and on surfaces, when energy transfer can be mitigated. Future studies of the nanocar's rotation rate using transient absorption spectroscopy and its photoactive behavior on surfaces are planned.

Experimental Section

General Methods. ^{1}H NMR and ^{13}C NMR spectra were recorded at 400 or 500 and 100 or 125 MHz, respectively. Solid-state ^{13}C NMR were recorded at 50 MHz, with a 5 KHz spinning rate and 90° ^{1}H pulse, using glycine as an internal shift reference (176.46

ppm). Proton chemical shifts (δ) are reported in ppm downfield from tetramethylsilane (TMS). Mass spectrometry was performed at the Rice University Mass Spectrometry Laboratory or the University of South Carolina Mass Spectrometry Laboratory. Infrared (IR) spectral assignments have 2 cm^{-1} resolution. All reactions were performed under an atmosphere of nitrogen unless stated otherwise. Reagent grade tetrahydrofuran (THF) was distilled from sodium benzophenone ketyl. Triethylamine (TEA) and CH_2Cl_2 were distilled over CaH_2. TBAF (1.0 M solution in THF), LHMDS (1.0 M solution in THF), bis(trifluoroacetoxy)iodobenzene and $PdCl_2(PhCN)_2$ were purchased from Sigma-Aldrich and used as received. $HP(^tBu)_3BF_4$ was purchased from Strem Chemicals and used as received. Organic starting materials for the synthesis of molecular rotors **6** and **7** as well as 4-bromobenzene-boronic acid were purchased from Acros Organics. Trimethylsilylacetylene (TMSA) was donated by FAR Research Inc. or Petra Research. Flash column chromatography was performed using 230-400 mesh silica gel from EM Science. Thin layer chromatography was performed using glass plates pre-coated with silica gel 40 F_{254} purchased from EM Science. The synthesis of compounds **5a**,[14] **b**,[17] **6**,[14] **7-8**,[17] **9**,[16] **11**[16] and **17**[8] were performed according to literature procedures. Compounds were named using Chemdraw Ultra 11.0.

General Procedure for the Coupling of a Terminal Alkyne with an Aryl Halide Using a Palladium-Catalyzed Cross-Coupling (Sonogashira) Protocol. To an oven-dried round bottom flask equipped with a magnetic stir bar were added the aryl halide, the terminal alkyne, $PdCl_2(PPh_3)_2$ (ca. 2 mol% per aryl halide), and CuI (ca. 4 mol% per aryl halide). A solvent system of TEA and/or THF was added depending on the substrates. Upon completion, the reaction was quenched with a saturated solution of

NH_4Cl. The organic layer was then diluted with hexanes, diethyl ether or CH_2Cl_2, and washed with water or saturated NH_4Cl (1×). The combined aqueous layers were extracted with hexanes, diethyl ether, or CH_2Cl_2 (2×). The combined organic layers were dried over $MgSO_4$, filtered, and the solvent was removed from the filtrate in vacuo to afford the crude product, which was purified by column chromatography (silica gel). Eluents and other slight modifications are described below for each compound.

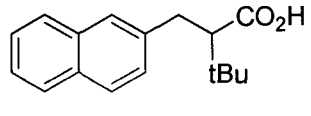

3,3-dimethyl-2-(naphthalen-2-ylmethyl)butanoic acid 4a. To an oven-dried 100 mL round-bottom flask equipped with magnetic stir bar was added LHMDS (9.05 mL, 9.05 mmol, 1.0 M in THF). The mixture was cooled to -78 °C via dry ice/acetone and methyl *tert*-butyl acetate (1.17 g, 9.05 mmol) was added dropwise over the period of 15 min. The mixture was then allowed to stir for 1 h at this temperature. In a separate oven-dried pear-shaped flask, 2-bromomethylnaphthalene (2.0 g, 9.05 mmol) was dissolved in 16 mL THF. This mixture was then added dropwise via cannula to the stirring enolate at -78 °C. The reaction was allowed to stir overnight, followed by quenching with NH_4Cl. The organics were then extracted with CH_2Cl_2 (2 × 40 mL), dried over magnesium sulfate, and dried by rotary evaporation. The crude material was then dispersed in a 1:1 mixture of $EtOH/H_2O$ (15 mL). KOH (2.02 g, 36.2 mmol) was added and the mixture heated in a sealed tube to 120 °C for 2 d. The ethanol was then removed by rotary evaporation, and CH_2Cl_2 (50 mL) was added. The mixture was then stirred and acidified by addition of concentrated HCl (approx. 4 mL). The organics were then separated, dried over $MgSO_4$,

and dried by rotary evaporation. The crude mixture was then purified by column chromatography using 10% EtOAc in hexanes as eluent to give compound **4a** (1.80 g, 79%, 2 steps) as an off-white solid. ^{1}H NMR spectroscopic data were in agreement with literature values.[14a]

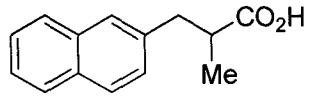

2-methyl-3-(naphthalen-2-yl)propanoic acid 4b. The protocol used was similar to that described for **4a**. Compounds used were LHMDS (61.7 mL, 61.7 mmol, 1.0 M in THF), methyl propionate (5.93 mL, 61.7 mmol), 2-bromonaphthalene (15.0 g, 67.9 mmol in 60 mL THF). Reaction time for the hydrolytic step was 12 h. Materials used in addition to the crude ester product were KOH (4.0 g, 71 mmol) and 1:1 EtOH/H_2O (60 mL). The material was purified as above to yield **4b** (7.1 g, 54%, 2 steps) as a light yellow oil that solidifies upon standing. ^{1}H NMR spectroscopic data were in agreement with literature values.[14a]

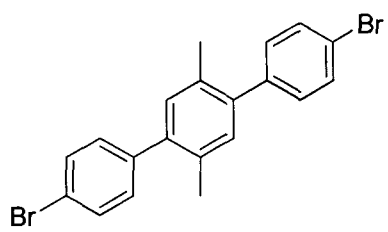

Compound 10. To a 250 mL round-bottom flask was added Ar-degassed H_2O (69.0 mL), K_2CO_3 (19.3 g, 140 mmol), THF (14.0 mL), $Pd(OAc)_2$ (0.156 g, 0.698 mmol), 4-

bromobenzene boronic acid (5.61 g, 27.9 mmol) and 1,4-diiodo-2,5-xylene **9**[16] (5.00 g, 13.9 mmol). The flask was fitted with a reflux condenser and allowed to stir at 65 °C overnight. The organics were then separated using CH_2Cl_2 (100 mL), dried over $MgSO_4$, and the solvent was removed using rotary evaporation. The solid mixture was then re-dissolved in hot CH_2Cl_2 (50 mL) and allowed to cool immediately to 5 °C after which the product, a white precipitate, formed. The solid was filtered to give 0.99 g (18%) of **10**. Additionally, the mother liquor was chromatographed using silica flash chromatography and 100% hexanes as eluent to yield a total (including precipitated product) of 3.70 g (64%) of **10** as a white solid. ^{1}H NMR data were in agreement with reported literature values.[16]

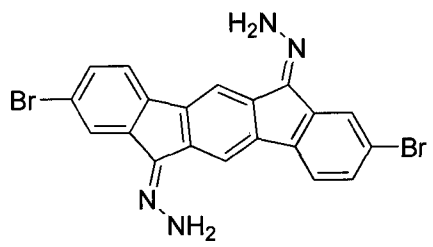

(2,8-dibromoindeno[1,2-b]fluorene-6,12-diylidene)bis(hydrazine) 12. **11** (0.416 g, 1.00 mmol) was suspended in a 1:1 mixture of hydrazine monohydrate:EtOH (200 mL). The purplish slurry was allowed to stir at 90 °C for 12 h, during which the color changed from purple to yellow. The mixture was cooled, poured into 200 mL H_2O, and the precipitate was collected by filtration. Multiple washings with warm EtOH and THF, followed by drying in vacuo yielded **12** (0.355 g, 76%) as a pale yellow solid. Due to the insoluble nature of the compound, solution-state NMR spectra could not be obtained. CPMAS NMR (50 MHz) δ 144.3, 139.4, 136.5, 130.8, 121.0, 117.8, 110.3; FTIR (KBr)

2359, 1625, 1603, 1585, 1438, 1410, 1298, 1261, 1167, 1063 cm^{-1}; DI-MS *m/z* calcd for $C_{20}H_{12}Br_2N_4$ 465.94, found 465.93.

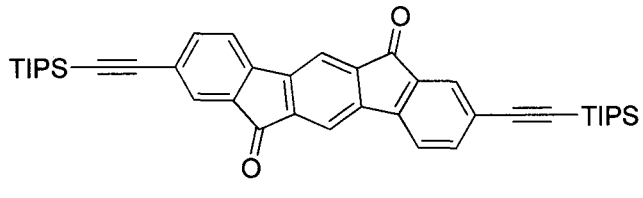

2,8-bis((triisopropylsilyl)ethynyl)indeno[1,2-b]fluorene-6,12-dione 13. 11 (0.600 g, 1.36 mmol), $PdCl_2(PhCN)_2$ (0.052 g, 0.136 mmol), $HP^tBu_3BF_4$ (0.118 g, 0.408 mmol) and CuI (0.011 g, 0.060 mmol) were added to an oven-dried pressure tube reactor with stir bar under nitrogen. PhMe (20 mL) and Et_3N (20 mL) were then added followed by TIPSA (0.920 mL, 4.08 mmol), and the tube was sealed with a Teflon screw-cap. The mixture was then heated to 80 °C and stirred for 18h, after which the insoluble reddish-purple slurry turned to an electric-red solution. The crude reaction mixture was then subjected to the standard workup protocol for Sonogashira couplings (see above) with an extra washing of 1×10^{-3} M EDTA (50 mL, dibasic) during separation. The crude mixture was then purified via column chromatography using 30% CH_2Cl_2 in hexanes as eluent to give 0.560 g, 64% of **13** as a red solid. FTIR (KBr) 2939, 2862, 1715, 1444, 1384, 1123, 828, 776 cm^{-1}; ^1H NMR (400 MHz, $CDCl_3$) δ 7.80 (s, 1H), 7.76 (dd, J_1 = 1.5 Hz, J_2 = 0.6 Hz, 2 H), 7.66 (d, J = 1.5 Hz, 1H), 7.64 (d, J = 1.5 Hz, 1H), 7.51 (d, J = 0.6 Hz, 1H)), 7.49 (d, J = 0.6 Hz, 1H), 1.1 (s, 42H); ^{13}C NMR (100 MHz, $CDCl_3$) δ 192.2, 145.8, 142.9, 139.8, 138.9, 134.1, 128.3, 125.3, 120.7, 116.6, 105.9, 94.0, 18.9, 11.5; HRMS *m/z* calcd for $C_{42}H_{50}O_2Si_2$ 642.3349, found 642.3349.

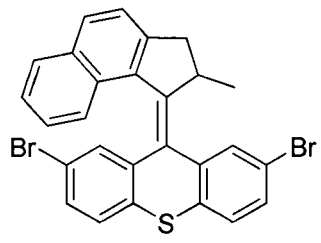

2,7-dibromo-9-(2-methyl-2,3-dihydro-1*H*-cyclopenta[a]naphthalen-1-ylidene)-9*H*-thioxanthene 18. Azo **8** was freshly prepared by reacting hydrazone **7** (0.200 g, 0.950 mmol) with active MnO_2 (0.290 g, 3.33 mmol) in dry CH_2Cl_2 (4.00 mL) in the presence of $MgSO_4$ (0.100 g) for 2 h at -5 °C. The resulting slurry was gravity filtered to yield a reddish-brown solution of azo **8**. To this solution was added thioketone **17**[8] (0.366 g, 0.950 mmol) at room temperature under nitrogen. After approximately 20 s, the solution began to rapidly evolve nitrogen, indicating successful reaction. The solution was allowed to stir another 12 h, after which an insoluble precipitate was filtered away. The filtrate was then washed with H_2O (100 mL) and the organics were extracted, dried over $MgSO_4$, and the solvent was removed by rotary evaporation. The crude product was then added to a pressure-tube reactor with stir-bar followed by PhMe (5.00 mL) and $P(OMe)_3$ (1.00 mL, 8.48 mmol). The tube was sealed with a teflon screw-cap and allowed to stir at 130 °C for 18 h. The mixture was then washed with copious amounts of water to remove the $P(OMe)_3$ and the organics were extracted with CH_2Cl_2. The organics were then dried over $MgSO_4$, passed through a short silica plug using 1:1 CH_2Cl_2:hexanes as eluent, and the solvent removed by rotary evaporation. The residual solid was then purified via column chromatography using 10% CH_2Cl_2 in hexanes as eluent to give 0.101 g (19%, 2 steps) of **18** as a light yellow solid. FTIR (KBr) 3050, 2955, 2922, 2842, 1437, 1382,

1082, 807 cm^{-1}; ^1H NMR (500 MHz, $CDCl_3$) δ 7.89 (d, J = 2.1 Hz, 1H), 7.79 (d, J = 8.2 Hz, 1H), 7.74 (d, J = 8.5 Hz, 1H), 7.45 (m, 2H), 7.42 (d, J = 8.3 Hz, 1H), 7.36 (dd, J_1 = 8.3 Hz, J_2 = 2.1 Hz 1H), 7.24 (m, 1H), 7.13 (dd, J_1 = 8.3 Hz, J_2 = 2.1 Hz 1H), 6.86 (m, 1H), 6.80 (d, J = 2.1 Hz 1H), 6.78 (d, J = 8.5 Hz, 1H), 4.19 (qd, J_1 = 6.6 Hz, J_2 = 6.6 Hz, 1H), 3.66 (dd, J_1 = 16 Hz, J_2 = 6.6 Hz, 1H), 2.67 (d, J = 16 Hz, 1H), 0.83 (d, J = 6.6 Hz, 3H); ^{13}C NMR (125 MHz, $CDCl_3$) δ 148.4, 146.5, 141.8, 139.7, 135.8, 135.0, 134.6, 134.3, 133.4, 131.8, 131.1, 130.9, 129.43, 129.37, 129.3, 128.89, 128.85, 128.3, 125.94, 125.2, 124.7, 124.0, 120.9, 120.6, 39.9, 38.0, 19.9; MS m/z calcd for $C_{27}H_{18}Br_2S$ 533.94, found 534.00.

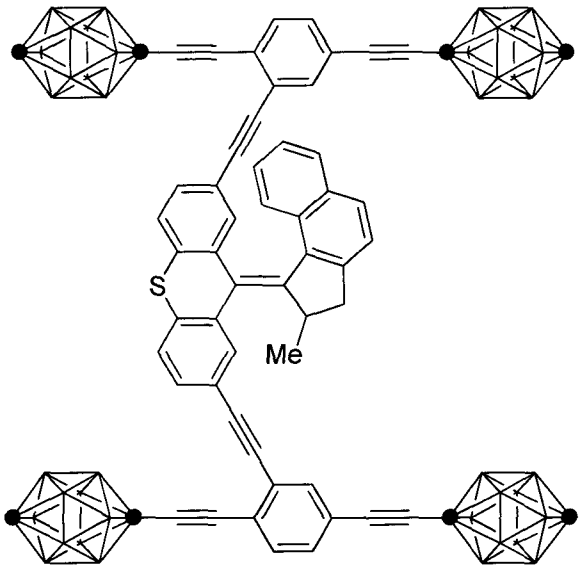

Motorized Nanocar 16. See the general procedure for Sonogashira couplings. Materials used were alkyne axle **19** (0.056 g, 0.129 mmol), motor **18** (0.023 g, 0.043 mmol), $PdCl_2PhCN_2$ (0.008 g, 0.021 mmol), $HP^tBu_3BF_4$ (0.018 g, 0.063 mmol) and CuI (0.004 g, 0.0021 mmol). The mixture was heated to 40 °C and allowed to stir overnight. Workup

according to the standard procedure and purification on silica gel using 10% CH_2Cl_2:hexanes yielded 0.008 g (15%) of nanocar **16** as a yellow solid. FTIR (KBr) 2957, 2923, 2852, 2615, 1614, 1463, 1384, 1261, 1084 cm^{-1}; ^1H NMR (500 MHz, $CDCl_3$) δ 7.89 (d, J = 1.9 Hz, 1H), 7.71 (d, J = 8.2 Hz, 1H), 7.63 (d, J = 9.0 Hz, 1H), 7.57 (d, J = 8.1 Hz, 1H), 7.55 (dd, J_1 = 8.1 Hz, J_2 = 0.34 Hz 1H), 7.41 (d, J = 8.2 Hz, 1H), 7.37 (dd, J_1 = 1.7 Hz, J_2 = 0.52 Hz, 1H), 7.36 (dd, J_1 = 8.0 Hz, J_2 = 1.7 Hz, 1H), 7.25-7.19 (m, 4H), 7.15 (dd, J_1 = 8.1 Hz, J_2 = 1.7 Hz 1H), 7.11-7.09 (m, 2H), 7.03 (dd, J_1 = 8.2 Hz, J_2 = 1.6 Hz, 1H), 6.90 (dd, J_1 = 1.8 Hz, J_2 = 0.39 Hz, 1H), 6.87 (d, J = 1.2 Hz, 1H), 4.32 (qd, J_1 = 6.1 Hz, J_2 = 6.1 Hz, 1H), 3.81 (dd, J_1 = 16 Hz, J_2 = 6.1 Hz, 1H), 3.30-1.60 (br, 45H, includes one proton from motor), 0.86 (d, J = 6.6 Hz, 3H) integration of aryl signals not corresponding to the nanocar indicate an inseparable impurity in the amount of 10% (see attached spectrum in supporting information of this chapter); ^{13}C NMR (125 MHz, $CDCl_3$) δ 147.7, 146.5, 140.2, 137.9, 136.8, 136.3, 135.1, 134.9, 134.4, 133.1, 132.2, 131.9, 131.7, 130.9, 130.7, 130.5, 129.7, 129.4, 128.7, 128.1, 127.9, 127.6, 126.7, 126.5, 126.45, 125.8, 125.0, 124.5, 123.9, 123.8, 123.7, 121.9, 121.7, 121.0, 94.5, 94.1, 91.4, 91.1, 88.1, 87.9, 87.3, 86.6, 69.6, 69.3, 60.6, 42.7, 40.8, 40.2, 38.2, 19.9; DI *m/z* calcd for $C_{59}H_{68}B_{40}S$ 1242, found 1243 [M+H].

References and Notes

(1) Feringa, B. L. *J. Org. Chem.* **2007**, *72*, 6635-6652 and references contained therein.

(2) a) Vives, G.; Rapenne, G. *Tetrahedron* **2008**, *64*, 11462-11468. b) Burdick, J. ; Laocharoensuk, R. ; Wheat, P. M. ; Posner, J. D. ; Wang, J. *J. Am. Chem. Soc.* **2008**, *130*,

8164-8165. c) Vives, G.; Gonzalez, A.; Jaud, J.; Launay, J.-P.; Rapenne, G. *Chem. – Eur. J.* **2007**, *13*, 5622-5631. d) Hawthorne, M. F.; Ramachandran, B. M.; Kennedy, R. D.; Knobler, C. B. *Pure Appl. Chem.* **2006**, *78*, 1299-1304. e) Jian, H.; Tour, J. M. *J. Org. Chem.* **2003**, *68*, 5091-5103. f) Sestelo, J. P.; Kelly, T . R. *Appl. Phys. A* **2002**, *75*, 337-343. g) Kelly, T. R. *Acc. Chem. Res.* **2001**, *34*, 514-522 h) Takeuchi, M.; Ikeda, M.; Sugasaki, A.; Shinkai, S. *Acc. Chem. Res.* **2001**, *34*, 865-873

(3) a) Kay, E. R.; Leigh, D. A. *Pure Appl. Chem.* **2008**, *80*, 17-29. b) Badjic′, J. D.; Ronconi, C. M.; Stoddart, J. F.; Balzani, V.; Silvi, S.; Credi, A. *J. Am. Chem. Soc.* **2006**, *128*, 1489-1499. c) Murakami, H.; Kawabuchi, A.; Matsumoto, R.; Ido, T.; Nakashima, N. *J. Am. Chem. Soc.* **2005**, *127*, 15891-15899. d) Wang, Q.-C.; Qu, D.-H.; Ren, J.; Chen, K.; Tian, H. *Angew. Chem.* **2004**, *116*, 2715 – 2719; *Angew. Chem., Int. Ed.* **2004**, *43*, 2661-2665. e) Badjic′, J. D.; Balzani, V.; Credi, A.; Silvi, S.; Stoddart, J. F. *Science* **2004**, *303*, 1845-1849. f) Stanier, C. A.; Alderman, S. J.; Claridge, T . D. W.; Anderson, H. L. *Angew. Chem.* **2002**, *114*, 1847-1850; *Angew. Chem., Int. Ed.* **2002**, 41,1769 – 1772. g) Wurpel, G. W. H.; Brouwer, A. M.; van Stokkum, I. H. M.; Farran, A.; Leigh, D . A. *J. Am. Chem. Soc.* **2001**, *123*, 11327-11328. h) Ashton, P. R.; Ballardini, R.; Balzani, V.; Boyd, S. E.; Credi, A.; Gandolfi, M. T.; Gomez-Lopez, M.; Iqbal, M. S.; Philp, D.; Preece, J. A.; Prodi, L.; Ricketts, H. G.; Stoddart, J. F.; Tolley, M. S.; Venturi, M.; White, A. J. P.; Williams, D. J. *Chem.- Eur. J.* **1997**, *3*, 152-170. i. Bissell, R. A.; Cordova, E.; Kaifer, A. E.; Stoddart, J. F. *Nature* **1994**, *369*, 133-137. j) Anelli, P. L.; Spencer, N.; Stoddart, J. F. *J. Am. Chem. Soc.* **1991**, *113*, 5131-5133.

(4) a) Xia, F.; Guo, W.; Mao, Y. ; Hou, X. ; Xue, J.; Xia, H.; Wang, L.; Song, Y.; Ji, H.; Ouyang, Q.; Wang, Y.; Jiang, L. *J. Am. Chem. Soc.* **2008**, *130*, 8345-8350. b) Muthukrishnan, G.; Hutchins, B. M.; Williams, M. E.; Hancock, W. O. *Small* **2006**, *2*, 626-630. c) Kelly T. R. *Angew. Chem., Int. Ed.* **2005**, *44*, 4124-4127. d) Sherman, W. B.; Seeman, N. C. *Nano Lett.* **2004**, *4*, 1203-1207. e) Shin, J. S.; Pierce, N. A. *J. Am. Chem. Soc.* **2004**, *126*, 10834-10835. f) Ye, T.; Mao, C. *J. Am. Chem. Soc.* **2004**, *126*, 11410-11411. g) Yin, P.; Yan, H.; Daniell, X. G.; Turberfield, A. J.; Reif, J. H. *Angew. Chem.* **2004**, *116*, 5014-5019; *Angew. Chem., Int. Ed.* **2004**, *43*, 4906-4911.

(5) a) Klok, M.; Boyle, N.; Pryce, M.; Meetsma, A.; Browne, W. R.; Feringa, B. L. *J. Am. Chem. Soc.* **2008**, *130*, 10484-10485. b) Hernandez, J. V.; Kay, E. R.; Leigh, D. A. *Science* **2004**, *306*, 1532-1537. c) Dahl, B. J.; Branchaud, B. P. *Tetrahedron Lett.* **2004**, *45*, 9599-9602. d) Leigh, D. A.; Wong, J. K. Y.; Dehez, F.; Zerbetto, F. *Nature* **2003**, *424*, 174-179. e) Kelly, T. R.; Silva, R. A.; De Silva, H.; Jasmin, S.; Zhao, Y. J. *J. Am. Chem. Soc.* **2000**, *122*, 6935-6949. f) Kelly, T. R.; De Silva, H.; Silva, R. A. *Nature* **1999**, *401*, 150-152.

(6) For a recent review see: a) Vives, G.; Tour, J. M. *Acc. Chem. Res.* **2009**, *42*, 473-487., and references therein. b) Khatua, S. ; Guerrero, J. M.; Claytor, K.; Vives, G.; Kolomeisky, A. B.; Tour, J. M. ; Link, S. *ACS Nano* **2009**, *3*, 351-356. For a review of early work see: c) Shirai, Y.; Morin, J. -F.; Sasaki, T.; Guerrero, J. M.; Tour, J. M. *Chem. Soc. Rev.* **2006**, *35*, 1043-1055., and references therein.

(7) Shirai, Y.; Osgood, A.; Zhao, Y.; Kelly, K. F.; Tour, J. M. *Nano Lett.* **2005**, *5*, 2330-2334.

(8) Morin, J. -F.; Shirai, Y.; Tour, J. M. *Org. Lett.* **2006**, *8*, 1713-1716.

(9) Shirai, Y.; Sasaki, T.; Guerrero, J. M.; Yu, B. C. ; Hodge, P.; Tour, J. M. *ACS Nano* **2008**, *2*, 97-106.

(10) Koumura, N.; Geertsma, E. M.; van Gelder, M. B.; Meetsma, A.; Feringa, B. L. *J. Am. Chem. Soc.* **2002**, *124*, 5037-5051.

(11) unpublished results

(12) For reviews on the manipulation of single molecules by STM see: a) Rosei, F.; Schunack, M.; Naitoh, Y.; Jiang, P.; Gourdon, A.; Laegsgaard, E.; Stensgaard, I.; Joachim, C.; Besenbacher, F. *Prog. Surf. Sci.* **2003**, *71*, 95-146. b) Chiang, S. *Chem. Rev.* **1997,** *97*, 1083-1096 c) Piorier, G. E. *Chem. Rev.* **1997,** *97*, 1117-1127 d) Acc. *Chem. Res.* **1995,** *28*, 95-102.

(13) a) Koumura, N.; Zijlstra, R. W. J.; van Delden, R. A.; Harada, N.; Feringa, B. L. *Nature* **1999**, *401*, 152-155. b) Koumura, N.; Geertsma, E. M.; Meetsma, A.; Feringa, B. L. *J. Am. Chem. Soc.* **2000,** *122,* 12005-12006.

(14) a) Vicario, J.; Walko, M.; Meetsma, A.; Feringa, B.L. *J. Am. Chem. Soc.* **2006**, *128*, 5127-5135. b) Klok, M.; Boyle, N.; Pryce, M.; Meetsma, A.; Browne, W. R.; Feringa, B. L. *J. Am. Chem. Soc.* **2008**, *130*, 10484-10485.

(15) a) Barton, D. H. R.; Willis, B. J. *J. Chem. Soc., Chem. Commun.* **1970**, 1225. b) Barton, D. H. R.; Smith, E. H.; Willis, B. J.; *J. Chem. Soc., Chem. Commun.* **1970**, 1226. c) Barton, D. H. R.; Willis, B. J.; *J. Chem. Soc., Perkin Trans. 1.* **1972**, 305. d) Staudinger, H.; Siegwart, J. *Helv. Chim. Acta* **1920**, *3*, 833.

(16) Vak, D.; Lim, B.; Lee, S.-H.; Kim, D.-Y. *Org. Lett* **2005**, *7*, 4229-4232.

(17) ter Wiel, M. K. J.; Vicario, J.; Davey, S. G.; Meetsma, A.; Feringa, B. L. *Org. Biomol. Chem.* **2005**, *3*, 28-30.

(18) Takashi Sasaki Ph.D. thesis, Rice University.

(19) Netherton, M. R.; Fu, G. C. *Org. Lett.* **2001**, *3*, 4295-4298.

Supporting Information for Chapter 2.1

Guerrero's dibromo-bis(hydrazo) aromatic compound. 4mm probe.
CPMAS with 5 kHz spinning (so that spinning sidebands are + or - 99 ppm from a centerband).
90degree 1H pulse = 2.96 usec at pl12 = 3.0 dB. 1-ms contact time.
H-H match optimized: 13C pl1 = 1.9 dB and 1H pl2 = 8.0 dB.
32.9-ms FID with TPPM decoupling (pl12 = 3.0 dB); p31 optimized at 5.0 usec.
5-s relaxation delay. 1000 scans. lb = 5 Hz (0.1 ppm).
Chemical shifts relative to glycine carbonyl defined as 176.46 ppm (sr = 152.34).

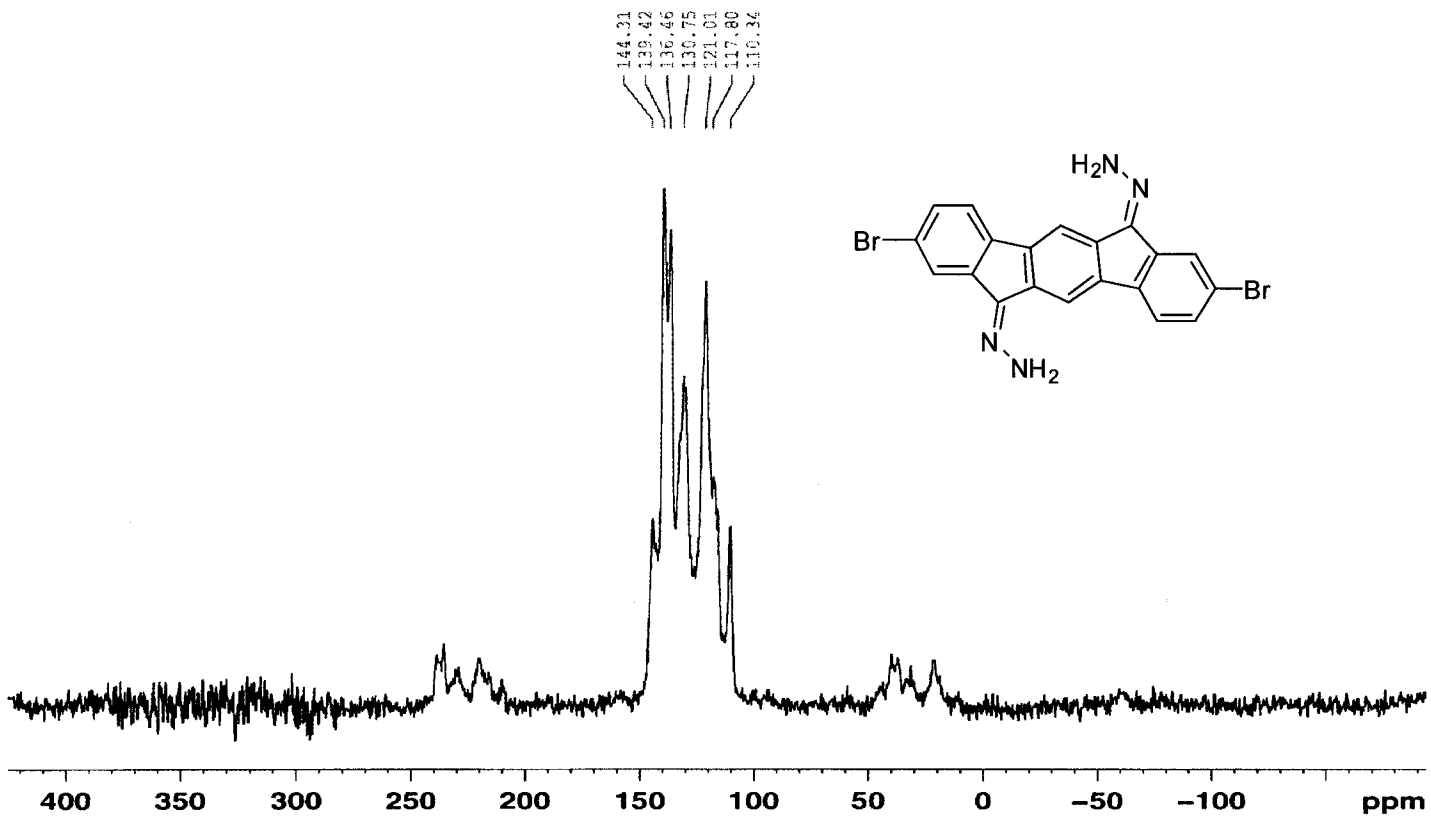

Figure S-2.1-1. ^{1}H NMR Spectrum of Compound **12**.

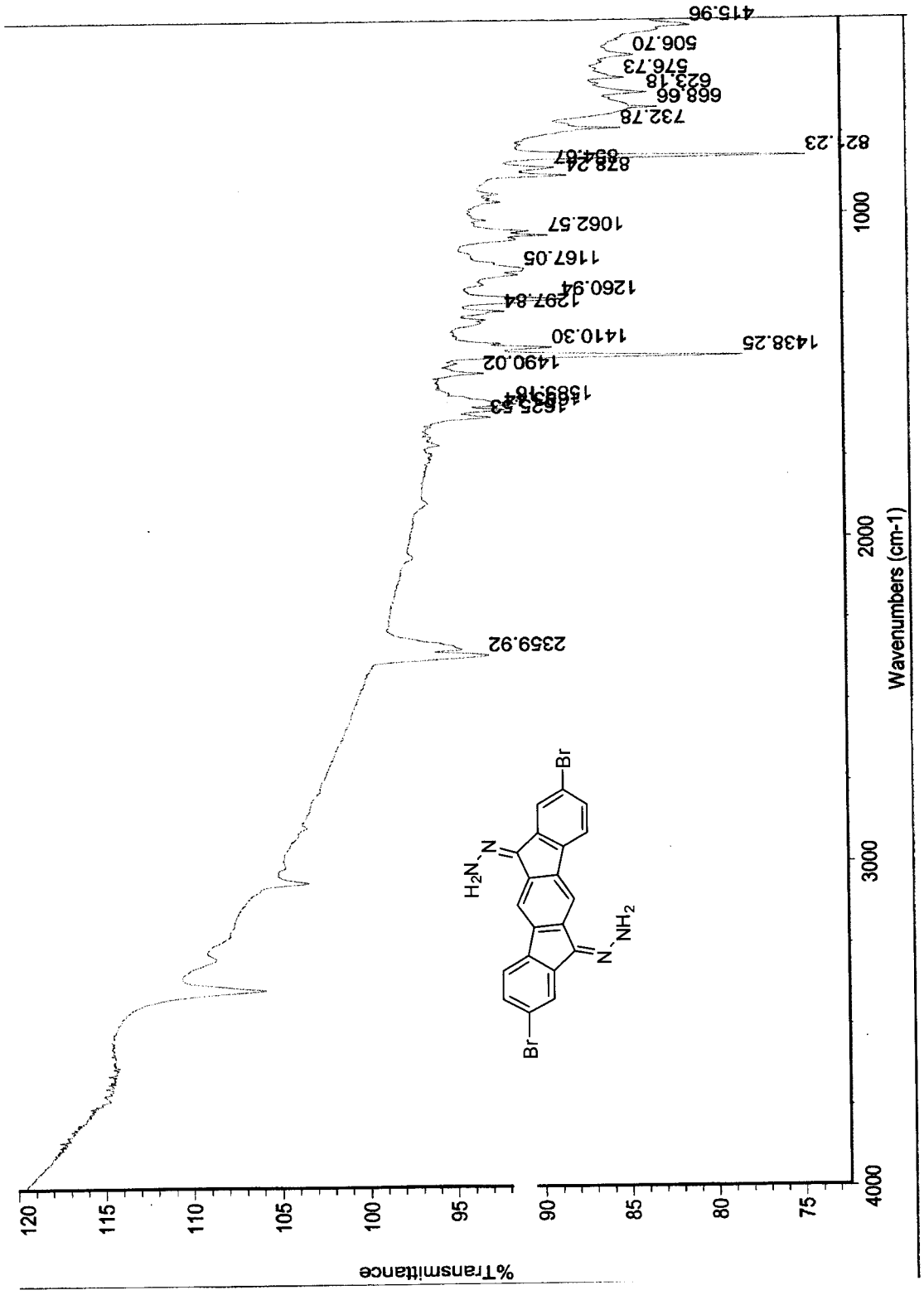

Figure S-2.1-2. IR Spectrum of Compound **12**.

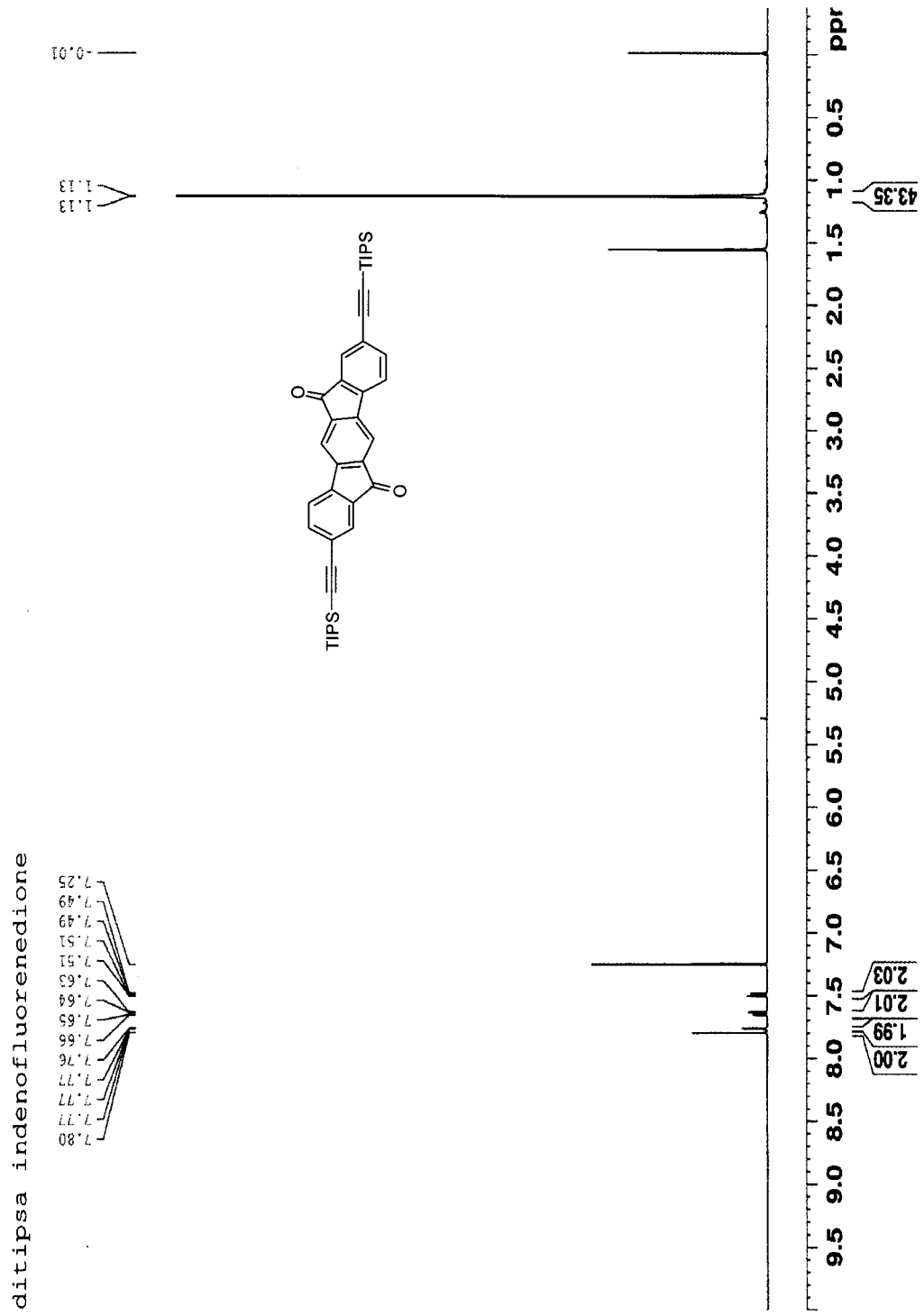

Figure S-2.1-3. ^{1}H NMR Spectrum of Compound **13**.

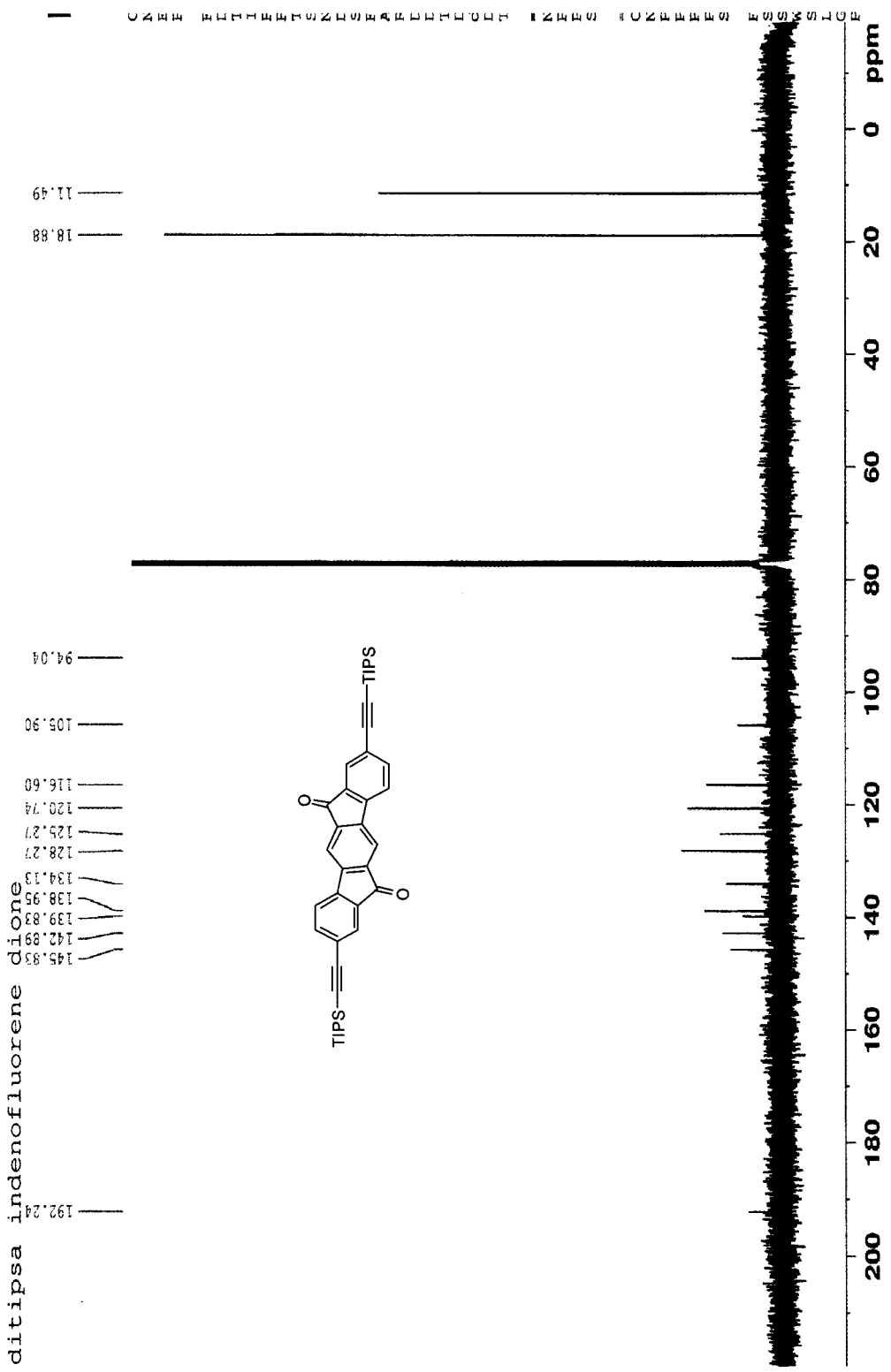

Figure S-2.1-4. ^{13}C NMR Spectrum of Compound **13**.

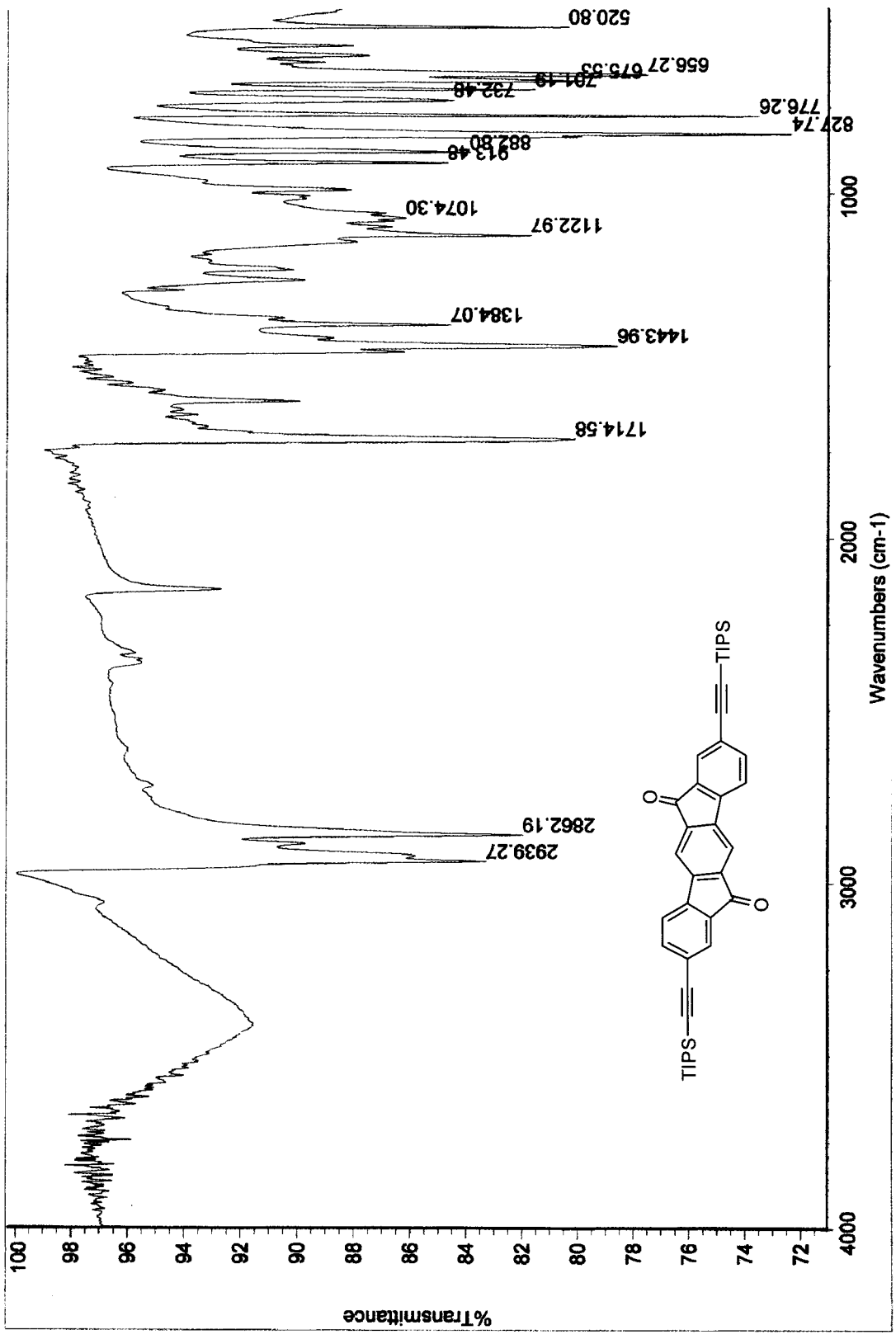

Figure S-2.1-5. IR Spectrum of Compound **13**.

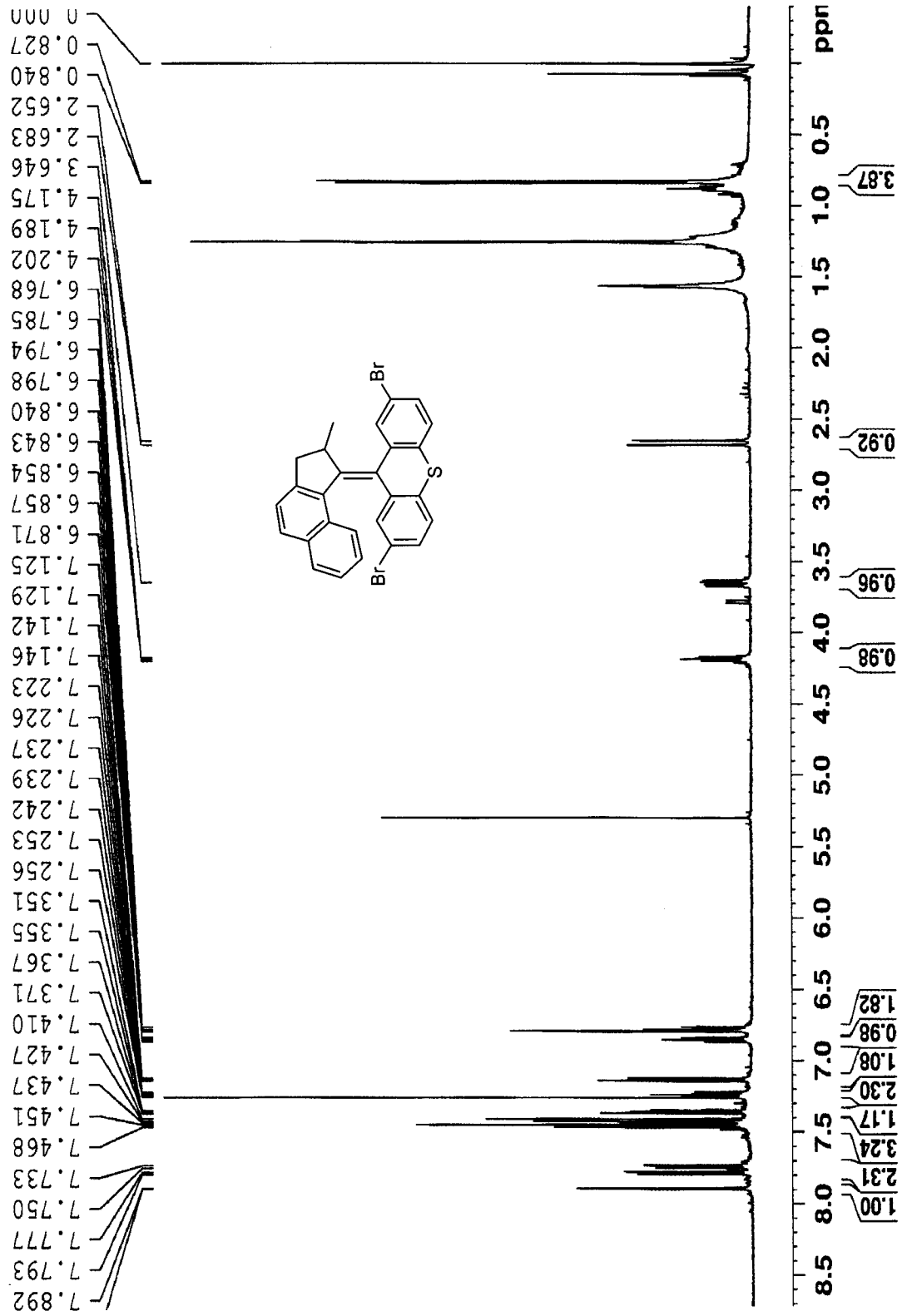

Figure S-2.1-6. ^{1}H NMR Spectrum of Compound **18**.

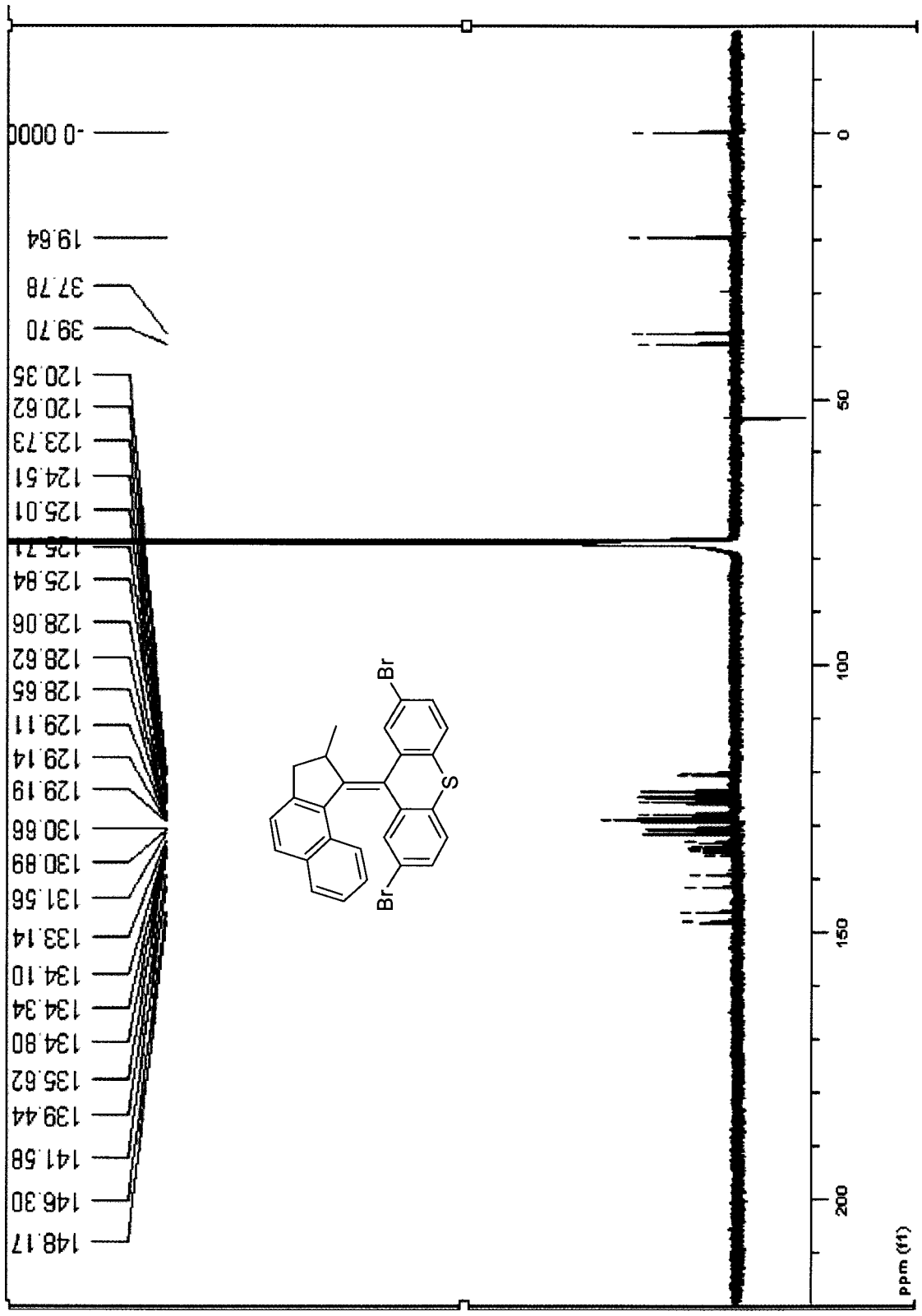

Figure S-2.1-7. ^{13}C NMR Spectrum of Compound **18**.

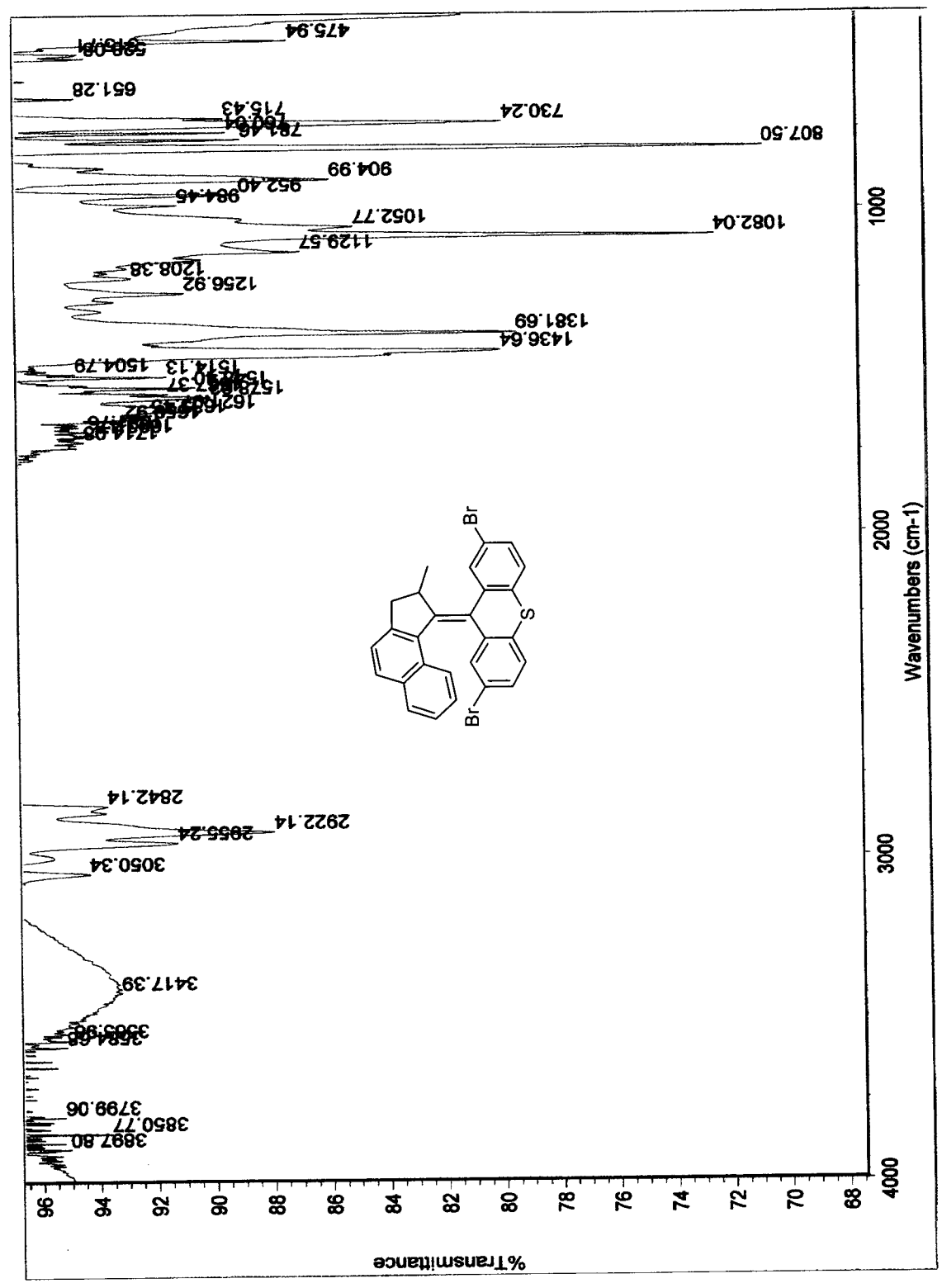

Figure S-2.1-8. IR Spectrum of Compound **18**.

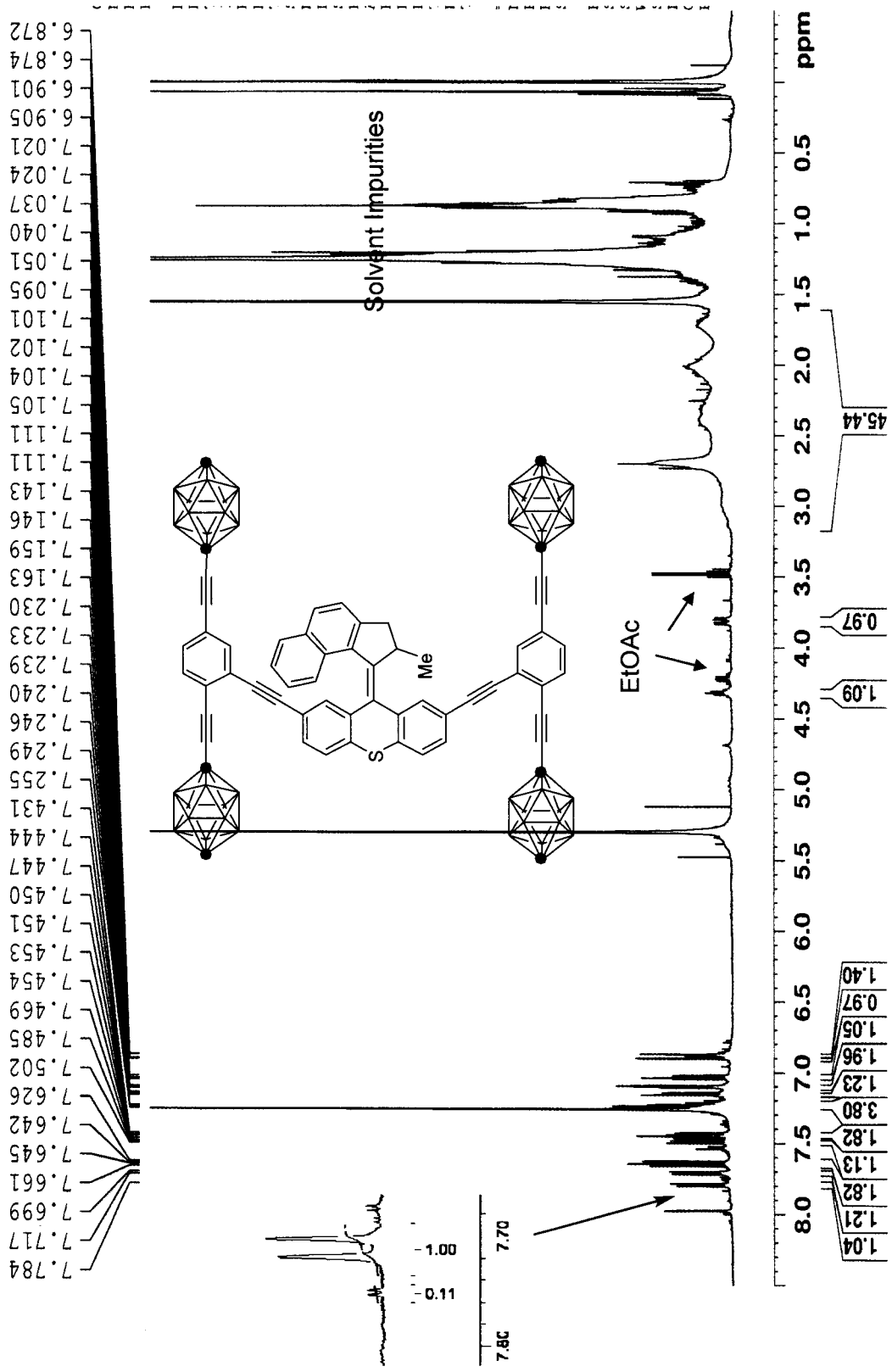

Figure S-2.1-9. ^{1}H NMR Spectrum of Nanocar **16**. Inset represents integration of impurity.

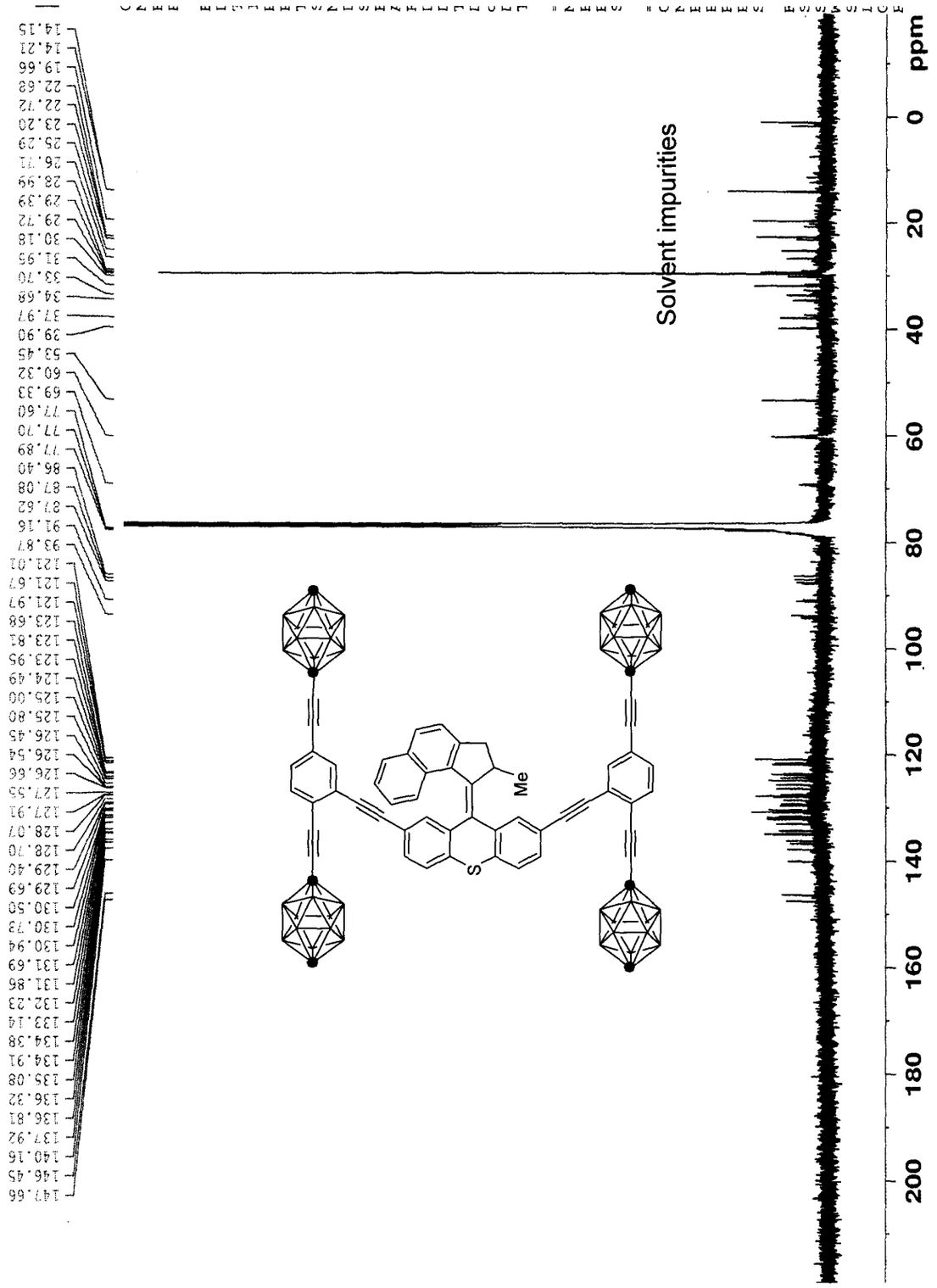

Figure S-2.1-10. ^{13}C NMR Spectrum of Nanocar **16**.

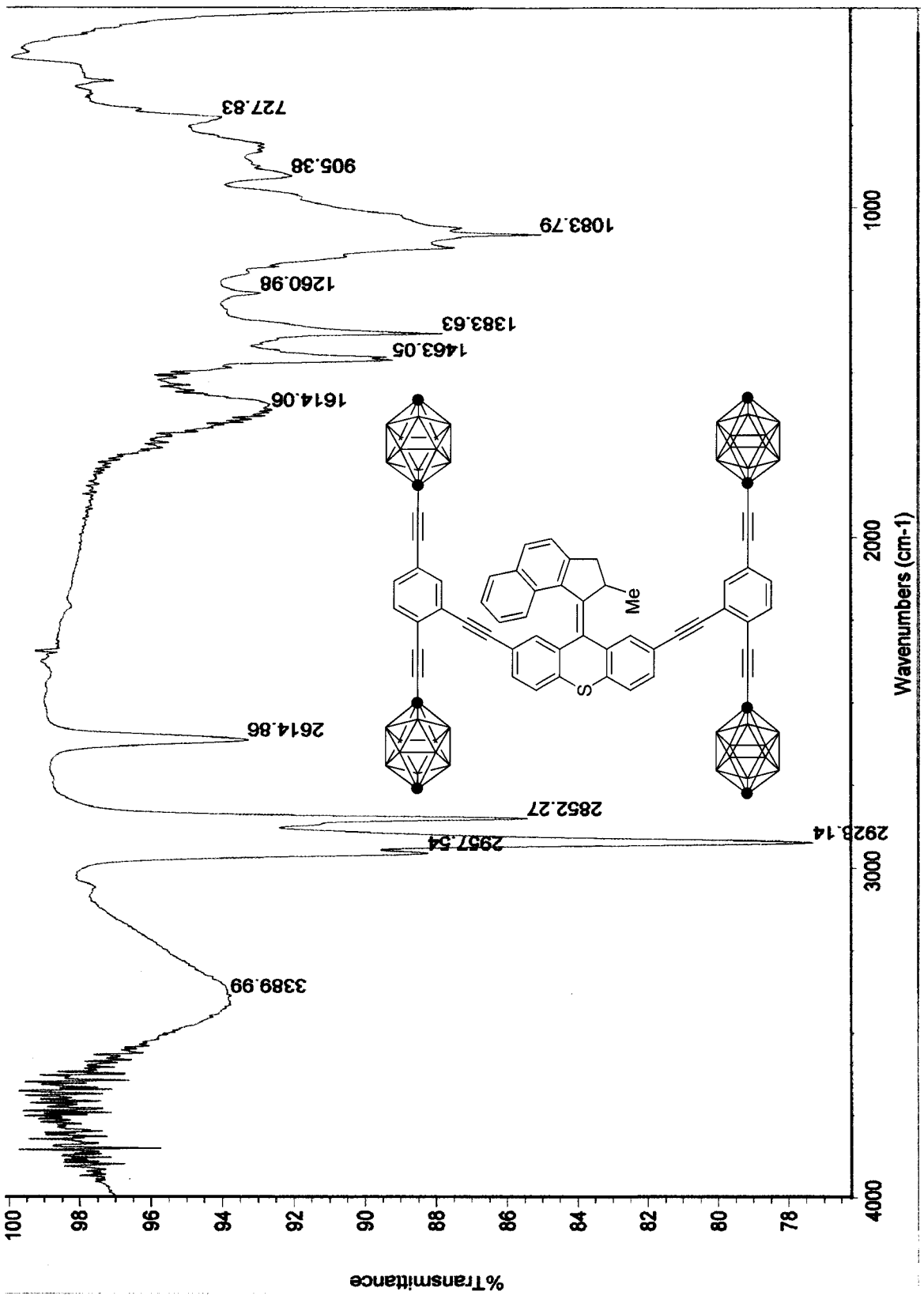

Figure S-2.1.11. IR Spectrum of Nanocar **16**.

Chapter 3

Synthesis and Studies of Fluorescently-Tagged Nanomachines

3.1

Micrometer-Scale Translation and Monitoring of Individual Nanocars on Glass

Introduction

Science and engineering on the nanoscale offers novel possibilities for the design and synthesis of functional materials. In contrast to the engineering of macroscopic objects where large pieces of materials are formed into smaller building blocks, nanoscale engineering is driven by a bottom-up materials synthesis. Inspiration for this approach can be drawn from nature where self-assembly of smaller molecules into larger networks through often weak interactions play an important role. Nanomachines are promising new materials that are designed to exhibit controlled mechanical motions resembling macroscopic rotors,[1-4] elevators,[5] shuttles,[6-8] ratchets,[9] turnstiles,[10] scissors,[11] and muscles.[12] Performing electronic and mechanical operations with specifically designed molecules presents the ultimate limit of miniaturization and has a profound impact on many diverse fields ranging from molecular computing to medicine. Among the most important tasks for molecular machines is the directed transport of molecules and charges. To accomplish molecular directed motion and transport, molecular machines that resemble the chassis and wheels of a car, hence called nanocars, have been synthesized.[13-15] The rotation of the nanocar wheels is thought to induce a directional rolling of the nanocars on a surface.[15] Understanding the mechanisms by which these molecular machines work under different conditions is crucial for the future design of even more complex machines and essential for finding novel ways to control the forces that are responsible for their mechanical nanoscale motion.

Ensemble characterization techniques often fail to measure the detailed mechanical action of molecular machines as a random alignment of the individual

molecules can lead to an orientational averaging, which is particularly problematic for the two-dimensional motion of a nanocar on a flat surface. Thermally activated rolling of individual fullerene-wheeled nanocars has previously been studied by scanning tunneling spectroscopy (STM) on a gold surface.[15] While STM is extremely powerful in resolving atomic scale details of single molecules,[16] the substrate surface must be conductive. As a complementary single molecule technique fluorescence imaging[17-19] is capable of monitoring the motion of single molecules on non-conductive glass. Although the resolution of optical single molecule spectroscopy is limited by diffraction, localization of individual molecules below 100 nm down to a few nanometers has become possible for large photon count rates[17,19] while, at the same time, acquiring images that are tens of microns large.

Here, we report on the translational motion of single dye-labeled carborane-wheeled nanocars on a glass surface, studied for the first time by single molecule fluorescence spectroscopy. Using polarization sensitive fluorescence detection in combination with a comparative analysis that employed three-wheeled nanocars and the dye tag only, we were able to investigate possible mechanisms for the movement of carborane-wheeled nanocars. Our results are consistent with a wheel-like rolling of the nanocars.

Imaging of the nanomachines was performed by S. Khatua, and I was responsible for molecular design and synthesis of the nanocar and trimer (synthetic details are reported in the following section). Dr. G. Vives performed TRITC tagging of the trimer, and K. Claytor developed the tracking program to monitor the motion of the nanovehicles.[30]

Results and Discussion

Fluorescence visualization of the nanocars with 532 nm excitation light was achieved by first attaching an appropriate dye label (tetramethylrhodamine isothiocyanate, TRITC) to the end of the nanocar chassis (Figure 1A). TRITC tagging of the nanocars was accomplished through an aniline-bearing nanocar reacting with the isothiocyanate residue on the fluorophore (supporting info). At room temperature without thermal activation, the dye-labeled carborane-wheeled nanocars showed significant displacement in successively scanned fluorescence images directly confirming movement of the nanocars on a glass surface. Individual nanocars were isolated on a glass surface by spin-casting from a 10^{-12} mol/L dimethylformamide (DMF) solution. Single photobleaching steps in fluorescence-time trajectories confirmed the presence of single molecules within the diffraction limited fluorescence signal.[19] 10 x 10 μm fluorescence images were acquired by scanning the sample over a focused laser beam in a home-built confocal microscope setup (Figure 1B). Movement of a single nanocar is shown in the images in Figs. 1C - 1F. The images were acquired continuously every 30 sec for a total time of 5 min.

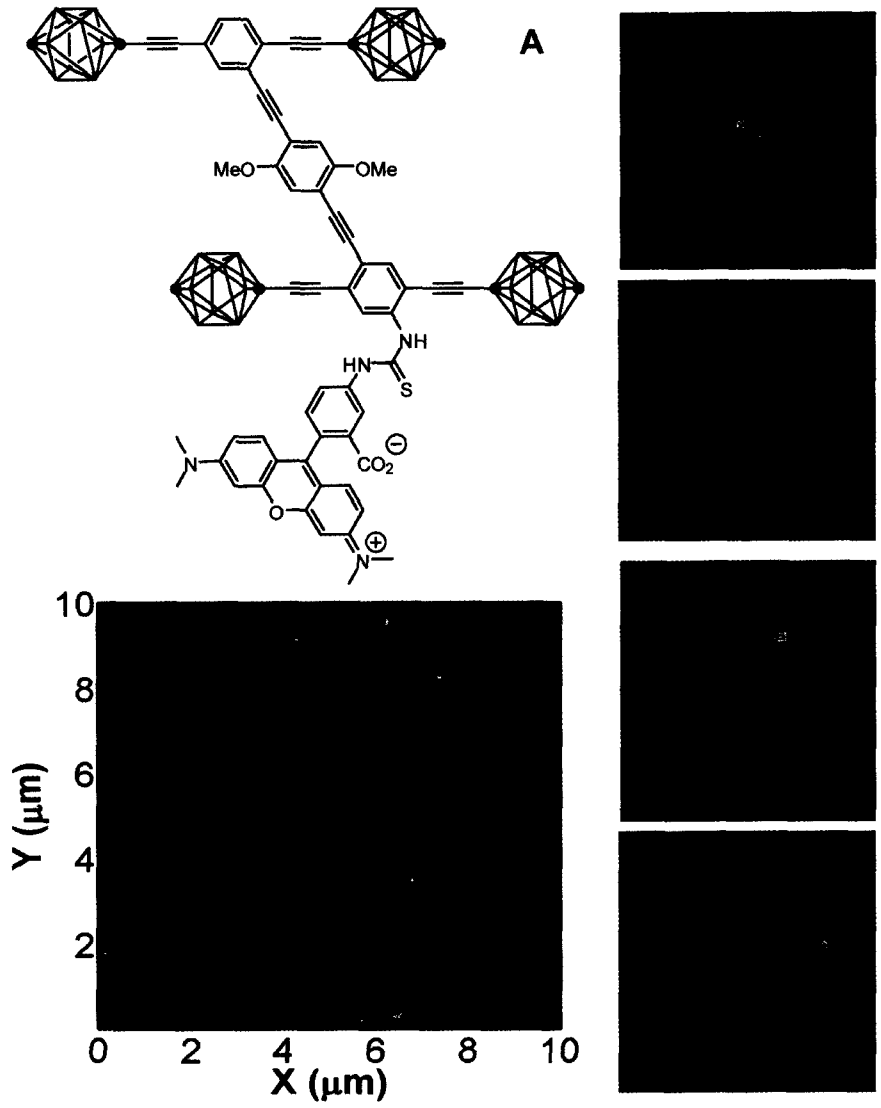

Figure. 1. **(A)** Dye labeled four-wheeled nanocar. The vertices in the carborane wheels correspond to B-H units while the black dots correspond to C and C-H units, *ipso* and *para*, respectively. The nanocar is ~2 x 2 nm and the dye "trailer" is ~1 x 1 nm. **(B)** Fluorescence image (10 µm x 10 µm, 128 x 128 pixels, 1 ms/pixel, $\lambda_{exc.}$ = 532 nm, 1 kW/cm^2) of single nanocars. **(C-F)** Time-lapse images (2.3 µm x 2.3 µm) for the nanocar circled in **(B)** demonstrating movement of the nanocar at room temperature. The red cross hair provides a stationary reference point.

Single nanocar trajectories were obtained by an automated routine that first identified individual molecules based on the intensity and size (e.g. number of pixels) of the fluorescent spot in the starting image for a time series of frames. If a molecule is found at the same position or within a search area in the subsequent frame, the molecule is associated with the corresponding one in the previous image. This procedure is repeated for all molecules and every frame. Large displacements within the relatively long image acquisition time of 30 sec, photo-blinking of the dye, and high single molecule coverage could lead to an incorrect association. Photo-blinking was addressed by searching in subsequent frames for molecules that blink on again. However, if an unambiguous assignment could not be made the corresponding molecules were excluded from further analysis. In addition, the dimensions of the search area and the concentration of nanocars were carefully adjusted in order to minimize intersecting search regions. A typical search radius was 600 nm for images with coverages of 10 - 15 molecules per 100 μm^2. Figure 2A shows the first analyzed frame of a time series of fluorescence images for carborane-wheeled nanocars together with superimposed trajectories obtained from the following images demonstrating that the displacements of individual nanocars can be as large as 500 nm between frames.

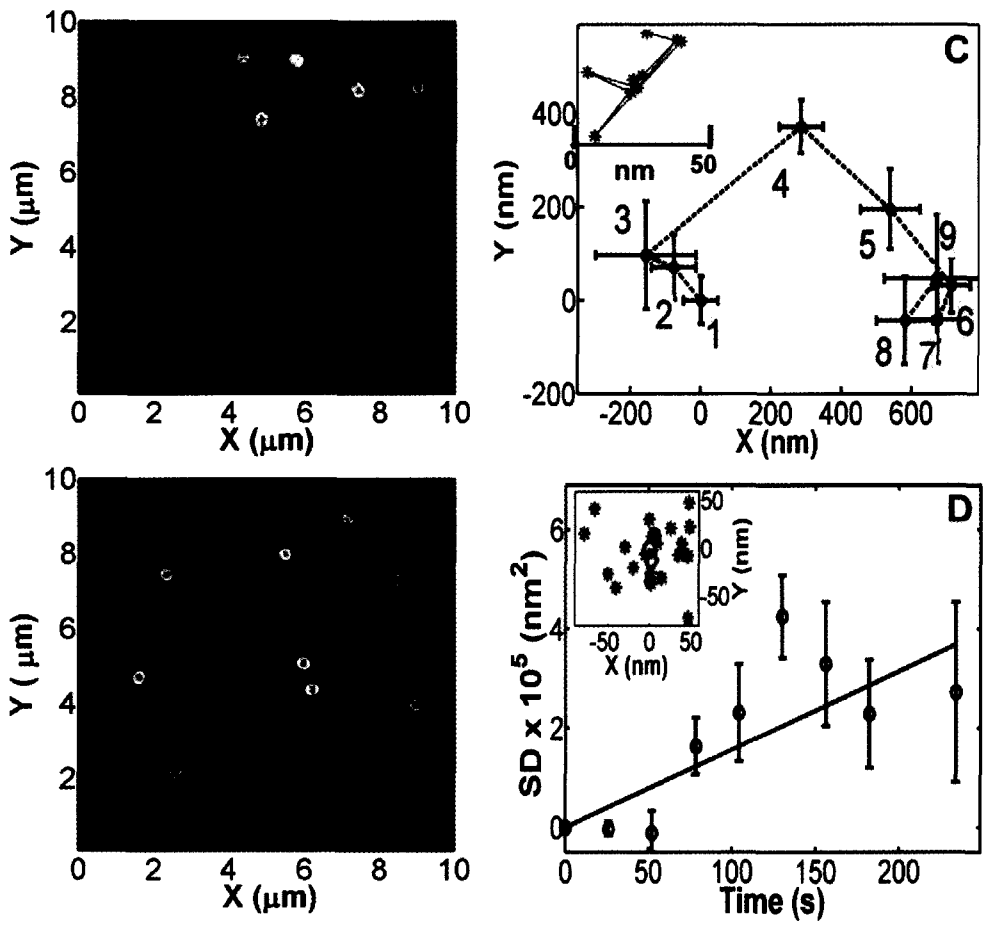

Figure 2. Analyzed images of nanocar **(A)** and TRITC **(B).** Molecules were identified based on intensity and size within the region marked by the red box. The positions of the molecules for a time series of images are shown superimposed on the first frame. 25% of the nanocars showed displacements greater than the error of 100 nm in at least two image frames and are color coded in red as 'moving' nanocars. **(C)** Single molecule trajectory of the nanocar indicated by the red circle in **(A)**. Displacements as large as 500 nm between frames far exceed the changes in position recorded for the representative TRITC molecule labeled with the green circle in **(B)** (upper left hand corner in **(C)**; note the scale bar). **(D)** Squared displacements SD (r^2) calculated from the single nanocar trajectory in **(C)** vs. time. A linear fit according to $SD = 4dt$ yields a squared displacement rate d of 6.0×10^{-16} m^2/s. The inset shows a scatter plot of the linear displacements between

images for each of the five 'non-moving' molecules in **(A)**. The 11 m shift between the blue and red points, corresponding to the origin and the mean position, confirms a negligible sample drift.

A non-specific movement of individual molecules on glass can be excluded here because fluorescence imaging of the dye only showed no measurable displacements outside our experimental error. We repeated the same single molecule experiments and analysis for individual TRITC molecules isolated on a glass surface (Figure 2B). The TRITC by itself showed no translational motion, which can be seen from the comparison of two typical trajectories obtained for the nanocar and TRITC (Figure 2C). The magnified nanocar trajectory in Figure 2C includes the error bars calculated from fitting each fluorescence spot to the microscope point spread function, which was approximated as a two-dimensional Gaussian.[18,19] For TRITC, the displacements are comparable or even smaller than the error bars verifying that the TRITC molecules remained stationary. On the other hand, the movement of the nanocars is much larger than our spatial resolution of 100 nm. The resolution is mainly limited by photon shotnoise and photo-blinking of the dye as well as a pixel size of 78 nm.[18] Despite a longer image acquisition time and reduced spatial resolution, the main advantage of our confocal sample scanning setup over wide-field imaging is that a non-constant laser illumination of all molecules allowed us to extend the total acquisition time and to obtain trajectories spanning several minutes.

It is interesting to note from Figure 2A that not all molecules that were identified actually moved. In fact, about 25 % of the nanocars (46 out of 191 molecules) showed

translational motion, which further illustrates the power and need for single molecule measurement techniques. A main factor contributing to the large fraction of 'non-moving' nanocars is most likely the surface roughness of the glass surface as it is not atomically flat; it is merely a glass cover slip (Fisher Scientific, 12-545-F) and the nanocars could become lodged at lattice defects. AFM measurements of a glass cover slip confirmed both smooth areas and surface height modulations of several nanometers exceeding the dimensions of the nanocars. Secondly, a fluorescent spot only indicates the presence of TRITC, which by itself did not move (Figure 2B), and the presence of some non-linked TRITC molecules due to decomposition cannot be excluded. In the following, we will concentrate only on the nanocars that showed a displacement which exceeded the error bar in at least 2 image frames. These 'moving' nanocars are colored red in Figure 2A. However, the 'non-moving' nanocars colored yellow in Figure 2A served the important role of an internal marker against overall sample drift. We found that sample drift (inset in Figure 2D) was 11 nm during the experiment shown in Figures 1 and 2, which is much smaller than the micron-scale movement of the nanocars as well as our spatial resolution of 100 nm.

We observed no biased movement of the nanocars on this amorphous surface. A histogram of angles obtained from the single molecule trajectories for all moving nanocars showed an equal distribution of all angles between 0 and 180 degrees (Figure S1). Polarization anisotropy analysis of the fluorescence images furthermore revealed that the nanocars, when they changed directions, underwent the change rapidly and within the time it took to scan the molecule over the laser beam (~ 500 ms, Figure 3A). The polarization anisotropy distribution of the nanocars is peaked at zero indicating

depolarization due to rotational movement. A rotation of the TRITC on the nanocar can be excluded as the major depolarization mechanism because an analysis of only the center pixel showed a broader polarization distribution (Figure S2). This is consistent with rotational dynamics on the 1-100 ms time scale and is much slower than a bond rotation. In contrast, TRITC only did not rotate as the polarization anisotropy values for TRITC (Figure 3B) ranged from -1 to 1 consistent with a random and stationary distribution of molecular orientations.[20,21] The fact that the molecules rotate is not surprising, considering that previous STM results[15] showed a combined pivot and translation motion of fullerene-wheeled nanocars on the nanometer length scale due to an independent wheel movement. The roughness of the glass surface is likely to further enhance pivoting of the nanocars.

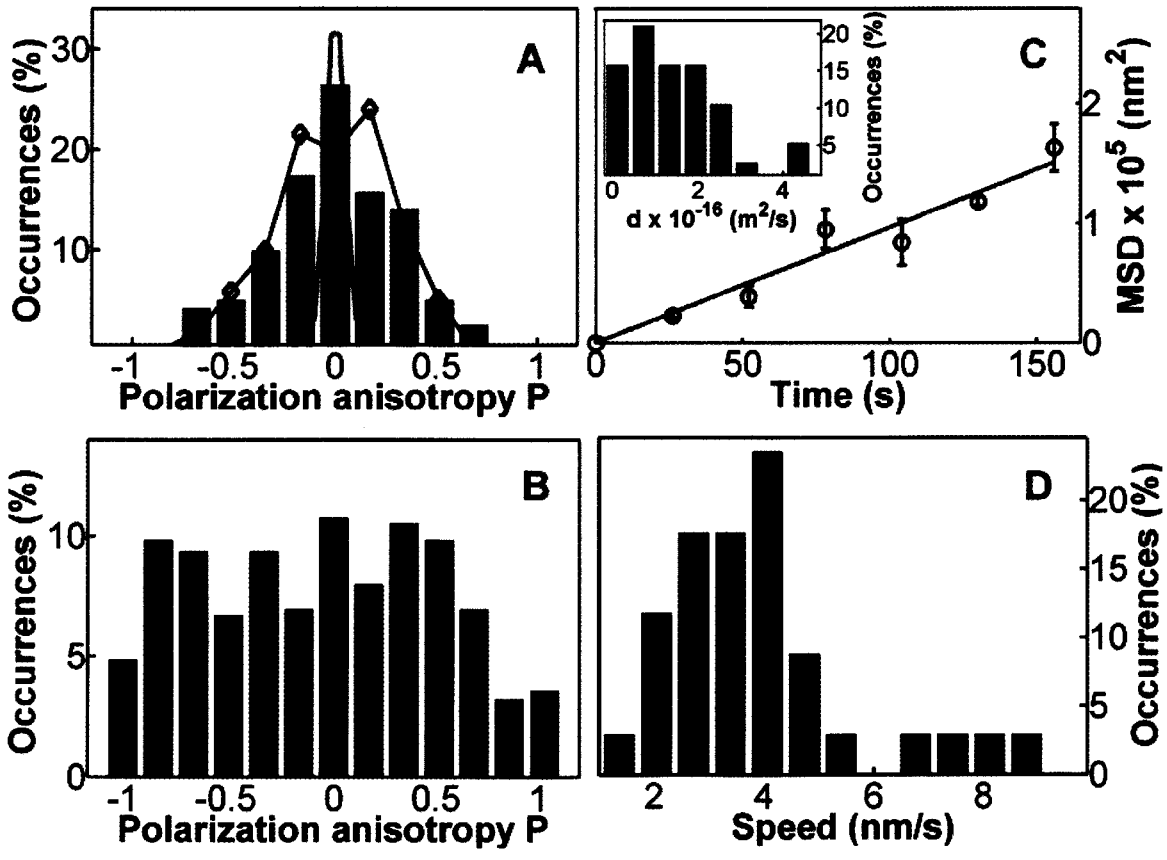

Figure 3. **(A)** Polarization anisotropy distribution of 'moving' four-wheeled nanocars (red bars). The polarization anisotropy values are peaked at zero, indicating rotation of the nanocars during the image acquisition time. Rotation much faster than the acquisition time would result in the distribution given by the green line for shotnoise limited polarization detection. The black points and line are a simulation of the polarization anisotropy distribution for random hopping with a minimum rate of 10 hops per second, assuming an equal weight for all hopping directions. Please note that the polarization distribution is also consistent with a rolling and continuous pivoting motion. **(B)** Polarization anisotropy distribution of TRITC confirming the absence of rotational motion during the image acquisition time. **(C)** Mean squared displacement MSD ($\langle r^2 \rangle - \langle r \rangle^2$) vs. time for all 'moving' nanocars. A linear fit according to $MSD = 4Dt$ yields a two-dimensional diffusion constant D of 2.7 x 10^{-16} ± 0.4 m^2/s. The inset shows a histogram of single molecule squared displacements rates d calculated from individual trajectories such as the one shown in Figure 2D. **(D)** Distribution of speeds of individual 'moving' nanocars. The average speed of the nanocars is 4.1 nm/s or two nanocar lengths per second.

Given the lack of long-range directionality, we analyzed the single nanocar trajectories to obtain displacement rates in analogy to two-dimensional surface diffusion.[22] Figure 2D shows the squared displacement SD of a single nanocar vs. time as obtained from the trajectory in Figure 2C. A linear fit according to $SD = 4dt$ yields a squared displacement rate d of 6.7 x 10^{-16} m^2/s. A histogram of single molecule diffusion constants is shown in the inset of Figure 3C. The average single molecule squared

displacement rate of 2.2 x 10^{-16} m^2/s agrees well with the diffusion constant D of 2.7 x 10^{-16} m^2/s calculated from a mean squared displacement MSD analysis ($MSD = 4Dt$, Figure 3C). We also calculated the average minimum speed of the four-wheeled nanocars at room temperature and found a value of 4.1 nm/s (Figure 3D). Based on a diameter of 0.8 nm for a carborane wheel and assuming here that the translation was purely due to a rolling mechanism, a minimum wheel rotation frequency of 2 rotations per second was calculated. In contrast, fullerene-wheeled nanocars on a gold surface only moved after increasing the temperature to 500 K.[15] The difference is due to the much larger surface interaction energy of 200 - 250 kJ/mol per fullerence wheel on gold.[23,24]

Instead of a wheel-like rolling motion, the nanocars could also translate by hopping as has been observed for a large organic molecule such as hexa-*tert*-butyldecacyclene (HtBDC, $C_{60}H_{66}$), on Cu (110) by STM imaging.[25] We evaluated this scenario using the measured diffusion constant and estimating a minimum hopping rate based on the polarization anisotropy distribution of the nanocars. A simulation of the polarization anisotropy distribution (Figure 3A), assuming random hopping with an equal weight for all directions, gives a minimum hopping rate h of 10 hops per second. According to $D = 1/4\ \lambda^2 h$,[26] a maximum hop length λ of 10 nm is calculated, which is several times the size of the nanocar. If the nanocars are unable to rotate freely while hopping, the hopping rate increases and the step size decreases, which eventually will become indistinguishable from a sliding or rolling motion.

Using a simple model, we can estimate the contributions due to rolling and hopping of the nanocars based on the activation energy for translational motion, which

can be estimated from the measured diffusion constant D according to $D = D_0 \exp\left(-\frac{E}{kT}\right)$.[26,27] Here, T is the temperature and k the Boltzmann constant. D_0 is the two-dimensional diffusion constant of the nanocar in air given by the Stokes-Einstein diffusion equation $D_0 = \frac{kT}{4\pi\eta a}$ where η is the viscosity of air and a is the radius of the nanocar. If the motion of the nanocar molecule on the surface were free it would have a diffusion constant D_0. However, because of interactions with the surface the diffusion is significantly smaller. This model yields an activation energy E of 42 ± 5 kJ/mol at room temperature. For a carborane wheel to sit on a surface, three hydrogen atoms are necessary to bond to the substrate, which is illustrated in Figure 4A together with a suggested rolling mechanism. The bond strength between a carborane hydrogen and an oxygen atom on the glass surface is estimated to be 4.8 kJ/mol.[28] In order for the nanocar to roll it has to break one hydrogen bond per wheel and overcome a rotational energy barrier of 4.2 kJ/mol per bond connecting the wheel to the chassis,[29] which equals a total energy of 36 kJ/mol for a total of four wheels per car, in good agreement with the measured activation energy. On the other hand, if the nanocars were hopping, 12 hydrogen bonds have to be broken yielding an activation energy of 57 kJ/mol. This exceeds the experimentally measured value making hopping the less likely mechanism.

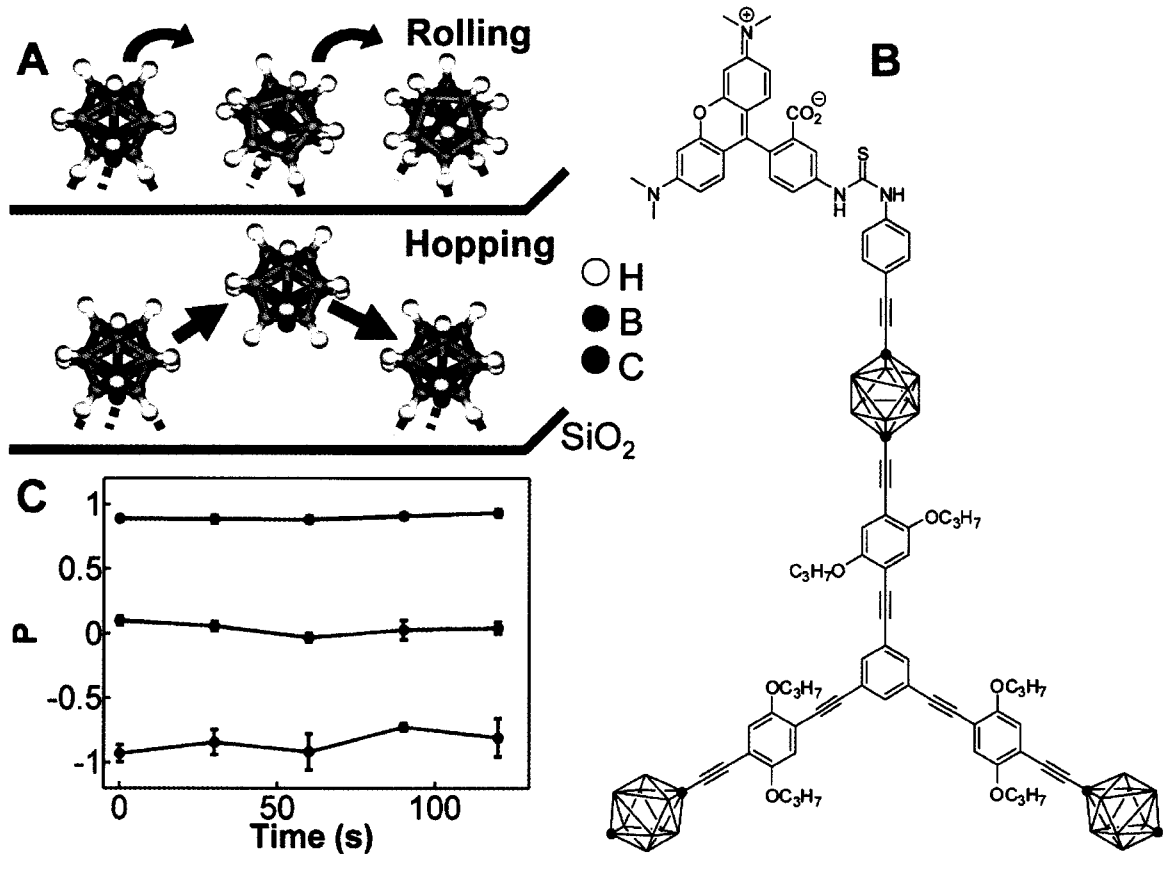

Figure 4. **(A)** Schematic comparison of a carborane wheel rolling (top) vs. hopping (bottom). A wheel on the glass surface forms three hydrogen bonds with the oxygen atoms (not shown for clarity) of the SiO_2. For rolling only one of the three hydrogen bonds has to break while for hopping the whole wheel has to detach from the surface. **(B)** Dye labeled three-wheeled nanocar. **(C)** Three representative polarization anisotropy time trajectories for trimer nanocars showing that rotational motion is absent on a time scale of several minutes. Similar results were also obtained for polarization measurements of 'non-moving' four-wheeled nanocars and TRITC only.

In order to further test this assignment, we measured single molecule trajectories and polarization anisotropy distributions for a TRITC-labeled three-wheeled nanocar,

(Figure 4B). Compared to the four-wheeled car, the trimer nanocar is expected to have only 75% of the interaction energy with the glass surface and would therefore be more likely to hop assuming that the interaction of the dye label with the surface is comparable. However, we found no movement of the trimer nanocars as the trajectories were similar to those measured for TRITC only or the non-moving four-wheeled nanocars. In addition to the absence of any translational movement in the trimer nanocars, we also did not observe rotational motion as confirmed by the polarization anisotropy distribution obtained from the fluorescence images (Figure S3) and the absence of a change of polarization anisotropy between image frames (Figure 4C). Although the trimer nanocar is expected to rotate, an important difference between the two nanocars is that TRITC is attached directly to the wheel of the trimer nanocar (Figures 1A and 4B) and could hinder a free wheel rotation. In order to test this hypothesis and to examine a possible role of the dye label on the nanocar movement we plan to also study non-labeled nanocars in the future.

Conclusion

Using single molecule fluorescence imaging, we have observed micrometer movement of dye-labeled carborane nanocars on a glass surface at room temperature. Polarization-sensitive measurements showed that translation is coupled with rotational motion. By comparing the four-wheeled nanocars to a three-wheeled nanocar analog and the unbound dye molecules, we conclude that the translation of the nanocars is consistent with a wheel-like rolling mechanism. While atomic resolution as with STM is not

possible using single molecule fluorescence imaging, the results presented here demonstrate that our approach yields complementary data and gives useful insights into the micrometer-scale motion of molecular machines.

It is interesting to speculate how a truly unidirectional motion of nanocars can be achieved. Our results suggest that the speed of the nanocars is dictated by the strength of the interactions between the nanocar wheels and the surface. Changing the surface should therefore have a large impact on the mobility of the nanocars. However, even more important for a controlled directional motion seems to be the reduction of pivoting, which was found to occur with a minimum frequency of 10 turns per second for the carborane-wheeled nanocars on glass. An extended nanocar chassis with an increased even number of wheels should be less susceptible to random pivot motion caused by an independent wheel movement, but at the expense of a reduced speed due to a stronger surface attraction and increased entropy for synchronized bond rotations.

Experimental Section[30]

Single molecule fluorescence imaging was performed on a home-built sample scanning confocal microscope consisting of a frequency doubled diode-pumped laser (Coherent, Verdi), an inverted microscope (Zeiss, Axiovert 200), and avalanche photodiode (APD) detectors. Samples were excited by circularly polarized 532 nm laser light with an average power of 500 nW focused to a diffraction limited spot size of 250 – 300 nm. To visualize the nanocars, a dye label (tetramethylrhodamine isothiocyanate, TRITC) was attached to the end of the nanocar chassis (Figure 1A). TRITC tagging of

the nanocars was accomplished through an aniline-bearing nanocar reacting with the isothiocyanate residue on the fluorophore (see supporting info for synthesis and characterization). We confirmed that the photophysical properties of TRITC labeled nanocars are similar to those of TRITC. TRITC and TRITC labeled nanocars were spin-casted (3500 rpm for 90 seconds) on plasma cleaned coverslips (Fisher Scientific, 12-545-F) from DMF solution with concentrations of 10^{-10} - 10^{-12} mol/L. Prior to spin-casting and plasma cleaning, the coverslips were sonicated in acetone for 15 minutes. Samples were mounted on a xyz piezo scanning stage (Physik Instrumente, P-517.3CL) connected to a surface probe microscope controller (RHK Technology, SPM 1000). Emitted fluorescence from individual molecules was collected by a 100X oil-immersion objective with a numerical aperture of 1.3 (Zeiss, Fluar) and filtered by a dichroic mirror and a notch filter to reduce scattered laser light. Fluorescence images were constructed by scanning the sample across the excitation laser. Typical images had dimensions of 10 x 10 μm and consisted of 128x128 pixels with an integration time of 1 ms/pixel (Figure 1B). Matlab software was written to automatically identify the position of each molecule in every image frame. For polarization sensitive detection, the fluorescence was separated into orthogonally polarized components I_x and I_y using a polarizing beamsplitter and detected by two APDs. After integrating the intensities over an area of 5x5 pixels corresponding to size of a single molecule, the polarization anisotropy was calculated according to $P = (I_y - I_x)/(I_y + I_x)$. For all of the samples studied we have measured about 200 molecules in order to extract statistically meaningful values.

References and Notes

(1) van Delden, R. A.; ter Wiel, M. K. J.; Pollard, M. M.; Vicario, J.; Koumura, N.; Feringa, B. L. *Nature* **2005**, *437*, 1337-1340.

(2) Fletcher, S. P.; Dumur, F.; Pollard, M. M.; Feringa, B. L. S*cience* **2005**, *310*, 80-82.

(3) Leigh, D. A.; Wong, J. K. Y.; Dehez, F.; Zerbetto, F. *Nature* **2003**, *424*, 174-179.

(4) Kelly, T. R.; De Silva, H.; Silva, R. A. *Nature* **1999**, *401*, 150-152.

(5) Badjic, J. D.; Balzani, V.; Credi, A.; Silvi, S.; Stoddart, J. F. *Science* **2004**, *303*, 1845-1849.

(6) Bissel, R. A.; Cordova, E.; Kaifer, A. E.; Stoddart, J. F. *Nature* **1994**, *369*, 133-137.

(7) Brouwer, A. M.; Frochot, C.; Gatti, F. G.; Leigh, D. A.; Mottier, L.; Paolucci, F.; Roffia, S.; Wurpel, G. W. H. *Science* **2001**, *291*, 2124-2128.

(8) Perez, E. M.; Dryden, D. T. F.; Leigh, D. A.; Teobaldi, G.; Zerbetto, F. *J. Am. Chem. Soc.* **2004**, *126*, 12210-12211.

(9) Serreli, V.; Lee, C.-F.; Kay, E. R.; Leigh, D. A. *Nature* **2007**, *445*, 523-527.

(10) Bedard, T. C.; Moore, J. S. *J. Am. Chem. Soc.* **1995**, *117*, 10662-10671.

(11) Muraoka, T.; Kinbara, K.; Aida, T. N*ature* **2006**, *440*, 512-515.

(12) Liu, Y.; Flood, A. H.; Bonvallet, P. A.; Vignon, S. A.; Northrop, B. H.; Tseng, H.-R.; Jeppesen, J. O.; Huang, T. J.; Brough, B.; Baller, M. *et al. J. Am. Chem. Soc.* **2005**, *127*, 9745-9759.

(13) Morin, J.-F.; Sasaki, T.; Shirai, Y.; Guerrero, J. M.; Tour, J. M. *J. Org. Chem.* **2007**, *72*, 9481-9490.

(14) Shirai, Y.; Morin, J.-F.; Sasaki, T.; Guerrero, J. M.; Tour, J. M. *Chem. Soc. Rev.* **2006**, *35*, 1043-1055.

(15) Shirai, Y.; Osgood, A. J.; Zhao, Y.; Kelly, K. F.; Tour, J. M. *Nano Lett.* **2005**, *5*, 2330-2334.

(16) Gimzewski, J. K.; Joachim, C. *Science* **1999**, *283*, 1683-1688.

(17) Yildiz, A.; Tomishige, M.; Vale, R. D.; Selvin, P. R. *Science* **2004**, *303*, 676-679.

(18) Thompson, R. E.; Larson, D. R.; Webb, W. W. *Biophys. J.* **2002**, *82*, 2775-2783.

(19) Qu, X.; Wu, D.; Mets, L.; Scherer, N. F. *Proc. Natl. Acad. Sci. U.S.A.* **2004**, *101*, 11298-11303.

(20) Forkey, J. N.; Quinlan, M. E.; Goldman, Y. E. *Prog. Biophys. Mol. Biol.* **2000**, *74*, 1-35.

(21) Ha, T.; Laurence, T. A.; Chemla, D. S.; Weiss, S. *J. Phys. Chem. B* **1999**, *103*, 6839-6850.

(22) Schmidt, T.; Shultz, G. J.; Baumgartner, W.; Gruber, H. J.; Schindler, H. *Proc. Natl. Acad. Sci. U.S.A.* **1996**, *93*, 2926-2929.

(23) Altman, E. I.; Colton, R. J. *Surf. Sci.* **1992**, *279*, 49-67.

(24) Akimov, A. I.; Nemukhin, A. V.; Moskovsky, A. A.; Kolomeisky, A. B.; Tour, J. M. *J. Chem. Theor. Comp.* **2008**, *4*, 652-656.

(25) Schunack, M.; Linderoth, T. R.; Rosei, F.; Laegsgaard, E.; Stensgaard, I.; Besenbacher, F. *Phys. Rev. Lett.* **2002**, *88*, 156102/1-156102/4.

(26) Rosei, F.; Schunack, M.; Naitoh, Y.; Jiang, P.; Gourdon, A.; Laegsgaard, E.; Stensgaard, I.; Joachim, C.; Besenbacher, F. *Prog. Surf. Sci.* **2003**, *71*, 95-146.

(27) Atkins, P.; de Paula, J. *Physical Chemistry, Chapter 28*; 7th ed.; Freeman and Company: New York, 2002.

(28) Andrews, P. C.; Hardie, M. J.; Raston, C. L. *Coord. Chem. Rev.* **1999**, *189*, 169–198.

(29) Shirai, Y.; Osgood, A. J.; Zhao, Y.; Yao, Y.; Saudan, L.; Yang, H.; Chiu, Y.-H.; Alemany, L. B.; Sasaki, T.; Morin, J.-F. *et al. J. Am. Chem. Soc.* **2006**, *128*, 4854-4864.

(30) Khatua, S.; Guerrero, J. M.; Claytor, K.; Vives, G.; Kolomeisky, A. B.; Tour, J. M.; Link, S. *ACS Nano* **2009** *ASAP*.

3.2

Synthesis of Fluorescent Dye-Tagged Nanomachines for Single Molecule Fluorescence Spectroscopy

Introduction

Watershed moments in the construction of nanomachines that exhibit controlled movements in solution[1] have lead researchers to explore the design, synthesis and manipulation of more complex, highly functional devices that can be studied not only as an ensemble, but as single entities.[2] Adapting the approach taken by biological systems, synthetic strategies often arrive at these structures via bottom-up construction - quickly generating nanometer-sized configurations from the most basic organic building blocks.[3] Concomitantly, the development of increasingly powerful imaging tools has enabled nanoscale engineers to study the individual rotational, translational and transportation dynamics of biological[4] and synthetic[5] nanomachines on surfaces.

Though many interesting results have been obtained using other methods,[5b,5c] STM remains unparalleled in its ability to resolve and manipulate single atoms as well as track the translational movement of nanoscale objects.[6] To this end, various groups have synthesized landers,[7] wheelbarrows,[3b,8] nanowalkers,[9] and poly-aromatic systems[10] for the purpose of observing their behavior on metallic surfaces. Similarly, our group has combined various nanocomponentry with molecular axles containing fullerene, *p*-carborane or organometallic wheels to construct a number of nanovehicles designed for directed motion and transport along atomically flat surfaces.[3a,f] Proof-of-concept experiments have shown, using STM, the directed movement of fullerene-wheeled nanocars on atomically-flat Au(111) surfaces upon thermal and electrostatic activation.[11]

Although STM remains invaluable in the study of atomic detail and mechanism, conditions required for precise measurement are often less than ideal and time consuming; conductive substrate surfaces must be used, and cryogenic and high-vacuum settings are often required to obtain clean images.[6b, 12] Single molecule fluorescence spectroscopy (SMFS), which has been widely used to track motion in biological systems,[13] offers a complementary technique to STM to study single molecules on non-conductive surfaces. While SMFS does not have the atomic resolution of STM, nanometer localization is possible with large photon count rates[14] and fast measurement of distances as low as several nanometers has been realized on larger scan areas.[15] To exploit these advantages, we recently employed single molecule fluorescence imaging as a complementary technique to STM for monitoring the motion of fluorescent nanocars on non-conductive glass under ambient conditions.[16]

To obtain accurate measurements of single molecules, it is of paramount importance to ensure that a) the molecules of interest fluoresce well and b) fluorescence from impurities, optic and substrate surfaces is avoided.[17] Molecular design ensures that the first requirement is met, while the other is typically met by the utilization of excitation light with wavelengths greater than 500 nm, as few molecules and substrates are known to absorb in this region.[18] In our case, utilization of such light came with a caveat, as our previously synthesized *p*-carborane nanocars[19] do not possess absorption bands in this region. In general, molecules are tagged with a high-quantum-yield fluorescent dye to provide the capability for visualization at longer wavelengths.[20] For our purposes, tetramethylrhodamine isothiocyanate (TRITC) was an attractive dye, as it possesses an excitation wavelength centered at the emission line of our Nd:Vn laser (532

nm), good quantum yield of fluorescence, and is appended to structures via a simple urea formation by reaction with amines.[21] The attachment of TRITC to nanovehicular structures should afford the ability to unabatedly study the behavior of nanocars on surfaces.

In an effort to elucidate the mechanism of movement and control the directionality of nanovehicles via specific arrangements of their molecular axles and wheels, reported here is the synthesis of three fluorescently-tagged nanovehicles (Figure 1) specifically designed for SMFS studies. The molecules all bear a TRITC fluorescent tag for excitation at 532 nm and *p*-carborane wheels. Our main reasons for choosing *p*-carborane were two-fold: (1) its ability to be substituted at both carbon atoms *para* to one another and (2) its stability towards many organometallic and photoinitiated processes. My research consisted of the synthesis of **1** and **2** as well as the starting nanocooper for nanocar **3**, while the synthesis of nanocar **3** was completed by Dr. G. Vives. As shown in Figure 1, nanocar **1** was designed to move along a straight trajectory due to the placement of the axles parallel to one another. Analogous to our previous work with fullerene nanomachines, trimer **2** was designed to exhibit a pivoting motion with no translation. Due to the initial results from imaging trimer **2**,[16] nanocar **3** was designed to ascertain the effect of TRITC on wheel rotation/nanocar movement.

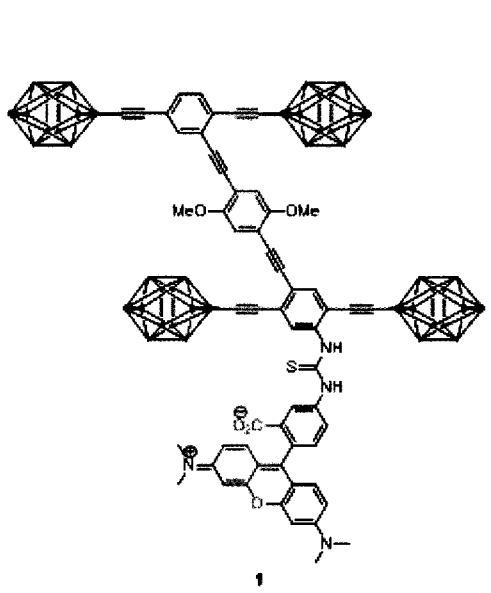

1

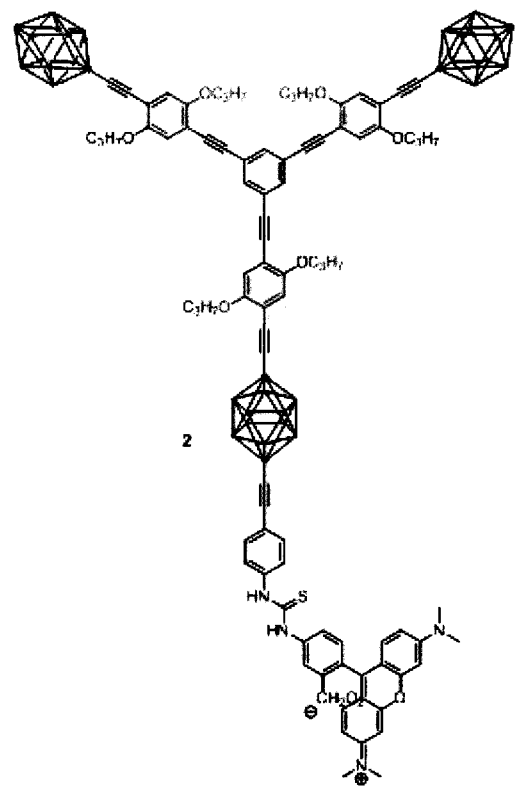

2

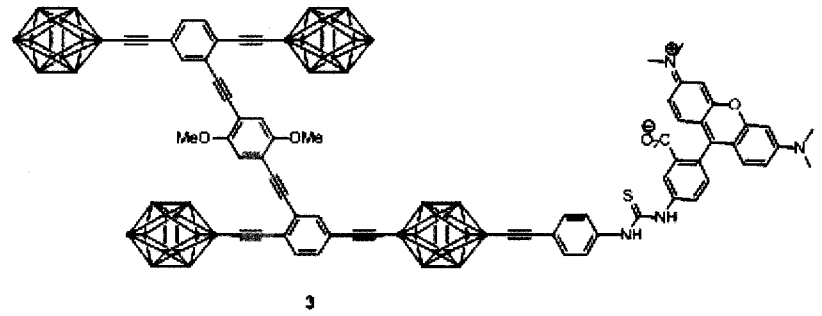

3

Figure 1. Structure of TRITC-Tagged nanovehicles **1-3** and their expected directional motion. Every vertex of the carborane wheel is BH except the darkened sites, where the outer is CH and the inner is alkynyl-substituted when in a molecular axle. Only the 5-isomer adduct of TRITC is shown.

Results and Discussion

Design and Synthesis. The strategy to arrive at each target adopts a convergent approach, where the inner components of each nanovehicle are synthesized and then attached to versatile *p*-carborane-containing axles (arms in the case of the trimer). The design of nanocar **1** dictated the use of two different molecular axles, with one axle bearing a pendant aniline for the attachment to amine-reactive TRITC. To arrive at trimer **2** and nanocar **3**, we used a convergent, symmetric approach to synthesize a late-stage intermediate, followed by statistical attachment of an extended aniline to one wheel for the purposes of TRITC tagging.

Scheme 1. Synthesis of TRITC-tagged Nanocar **1**

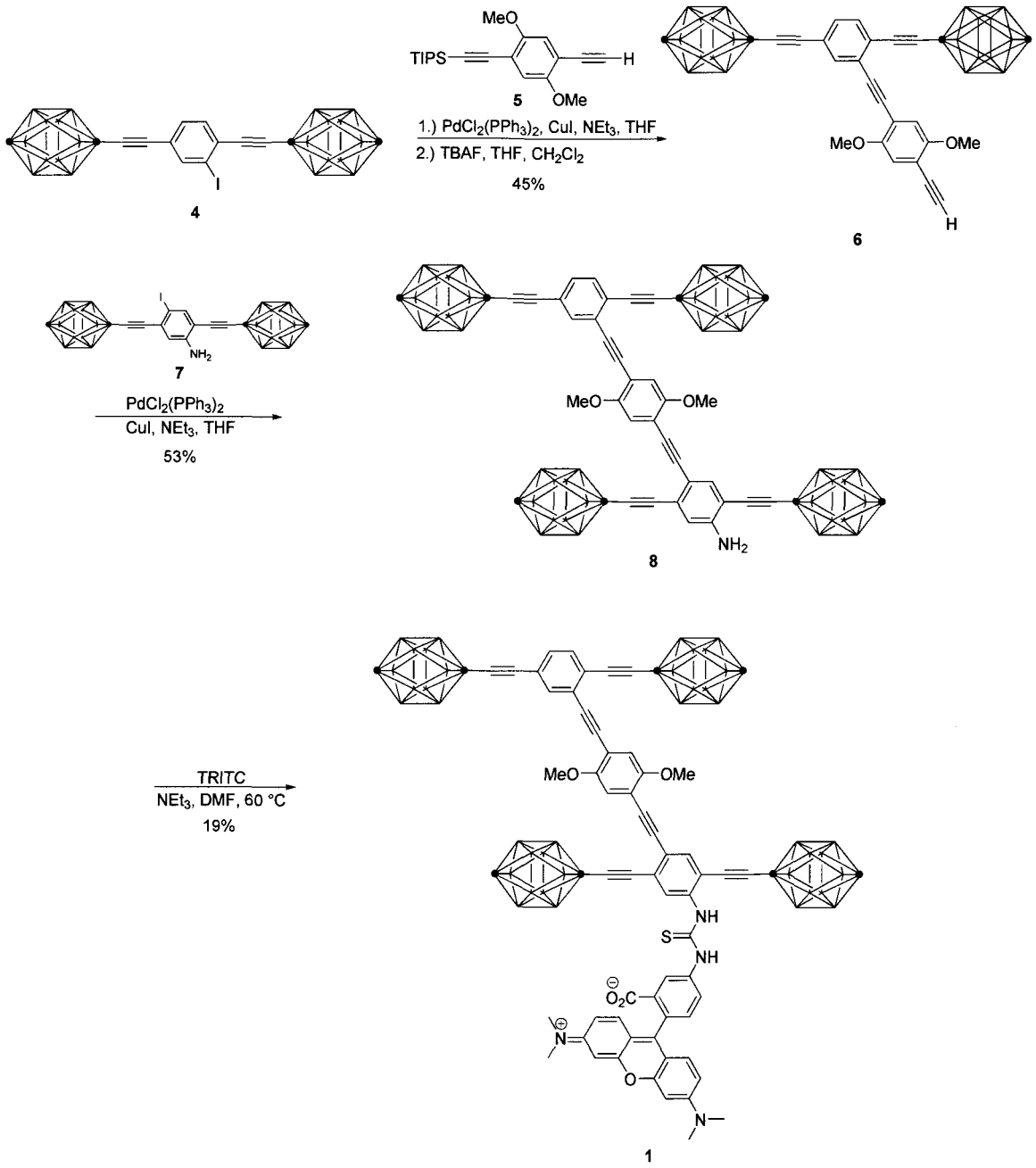

In Scheme 1, iodide axle **4**[22] is coupled to the methoxy-containing inner chassis of the nanocar **5**[23] using normal Sonogashira conditions followed by deprotection to yield terminal alkyne **6**. Immediate coupling with known aniline axle **7**[23] was performed to give the aniline nanocar **8**. In a final step, the aniline was reacted with TRITC in DMF at

elevated temperature, with triethylamine as base to give target nanocar **1** in 19% yield. It is possible that the low yield was a result of steric bulk around the reacting aniline.

SMFS results show that the axle-tagged nanocar **1** has sufficient energy at room temperature to move along the glass surface at high rates of displacement.[16] This was an encouraging result, as the attachment of a large moiety to the axle of nanocar **1** demonstrates the ability to transport on the nanoscale, albeit with a lack of long-range directionality. To further explore our ability to study directionality and molecular behavior, trimer **2** was designed and synthesized to have analogous properties to those of a previously studied fullerene-wheeled trimer, where the molecule undergoes no translation, but rotates about the central trialkynylated benzene.[11]

Scheme 2. Synthesis of Trimer **2**

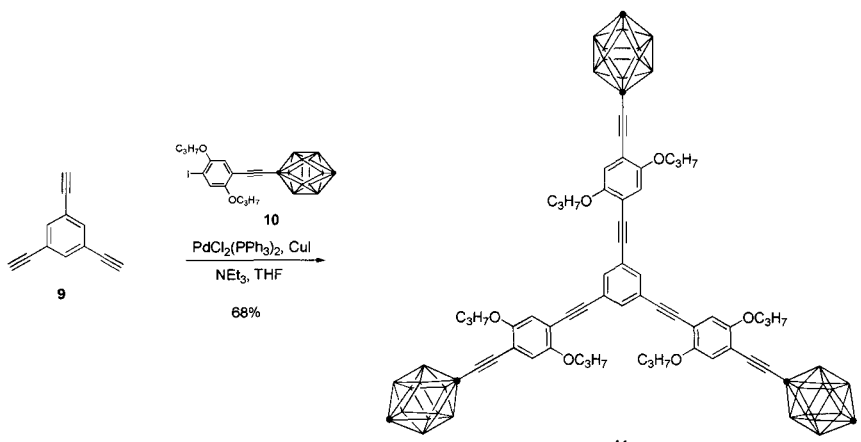

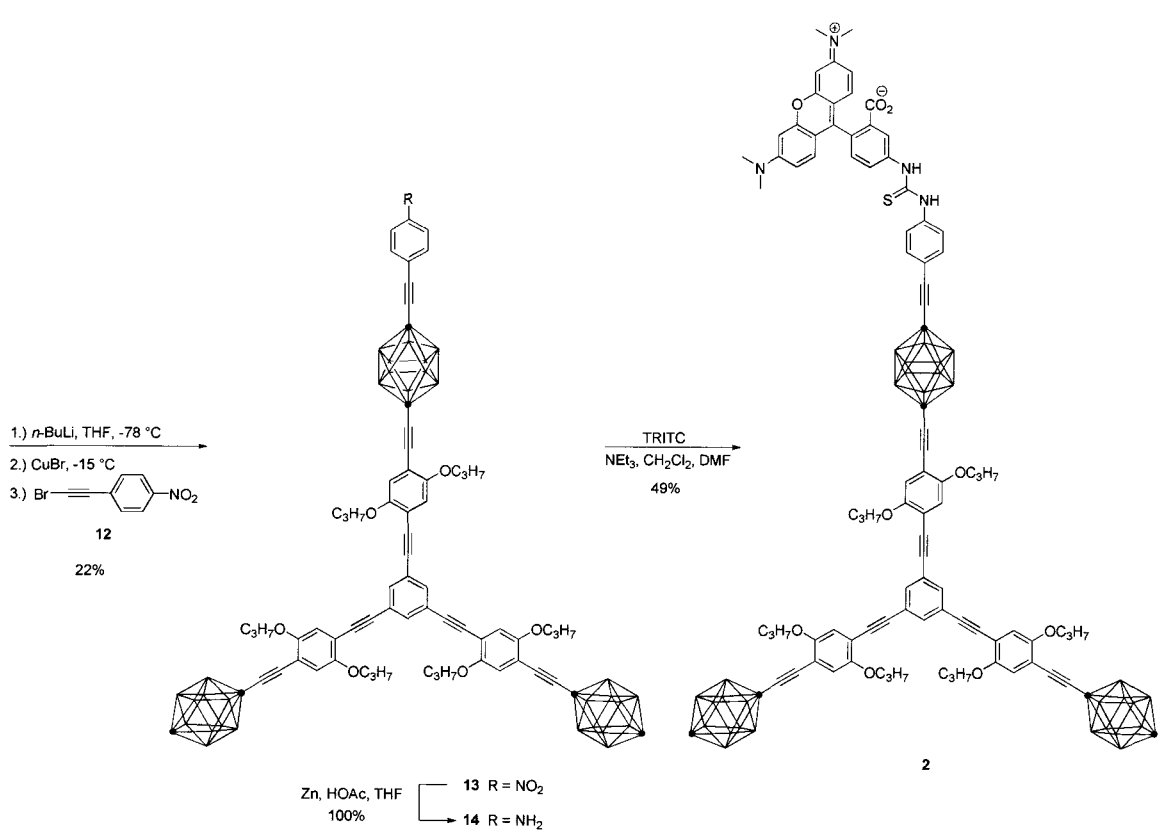

To synthesize trimer **2** (Scheme 2), we first attempted to use an early-stage statistical coupling to 1,3,5-tribromobenzene, followed by the coupling of a fully-elaborated pendant aniline arm to the benzene core. This method, however, proved to be lengthy and low yielding. Using a late-stage statistical approach, we were able to synthesize potentially useful intermediates which may be used in other future STM and

fluorescence studies. Thus, trimer **2** is convergently constructed in four synthetic steps, where 1,3,5-triethynylbenzene **9**[19] is coupled to 3 equiv. of known carborane arm **10**[19] to give the symmetrical trimer **11** in good yield. Initially, statistical attachment of the *p*-ethynylnitrobenzene (**12**) unit was carried out under standard conditions for unsubstituted *p*-carborane functionalization: the molecule is deprotonated using 1 equiv. of *n*-butyllithium at -78 °C, followed by equilibration at room temperature for 30 min, then cooled again to -78 °C. Transmetalation is then performed by addition of CuBr and allowing the mixture to warm to room temperature, follwed by coupling with the alkynyl bromide. Unfortunately, no product was obtained using this protocol and the starting material was almost totally recovered. In monosubstituted *p*-carboranes, Fox and co-workers have reported an influence of the substituent on the unsubstituted carbon.[24] Substitutions by electron-donating groups increase electron density on the *para* carbon, following a Hammet σ_p plot with good correlation. In our case, it is likely that the resulting anion and/or organocopper intermediates decompose during the room temperature equilibration step of the substitution process due to the highly electron-donating nature of the chassis/inner core. Consequently, modification of the procedure by lowering the temperature of the equilibration steps to -15 °C and increasing the equilibration times to 1 h led to formation of *p*-ethynylnitrobenzene-substituted trimer **13** in 22% yield. The pendant nitro was then reduced smoothly using zinc powder and acetic acid in THF to provide the aniline **14** in quantitative yield. Reaction with TRITC provided fluorescently-tagged trimer **2** in 49% yield.

Scheme 3. Synthesis of Wheel-Tagged Nanocar **3**

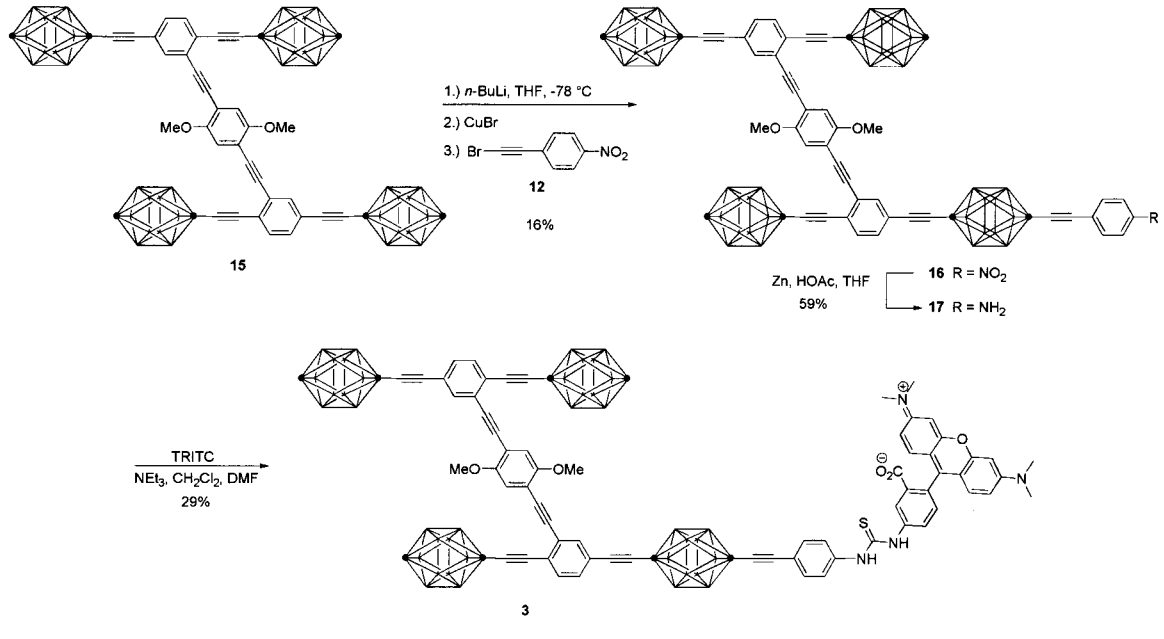

SMFS imaging of TRITC-tagged trimer **2** showed that the molecule is quite stationary, exhibiting no translational motion. While a lack of translational motion was expected, the molecule also failed to show any rotational movement by polarization anisotropy measurements.[16] This lack of rotation could be due to molecular design, where TRITC is attached via a pendant group directly off of one wheel, causing it to act as a brake.

To test our hypothesis, we synthesized a wheel-tagged fluorescent nanocar (Scheme 3). Known nanocooper **15**[19] was subjected to similar statistical carborane substitution conditions to those developed for the synthesis of the trimer, resulting in a 16% yield of **16**, lower when compared to the trimer due to the statistical contribution of one extra wheel. The substitution of only one of the four wheels of nanocar **15** leads to two regioisomers, corresponding to substitution on the ortho- or meta-positioned ethynyl carborane relative to the inner chassis. The two isomers are obtained as a 1:1 mixture that

is inseparable by column chromatography. The current mechanism of translocation suggests that the two isomers should exhibit similar behavior on the glass surface, so their mixture is carried on through the rest of the synthetic sequence. Subsequent reduction to aniline **17** and TRITC attachment gave wheel-tagged nanocar **3** in a 29% yield. Initial SMFS results indicate that TRITC may indeed act as a brake, as only 5% of the nanocars exhibit translational motion, compared to 25% for nanocar **1**.

Conclusion

The design and synthesis of three fluorescently-tagged nanovehicles for the purpose of SMFS imaging is reported. Due to our recent findings where TRITC may hinder movement when attached directly to molecular wheels, we are currently undertaking the synthesis of a non-wheel tagged trimer. Other nanocars with varying orientations and numbers of axles are near completion, and their imaging, in combination with a non-wheel-tagged trimer, should provide more insight into the nature of the translational movement of nanocar **1**. Encouraged by our initial results, we are undertaking the synthesis of other highly functionalized fluorescent nanomachines and the development of new techniques for the purpose of blue excitation light fluorescence visualization (imaging of non-tagged nanovehicles).

Experimental Section

General Methods. ^{1}H NMR and ^{13}C NMR spectra were recorded at 400 and 100 MHz, respectively. Proton chemical shifts (δ) are reported in ppm downfield from tetramethylsilane (TMS). Mass spectrometry was performed at the Rice University and University of South Carolina Mass Spectrometry Laboratory. Infrared spectra (IR) assignments have 2 cm^{-1} resolution. All reactions were performed under an atmosphere of nitrogen unless stated otherwise. Reagent grade tetrahydrofuran (THF) was distilled from sodium benzophenone ketyl. Triethylamine (TEA) and CH_2Cl_2 were distilled over CaH_2. TRITC, TBAF (1.0 M solution in THF) and *n*-butyllithium (2.5 M solution in hexanes) were purchased from Sigma-Aldrich and used as received. Trimethylsilylacetylene (TMSA) was donated by FAR Research Inc. or Petra Research. CuBr was purified by suspension in hot methanol and filtration. Flash column chromatography was performed using 230-400 mesh silica gel from EM Science. Thin layer chromatography was performed using glass plates pre-coated with silica gel 40 F_{254} purchased from EM Science. The synthesis of compounds **4**,[19] **5**,[23] **7**,[23] **9**,[19] **10**,[19] and **15**[19] was performed according to literature procedures.

General Procedure for the Coupling of a Terminal Alkyne with an Aryl Halide Using a Palladium-Catalyzed Cross-Coupling (Sonogashira) Protocol. To an oven-dried round bottom flask equipped with a magnetic stir bar were added the aryl halide, the terminal alkyne, $PdCl_2(PPh_3)_2$ (ca. 2 mol% per aryl halide), and CuI (ca. 4 mol% per aryl halide). A solvent system of TEA and/or THF was added depending on the substrates. Upon completion, the reaction was quenched with a saturated solution of

NH_4Cl. The organic layer was then diluted with hexanes, diethyl ether or CH_2Cl_2, and washed with water or saturated NH_4Cl (1×). The combined aqueous layers were extracted with hexanes, diethyl ether, or CH_2Cl_2 (2×). The combined organic layers were dried over $MgSO_4$, filtered, and the solvent was removed from the filtrate in vacuo to afford the crude product, which was purified by column chromatography (silica gel). Eluents and other slight modifications are described below for each compound.

General Procedure for Deprotection of TIPS-Protected Alkynes using TBAF. In a round-bottomed flask equipped with a magnetic stir bar, the protected alkyne was dissolved in CH_2Cl_2 ([protected alkyne] = 0.05 - 0.1 M). TBAF in THF (1.0 M, 1.1 equiv per alkyne) was added. The mixture was stirred at room temperature for 0.5 h or until the reaction was complete (monitored by TLC). Silica gel was added and the solvent was removed in vacuo. The resulting product loaded onto silica gel was then purified by column chromatography (silica gel as the stationary phase) to provide the product.

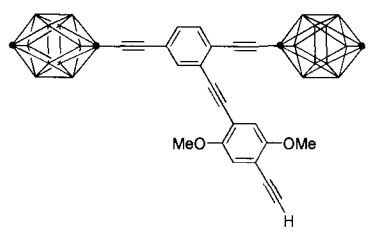

Compound (6). See the general procedure for the Pd/Cu coupling reaction. The materials used were **4**[19] (0.150 g, 0.28 mmol), **5**[23] (0.091 g, 0.27 mmol), $PdCl_2(PPh_3)_2$ (0.020 g, 0.028 mmol), CuI (0.012 g, 0.063 mmol), TEA (0.32 mL), and THF (4.0 mL) at room temperature overnight. The residue was purified by flash column chromatography with 20 % CH_2Cl_2 in hexanes; the product-containing fractions were combined, concentrated and the residue was subjected to the general procedure for the deprotection of TIPS-protected alkynes. The materials used were the TIPS protected intermediate

(0.090 g, 0.12 mmol), TBAF (0.20 mL, 1.0 M in THF) and CH_2Cl_2 (3 mL). The mixture was stirred at room temperature for 0.5 h, then passed through a silica plug using 30 % CH_2Cl_2 in hexanes as eluent to yield **6** (0.071 g, 45%, 2 steps) as an off-white solid. FTIR (KBr) 2926, 2615, 1502, 1463, 1408, 1385, 1221, 1064, 1041, 785, 665 cm^{-1}; ^1H NMR (400 MHz, $CDCl_3$) δ 7.45 (d, J = 1.2 Hz, 1H), 7.22 (d, 1H, J = 8.0 Hz), 7.13 (dd, J_1 = 8.0 Hz, J_2 = 1.2 Hz, 1H), 7.04 (s, 1H), 7.01 (s, 1H), 3.97 (s, 3H), 3.89 (s, 3H), 3.44 (s, 1H), 3.40-1.45 (br, 22H); ^{13}C NMR (100 MHz, $CDCl_3$) δ 154.5, 154.0, 135.3, 132.1, 131.0, 126.4, 123.8, 122.0, 116.2, 115.6, 113.4, 112.5, 91.8, 91.0, 90.4, 87.8, 82.8, 79.9, 77.9, 77.7, 60.3, 56.5, 56.4; EI-HRMS m/z calcd for $C_{26}H_{34}B_{20}O_2$ 595.4549, found 595.4552.

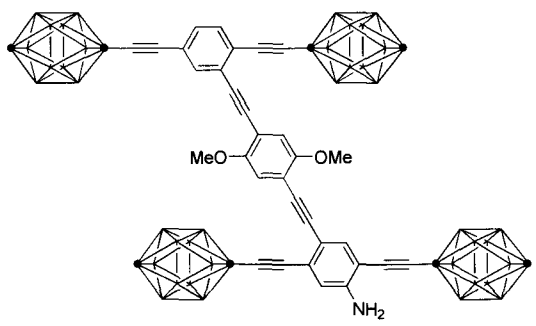

Compound (8). Terminal alkyne **6** (0.019 g, 0.031 mmol) was subjected to the general Sonogashira protocol, using **7**[23] (0.019 g, 0.034 mmol), $PdCl_2(PPh_3)_2$ (0.002 g, 0.003 mmol), CuI (0.001 g, 0.006 mmol), TEA (1 mL), and THF (5 mL) and stirred at room temperature overnight. The resulting residue was purified by column chromatography with 25 % CH_2Cl_2 in hexanes to give product **8** (0.017 g, 53%) as a light yellow solid. IR (drop cast) 3493, 3395, 3061, 2924, 2853, 2614, 2358, 2205, 1615, 1507, 1220, 1063, 727 cm^{-1}; ^1H NMR (400 MHz, $CDCl_3$) δ 7.47 (d, J = 1.5 Hz, 1H), 7.33, (s, 1H), 7.22 (d, J = 8 Hz, 1H), 7.13, (dd, J = 8 Hz, J = 1.5 Hz, 1H), 7.04 (d, J = 1.3 Hz, 2H), 6.59 (s, 1H), 4.13 (brs, 1H), 3.98 (d, J = 2 Hz, 6 H), 2.6 (br, 44 H); ^{13}C NMR (100 MHz, $CDCl_3$) δ 154.0, 153.7, 147.4, 136.1, 135.3, 132.1, 130.8, 126.6, 125.1, 123.7, 121.9,

117.2, 115.5, 115.4, 114.1, 112.2, 106.6, 92.7, 92.6, 91.6, 90.9, 87.7, 77.9, 77.8, 74.8, 60.2, 56.3, 29.6; MALDI calc'd for $C_{40}H_{59}B_{40}NO_2$: 1018.9, found: 1019.0.

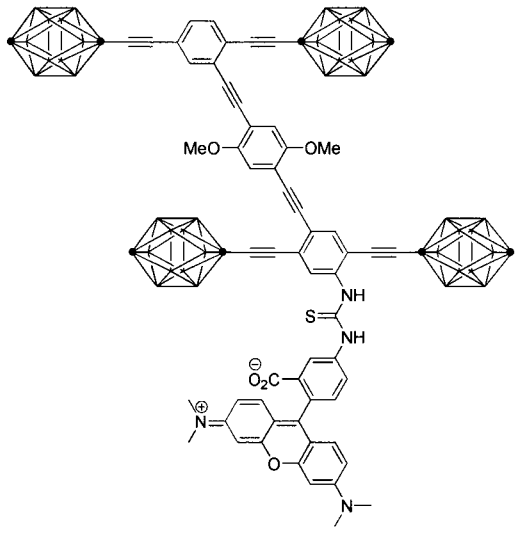

Nanocar (1). In a Schlenk tube under nitrogen **8** (0.021 g, 0.026 mmol) was dissolved in DMF (1.0 mL) and Et_3N (0.1 mL). TRITC (5.8 mg, 0.013 mmol) in solution in DMF (1.0 mL) was added dropwise and the mixture was heated to 60 °C, then stirred overnight in the dark. The solvents were then removed by rotary evaporation under reduced pressure. The resulting solid was purified by flash column chromatography with 10 % methanol in CH_2Cl_2 to yield **1** as a purple solid (0.003 g, 16%). IR (drop cast) 3349, 2960, 2921, 2851, 2615, 2359, 2342, 1737, 1596, 1510, 1249, 1185, 1112, 1039, 828, 803 cm^{-1}; ^1H NMR (400 MHz, $CDCl_3$) δ 7.98 (br s, 1H), 7.82 (d, J = 8.8 Hz, 1H), 7.48 (m, 1H), 7.15 (m, 5H), 6.82 (m, 2H), 6.69 (d, J = 8.6 Hz, 2H), 6.50 (d, J = 2.0 Hz, 2H), 6.42 (dd, J = 7.6 Hz, J = 2.0 Hz, 2H), 4.01 (s, 6H), 3.00 (s, 12H), 3.00-1.47 (br m, 44H). The material was not soluble enough for ^{13}C analysis. MALDI calc'd: 1461.9, found: 1462.2.

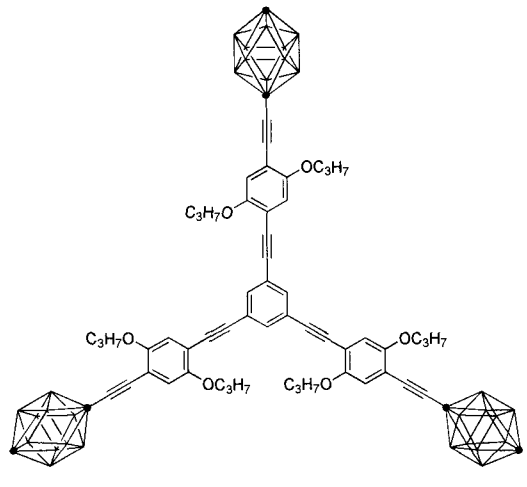

Compound (11). Trialkyne **9**[19] (0.100 g, 0.667 mmol) was subjected to the general Sonogashira protocol, using **10** (0.978 g, 2.00 mmol), $PdCl_2(PPh_3)_2$ (0.126 g, 0.179 mmol), CuI (0.066 g, 0.346 mmol), TEA (3.0 mL), and THF (10.0 mL) and stirred at room temperature overnight. The resulting residue was purified by column chromatography with 25 % CH_2Cl_2 in hexanes to give product **8** (0.557 g, 68%) as a light yellow solid. FTIR (KBr) 2963, 2613, 1579, 1502, 1423, 1218, 1061 cm^{-1}; ^1H NMR (400 MHz, $CDCl_3$) δ 7.57 (s, 3H), 6.89 (s, 3H), 6.76 (s, 3H), 3.92 (t, J = 5.2 Hz, 6H), 3.87 (t, J = 5.2 Hz, 6H), 3.15 – 1.90 (br, 33H), 1.82 (m, 12H), 1.08 (m, 18H); ^{13}C NMR (100 MHz, $CDCl_3$) δ 154.5, 153.7, 134.2, 124.3, 117.2, 117.1, 114.5, 112.5, 93.5, 91.0, 87.1, 76.2, 71.4, 71.1, 22.9, 22.8, 10.8, 10.7; MALDI *m/z* calcd for $C_{60}H_{84}B_{30}O_6$ 1226.0, found 1226.0.

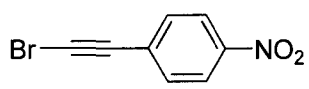

Compound (12). 1-Nitro-4-trimethylsilylacetylene-benzene (2.19 g, 10.00 mmol) was combined with $AgNO_3$ (0.340 g, 2.00 mmol), NBS (1.80 g, 10.1 mmol) and acetone (100 mL). The mixture was stirred for 2 h in the dark, and poured onto a pad of silica gel. The pad was then eluted with 40% CH_2Cl_2 in hexanes and the solvents removed to yield

12 (2.37 g, 91%) as a light yellow solid. *Caution: alkynyl bromides decompose over time and evolve HBr. Care should be taken when handling.* (FTIR (KBr) 3105, 2196, 1772, 1698, 1591, 1508, 1346, 1192, 853, 748 cm^{-1}; ^{1}H NMR (400 MHz, $CDCl_3$) δ 8.18 (d, J = 8.8 Hz, 2H), 7.58 (d, J = 8.8 Hz, 2H); ^{13}C NMR (100 MHz, $CDCl_3$) δ 133.0, 123.8; EI-HRMS *m/z* calcd for $C_8H_4BrNO_2$ 224.9425, found 224.9419.

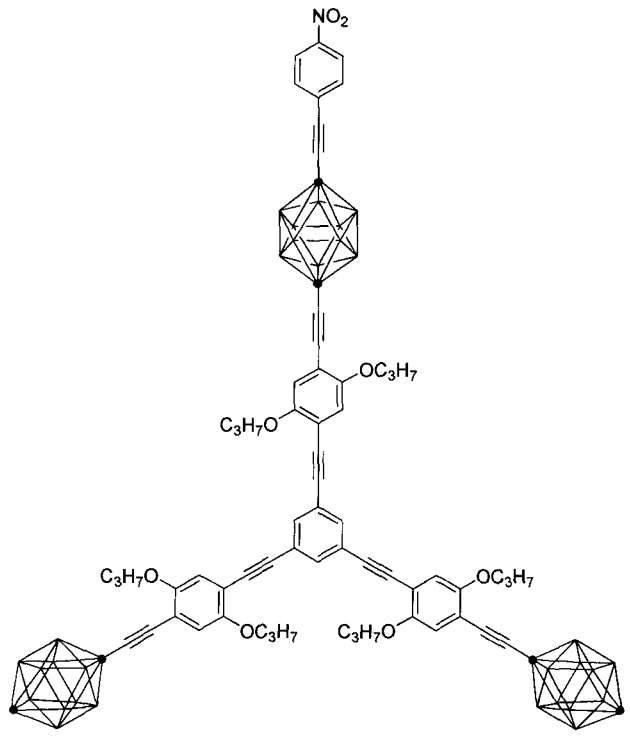

Compound (13). Trimer **11** (0.40 g, 0.33 mmol) was added to an oven-dried three-neck round bottom flask, followed by THF (4.66 mL). The mixture was cooled to -78 °C, and *n*-BuLi (2.5 M in hexanes, 0.13 mL, 0.033 mmol) was added dropwise. The mixture was allowed to stir at -15 °C for 1 h, followed by cooling to -78 °C. To the blue mixture was then added CuBr (0.061 g, 0.424 mmol), followed by warming to -15 °C and stirring for 1 h. Alkynyl bromide **12** (0.096 g, 0.424 mmol) was then added all at once as a solid, and the mixture was allowed to warm to room temperature and stirred overnight. The reaction was quenched by addition of 1 drop of water, followed by elution through a

celite pad with CH_2Cl_2. The resulting residue was then purified using flash chromatography with 25 % CH_2Cl_2 in hexanes as eluent to give product **13** (0.098 g, 22%) as a light yellow solid. FTIR (KBr) 2963, 2925, 2875, 2855, 2615, 1579, 1502, 1467, 1423, 1387, 1343, 1276, 1218, 1062, 1017, 989 cm^{-1}; ^1H NMR (400 MHz, $CDCl_3$) δ 8.14 (d, J = 7.2 Hz, 2H), 7.57 (s, 3H), 7.47 (d, J = 6.8 Hz, 2H), 6.89 (s, 3H), 6.76 (s, 3H), 3.92 (t, J = 5.2 Hz, 6H), 3.86 (t, J = 5.2 Hz, 6H), 3.20 – 1.90 (br, 33H), 1.81 (m, 12H), 1.07 (m, 18H) ; ^{13}C NMR (100 MHz, $CDCl_3$) δ 154.5, 153.7, 147.8, 134.2, 133.1, 128.2, 124.3, 124.2, 123.7, 117.19, 117.17, 117.1, 117.0, 114.8, 114.5, 93.7, 93.5, 91.1, 87.1, 71.4, 71.3, 71.1, 71.0, 29.9, 22.9, 22.8, 10.8; MALDI m/z calcd for $C_{68}H_{87}B_{30}NO_8$ 1371.0, found 1371.0.

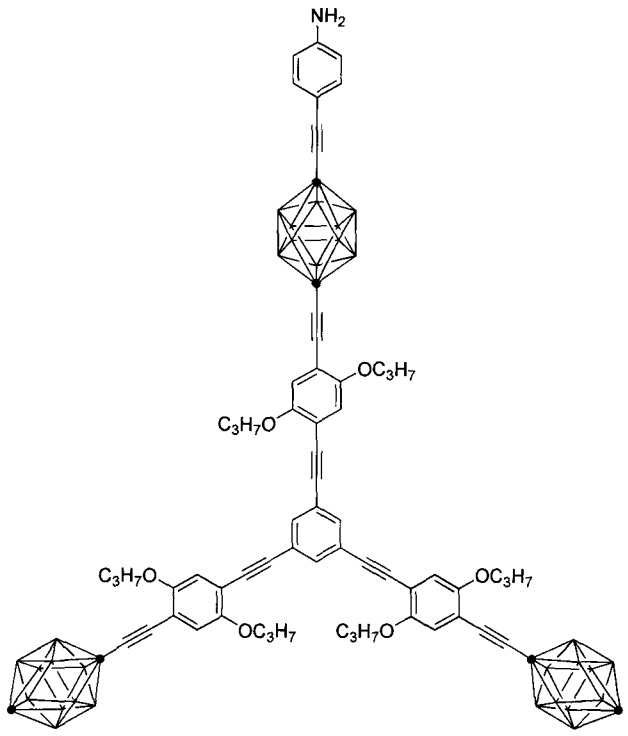

Compound (14). To a round bottom flask with stir bar was added trimer **13** (0.074 g, 0.054 mmol), Zn powder (0.353 g, 5.39 mmol), 1 drop AcOH and THF (3.0 mL). The mixture was allowed to stir for 1 h and the reaction quenched by elution

through a celite pad with CH_2Cl_2. The resulting residue was then purified using flash chromatography with 25 % CH_2Cl_2 in hexanes as eluent to give product **14** (0.072 g, 100%) a light yellow solid. IR (drop cast) 3568, 3386, 2964, 2934, 2876, 2614, 2364, 2229, 1619, 1605, 1578, 1501, 1422, 1386, 1276, 1217, 1062, 1015 cm^{-1}; ^1H NMR (400 MHz, $CDCl_3$) δ 7.57 (s, 3H), 7.11, (d, J = 8.7 Hz, 2H), 6.89 (s, 3H), 6.75, (s, 3H), 6.53 (d, J = 8.7 Hz, 2H), 3.92 (t, J = 6.5 Hz, 6H), 3.86 (t, J = 6.2 Hz, 6H), 2.6 (brm, 46H), 1.06 (t, J = 7.4 Hz, 18H); ^{13}C NMR (100 MHz, $CDCl_3$) δ 154.5, 153.7, 134.2, 133.5, 124.3, 117.2, 117.1, 115.7, 114.7, 114.5, 112.5, 112.4, 93.6, 87.1, 76.2, 71.4, 71.1, 29.9, 22.9, 10.8; MALDI calc'd for $C_{68}H_{90}B_{30}NO_6$: 1341.0, found: 1342.1 (M+H).

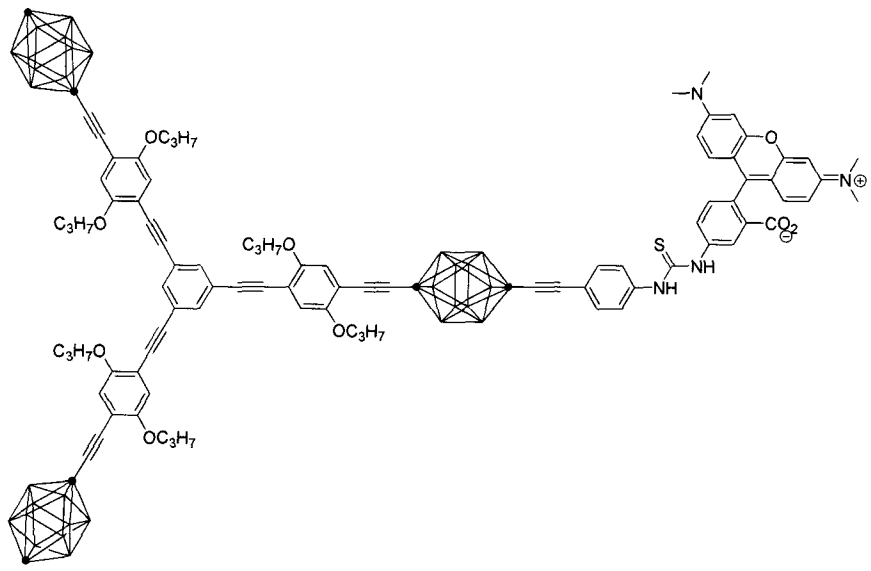

Trimer 2. Into a Schlenk tube under nitrogen, trimer **14** (15 mg, 0.011mmol) was dissolved in CH_2Cl_2 (1 ml) and TEA (0.1 ml). TRITC (5 mg, 0.011 mmol) in solution in DMF (1 ml) was added dropwise and the mixture was stirred overnight in the dark at room temperature. The solvents were removed by rotary evaporation. The resulting residue was then purified using flash chromatography with 10% MeOH in CH_2Cl_2 as eluent to give **2** (9 mg, 45%) as a purple solid. IR (drop cast) 3350, 2961, 2924, 2853,

2615, 2369, 1596, 1500, 1421, 1365, 1349, 1218, 1188 cm^{-1}; ^1H NMR (400 MHz $CDCl_3$) δ 8.05 (br s, 1H), 7.89 (d, J = 8.8 Hz, 1H), 7.74 (br s, 1H), 7.58 (m, 1H), 7.52 (s, 3H), 7.20 (m, 4H), 7.05 (d, J = 9.5 Hz, 1H), 6.85 (s, 3H), 6.72 (dd, J = 8.3 Hz J = 2.0 Hz, 2H), 6.71 (s, 3H), 6.67 (d, J = 2.0 Hz, 2H), 3.88 (t, J = 6.5 Hz, 6H), 3.82 (t, J = 6.5 Hz, 6H), 3.21 (s, 12H), 3.00-1.47 (br m, 33H), 1.77 (m, 12H), 1.02 (m, 18H); MALDI calc'd for $C_{93}H_{110}B_{30}N_4O_6S$: 1784.1, found: 1785.1 (M+H).

References and Notes

(1) For examples of early work see Balzani, V.; Credi, A.; Venturi, M. *Molecular Devices and Machines: A Journey Into the Nanoworld*; Wiley-VCH: Weinheim, Germany, 2003.

(2) For a comprehensive review of molecular machine work see Kay, E. R.; Leigh, D. A.; Zerbetto, F. *Angew. Chem. Int. Ed.* **2007**, *46* 72-191.

(3) For recent monumentalization (synthetic) approaches see: a) Shirai, Y.; Morin, J.-F.; Sasaki, T.; Guerrero, J.; Tour, J. M. *Chem. Soc. Rev.* **2006**, *35*, 1043-1055. b) Jimenez-Bueno, G.; Rapenne, G. *Tetrahedron* **2007**, *63*, 7018-7026. c) Spruell, J. M.; Dichtel, W. R.; Heath, J. R.; Stoddart, J. F. *Chem. Eur. J.* **2008**, *14*, 4168-4177. For recent self-assembly approaches see: d) *Molecular motors and muscles*; S. Saha, S; J. F. Stoddart, J. F. Wiley-VCH: Weinheim, Germany 2007, 295-327. e) Aprahamian, I.; Yasuda, T.; Ikeda, T.; Saha, S.; Dichtel, W. R.; Isoda, K.; Kato, T.; Stoddart, J. F. *Angew. Chem. Int. Ed.* **2007**, *119*, 4759-4763. f) Vives, G.; Tour, J. M. *Acc. Chem. Res.* in press.

(4) a) Takano, H.; Kenseth, J. R.; Wong, S.-S.; O'Brien, J. C.; Porter, M. D. *Chem. Rev.* **1999**, *99*, 2845-2890. b) Soong, R. K.; Bachand, G. D.; Neves, H. P.; Olkhovets, A. G.; Craighead, H. G.; Montemagno, C. D. *Science* **2000**, *290*, 1555-1558. c) Bachand, G. D.; Soong, R. K.; Neves, H. P.; Olkhovets, A. G.; Craighead, H. G. Montemagno, C. D. *Nano Lett.* **2001**, *1*, 42-44. d) Park, H.; Toprak, E.; Selvin, P. R. *Quarterly Reviews of Biophysics* **2007**, *40*, 87-111.

(5) a) Rosei, F.; Schunack, M.; Naitoh, Y.; Jiang, P.; Gourdon, A.; Laegsgaard, E.; Stensgaard, I.; Joachim, C.; Besenbacher, F. *Prog. Surf. Sci.* **2003**, *71*, 95-146. b) Tinnefeld, P.; Sauer, M. *Angew. Chem. Int. Ed.* **2005**, *44*, 2642-2671. c) Sasaki, T.; Guerrero, J. M.; Leonard, A. D.; Tour, J. M. *Nano Research* **2008**, *5*, 412-419.

(6) a) Avouris, P. *Acc. Chem. Res.* **1995**, *28*, 95-102. b) Anderson, H. *Angew. Chem. Int. Ed.* **2000**, *39*, 2451-2453 and references contained within.

(7) Rosei, F.; Schunack, M.; Jiang, P.; Gourdon, A.; Legsgaard, E.; Stensgaard, I.; Joachim, C.; Besenbacher, F. *Science* **2002**, *296*, 328-331.

(8) Grill, L.; Rieder, K.-H.; Moresco, F.; Jimenez-Bueno, G.; Wang, C.; Rapenne, G.; Joachim, C. *Surf. Sci.* **2005**, *584*, L153-L158.

(9) Kwon, K.-Y.; Wong, K. L.; Pawin, G.; Bartels, L.; Stolbov, S.; Rahman, T. S. *Phys. Rev. Lett.* **2005**, *95*, 166101-166104.

(10) Gimzewski, J. K.; Joachim, C.; Schlittler, R. R.; Langlais, V.; Tang, H.; Johannsen, I. *Science* **1998**, *281*, 531. b) Gross, L.; Rieder, K. –H.; Moresco, F.; Stojkovic, S. M.; Gourdon, A.; Joachim, C. *Nat. Mater.* **2006**, *4*, 892.

(11) Shirai, Y.; Osgood, A. J.; Zhao, Y.; Kelly, K. F.; Tour, J. M. *Nano Lett.* **2005**, *5*, 2330-2334.

(12) Eigler, D. M.; Lutz, C. P. ; Rudge, W. E. *Nature* **1991**, *352*, 600-603.

(13) Haustein, E.; P. Schwille, P. *Methods* **2003**, *29*, 153–166, and references within.

(14) a) Yildiz, A.; Forkey, J.N.; McKinney, S.A.; Ha, T.; Goldman, Y.E.; Selvin, P.R. *Science* **2003**, *300*, 2061-2065. b) Yildiz, A.; Tomishige, M.; Vale, R. D.; Selvin, P. R. *Science* **2004**, *303*, 676-678.

(15) Thompson, R. E.; Larson, D. R.; Webb, W. W. *Biophys. J.* **2002**, *82*, 2775-2783.

(16) Khatua, S. ; Guerrero, J. M. ; Claytor, K. ; Vives, G. ; Kolomeisky, A. B. ; Tour, J. M. ; Link, S. *ACS Nano* **2008**, ASAP.

(17) Rueda, D.; Walter, N. G. *J. Nanosci. Nanotechnol.* **2005**, *5*, 1990-2000.

(18) a.) Telford, W.G.; Murga, M.; Hawley, T.; Hawley, R.; Packard, B.; Komoriya, A.; Haas, F.; Hubert, C. *Cytometry A* **2005**, *68A*, 36–44. b) Van Hoof, D.; Pinkse, M. W. H.; Ward-Van Oostwaard, D.; Mummery, C. L.; Heck, A. J. R.; Krijgsveld, J. *Nature Methods* **2007**, *4*, 678-679. c.) Perfetto, S.P.; Roederer, M. *Cytometry* A **2007**, *71A*, 73–79.

(19) Morin, J. –F.; Sasaki, T.; Shirai, Y.; Guerrero, J. M.; Tour, J. M. *J. Org. Chem.* **2007**, *72*, 9481-9490.

(20) Zarrin, F.; Dovichi, N. J. *Anal. Chem.* **1985**, *57*, 2690-2692.

(21) a.) Corrie, J. E. T. ; Craik, J. S. *J. Chem. Soc., Perkins Trans.* **1994**, 2967-2973. b.) Buchynskyy, A. ; Kempin, U.; Vogel, S. ; Hennig, L. ; Findeisen, M.; Müller, D.; Giesa, S.; Knoll, H.; Welzel, P. *Eur. J. Org. Chem.* **2002**, 1149-1162. c.) Hernando, J.; van der Schaaf, M.; van Dijk, E. M. H. P.; Sauer, M.; García-Parajó, M. F.; van Hulst, N. F. *J. Phys. Chem. A* **2003,** *107,* 43-52. d.) Reizelman, A.; Wigchert, S. C. M.; del-Bianco, C. ;

Zwanenburg, B. *Org. Biol. Chem.* **2003**, *1*, 950-959. e.) Sørensen, M. D. ; Martins, R. ; Hindsgaul, O. *Angew. Chem., Int. Ed.* **2007**, *46*, 2403-2407.

(22) Morin, J. –F.; Shirai, Y.; Tour, J. M. *Org. Lett.* **2006**, *8*, 1713-1716.

(23) Sasaki, T.; Tour, J. M. *Tetrahedron Lett.* **2007**, *48*, 5821-5824.

(24) Fox, M.A.; MacBride, J.A.H.; Peace, R.J.; Wade, K. *J. Chem. Soc., Dalton Trans.* **1998**, 401-411.

Supporting Information for Chapter 3.1

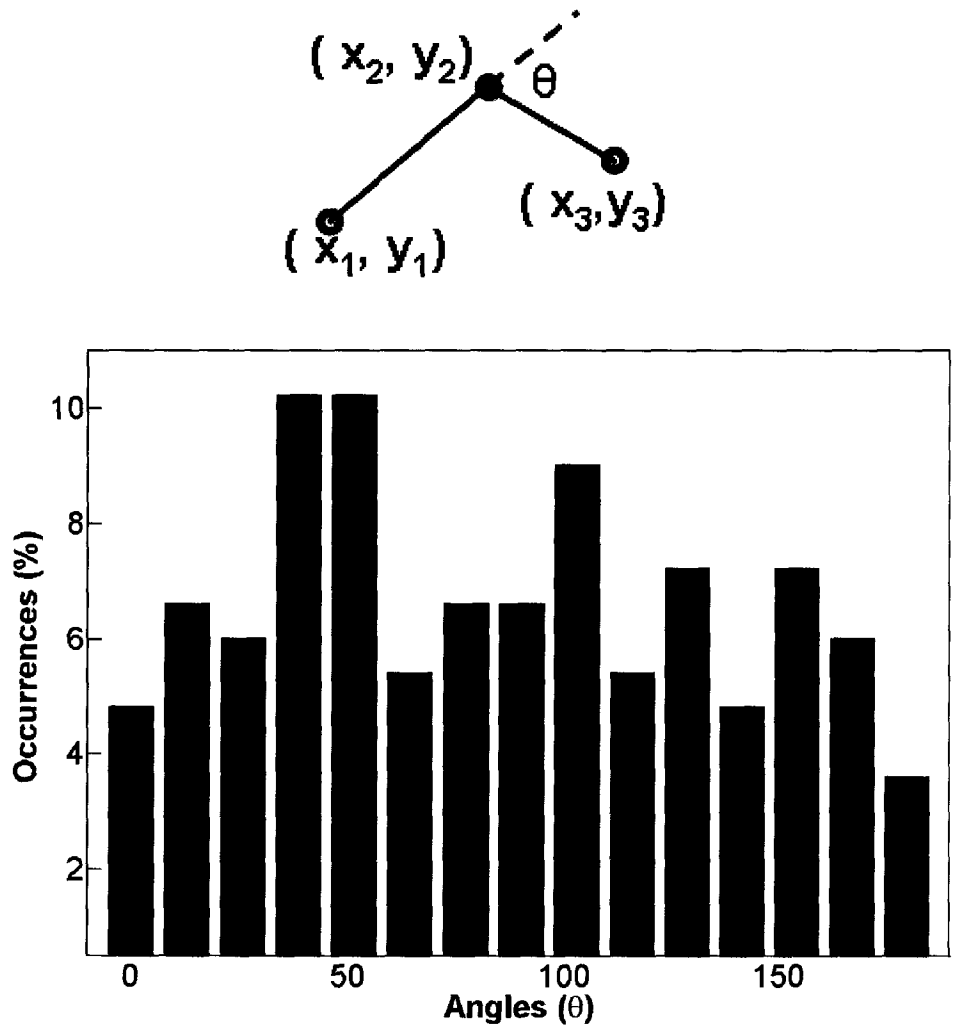

Figure S-3.1-1. Directionality of nanocar movement. To evaluate if the nanocars showed motion with a preferential direction, we calculated the angular displacements θ from unidirectional translation using the single molecule trajectories. The definition of the angle θ is shown on the top and the histogram of θ is given on the bottom. The equal distribution over all possible values of θ indicates movement in all directions without a bias for directional motion. Translation along a straight line would result in a histogram that is peaked at zero.

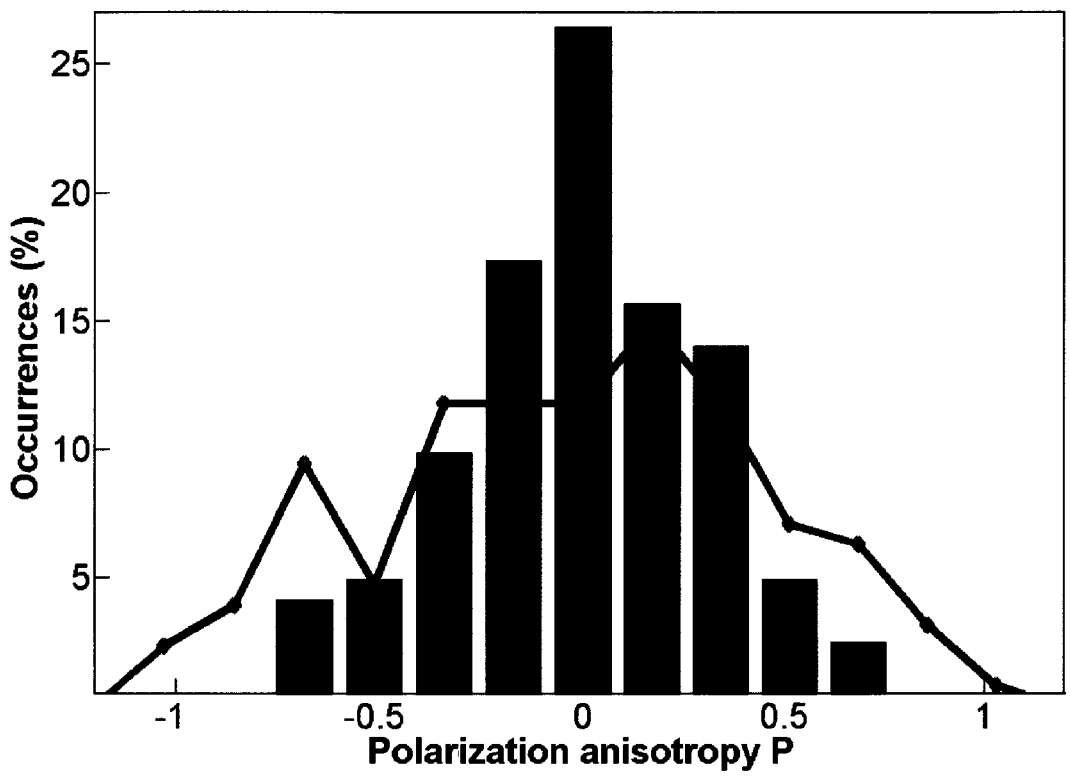

Figure S-3.1-2: Polarization anisotropy distribution of 'moving' four-wheeled nanocars. The polarization anisotropies were calculated by integrating over the area of the single molecules (5x5 pixels, red bars) and the center pixel with the highest intensity only (black line). Because of the scanning image acquisition, the different integration areas correspond to integration times of 500 ms and 1 ms, respectively. The polarization anisotropy distributions are peaked at zero indicating depolarization due to rotational movement. However, the larger width in the polarization anisotropy distribution for the center pixel suggests that rotational dynamics occur on the 1-100 ms time.

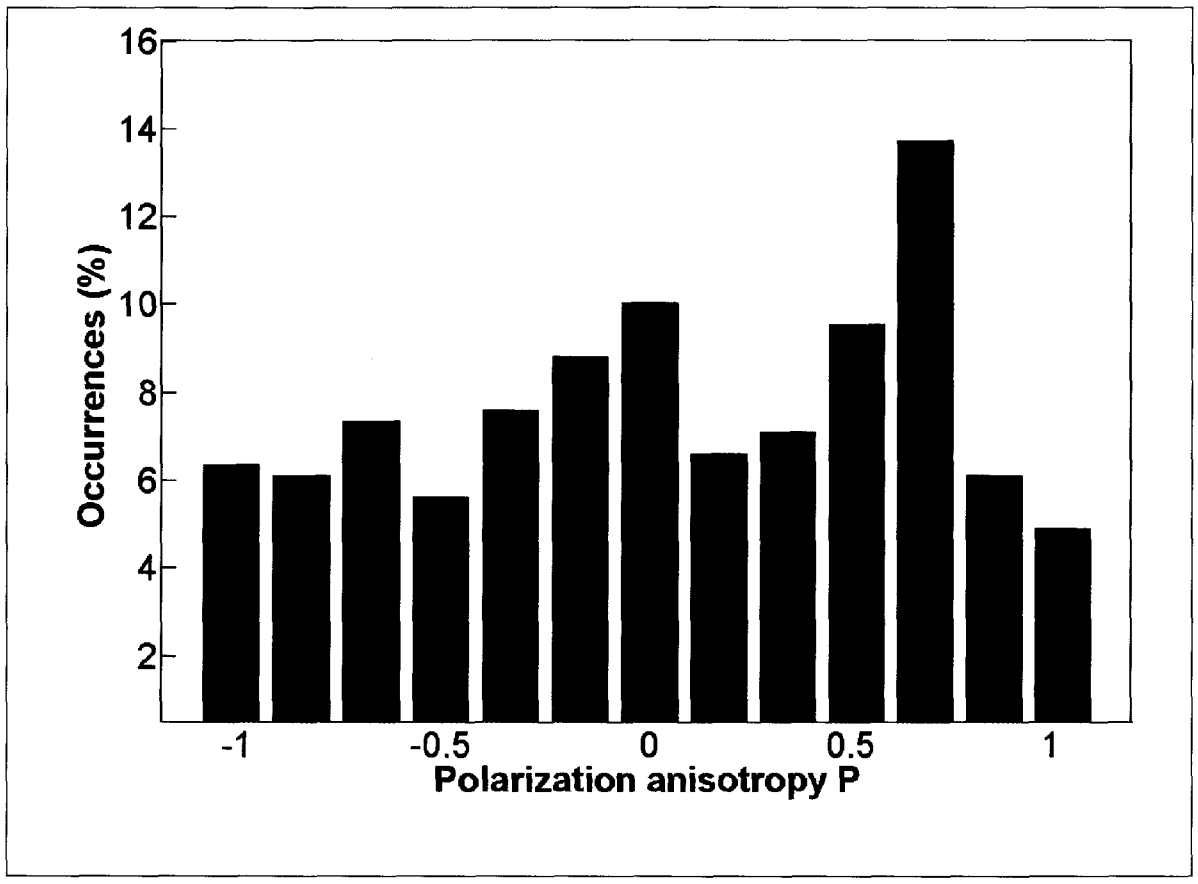

Figure S-3.1-3 Polarization anisotropy distribution of three-wheeled nanocars. The equal distribution of polarization anisotropies over the entire region from -1 to +1 indicates the absence of rotational movement of the trimer nanocars within the acquisition time of 500 ms.

Supporting Information for Chapter 3.2

Compound 6.

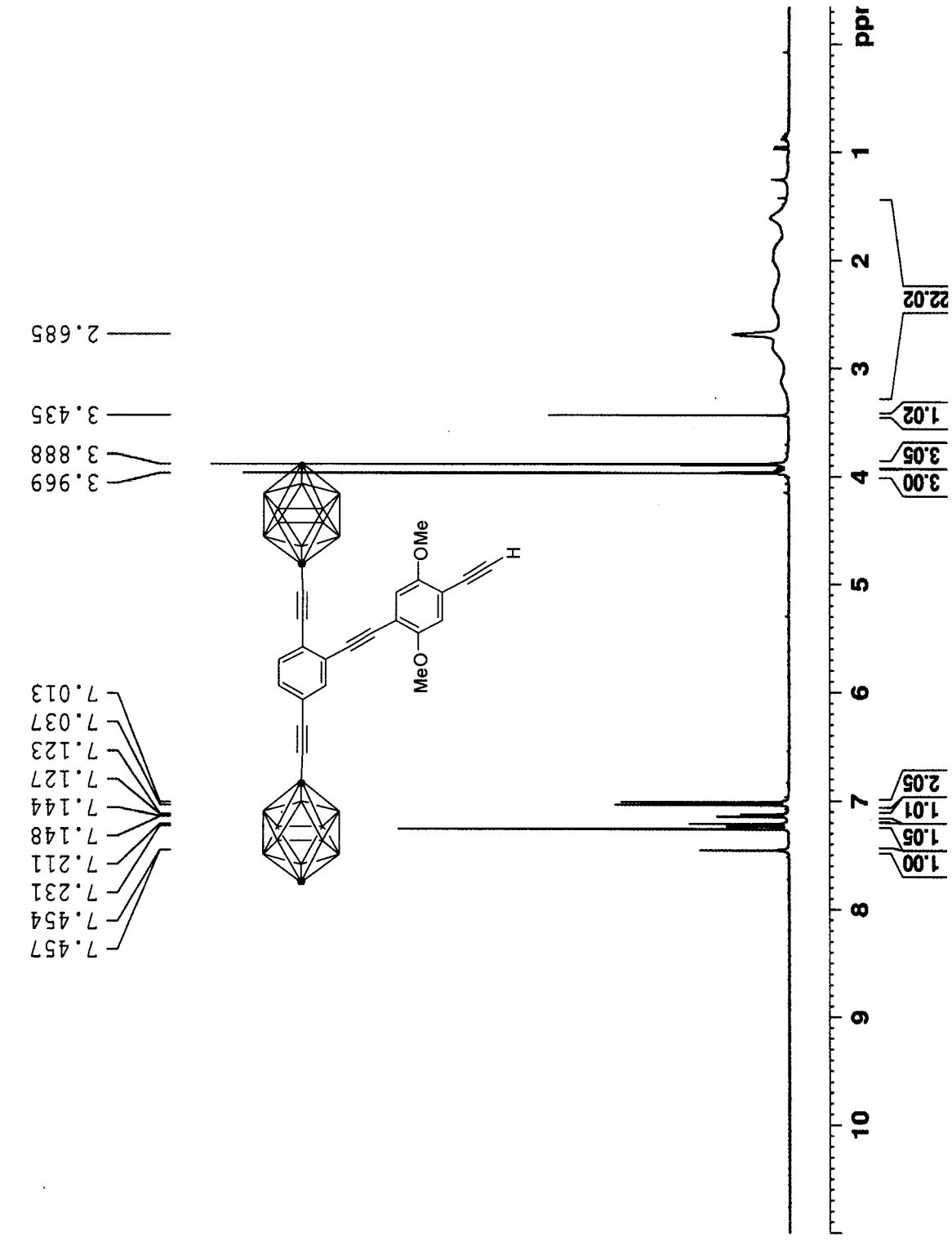

Figure S-3.2-1. ^{1}H NMR Spectrum of Compound **6**.

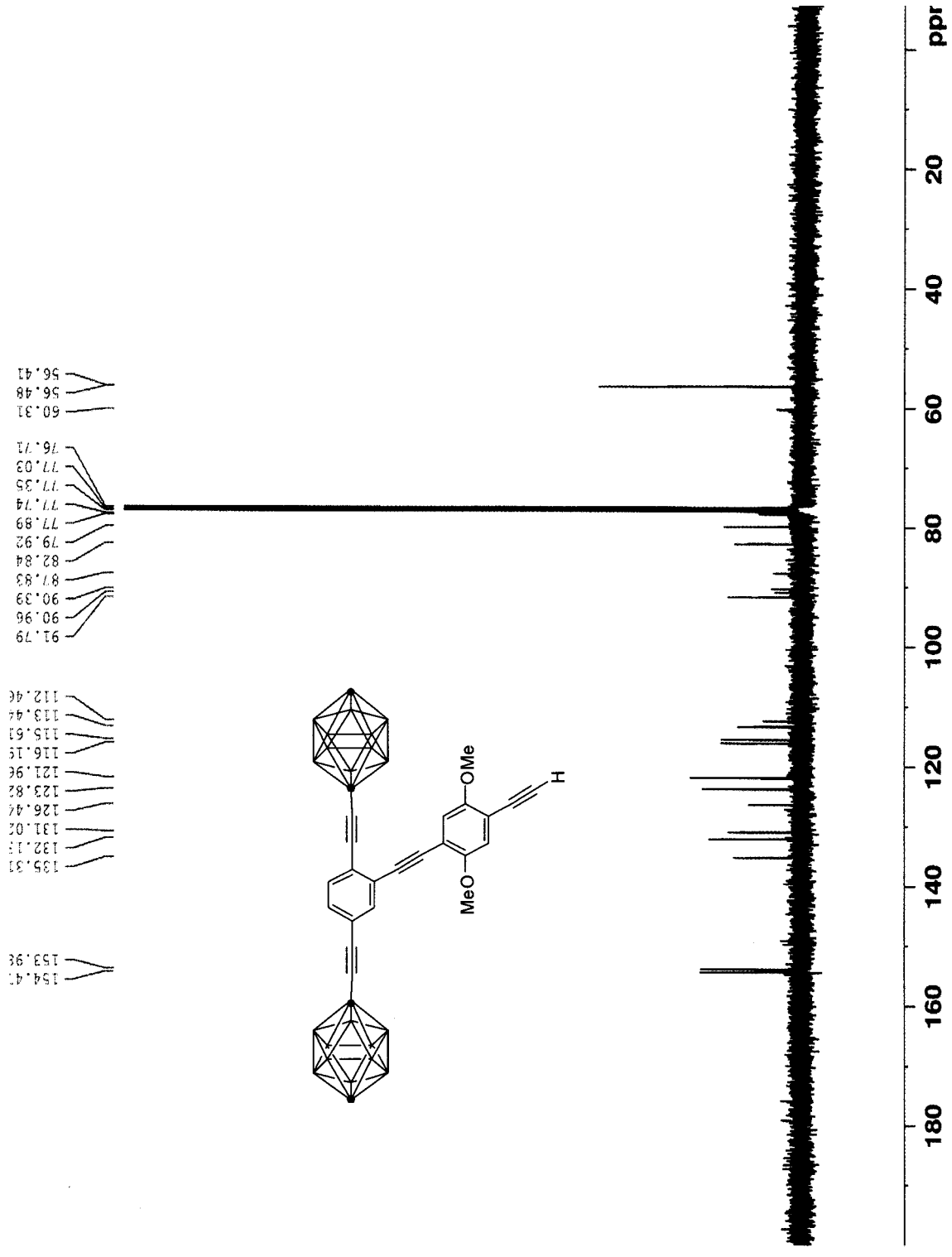

Figure S-3.2-2. ^{13}C NMR Spectrum of Compound **6**.

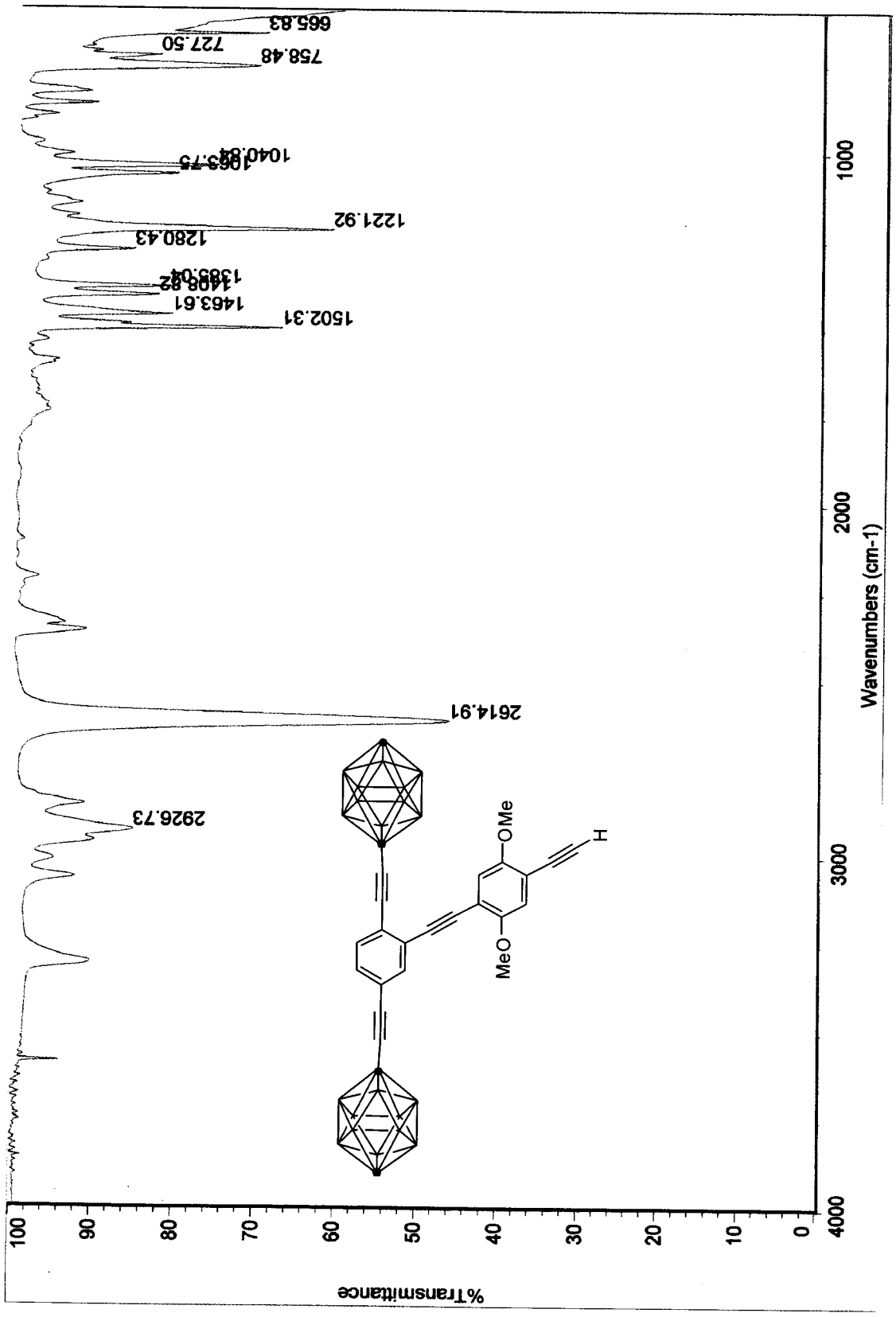

Figure S-3.2-3. IR Spectrum of Compound **6**.

Compound 8.

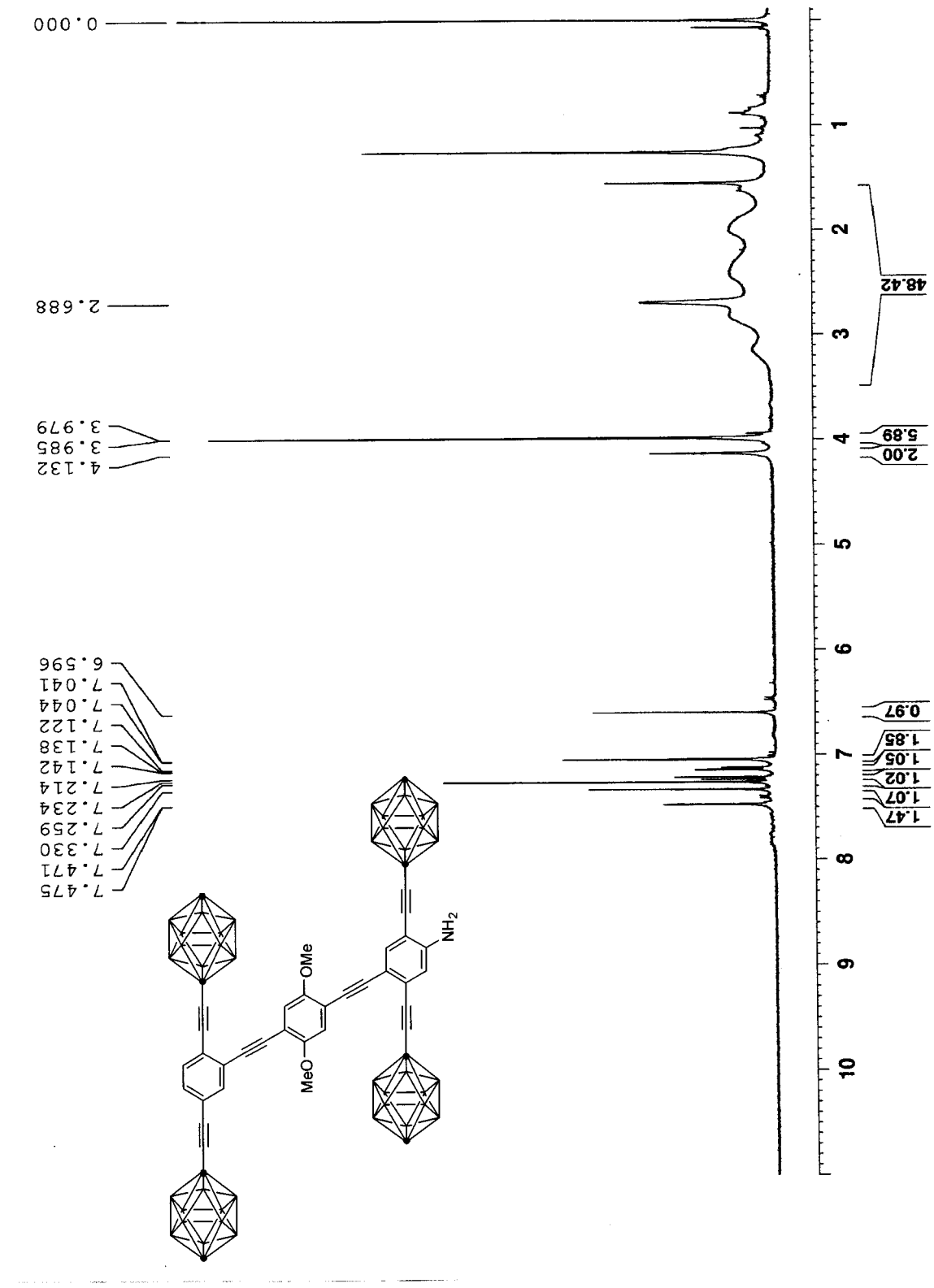

Figure S-3.2-4. ^{1}H NMR Spectrum of Compound **8**.

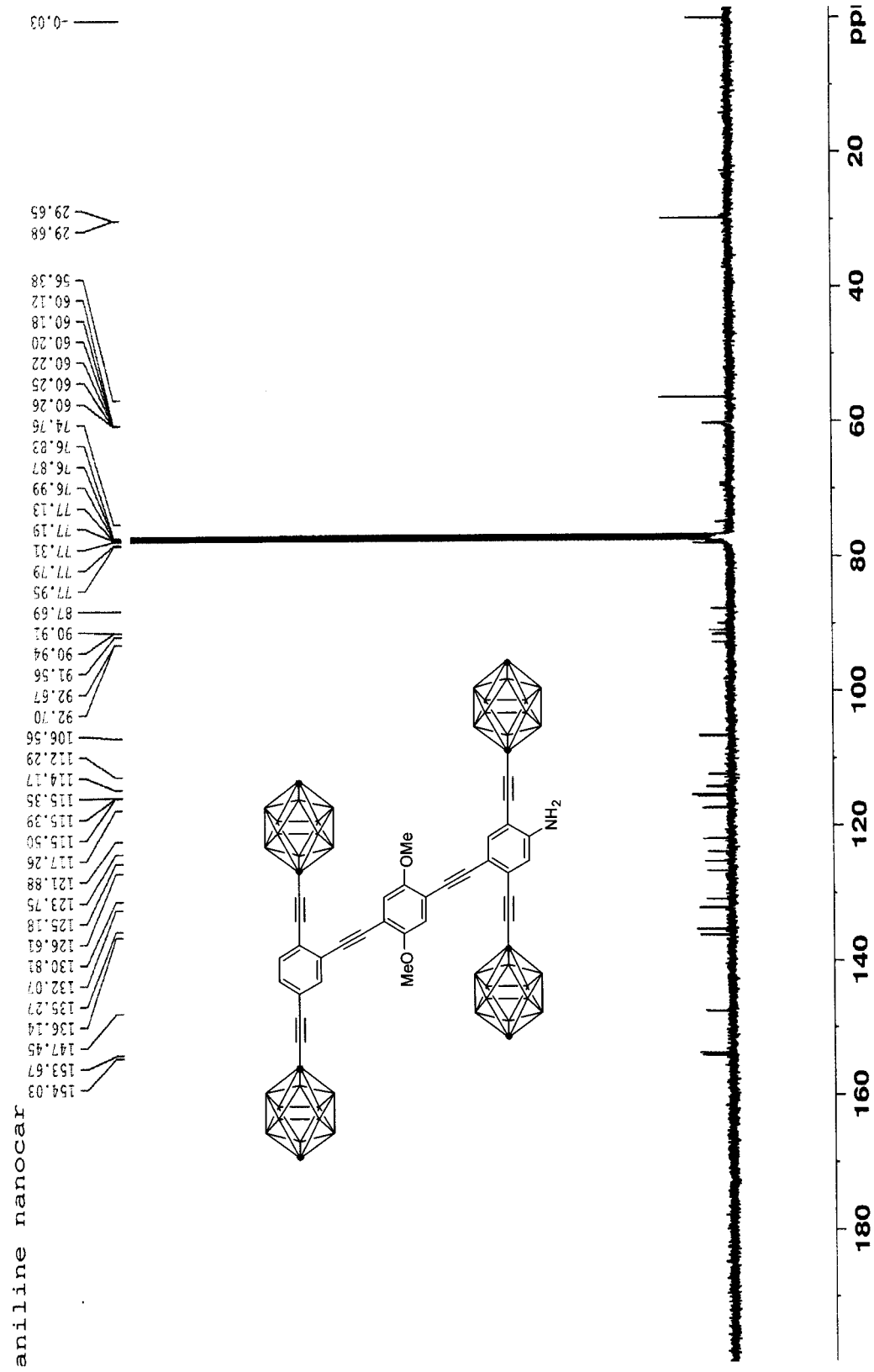

Figure S-3.2-5. ^{13}C NMR Spectrum of Compound **8**.

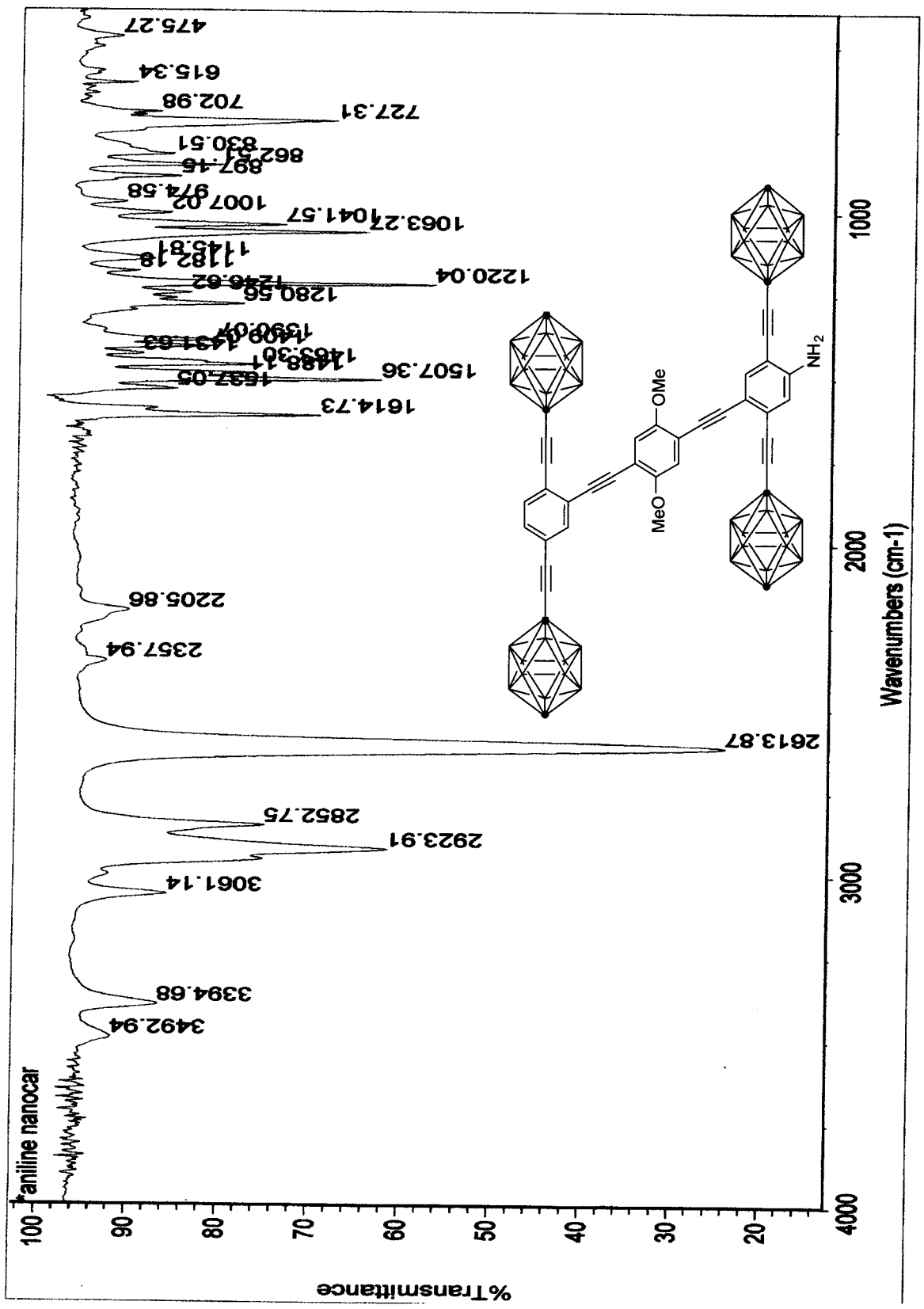

Figure S-3.2-6. IR Spectrum of Compound **8**.

Nanocar 1.

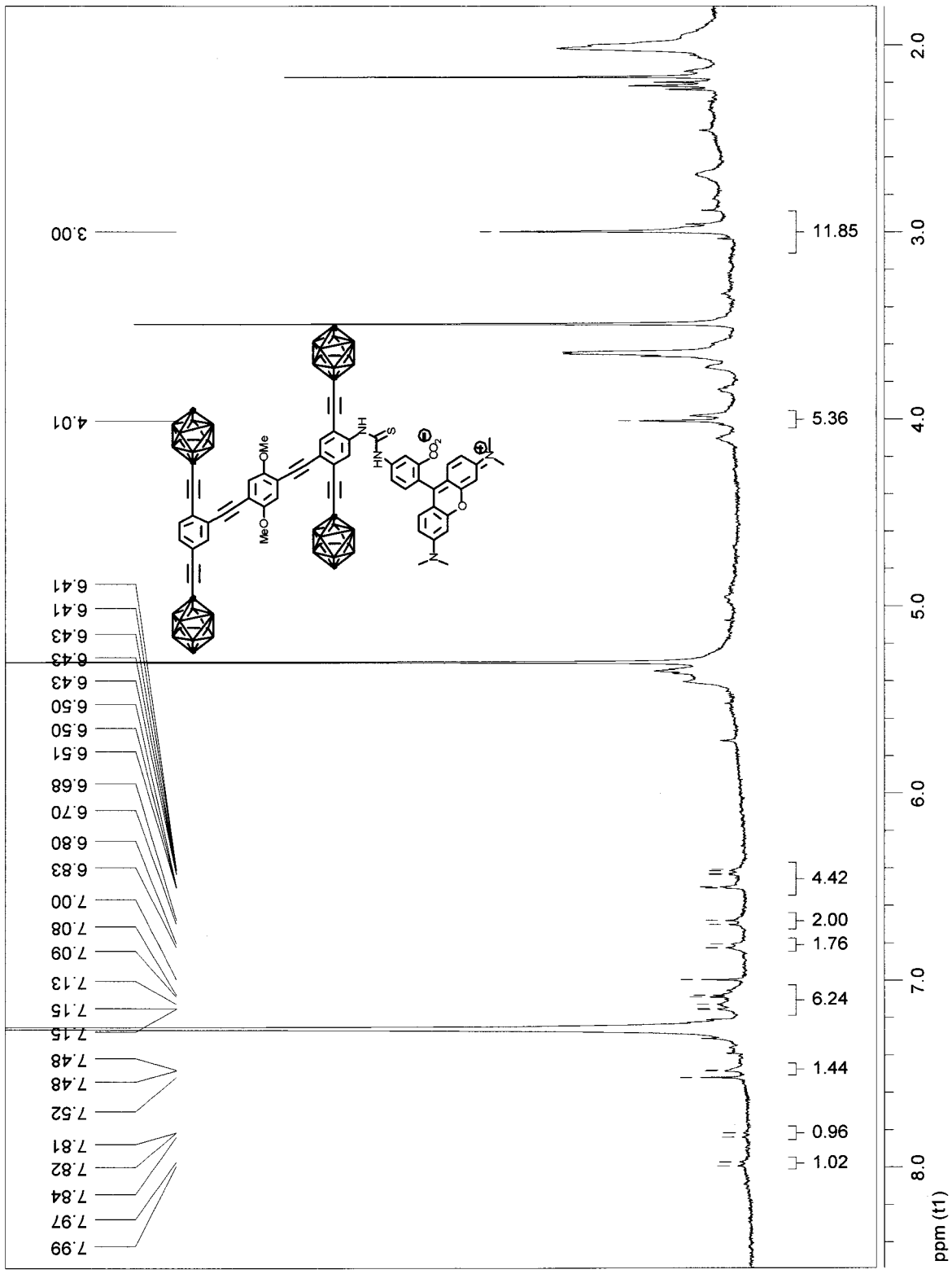

Figure S-3.2-7. ^{1}H NMR Spectrum of Nanocar **1**.

^{13}C could not be obtained for this product.

Figure S-3.2-8. ^{13}C NMR Spectrum of Nanocar **1**.

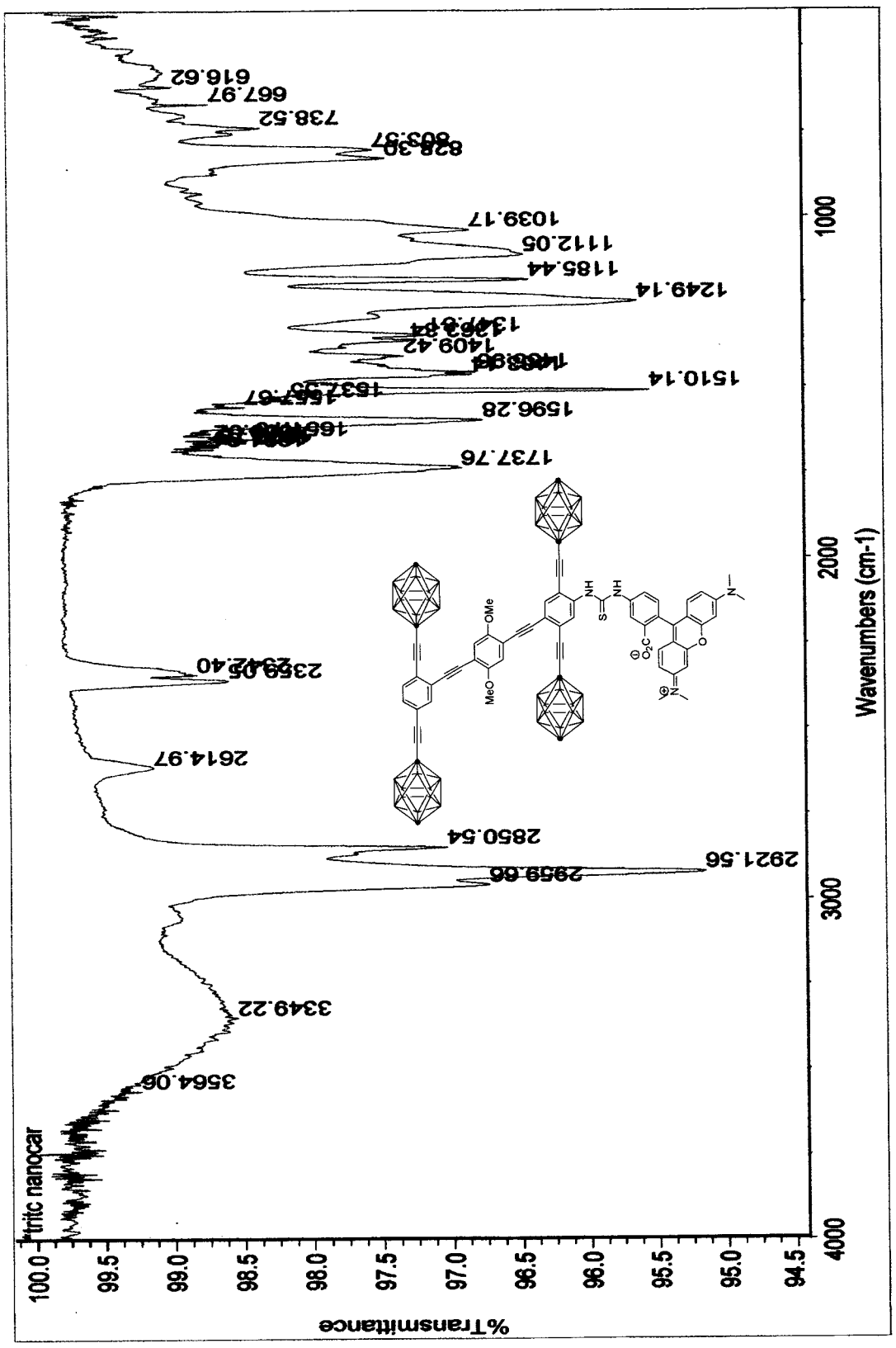

Figure S-3.2-9. IR Spectrum of Nanocar **1**.

Compound 11.

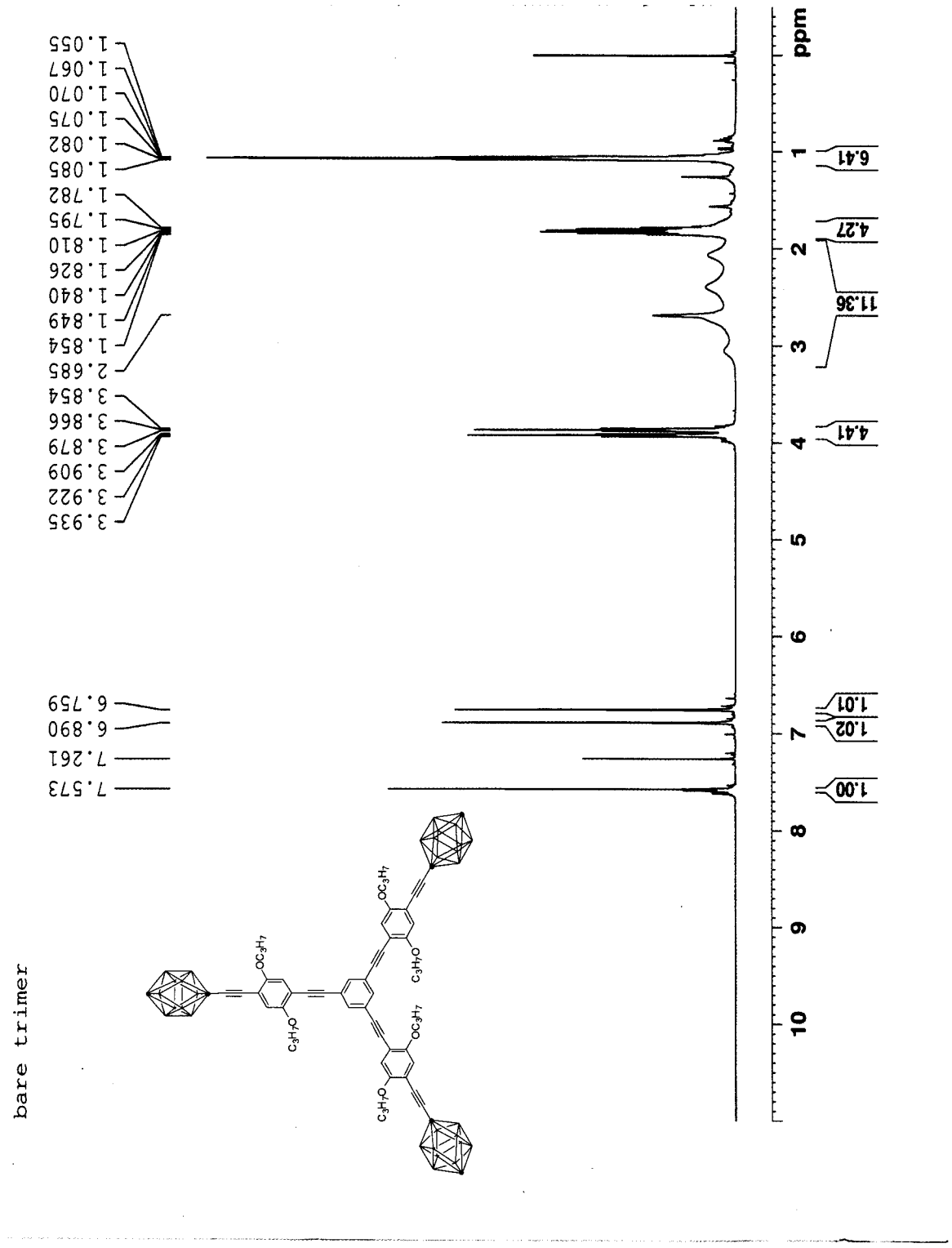

Figure S-3.2-10. ^{1}H NMR Spectrum of Compound **11**.

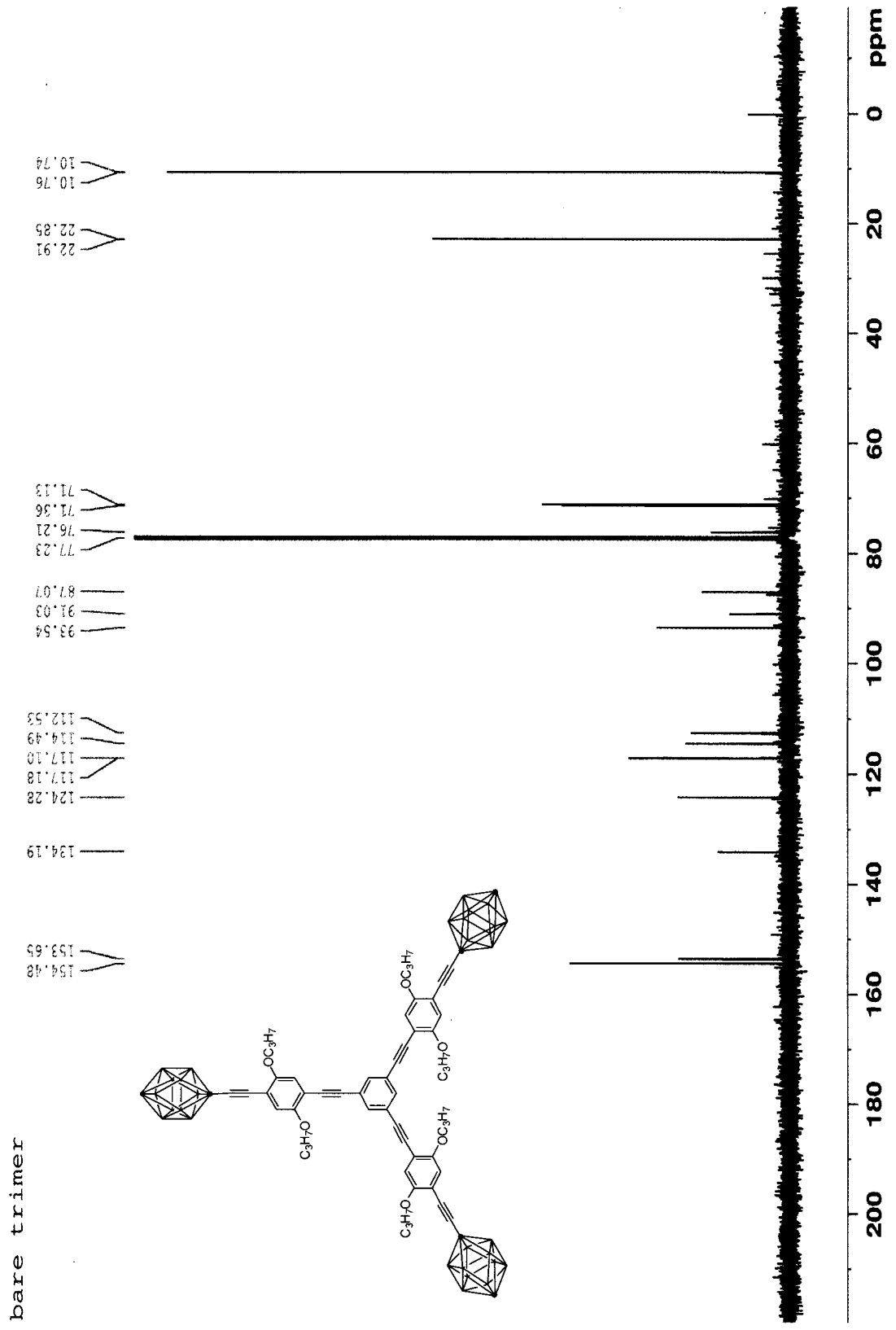

Figure S-3.2-11. ^{13}C NMR Spectrum of Compound **11**.

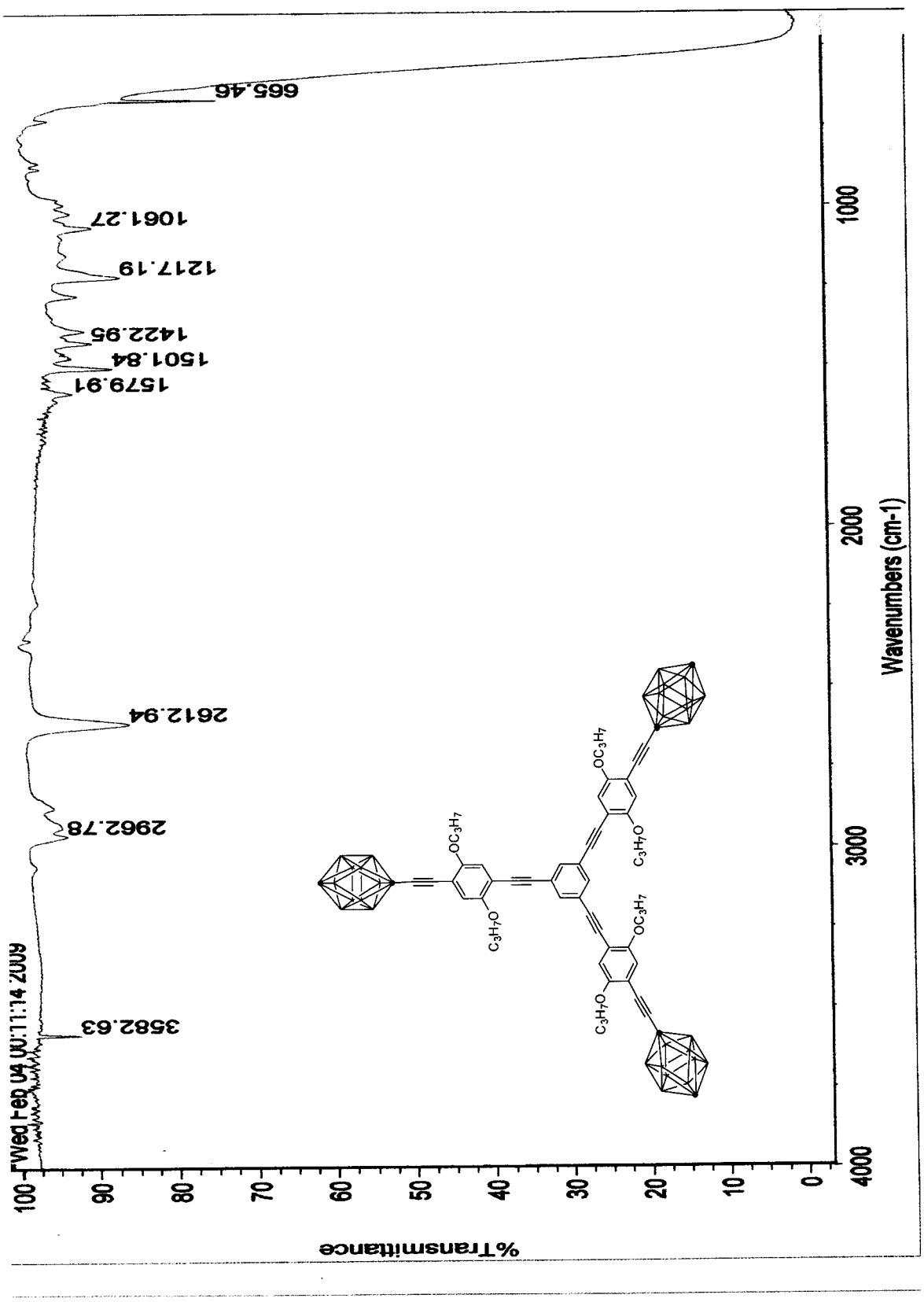

Figure S-3.2-12. IR Spectrum of Compound **11**.

Compound 12.

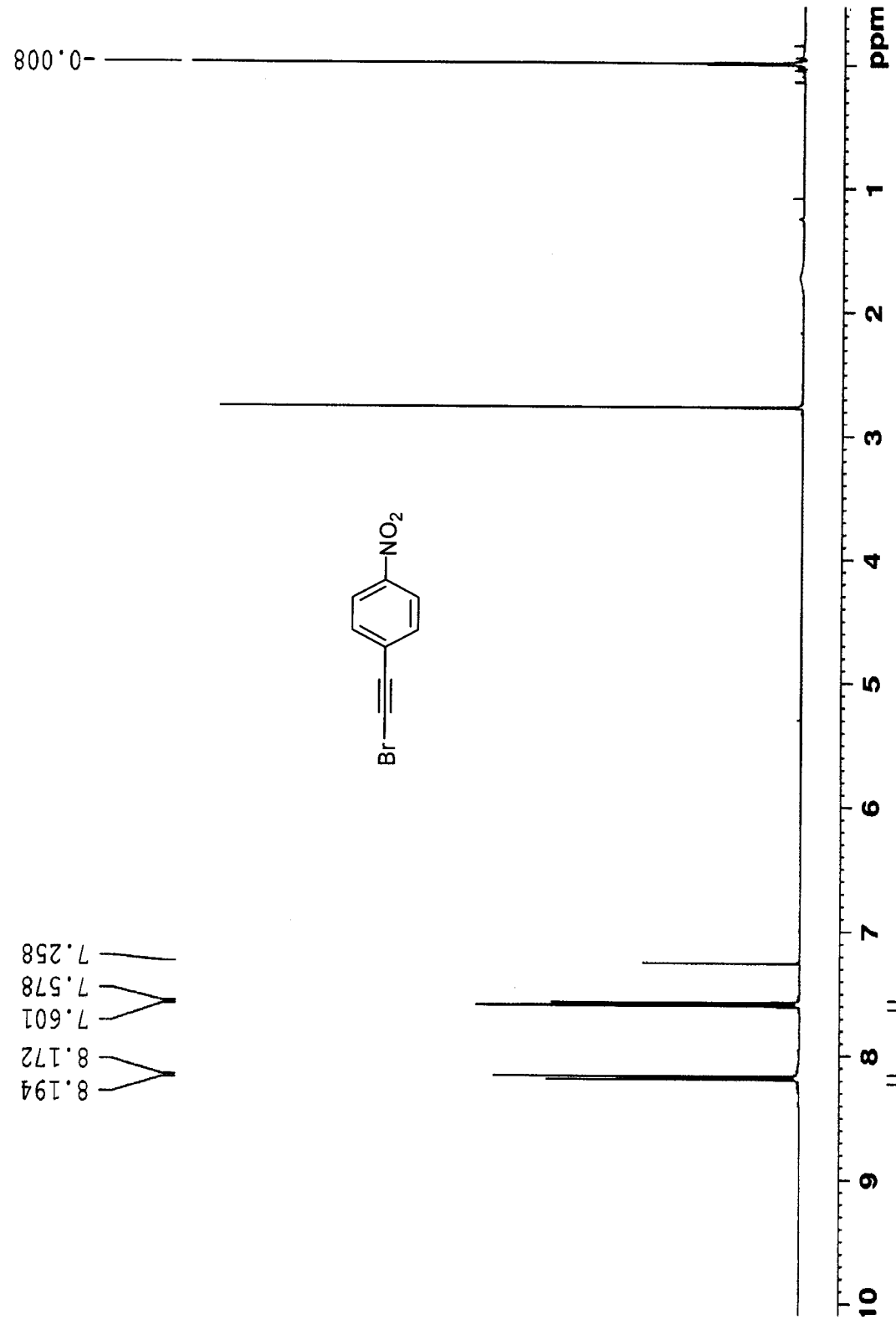

Figure S-3.2-13. ^{1}H NMR Spectrum of Compound **12**.

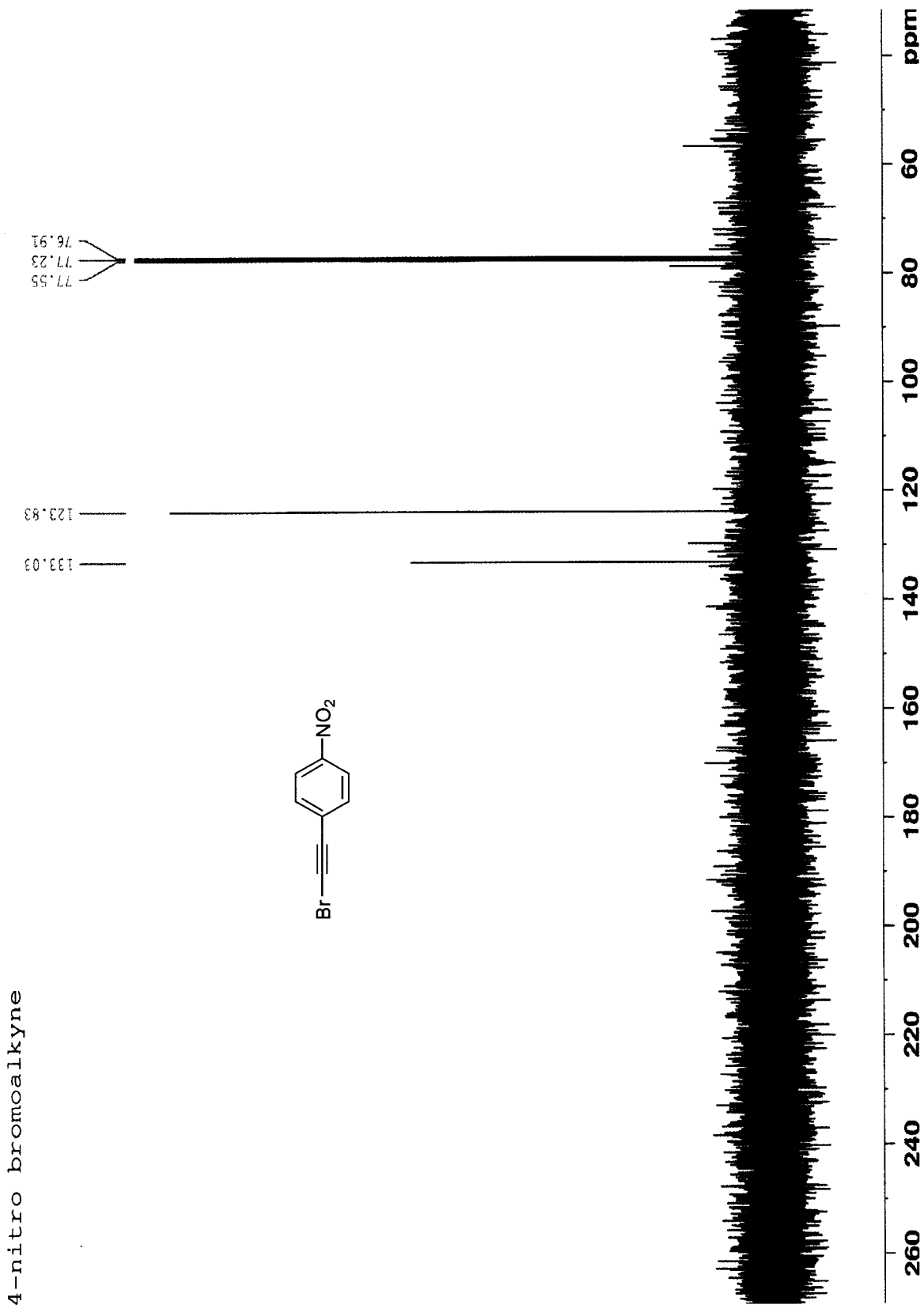

Figure S-3.2-14. ^{13}C NMR Spectrum of Compound **12**.

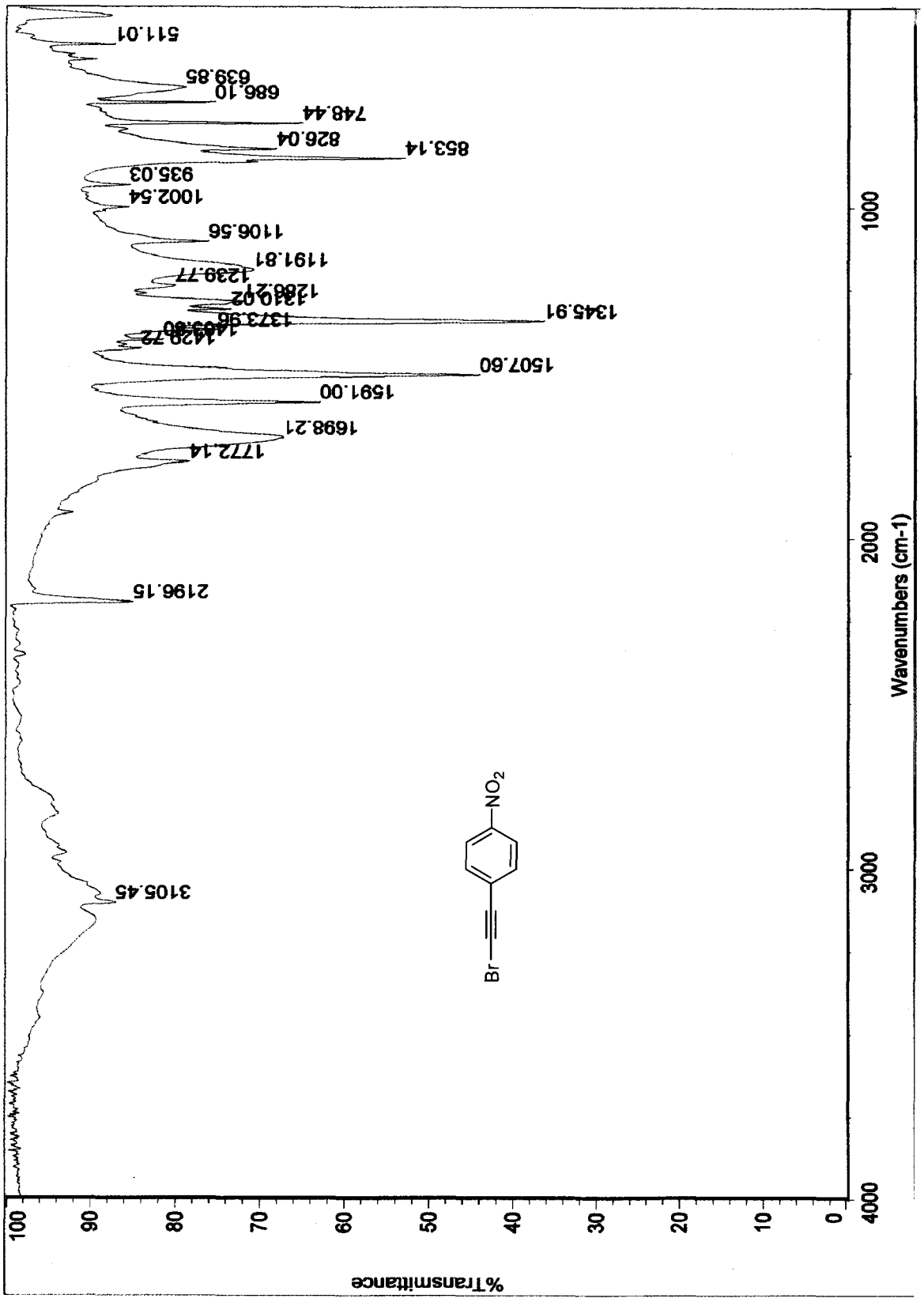

Figure S-3.2-15. IR Spectrum of Compound **12**.

Compound 13.

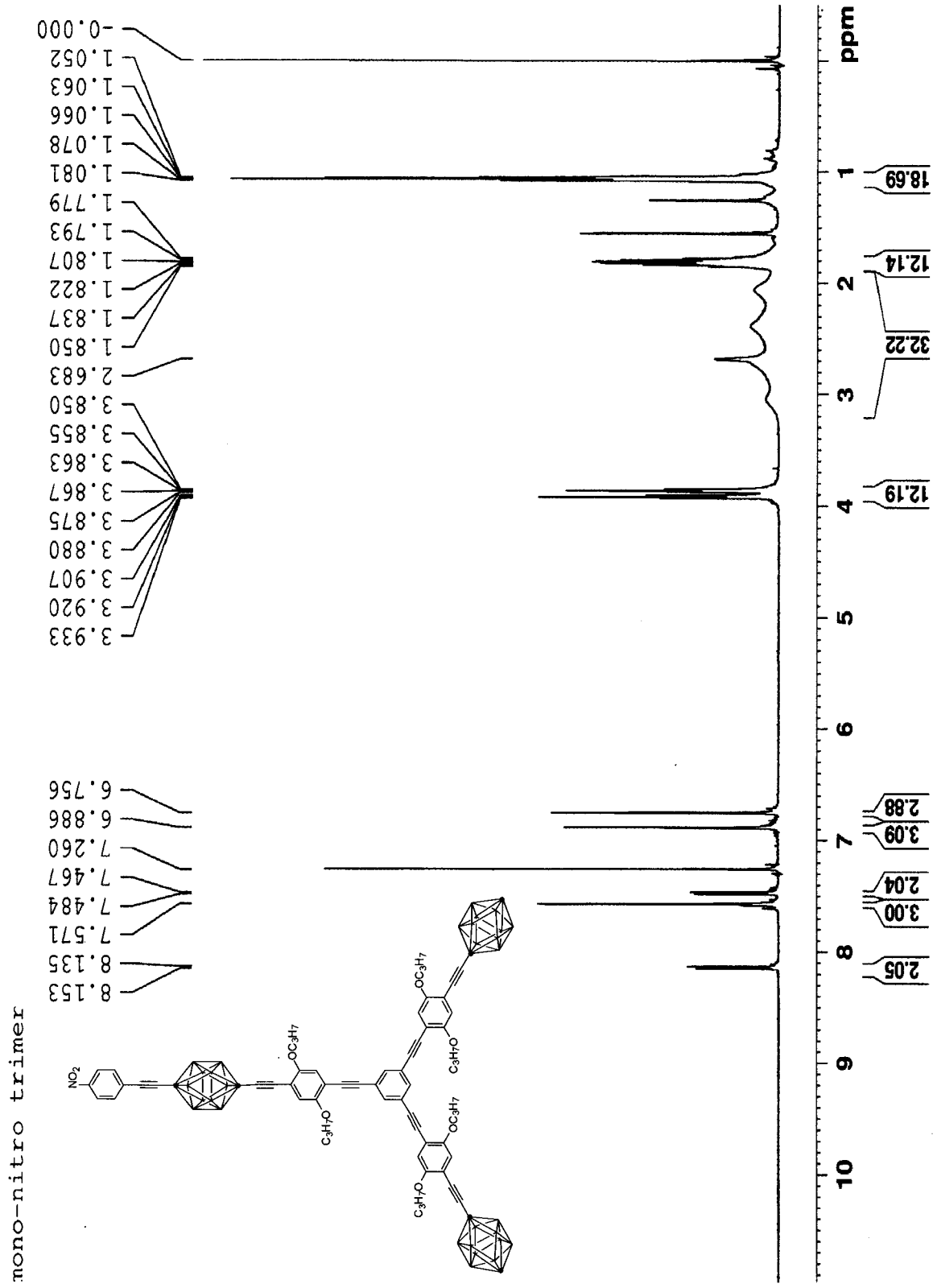

Figure S-3.2-16. ^{1}H NMR Spectrum of Compound **13**.

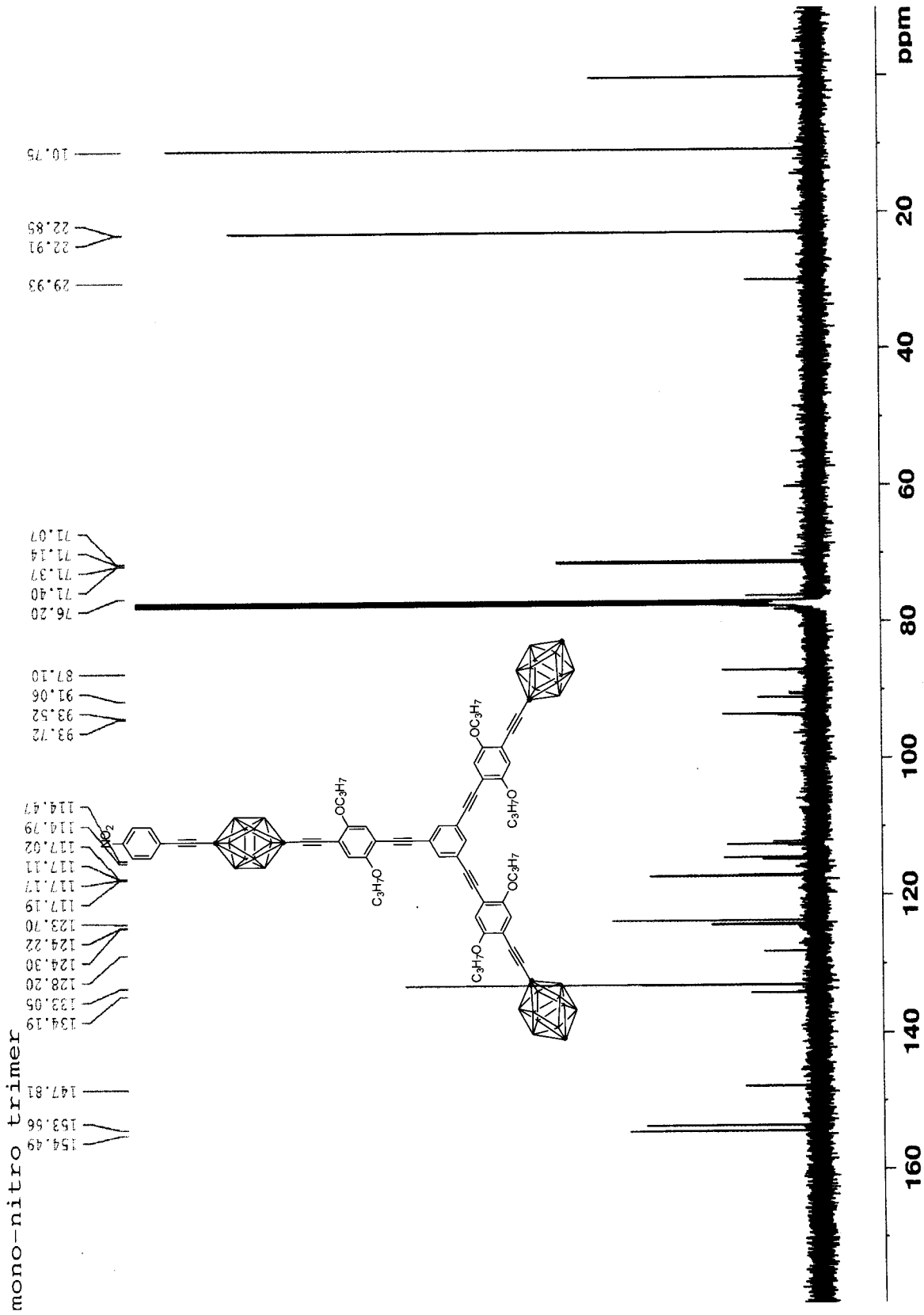

Figure S-3.2-17. ^{13}C NMR Spectrum of Compound **13**.

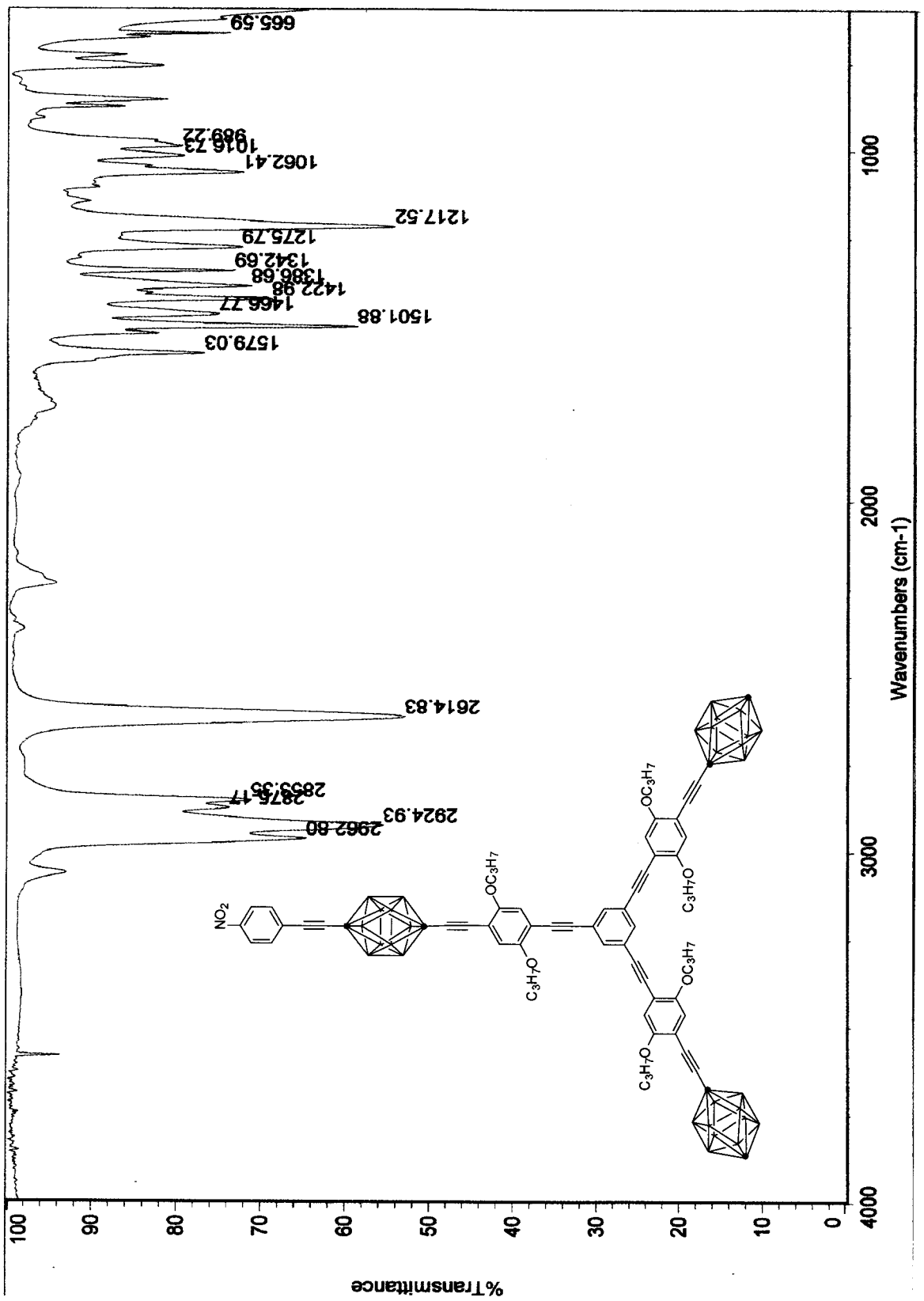

Figure S-3.2-18. IR Spectrum of Compound **13**.

Compound 14.

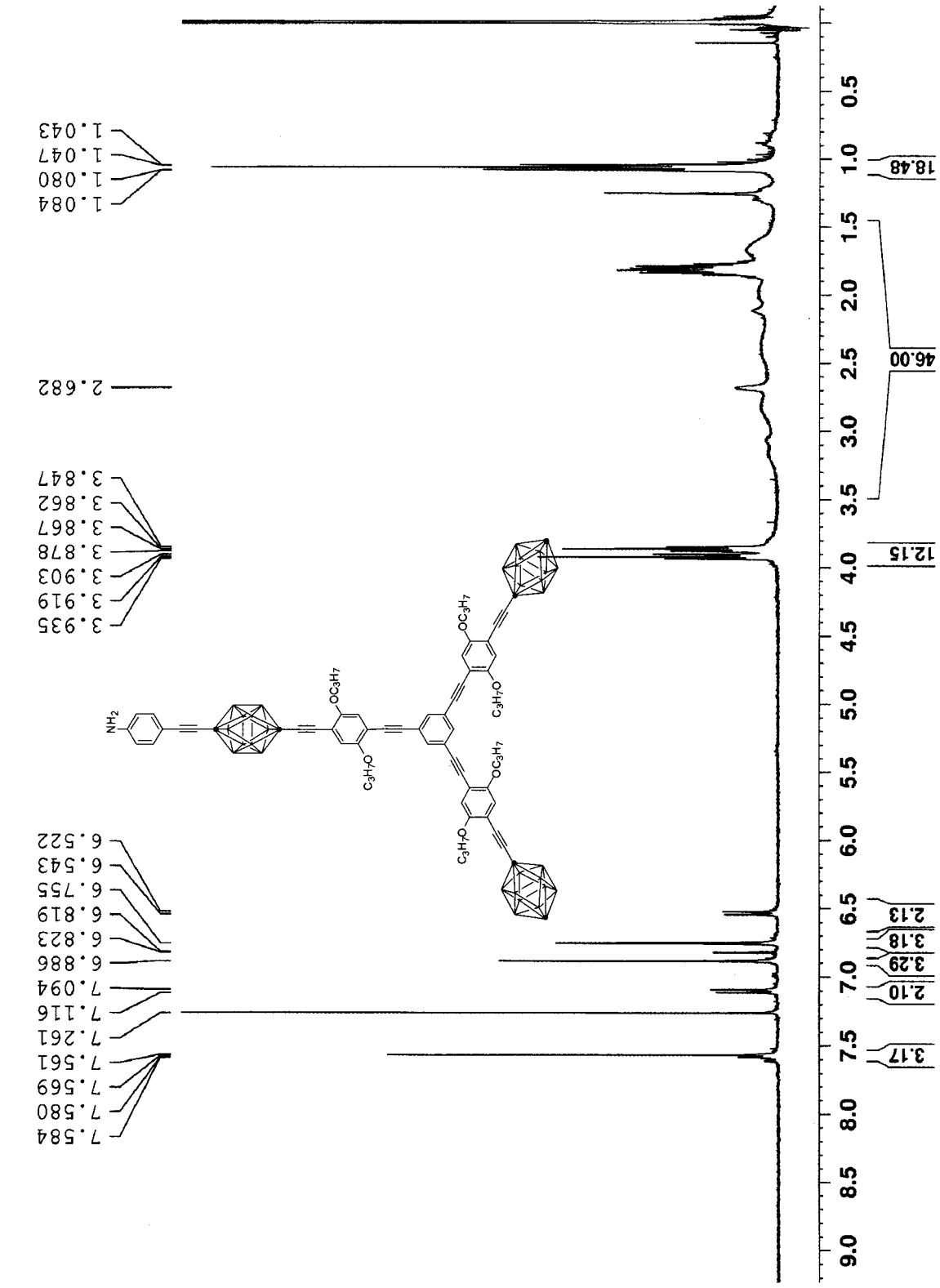

Figure S-3.2-19. ^{1}H NMR Spectrum of Compound **14**.

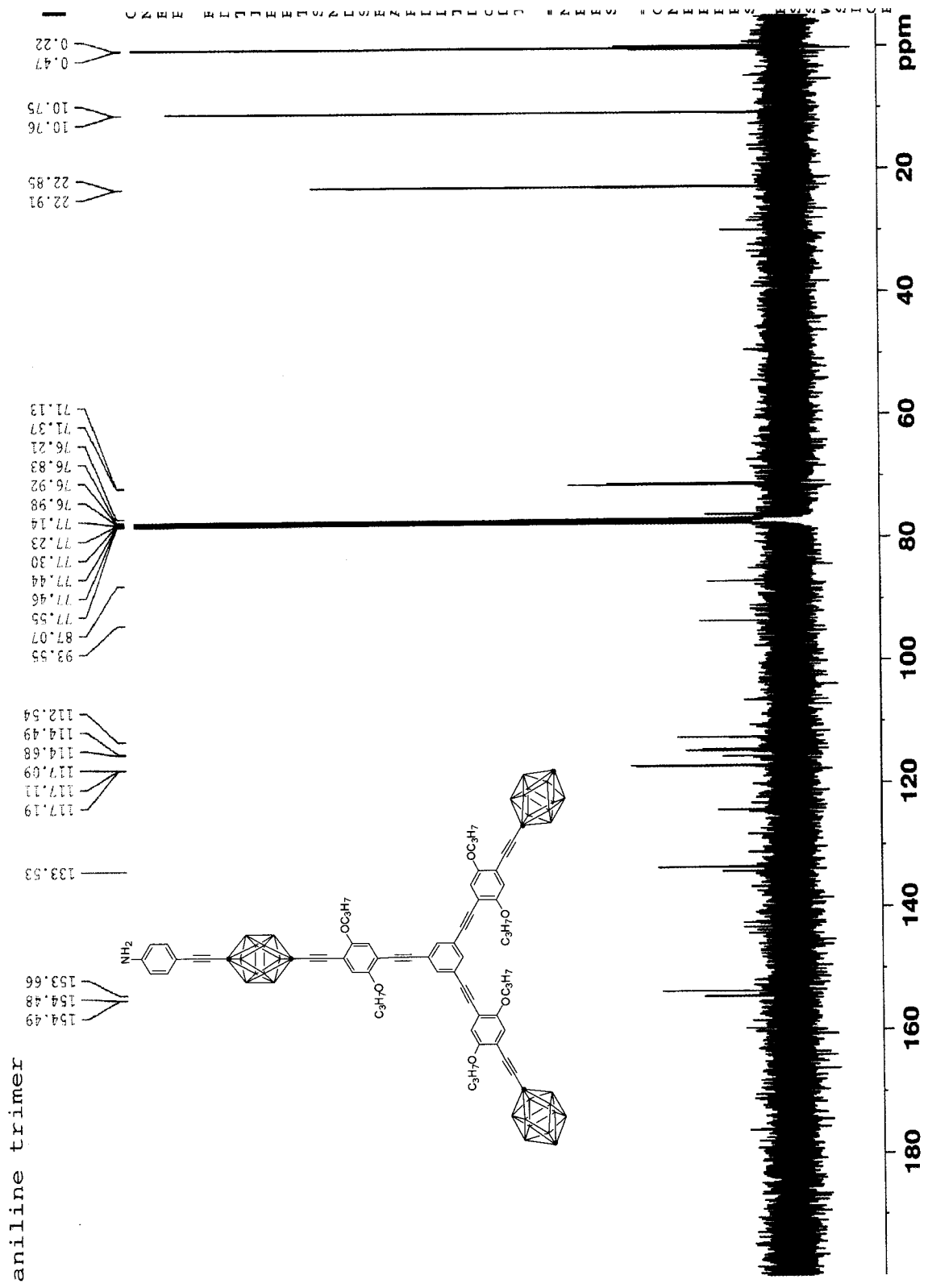

Figure S-3.2-20. ^{13}C NMR Spectrum of Compound **14**.

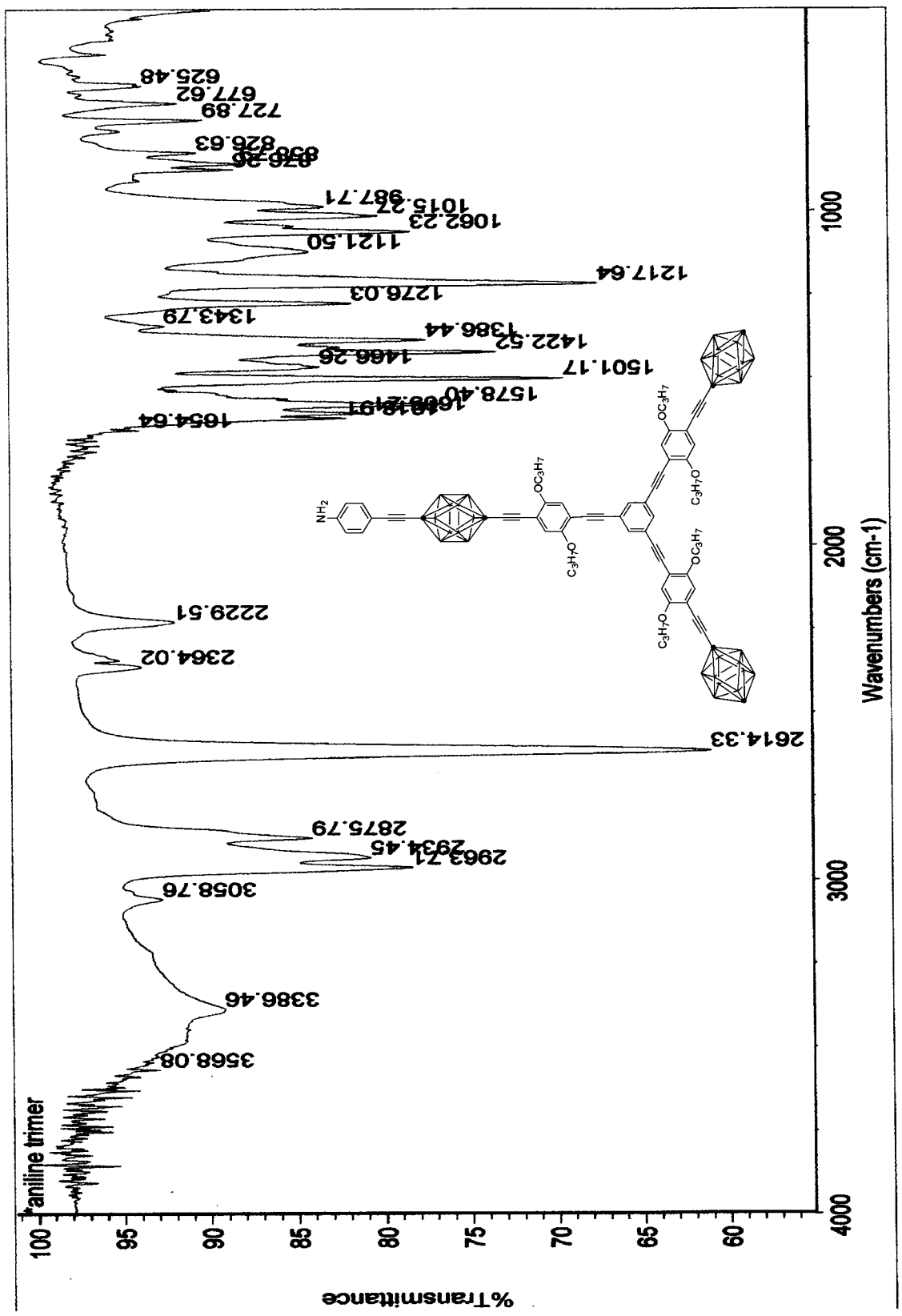

Figure S-3.2-21. IR Spectrum of Compound **14**.

Chapter 4

Construction of Nanovehicles through Self-Assembly

4.1

Towards an Assembly Line: Self-Assembling Nanocars

Introduction

In recent years there have been significant advancements and increased attention in the field of molecular machinery.[1] To further the development of nanomachines and devices, researchers have looked for information and solutions in nature and its biological processes. The concept of self-assembly is a "bottom-up" approach that has inspired scientists to develop numerous new structures. However, there are ideas that are not reminiscent of biological systems. In our present work, our inspiration comes from both the process of self-assembly and the concept of a mechanical assembly line, such as used for automobiles. In our efforts to develop machines and devices at the molecular level, our research has recently focused on the synthesis and manipulation of surface-rolling molecular machines called nanocars.[2] To facilitate syntheses and to further our understanding and development of new-generation nanocars, we have integrated the ideas of assembly lines and self-assembly to construct new nanocar models.

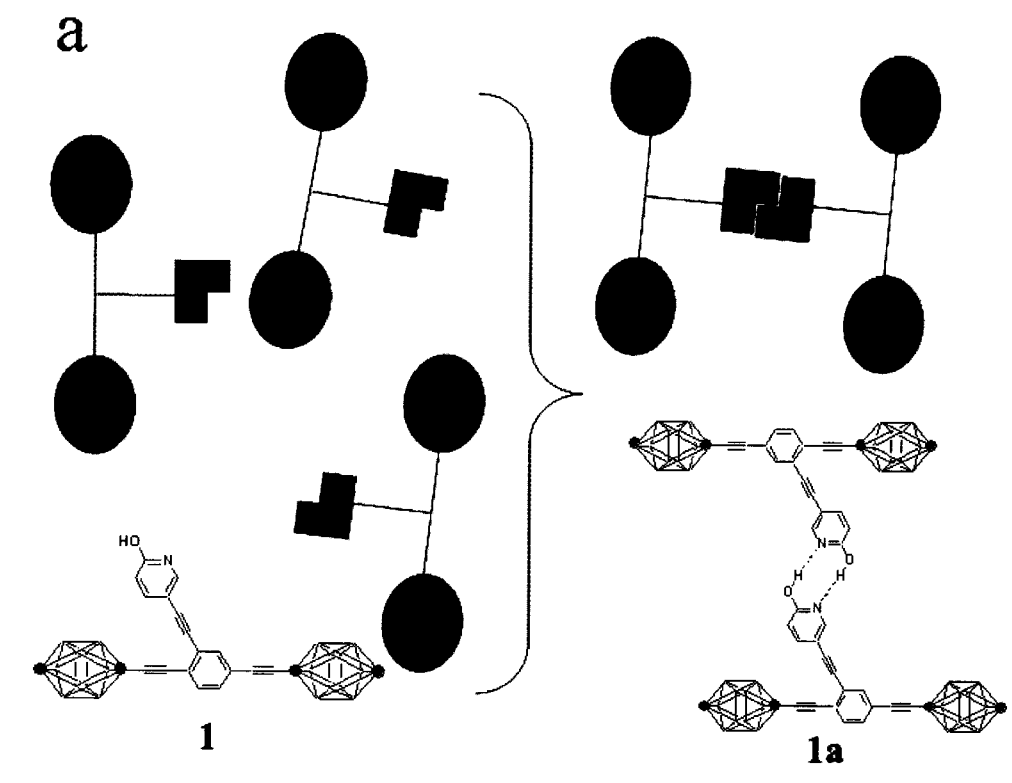
a
HO
N
1
1a
b
= Metal
w/o Metal
w/ Metal
2
2+
2PF6
M = Fe 2a
Ru 2b

Figure 1. Illustration of the self-assembled (a) hydrogen-bond nanocar **1** and (b) metal-complex nanocar **2**. The *p*-carborane moieties have BH at every intersection except at the points denoted by (●), which represents C and CH positions, *ipso* and *para*, respectively.

There are a wide range of noncovalent interactions such as hydrogen bonding, π-π stacking, van der Waals forces, hydrophobic/hydrophilic interactions, Coulombic interactions, and metal-complexation that have been used to generate impressive structures[3] in applications such as bioactive systems, sensors, field-effect transistors (FETs), thermoplastic elastomers and optoelectronic devices.[4-8] In particular, hydrogen-bond and metal-ligand interactions are attractive for obtaining well-defined supramolecular structures due to their spatial arrangement and directionality.[9] Reported here are the syntheses of self-assembled nanocars via hydrogen bonding and metal-complexation as prepared by T. Sasaki (Figure 1). My research consisted of the synthesis of late intermediates (axles) for nanocars **1** and **2**, as well as spectroscopic measurements.[10]

Well-defined hydrogen bonding structures are realized through DNA nucleotide-like molecules offering multiple binding sites for its increased binding strength and organization.[11] However, simpler hydrogen-bonding molecules should not be overlooked for generating self-assembled structures. 2-Pyridones and their tautomers, hydroxypyridines, are well-documented for their ability to form hydrogen-bonded dimeric structures in both solution and solid phases.[12] Therefore the 2-pyridone moiety has been incorporated into the design of nanocar **1a** (Scheme 1).

Results and Discussion

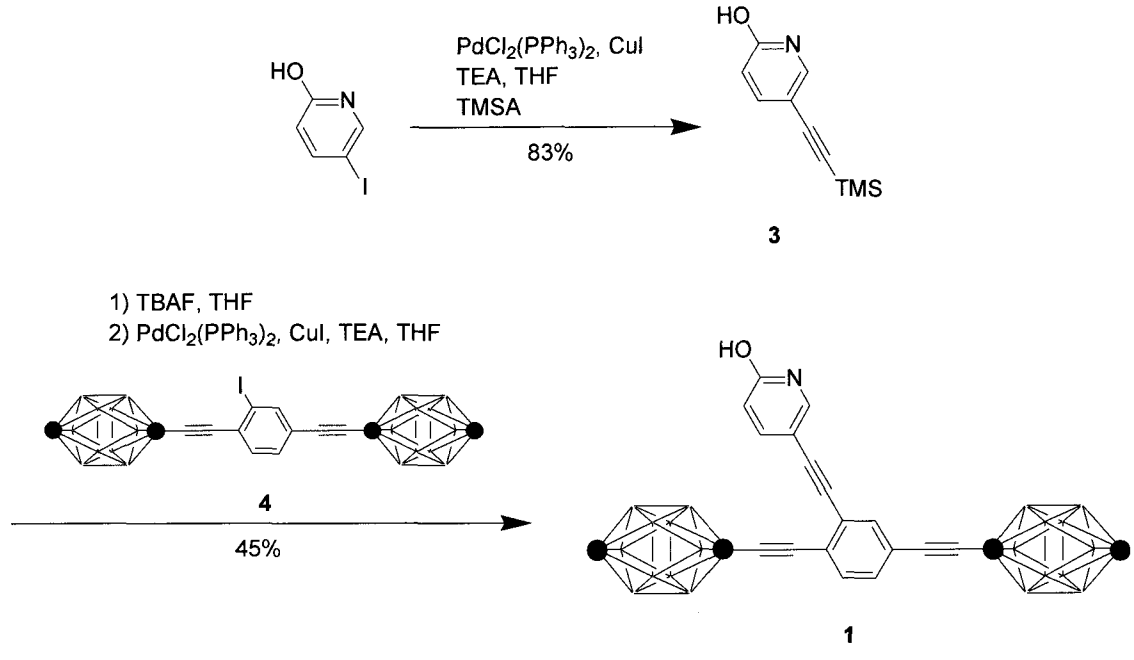

Scheme 1. Synthesis of hydroxypyridine half-car **1a**.

The synthesis of the hydrogen-bonded nanocar **1a** started by coupling trimethylsilylacetylene (TMSA) via palladium-catalyzed Sonogashira coupling with 2-hydroxy-5-iodopyridine to afford **3**. The TMS-protecting group was removed by treatment with tetrabutylammonium fluoride (TBAF) and the resulting crude product was used immediately for coupling with wheel/axle molecule **4**, a common component used in prior carborane-wheeled nanocars, to afford the half-car **1**. Incorporation of the *p*-carborane wheel into the nanocars structures has proven to be useful because of its stability, its ease of imaging by STM,[2a,13] and its compatibility with the required Pd-catalyzed coupling reactions.[2,14]

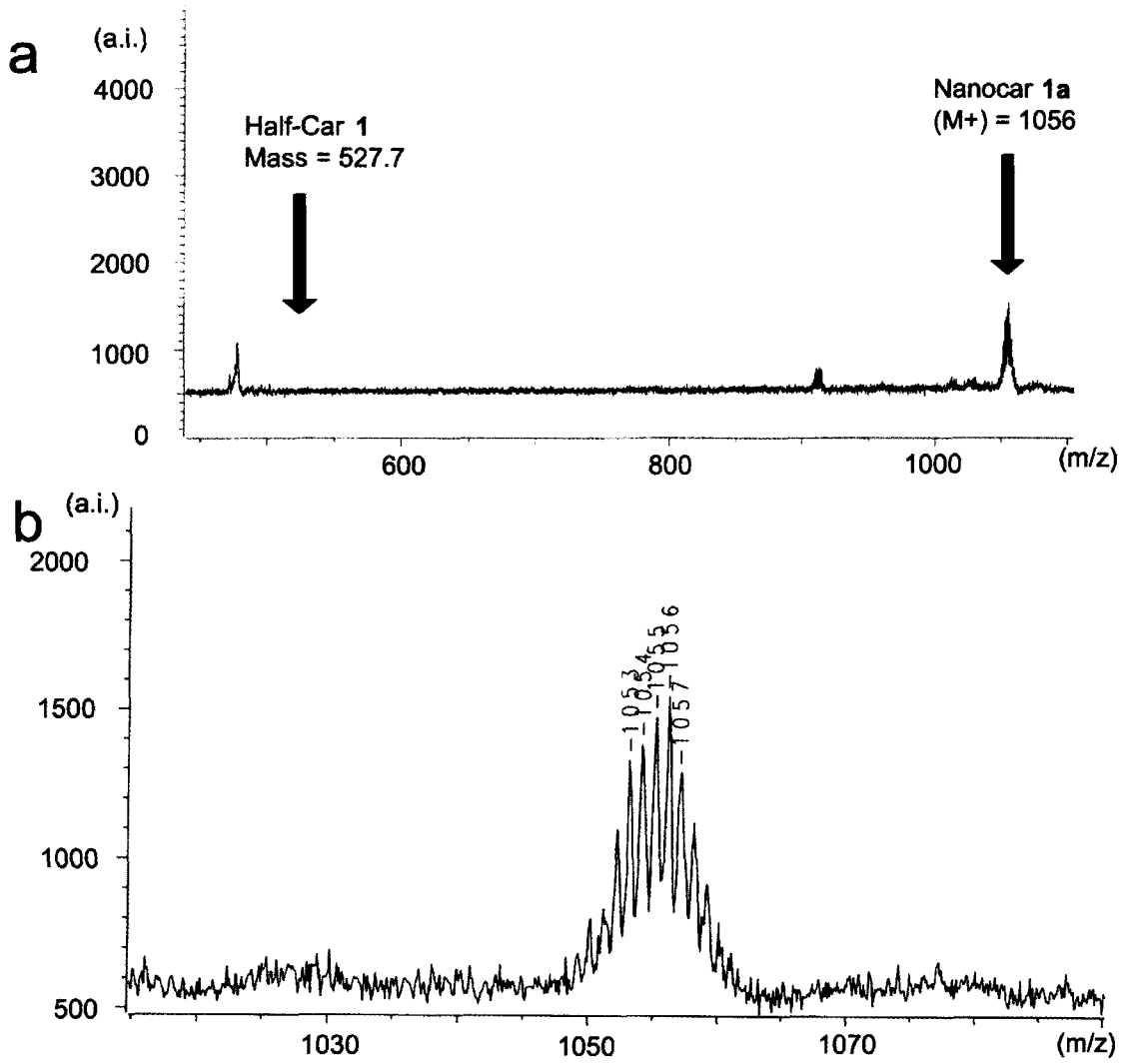

Figure 2. MALDI-TOF mass spectrometry of hydrogen-bonding nanocar **1a**. a) There is no peak that would correspond to the exact mass for the half-car **1** while the peak for the exact mass of nanocar **1a** is clearly discernable; b) an expansion of the exact mass peak for **1a**.

Analysis of the half-car **1** by MALDI-TOF (Fig 2.) direct ionization showed no monomer peaks **1** but only the self-assembled nanocar **1a** at peak *m/z* 1056 (M+). Thus we were able to successfully construct a system that spontaneously self-assembles into a hydrogen-bonded nanocar **1a**.

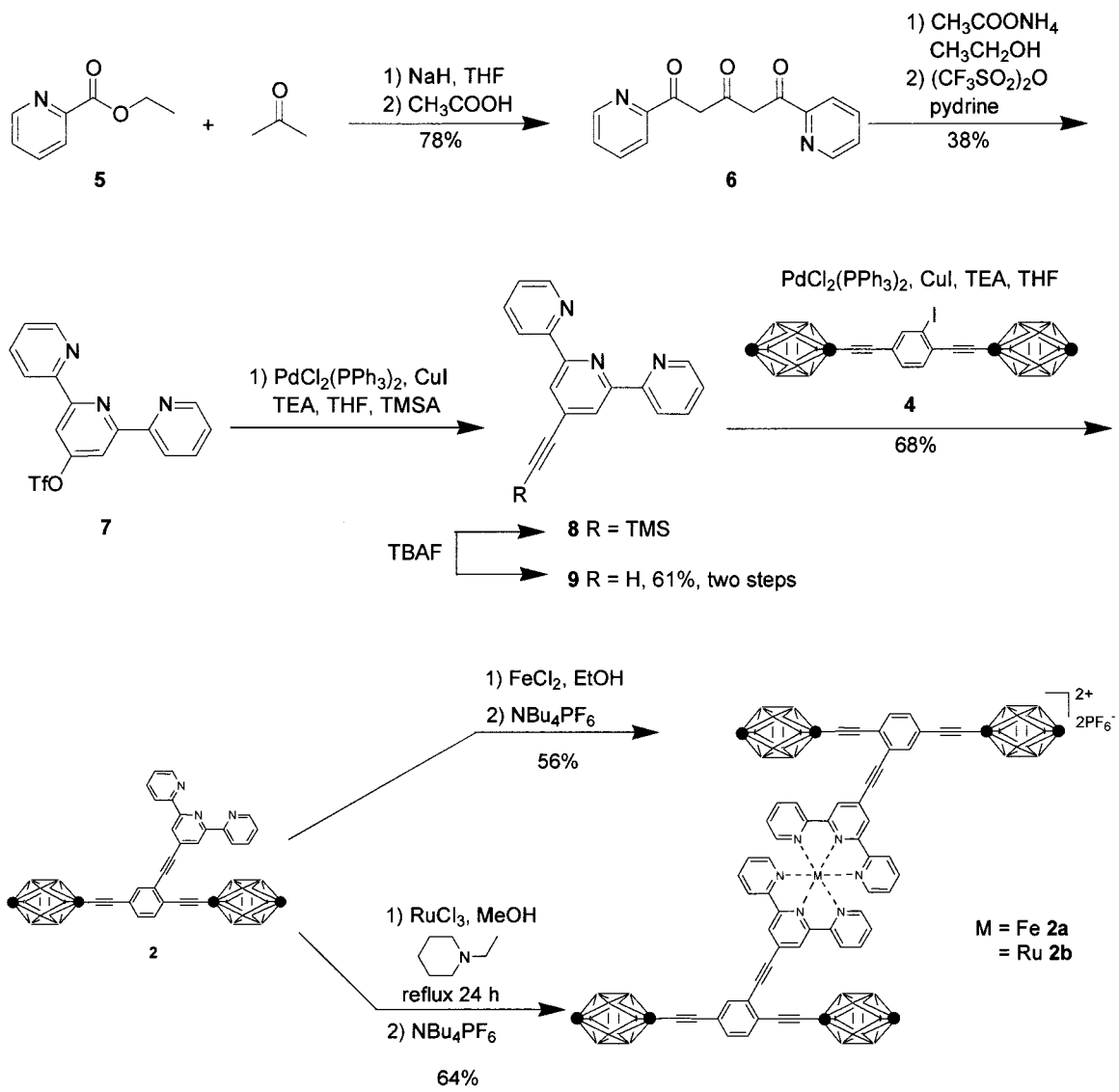

Scheme 2. Synthesis of metal-complexed nanocars **2a** and **2b**.

To retain a relatively rigid chassis as well as a molecule compatible with palladium-catalyzed Sonogashira couplings, terpyridines were used as an initial strategy to synthesize a metal-complexing nanocar. Due to the electrochemical properties and ease of isolation with different metals, terpyridyl ligands are used in variety of applications such as redox polymers, electrocatalysis, photovoltaics and electrochromic devices.[15-17]

The most attractive metals for complexation for the self-assembling nanocars **2a**, and **2b** were iron and ruthenium due to their simple solution complexation at room temperature.

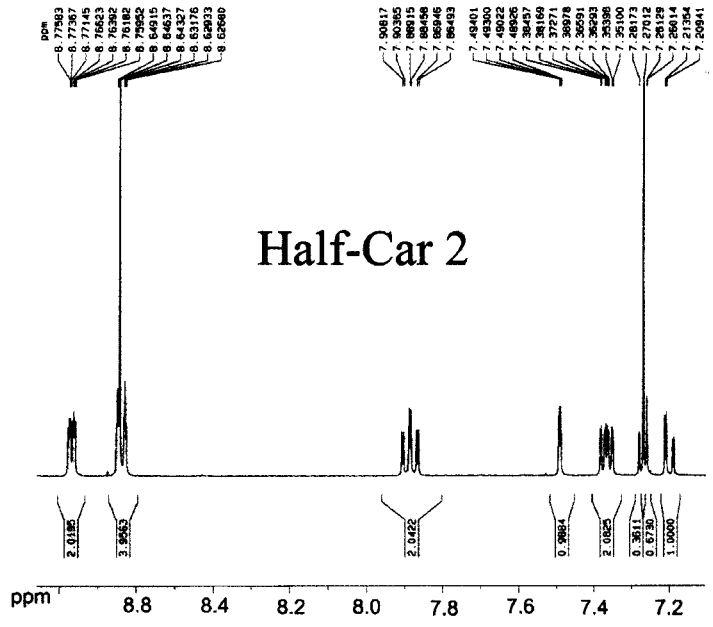

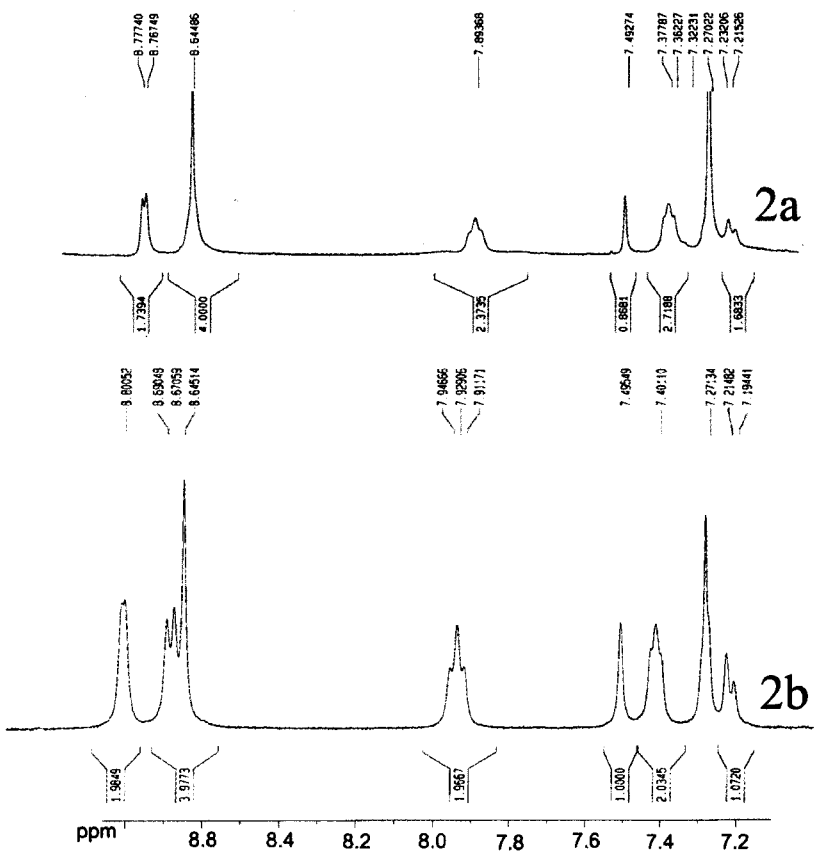

Figure 3. Evidence for nanocar **2a** and **2b** formation; ^{1}H NMR aromatic region of the half-car **2** (top); ^{1}H NMR of the aromatic region of nanocar **2a** with peak broadening due to the presence of iron (middle); ^{1}H NMR of the aromatic region of nanocar **2b** with peak broadening due to the presence of ruthenium (bottom).

The terpyridyl ligand suitable for the half-car **2** was synthesized using known protocols (Scheme 2) to form the OTf-terpyridine **7**.[18] Under Sonogashira conditions, **7** was coupled to TMSA to form **8**, which was immediately deprotected with TBAF in THF to afford **9**. To complete the synthesis, the alkyne **9** and the carborane wheel/axle **4** were again coupled to afford half-car **2**.

The self-assembled nanocar **2a** was obtained by mixing a 2.5:1 ratio of **2** to $FeCl_2$ in ethanol at room temperature for 1 h followed by adding the counter ion tetrabutylammonium hexafluorophosphate (NBu_4PF_6).[18] Characterization using ^{1}H NMR (Fig. 3) showed clear differences between the half-car **2** and complexed **2a**. Due to the presence of iron in the complex, the T_2 relaxation time is shortened thus producing line-broadening of the peaks. Similarly, the ruthenium complex **2b** was synthesized by mixing a 2.5:1 ratio of **2** and $RuCl_3$, respectively, in MeOH. After adding a drop of 1-ethylpiperidine, the mixture was heated to reflux for 24 h. NBu_4PF_6 was added as the counter ion and the reaction was heated to reflux for an additional 2 h. Analysis by NMR resulted in similar ^{1}H NMR broadening with the terpyridyl peaks being slightly more downfield in the ruthenium complex than in the iron complex.

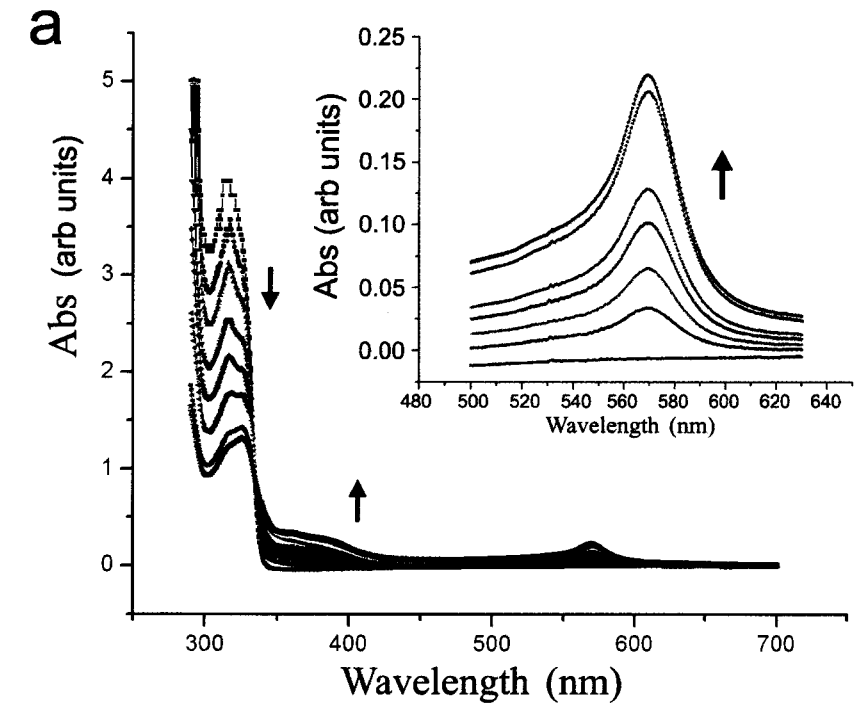

Figure 4. (a) Absorption spectra of **2** (2.0×10^{-4} M) in CH_3CN with increased amount of $FeCl_2$ in CH_3CN. (b) Changes observed at MLCT at 570 nm from 0 → 1.5 equiv of Fe(II) added.

From the visible absorption spectrum (Fig. 4a), a new band was formed after the addition of Fe(II) to a solution of **2** in CH_3CN that is indicative of metal-to-ligand charge transfer (MLCT). Changes at 570 nm shown in Figure 4b indicate that the formation of **2a** is complete after a stoichiometric amount (0.5 equiv) of Fe(II) is added. Gradual formation of monoterpyridyl Fe(II) results from further addition of Fe(II), as evidenced by the slight decrease in the absorption spectra. The small shoulder formed at ~375 nm is due to changes in π-π^* transition. The two distinct maxima (315 nm and 325 nm) observed are blue-shifted compared to our past optical studies on carborane-containing conjugated molecules.[2g] The blue-shift can be attributed to the steric hindrance between the carborane wheels and the terpyridyl core, which leads to a high dihedral angle between the axle and the core. The two maxima indicate that the molecule adopts a rigid conformation in its ground state, a confirmation that is frequently observed in cases of rigid ladder-shaped molecules.[19] The rigidity of the complex after self-assembly may be a problem during surface studies because the terpyridyl-complexed core of the molecule may act to lift the wheel moieties off the surface. The synthesis of a less rigid, more nearly planar metal-complex is planned in the future.

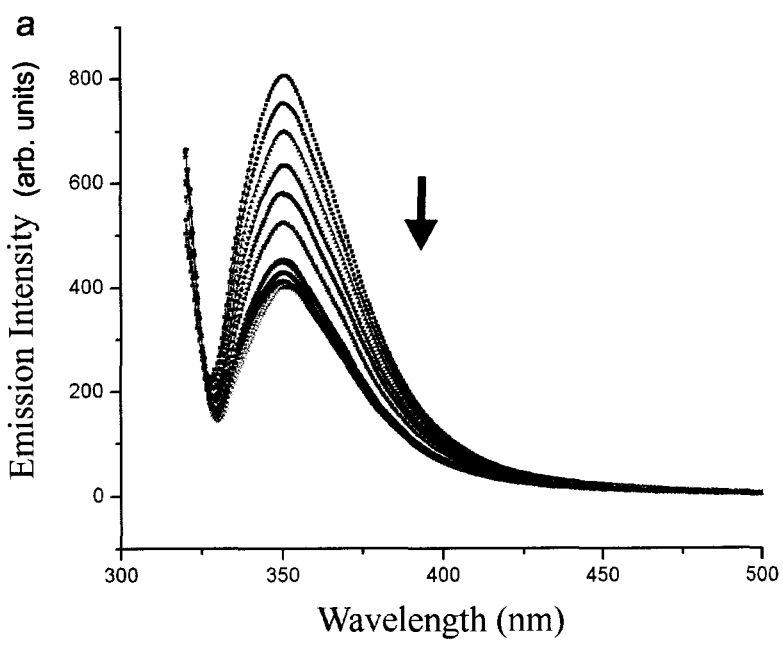

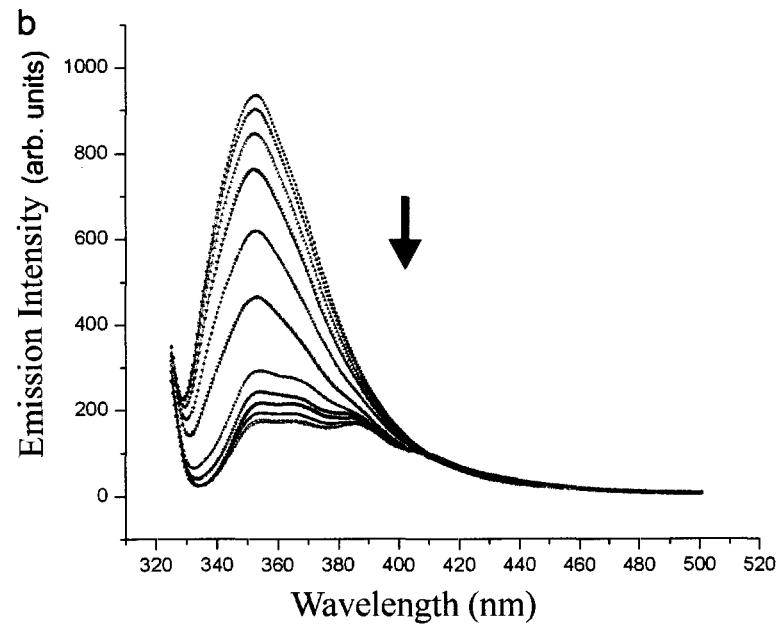

Figure 5. (a) Emission spectra of **2** (5.0 x 10^{-7} M) in CH_3CN excited at 315 nm with increased amounts of $FeCl_2$ in CH_3CN. (b) Emission spectra of **2** (7.0 x 10^{-7} M) in CH_3CN excited at 315 nm with increased amount of $RuCl_3$ in CH_3CN.

Fluorescent optical studies of carboranes are scarcely reported,[2g] but fluorescent imaging could be an alternate to STM for discerning movement of these molecules on surfaces. The emission spectrum of **2** in CH_3CN (Fig. 5), when excited at 315 nm, gave rise to an emission band in the UV-blue region. The quenching behavior as a result of $FeCl_2$ addition is due to the coordination of Fe(II) to the terpyridyl units (Fig. 5a). Similar results were obtained as a solution of $RuCl_3$ in CH_3CN was added in the same manner (Fig. 5b).

Conclusion

In summary, incorporating an assembly line approach to the synthesis of two types of self-assembled nanocars has been successful. Work continues on assembling these molecules on surfaces to demonstrate both self-assembly and rolling of these nanocars. With the use of these simple moieties for self-assembly, one can envision other complex nanomachine architectures such as nanotrains being constructed through a similar complexation process.

Experimental Section

General Methods. Starting materials were purchased from Aldrich and Acros Chemicals. All reactions were performed under an atmosphere of nitrogen unless stated otherwise. Reagent grade tetrahydrofuran (THF) was distilled from sodium benzophenone ketyl.

Triethylamine (TEA) and CH_2Cl_2 were distilled over CaH_2. TBAF (1 M solution in THF) was obtained from Aldrich and used as received. Trimethylsilylacetylene (TMSA) was donated by FAR Research Inc. or Petra Research. Flash column chromatography was performed using 230-400 mesh silica gel from EM Science. Thin layer chromatography was performed using glass plates pre-coated with silica gel 40 F_{254} purchased from EM Science. Compounds **4**,[2g] **6**[18] and **7**[18] were prepared according to literature procedure. Compounds **1** – **3**, **8** and **9** were prepared as described by Sasaki and co-workers.[10]

References and Notes

(1) (a) Gross, L.; Rieder, K. -H.; Moresco, F.; Stojkovic, S. M.; Gourdon, A.; Joachim, C. *Nature Mater.* **2005**, *4*, 892-895. (b) Grill, L.; Rieder, K. –H.; Moresco, F.; Rapenne, G.; Stojkovic, S.; Bouju, X.; Joachim, C. *Nature Nanotechnology* **2007**, *2*, 95-98. (c) Serreli, V.; Lee, C. –F.; Kay, E. R.; Leigh, D. A. *Nature* **2007**, *445*, 523-527., *300*, 2061-2065. Not STM (d) Wong, K. L.; Pawin, G.; Kwon, K. Y.; Lin, X.; Jiao, T.; Solanki, U.; Fawcett, R. H. J.; Bartels, L.; Stolbov, S.; Rahman, T. S. *Science* **2007**, *315*, 1391-1393. (e) Joachim, C.; Tang, H.; Moresco, F.; Rapenne, G.; Meyer, G. *Nanotechnology* **2002**, *13*, 330. (f) Jimenez-Bueno, G.; Rapenne, G; *Tetrahedron Lett.* **2003**, *44*, 6261. (g) Rapenne, G. *Org. Biomol. Chem.* **2005**, *7*, 1165. (g) Balzani, V.; Credi. A.; Venturi, M. Molecular Devices and Machines: A journey into the Nano World; WILEY-VCH, Weinheim, Germany, 2004. (h) Balzani, V.; Credi. A.; Ryamo, F. M.; Stoddart, J. F. *Angew. Chem., Int. Ed.* **2000**, *39*, 3349-3391. (i) Berná, J.; Leighm D. A.; Lubomska, M.;

Mendoza, S. M.; Pérez, E. M.; Rudolf, P.; Teobaldi, G.; Zerbetto, F. *Nature Mater.* **2005**, *4*, 704-710. (j) Badjié, J. D.; Balzani, V.; Credi, A.; Silvi, S.; Stoddart, J. F. *Science* **2004**, *303*, 1845-1849. (k) Kottas, G. S.; Clarke, L. I.; Horinek, D.; Michl, J. *Chem. Rev.* **2005**, *105*, 1281-1376. (l) Muraoka, T.; Kinbara, K.; Kobayashi, Y.; Aida, T. *J. Am. Chem. Soc.* **2003**, *125*, 5612-5613. (m) Koumura, N.; Geertsema, E. M.; Meetsma, A.; Feringa, B. L. *J. Am. Chem. Soc.* **2000**, *122*, 12005-12006. (n) Garcia-Garibay, M. A. *Proc. Natl. Acad. Sci.* **2005**, *102*, 10771-10776. (o) Kwon, K.-Y.; Wong, K. L.; Pawin, G.; Bartels, L.; Stolbov, S.; Rahman, T. S. *Phys. Rev. Lett.* **2005**, *95*, 166101/1-166101/4. (p) Kay, E. R.; Leigh, D. A.; Zerbetto, F. *Angew. Chem., Int. Ed.* **2006**, *46*, 72-191.

(2) (a) Shirai, Y.; Osgood, A. J.; Zhao, Y.; Kelly, K. F.; Tour, J. M. *Nano Lett.* **2005**, *5*, 2330-2334. (b) Shirai, Y.; Osgood, A. J.; Zhao, Y.; Yao, Y.; Saudan, L.; Yang, H.; Yu-Hung, C.; Sasaki, T.; Morin, J.-F.; Guerrero, J. M.; Kelly, K. F.; Tour, J. T. *J. Am. Chem. Soc.* **2006**, *128*, 4854. (c) Shirai Y.; Morin, J. -F.; Sasaki, T.; Guerrero, J. M.; Tour, J. M. *Chem. Soc. Rev.* **2006**, *35*, 1043. (d) Morin, J.-F.; Shirai, Y.; Tour, J. M. *Org. Lett.* **2006**, *8*, 1713. (e) Sasaki, T.; Tour, J. M. *Tetrahedron Lett.* **2007**, 48, 5821-5824. (f) Sasaki, T.; Morin, J.–F.; Lu, M.; Tour, J. M. *Tetrahedron Lett.* **2007**, 48, 5817-5820. (g) Morin, J.–F.; Sasaki, T.; Shirai. Y.; Guerrero J. M.; Tour, J. M. *J. Org. Chem.* **2007**. *72*, 9481-9490. (h) Sasaki, T, Osgood, A. J.; Alemany, L. B.; Kelly, K. F.; Tour, J. M. *Org. Lett.* **2008**, *10*, 229-232. (i) Sasaki, T.; Tour, J. M. *Org. Lett.* **2008**, *10*, 897-900. (j) Sasaki, T.; Osgood, A. J.; Kiappes, J. L. Kelly, K. F.; Tour, J. M. *Org. Lett.* **2008**, 1377-1380.

(3) (a) Yamamoto, T.; Fukushima, T.; Yamamoto, Y.; Kosaka, A.; Jin, W.; Ishii, N.; Aida, T. *J. Am. Chem. Soc.* **2006**, *128*, 14337–14340. (b) Jonkheijm, P.; Miura, A.; Zdanowska M.; Hoeben F. J. M.; Feyter, S. D.; Schenning, A. P. H. J.; de Schryver, F.

C.; Meijer, E. W. *Angew. Chem., Int. Ed.* **2004**, *43*, 73-78. (c) Ghadiri, M. R.; Granja, J. R.; Milligan, R. A.; Mcree, D. E.; Lhazanovich, N. *Nature*, **1993**, *366*, 324-327. (d) Yan, D. Y.; Zhou, Y. F.; Hou, J. *Science* **2004**, *303*, 65-67. (e) Bazter, R. N. W.; Lehn, J. M.; Fischer, J.; Youinou, M. *Angew. Chem., Int. Ed.* **1994**, *33*, 2284-2287. (f) Weissbuch, I.; Baxter, P. N. W.; Cohen, S.; Cohen, H.; Kjaer, K.; Howes, P. B.; Als-Nielsen J.; Hanan, G. S.; Schubert, U. S.; Lehn, J, M.; Leiserowitz, L.; Lahav, M. *J. Am. Chem. Soc.* **1998**, *120*, 4850-4860. (g) Ruben, M.; Rojo, J.; Romero-Saluguero, F. J.; Uppadine, L. H.; Lehn, J. M. *Angew. Chem., Int. Ed.* **2004**, *43*, 3644-3662. (h) Zerowski, J. A.; Whitesides, G. M. *J. Am. Chem. Soc.* **1994**, *116*, 4298-4304. (i) Ranganathan, A.; Pedireddi, V. R.; Rao, C. N. R. *J. Am. Chem. Soc.* **1999**, *121*, 1752-1753. (j) Prins, L. J.; de Jong, F.; Timmerman, P.; Reinhoudt, D. N. *Nature* **2000**, *408*, 181-184. (k) Whiteside, G. M.; Simanek, E. E.; Mathias, J. P.; Seto, C. T.; Chin, D. N.; Mammen, M.; Gordon, D, M. *Acc. Chem. Res.* **1995**, *28*, 37-44. (l) Highfill, M. L.; Chandrasekaran, A.; Lynch, D. E.; Hamilton, D. A. *Crystal Growth & Design.* **2002**, *1*, 15-20. (m) Kolotuchin S. C. Zimmerman, *J. Am. Chem. Soc.* **1998**, *120*, 9092-9093. (n) Marsh, A.; Silverstri, M.; Lehn, J. M. *Chem. Commun.* **1996**, 1527-1528. (o) Jeffrey, G. A. *An Introduction to hydrogen bonding*, Oxford, University, Oxford, **1997**.

(4) Bong, D. T.; Clark, T. D.; Granja, J. R.; Ghadiri, M. R.; *Angew. Chem., Int. Ed.* **2001**, *40*, 988-1011.

(5) Miao, Q.; Lefenfeld, M.; Nguyen, T. –Q.; Siegrist, T.; K., Christian; N., C. *Adv. Mater.* **2005**, *17*, 407-412.

(6) (a) Yip, H, -L.; Ma, H.; Jen, A. K. –Y.; Dong, J.; Parviz, B. A. *J. Am. Chem. Soc.* **2006**, *128*, 5672-5679. (b) Sirringhaus, H.; Brown, P. J.; Frieds, R. H.; Nielsen, M. M.;

Bechgaard, K.; Langeveld-Voss, B. M. W.; Spiering, A. J. H.; Jamssen, R. A. J.; Meijer, E. W.; Herwig, P.; de Leeuw, D. M. *Nature* **1998**, *401*, 685-688. (c) van de Craats, A. M.; Stutzmann, N.; Bunk, O.; Nielsen, M. M.; Watson, M.; Mullen, K.; Chanzy, H. D.; Sirrnghaus, H.; Friends, R. H. *Adv. Mater.* **2004**, *15*, 495-499. (d) Faccheti, A.; Mushrush, M.; Yoon, M.H.; Hutchison, G. R.; Ratner, M. A.; Marks, T. J. *J. Am. Chem. Soc.* **2004**. *126*, 13859-13874. (e) Wu, Y.; Li, Y.; Gardner, S.; Ong, B. S. *J. Am. Chem. Soc.* **2004**, *127*, 614-618.

(7) Kautz, H.; van Beek, D. J. M.; Sijbesma, R. P.; Meijer, E. W. *Macromolecules* **2006**, *39*, 4265-4267.

(8) (a) Schmidt-Mende, L.; Fehtenkotter A.; Mullen, K.; Moons, E.; Friend, R. H.; Mackenzie, J. D. *Science* **2001**, *293*, 1119-1122. (b) Yang, X. N.; van Duren, J. K. J.; Rispens, M. T.; Hummelen, J. C.; Janssen, R. A. J.; Michels, M. A. J.; Loos, J. *Adv. Mater.* **2004**, *16*, 802-806.

(9) (a) Hammes, G. G.; Park, A. C. *J. Am. Chem. Soc.* **1968**, *91*, 956–961. (b) Gallant, M.; Viet, M. T. P.; Wuest, J. D. *J. Org. Chem.* **1991**, *56*, 2284–2286. (c) Beak, P.; Fry, F. S., Jr.; Lee, J.; Steele, F. *J. Am. Chem. Soc.* **1976**, *98*, 171-179. (d) Schlegel, H. B.; Gund, P.; Fluder, E. M. *J. Am. Chem. Soc.* **1982**, *104*, 5347-5351. (e) Beak, P.; Covington, J. B.; Smith, S. G.; White, M.; Zeigler, J. M. *J. Org. Chem.* **1980**, *45*, 1354-1362. (f) Beak, P. *Acc. Chem. Res.* **1977**, *10*, 186-192.

(10) Sasaki, T.; Guerrero, J. M.; Tour, J. M. *Tetrahedron* **2008**, *36*, 8522-8529.

(11) (a) Park, T.; Zimmerman, S. C. *J. Am. Chem. Soc.* **2006**, *128*, 11582-11590. (b) Ohkawa, H.; Takayama, A.; Nakajima, S.; Nishide, H. *Org. Lett.* **2006**, *8*, 2225-2228. (c) Wong, C. –Ho.; Chow, H. –F.; Hui, S. –K.; Sze, K. -H. *Org. Lett.* **2006**, *8*, 1811-1814.

(12) (a) Simard, M.; Su, D.; Wuest, J. D. *J. Am. Chem. Soc.* **1991**, *113*, 4696-4698. (b) Edwards, M. R.; Jones, W.; Motherwell, W. D. S. *Cryst. Eng.* **2002**, *5*, 25-36

(13) Zhang, J.; Sasaki, T.; Kelly, K. F.; Tour, J. M. manuscript in preparation.

(14) (a) Zhao, Y.; Shirai, Y.; Slepkov, D. A.; Alemany, L. B.; Sasaki, T.; Hegmann, F. A.; Tour, J. M. *Chem. Eur. J.* **2005**, *11*, 3643. (b) Shirai, Y.; Zhao, Y.; Chen, L.; Tour, J. M. *Org. Lett.* **2004**, *6*, 2129.

(15) (a) Chen, Y.-Y.; Tao, Y.-T.; Lin, H.-C. *Macromolecules* **2006**, *39*, 8559-8566.

(16) (a) Chen, S.-M.; Wang, C.-H. *Bioelectrochemistry* **2007**, *70*, 452-461. (b) Geneste, F.; Moinet, C. *J. Electroanal. Chem.* **2006**, *594*, 105-110.

(17) (a) Hagemann, O.; Jorgensen, M.; Krebs, F. C. *J. Org. Chem.* **2006**, *71*, 5546-5559. (b) Houarner, C.; Blart, E.; Buvat, P.; Odobel, F. *Photochem. Photobiol. Sci.*, **2005**, *4*, 200-204.

(18) Bernhard, S.; Goldsmith, J. I.; Takada, K.; Abruna, H. D. *Inorg. Chem.* **2003**, *42*, 4389-4393.

(19) Wakim, S.; Bouchard, J.; Blouin, N.; Michaud, A.; Leclerc, M. *Org. Lett.* **2004**, *6*, 3413-3416.

4.2

Nanotrains and Self-Assembled Two-Dimensional Arrays Built from Carboranes Linked by Hydrogen Bonding of Dipyridones

Introduction

Supramolecular engineering through noncovalent interactions is a promising tool for nanotechnological advances,[1-3] such as potential applications in bioactive systems, sensors, field-effect transistors, thermoplastic elastomers, and optoelectronic devices.[4-13] With the use of interactions such as hydrogen bonding, π π stacking, van der Waals forces, hydrophobic/hydrophilic interactions, and Coulombic interactions, separately or in combinations, impressive structures including helices, cylindrical tubes, grids and cyclic assemblies[14-31] have been realized through specific molecular design. In particular, hydrogen bond interactions are attractive for obtaining well-defined supramolecular structures due to their spatial arrangement, selectivity and directionality.[32]

Well-defined hydrogen-bonded structures have been realized through an understanding of biological systems.[33] Multiple binding sites seen in DNA nucleotide-like molecules offer increased binding strength and organization. However, simpler hydrogen bonding molecules should not be overlooked for generating self-assembled structures. Both 2-pyridone and its tautomer, hydroxypyridine, are well-documented for their ability to form hydrogen bonded dimeric structures in both solution and the solid phase.[34, 35] Although simple methods have been proposed to modify the bond strength of these dimers, such as cocrystallization between carboxylic acid units,[36] there are few reports of imaging or the use of multiple 2-pyridone moieties to generate more complex assemblies.[36-38]

There are two notable difficulties in imaging assembled structures of 2-pyridones. Firstly, imaging via scanning tunneling microscopy (STM), requires conductive substrates. The substrate-molecule interactions for 2-pyridones on metallic surfaces or metal atoms are stronger than the hydrogen bonds between 2-pyridone molecules,[39-43] although there is one example of 2-pyridone species forming a dimeric 2-D adlayer imaged via STM on modified, highly oriented pyrolytic graphite (HOPG).[38] There are also atomically resolved STM images of other hydrogen bonding moieties that self-assemble into unique architectures but the substrate-molecule binding energies are usually lower.[44,45] Despite the disadvantages of using STM as an imaging technique, its lateral resolution remains unparalleled. The second difficulty is that 2-pyridones form one-molecule thin self-assembled structures that are difficult to image with good lateral resolution. To address these difficulties, in the present work, imaging with atomic force microscopy (AFM) allows for the use of a wide range of surfaces including non-conductive ones for imaging the self-assembly of 2-pyridones. The resolution in AFM imaging, however, depends upon both the in-plane (*X Y*) and *Z*-axis effects. The tip effect results in geometrical broadening (the approximate molecular width + 2 × tip diameter) of the molecules.[46] Although there are reports suggesting the use of a single molecule as a tip,[47] the sharpest tips currently available are at best 1 nm in radius,[48,49] thus resolution at the atomic or small molecule scale is extremely difficult. Other factors in AFM resolution are shot noise in the cantilever deflection photo detector and thermal vibration noise of the cantilever that occurs in the *Z*-axis. The combination of the noise effects contributes from ~0.2 to 0.7 nm in lost resolution depending on probe type, optical detection

technique, and surface roughness,[46] and thus resolving a monolayer of planar molecules is very difficult.

Our research in recent years has generated a class of surface-rolling molecules termed nanocars.[50-60] Preferential rolling versus sliding motion was observed on surfaces with the incorporated wheels interacting strongly with the substrate. The wheels, fullerenes (1 nm in diameter) or *p*-carboranes (0.8 nm in diameter),[61] that have been used can potentially serve as height-enhancing units for AFM imaging to enable imaging despite noise and tip effects. As an extension to the nanocar work, the synthesis of monomer **1** containing 2-pyridones and a resulting self-assembled structure, a nanotrain, imaged by AFM is reported. For control purposes, monomer **2** without the wheels was also synthesized.

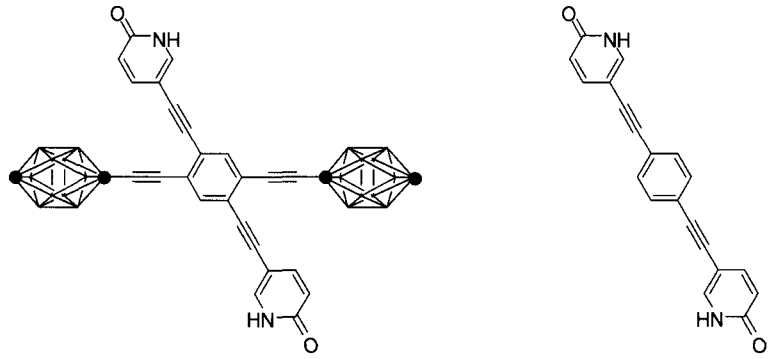

1 **2**

Figure 1. Target monomer molecules for hydrogen-bonded self-assembled structures. Monomer **1** contains *p*-carborane moieties to produce heightened images for AFM analysis. Monomer **2** serves as a control. The carborane has a B-H at each vertex except the darkened positions that have C-H para and C ipso to the alkyne.

Results and discussion

The synthesis of compounds **1** and **2** as well as the AFM imaging on SiO_2 was done by T. Sasaki. To complete the project,[62] I synthesized the dialkynylated axle **3** and compound **1**(as follow-up experiments were necessary) and carried out the self-assembly of the nanotrains on mica prepared from different solvents. I was also responsible for some AFM data collection in collaboration with A. Leonard. Compound **1** was synthesized using a known procedure,[56] starting with the installation of the *p*-carborane wheels with the alkynyl bromide **3**, to give **4** (Scheme 1). This was followed by the deprotection of the triisopropylsilylacetylene (TIPSA) groups to give **5**. Finally, Pd-catalyzed coupling of the 2-pyridone moieties gave nanotrain monomer **1** (Fig. 1).

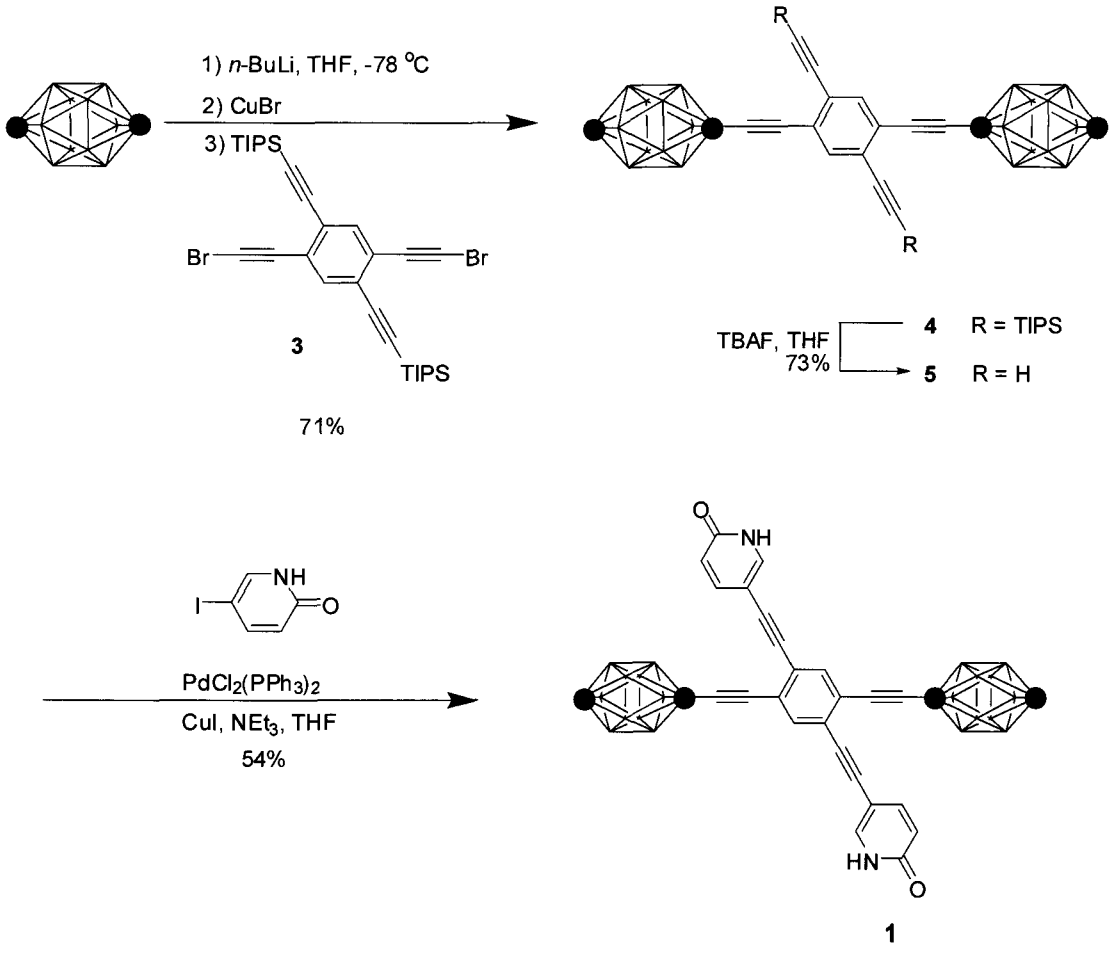

Scheme 1. Synthesis of compound **1**.

Similarly, the dialkynyl benzene precursor 6[63] was coupled via a simple Sonogashira protocol to obtain control monomer **2** (Scheme 2). In some cases, the NMR analyses do not give first order spectra. We assume that there is some degree of hydrogen bonding and/or tautomerization detected in the NMR analyses, and that causes peak broadening as well as the presence/absence of peaks.

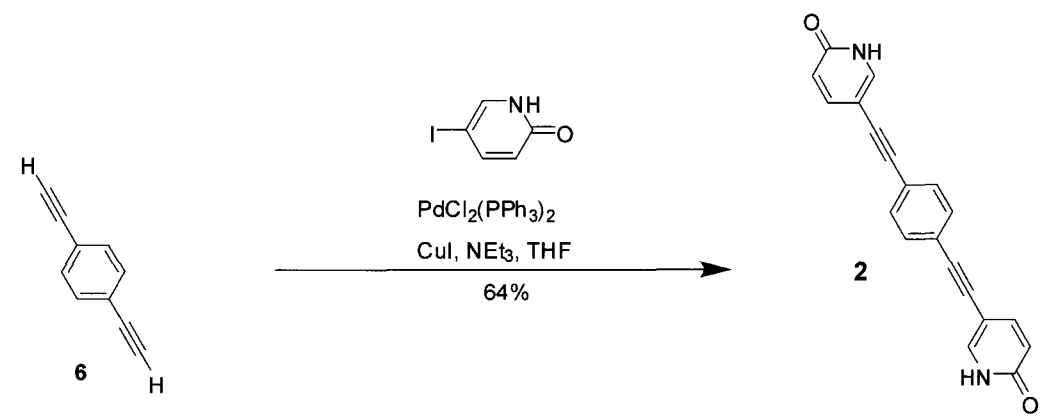

Scheme 2. Synthesis of compound **2**

To study the self-assembling nature of these 2-pyridone derivatives, a 10 μmol/L solution of the monomer in tetrahydrofuran (THF) was drop-cast onto a SiO_2 or a freshly cleaved mica surface, vacuum dried (in the case of the samples on SiO_2; vacuum drying the mica samples did not produce good results), and observed by AFM.[64] Conventional tapping-mode etched silicon probes (TESP) with tip sizes of approximately 25 nm in diameter were used in ambient atmosphere.

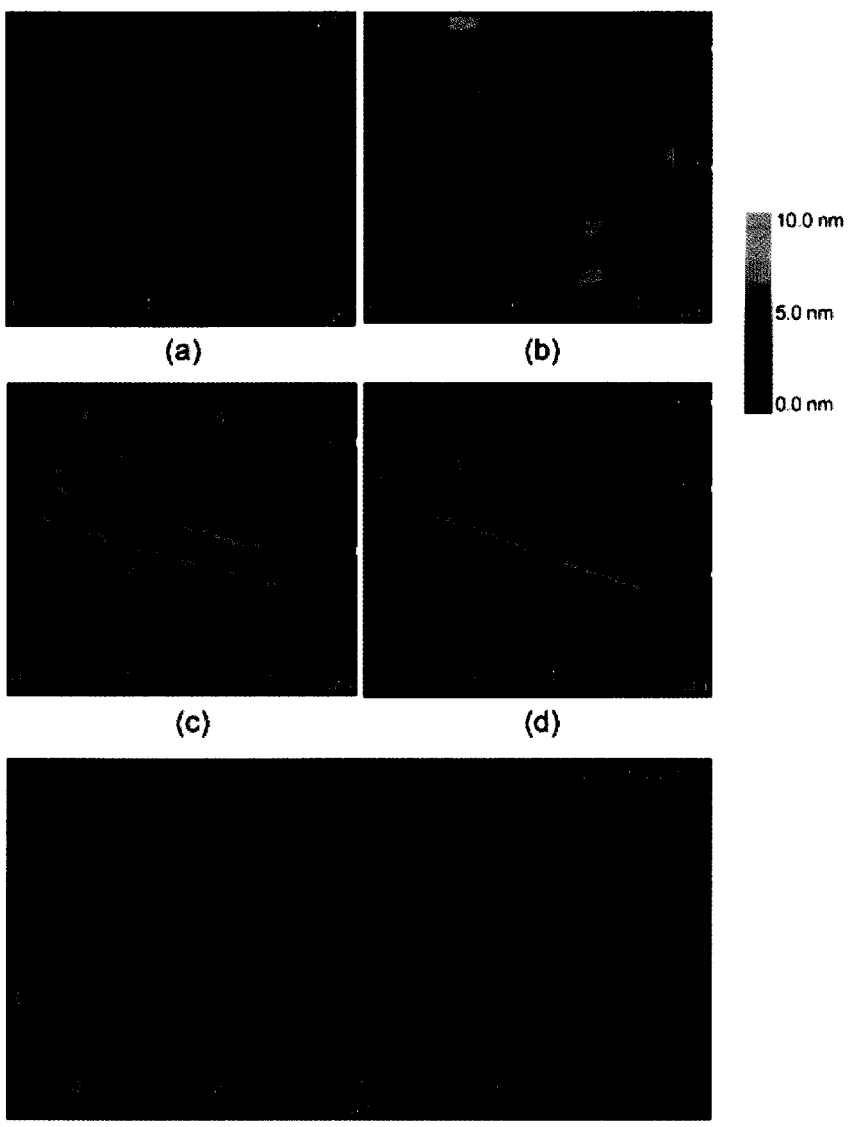

Figure 2. (a-d) Four AFM images of drop-cast nanotrain **1** and control **2** in THF (1×10^{-5} M) on SiO_2; scan rate 1.30 Hz, sample resolution 512; (a) **2**, 20.0 μm × 20.0 μm; (b) **1**, 0.90 μm × 0.90 μm; (c) **1**, 2.5 μm × 2.5 μm; (d) **1**, 6.5 μm × 6.5 μm; (e) typical height profile of the self-assembled nanotrain. Scale bar is representative of all images.

For superior lateral resolution, high resolution (MikroMasch HI-RES) tips of diameter 1 nm were also used under similar conditions. Without the height-enhancing carborane

structures, monomer **2** showed no recognizable self-assembled structures anywhere on the SiO_2surface (Fig. 2(a)) whereas monomer **1** self-assembled into linear structures (Figs. 2(b)-(d)) with lengths as long as ~5 μm. Heights were in the range of 0.7 - 1.6 nm, within the range of the molecular height of carboranes or carboranes with axles.[61] Although imaging of the nanotrain using MikroMasch HI-RES tips on mica surfaces indeed provided sharper images than their conventional counterparts (Figure 3), the data from Figs. 2 and 3 are in agreement that intra- or interchain interactions arising from folding, or multiple chains bound side-to-side, are quite possible due to the widths of the observed formations. Unfortunately, in an effort to obtain images of single nanotrains, AFM using the HI-RES tip of samples deposited from toluene or toluene/ THF on mica did not produce usable images.[65]

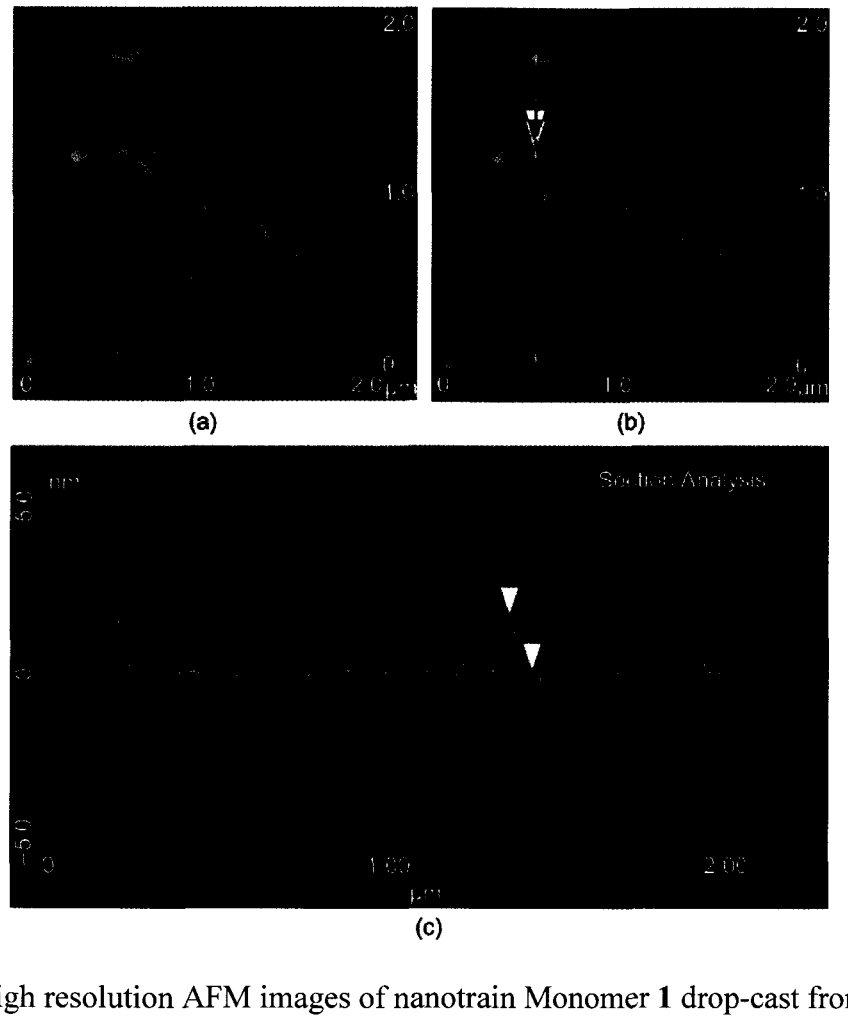

Figure 3. High resolution AFM images of nanotrain Monomer **1** drop-cast from THF (1 × 10–5 mol/L) onto a mica surface; scan rate 0.988 Hz, sample resolution 512; (a) 2.0 μm × 2.0 μm; (b and c) sectional analysis of (a)

There are three possible combinations of hydrogen bonding patterns through rotation about the alkyne bond linking the 2-pyridone to the rigid core (Fig. 4). In Fig. 4(a), with an assembly of the monomer in the *cis* conformation only, where both of the 2-pyridones are facing the same side, a linear chain is produced.

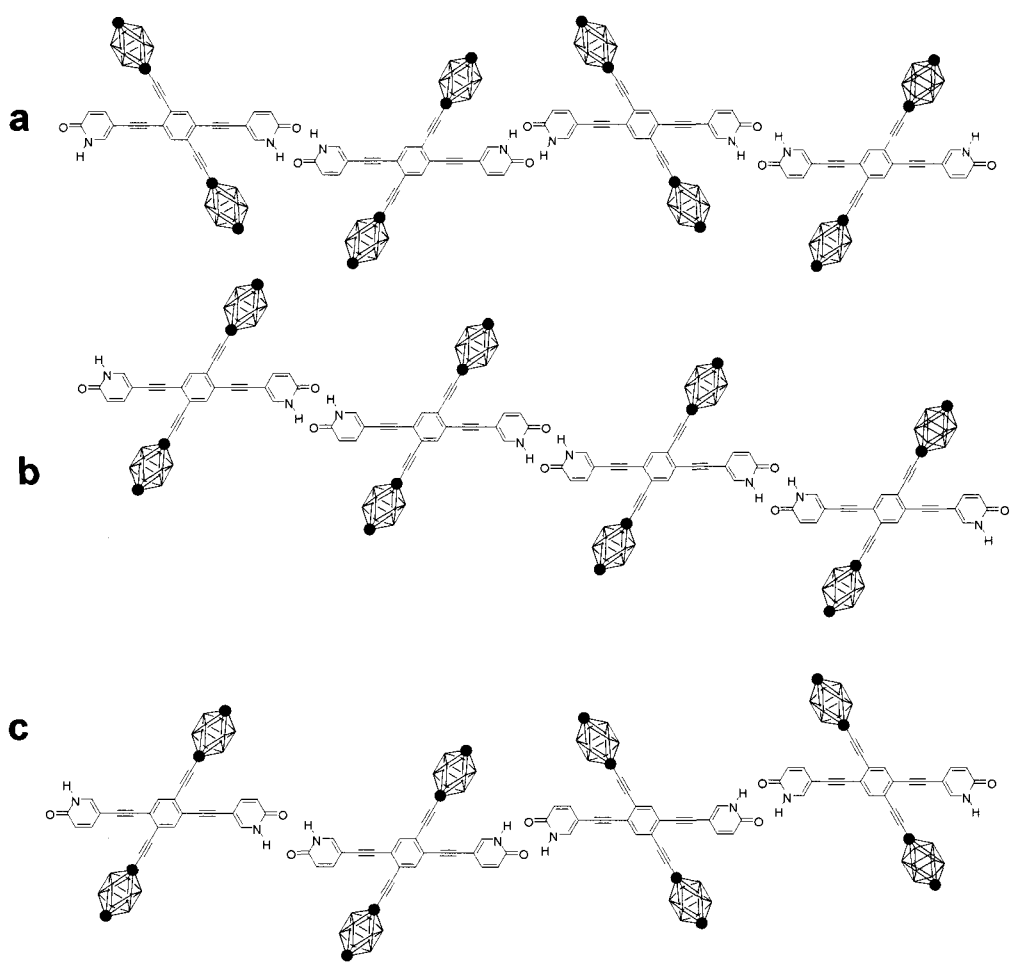

Figure 4. Nanotrain configurations from monomer **1**. Three possible patterns of 2-pyridone self-assembly, (a) *cis* only, linear assembly; (b) *trans* only, linear diagonal assembly; (c) combination of *cis* and *trans* in random fashion, which can result in curvature.

In Fig. 4(b), a linear chain is again produced with all the monomers in the *trans* conformation and the pyridones facing the opposite directions. In Fig. 4(c), the combination of both the *cis* and the *trans* confirmations of **1** linking randomly can result in a curved structure. We are not able to resolve the individual moieties responsible for hydrogen bonding, and all three structures could co-exist. In a report of similar hydrogen bonding via dipyridone structures linked by alkynes to a rigid core, X-ray crystallography

showed a preferential planar polymeric motif based on the *trans* pattern.[36] This result is based on a closely packed crystalline structure, whereas the diluted condition on the surface presents a different environment, and thus the exact hydrogen bonding scheme is unknown.

Conclusions

In summary, self-assembled structures using simple but strong hydrogen bonding of 2-pyridone moieties have been designed, synthesized and imaged by AFM. A linear nanotrain was synthesized with two hydrogen bonding sites at opposite positions. Imaging of the nanotrain at the atomic level on modified substrates is underway with the eventual goal of imaging concerted rolling motion.

Experimental Section

General Methods. All reactions were performed under an atmosphere of nitrogen unless otherwise stated. ^{1}H NMR and ^{13}C NMR spectra were recorded at 400 and 100 MHz respectively. Proton chemical shifts (δ) are reported in ppm downfield from tetramethylsilane (TMS). Mass spectrometry was performed at the Rice University and University of South Carolina Mass Spectrometry Laboratory. Infrared spectra (IR) assignments have 2 cm^{-1} resolution. Reagent grade tetrahydrofuran (THF) was distilled from sodium and benzophenone under a N_2 atmosphere. Triethylamine (NEt_3) was distilled from CaH_2. All other reagents were purchased from commercial suppliers and

used without further purification. Trimethylsilylacetylene (TMSA) was donated by FAR Research Inc or Petra Research. Flash column chromatography was performed using 230-400 mesh silica gel from EM. TLC was performed using glass plates precoated with silica gel 40 F_{254} purchased from EM Science. Compounds **1** and **2** were synthesized as described by Sasaki and co-workers.[62]

Typical Procedure for Self-Assembly onto Silica Surfaces

A solution of self-assembling molecule **1** or **2** was prepared in THF (1.0×10^{-5} M), and drop-cast onto a freshly-cleaned SiO_2 surface[66] attached to an AFM puck via double-sided tape. The puck was then placed into a dessicator and vacuum dried for 1 h. The dessicator was back-filled with nitrogen and AFM measurements were taken.

Typical Procedure for Self-Assembly onto Mica Surfaces

A solution of self-assembling molecule **1** or **2** was prepared in THF (1.0×10^{-5} M), and drop-cast onto a freshly-cleaved silica surface[67] attached to an AFM puck via double-sided tape. The puck was then placed into a dessicator and allowed to stand for 1 h under nitrogen and AFM was taken.

References and Notes

(1) Whitesides, G. M.; Mathias, J. P.; Seto, C. T. *Science* **1991**, *254*, 1312-1319.

(2) Lindsey, J. S. *New J. Chem.* **1991**, *15*, 153-180.

(3) Philp, D.; Stoddart, J. F. *Angew. Chem. Int. Ed.* **1996**, *35*, 1154-1196.

(4) Bong, D. T.; Clark, T. D.; Granja, J. R.; Ghadiri, M. R. *Angew. Chem., Int. Ed.* **2001**, *40*, 988-1011.

(5) Miao, Q.; Lefenfeld, M.; Nguyen, T. –Q.; Siegrist, T.; Kloc, C.; Nuckolls, C. *Adv. Mater.* **2005**, *17*, 407-412.

(6) Yip, H, -L.; Ma, H.; Jen, A. K. –Y.; Dong, J.; Parviz, B. A. *J. Am. Chem. Soc.* **2006**, *128*, 5672-5679.

(7) Sirringhaus, H.; Brown, P. J.; Frieds, R. H.; Nielsen, M. M.; Bechgaard, K.; Langeveld-Voss, B. M. W.; Spiering, A. J. H.; Jamssen, R. A. J.; Meijer, E. W.; Herwig, P.; et. al. *Nature* **1999**, *401*, 685-688.

(8) van de Craats, A. M.; Stutzmann, N.; Bunk, O.; Nielsen, M. M.; Watson, M.; Mullen, K.; Chanzy, H. D.; Sirrnghaus, H.; Friends, R. H. *Adv. Mater.* **2003**, *15*, 495-499.

(9) Faccheti, A.; Mushrush, M.; Yoon, M.H.; Hutchison, G. R.; Ratner, M. A.; Marks, T. J. *J. Am. Chem. Soc.* **2004**, *126*, 13859-13874.

(10) Wu, Y.; Li, Y.; Gardner, S.; Ong, B. S. *J. Am. Chem. Soc.* **2005**, *127*, 614-618.

(11) Kautz, H.; van Beek, D. J. M.; Sijbesma, R. P.; Meijer, E. W. *Macromolecules* **2006**, *39*, 4265-4267.

(12) Schmidt-Mende, L.; Fehtenkotter A.; Mullen, K.; Moons, E.; Friend, R. H.; Mackenzie, J. D. *Science* **2001**, *293*, 1119-1122.

(13) Yang, X. N.; van Duren, J. K. J.; Rispens, M. T.; Hummelen, J. C.; Janssen, R. A. J.; Michels, M. A. J.; Loos, J. *Adv. Mater.* **2004**, *16*, 802-806.

(14) Koert, U.; Harding, M. M.; Lehn, J. M. *Nature* **1990**, *346*, 339-342.

(15) Engelkamp, H.; Middelbeek, S.; Nolte, R. J. M. *Science* **1999**, *284*, 785-788.

(16) Hirsschberg, J. H. K. K.l Brunsverld, L.; Ramzi, A.; Vekemans, J. A. J. M.; Sibesma, R. P.; Meijer, E. W. *Nature* **2000**, *407*, 167-170.

(17) Percec, V.; Glodde, M.; Bera, T. K.; Miura, Y.; Shiyanovskaya, I.; Singer, K. D.; Balagurusamy, V. S. L.; Heiney, P. A.; Schnell, I.; Rapp, A.; et al *Nature* **2002**, *419*, 384-387.

(18) Yamamoto, T.; Fukushima, T.; Yamamoto, Y.; Kosaka, A.; Jin, W.; Ishii, N.; Aida, T. *J. Am. Chem. Soc.* **2006**, *128*, 14337–14340.

(19) Jonkheijm, P.; Miura, A.; Zdanowska M.; Hoeben F. J. M.; Feyter, S. D.; Schenning, A. P. H. J.; de Schryver, F. C.; Meijer, E. W. *Angew. Chem., Int. Ed.* **2004**, *43*, 74-78.

(20) Ghadiri, M. R.; Granja, J. R.; Milligan, R. A.; Mcree, D. E.; Lhazanovich, N. *Nature*, **1993**, *366*, 324-327.

(21) Yan, D. Y.; Zhou, Y. F.; Hou, J. *Science* **2004**, *303*, 65-67.

(22) Bazter, R. N. W.; Lehn, J. M.; Fischer, J.; Youinou, M. *Angew. Chem., Int. Ed.* **1994**, *33*, 2284-2287.

(23) Weissbuch, I.; Baxter, P. N. W.; Cohen, S.; Cohen, H.; Kjaer, K.; Howes, P. B.; Als-Nielsen J.; Hanan, G. S.; Schubert, U. S.; Lehn, J, M.; et al. *J. Am. Chem. Soc.* **1998**, *120*, 4850-4860.

(24) Ruben, M.; Rojo, J.; Romero-Saluguero, F. J.; Uppadine, L. H.; Lehn, J. M. *Angew. Chem., Int. Ed.* **2004**, *43*, 3644-3662.

(25) Zerowski, J. A.; Whitesides, G. M *J. Am. Chem. Soc.* **1994**, *116*, 4298-4304.

(26) Ranganathan, A.; Pedireddi, V. R.; Rao, C. N. R. *J. Am. Chem. Soc.* **1999**, *121*, 1752-1753.

(27) Prins, L. J.; de Jong, F.; Timmerman, P.; Reinhoudt, D. N. *Nature* **2000**, *408*, 181-184.

(28) Whiteside, G. M.; Simanek, E. E.; Mathias, J. P.; Seto, C. T.; Chin, D. N.; Mammen, M.; Gordon, D, M. *Acc. Chem. Res.* **1995**, *28*, 37-44.

(29) Highfill, M. L.; Chandrasekaran, A.; Lynch, D. E.; Hamilton, D. A. *Crystal Growth & Design.* **2002**, *2*, 15-20.

(30) Kolotuchin, S. V.; Zimmerman, S. C. *J. Am. Chem. Soc.* **1998**, *120*, 9092-9093.

(31) Marsh, A.; Silverstri, M.; Lehn, J. M. *Chem. Commun.* **1996**, 1527-1528.

(32) Jeffrey, G. A. *An Introduction to hydrogen bonding*, Oxford University, Oxford, **1997**.

(33) Atwood, J. L.; Davies, J. E. D.; MacNicol, D. D.; Vögtle, F.; Lehn, J. –M. *Comprehensive Supramolecular Chemistry*, Pergamon, New York, **1996**.

(34) Simard, M.; Su, D.; Wuest, J. D. *J. Am. Chem. Soc.* **1991**, *113*, 4696-4698.

(35) Edwards, M. R.; Jones, W.; Motherwell, W. D. S. *Cryst. Eng.* **2002**, *5*, 25-36

(36) Ducharme, Y.; Wuest, J. D. *J. Org. Chem.* **1988**, *53*, 5787–5789.

(37) Gallant, M.; Viet, M. T. P.; Wuest, J. D. *J. Org. Chem.* **1991**, *56*, 2284–2286.

(38) Heinz, R.; Rabe, J. P.; Meister, W. –V.; Hoffmann, S. *Thin Solid Films* **1995**, *264*, 246-249.

(39) Thwaite, S.; Schier, A.; Schmidbaur, H. *Inorg. Chim. Acta.* **2004**, *357*, 1549-1557.

(40) Miyabayashi, T.; Hara, T.; Yamagata, T.; Mashima, K. *Act Cryst.* **2007**, *E63*, m576 – m578.

(41) Nichol, G. S.; Clegg, W. *Inorg. Chim. Acta* **2006**, *359*, 3474-3480.

(42) Murugavel, R.; Kuppuswamy, S.; Boomishankar, R.; Steiner, A. *Angew. Chem,. Int. Ed.* **2006**, *45*, 5536-5540.

(43) Chuchuryukin, A. V.; Chase, P. A.; Mills, A. M.; Lutz, M.; Spek, A. L.; van Klink, G. P. M.; van Koten, G. *Inorg. Chem.* **2006**, *5*, 2045-2054.

(44) Barth, J. V.; Constantini, G.; Kern, K. *Nature* **2005**, *437*, 671-679.

(45) Barth, J. V.; Weckesser, J.; Cai, C.; Günter, P.; Burgi, L.; Jeandupeux O.; Kern, K. *Angew. Chem., Int. Ed.* **2000**, *39*, 1230-1234.

(46) West, P.; Ross. A. *An Introduction to Atomic Force Microscopy Modes*, Pacific Nanotoechnology, Inc., **2006**.

(47) Takamatsu, D.; Yamakoshi, Y.; Fukui, K. *Surf. Sci. Nanotech.* **2006**, *4*, 249-253.

(48) Marcus, R. B.; Ravi, T. S.; Gmitter, T.; Chin, K.; Orvis, W. J.; Ciarlo, D. R.; Hunt, C. E.; Trujillo, J. *Appl. Phys. Lett.* **1990**, *56*, 236-238.

(49) HI-RES tips with tip radius of ~1 nm are commercially available from μMasch, Inc.

(50) Shirai, Y.; Osgood, A. J.; Zhao, Y.; Kelly, K. F.; Tour, J. M. *Nano Lett.* **2005**, *5*, 2330-2334.

(51) Shirai, Y.; Osgood, A. J.; Zhao, Y.; Yao, Y.; Saudan, L.; Yang, H.; Yu-Hung, C.; Sasaki, T.; Morin, J.-F.; Guerrero, J. M.; Kelly, K. F.; Tour, J. M. *J. Am. Chem. Soc.* **2006**, *128*, 4854-4864.

(52) Shirai Y.; Morin, J. -F.; Sasaki, T.; Guerrero, J. M.; Tour, J. M. *Chem. Soc. Rev.* **2006**, *35*, 1043-1055.

(53) Morin, J.-F.; Shirai, Y.; Tour, J. M. *Org. Lett.* **2006**, *8*, 1713-1716.

(54) Sasaki, T.; Tour, J. M. *Tetrahedron Lett.* **2007**, *48*, 5821-5824.

(55) Sasaki, T.; Morin, J.–F.; Lu, M.; Tour, J. M. *Tetrahedron Lett.* **2007**, *48*, 5817-5820.

(56) Morin, J.–F.; Sasaki, T.; Shirai. Y.; Guerrero J. M.; Tour, J. M. *J. Org. Chem.* **2007**, *72*, 9481-9490.

(57) Sasaki, T, Osgood, A. J.; Alemany, L. B.; Kelly, K. F.; Tour, J. M. *Org. Lett.* **2008**, *10*, 229-232.

(58) Sasaki, T.; Tour, J. M. *Org. Lett.* **2008**, *10*, 897-900.

(59) Sasaki, T.; Osgood, A. J.; Kiappes, J. L. Kelly, K. F.; Tour, J. M. *Org. Lett.* **2008**, *10*, 1377-1380.

(60) Sasaki, T.; Guerrero J. M.; Tour, J. M. *Tetrahedron* **2008**, *64*, 8522-8529.

(61) Morgan, D. A.; Sloan, J.; Green, M. L. H. *Chem. Commun.* **2002**, 2442-2443.

(62) Sasaki, T.; Guerrero, J. M.; Leonard, A. D.; Tour, J. M. *Nano Research* **2008**, *1*, 412-419.

(63) Bodwell, G. J.; Miller, D. O.; Vermeij, R. J. *Org. Lett.* **2001**, *3*, 2093–2096.

(64) Images taken by the AFM were processed using Nanoscope 5.30r1. Nanotrain formation was unaffected when switching the substrate from SiO_2 to Mica.

(65) In an attempt to avoid possible pi-stacking interactions, drop-casting was also attempted using benzene and toluene as solvent but no trains were observed, presumably due to the low solubility of the molecules.

(66) The silica surface was cleaned via submersion into a freshly prepared solution containing 3:1 H_2SO_4 : H_2O_2 for 20 minutes. The surface was then washed with deionized, degassed water followed by degassed ethanol. Finally, the surface was dried under a steady stream of nitrogen and scored to give a silica "chip" roughly 1 cm in diameter.

(67) A freshly-cleaved mica surface was prepared by hole-punching a circle of multiple-layer mica (roughly 1 cm in diameter), followed by attachment via double sided tape to an AFM puck. The upper layer was cleaved off by placing scotch tape over the upper

surface and gentlly removing the tape. When the resulting layer on the puck was smooth to the naked eye, the surface was ready for use.

Chapter 5

Carborane-Wheeled Nanocars

5.1

Synthetic Routes Toward Carborane-Wheeled Nanocars

Introduction

The development of microscopy tools, particularly scanning tunneling microscopy (STM), has allowed scientists to study biological[1] and artificial[2] molecular machines on surfaces. The quickly expanding field of nanomachines has been reviewed.[3] Because translational motion is the easiest to monitor by STM, much effort has been devoted to observe single molecule translational movement on flat metallic surfaces. For instance, a family of molecular barrows with triptycene moieties as wheels has been developed.[4] Although these molecules can be imaged and manipulated by STM in the direction perpendicular to the axles, calculations suggest sliding rather than rolling of the molecules due to the lack of positive interactions with the surface.[4a] Furthermore, other molecules have been imaged to slide or migrate across surfaces.[5] To improve directionality, four fullerene-wheeled nanocars were recently synthesized by our group.[6] Fullerene's spherical and smooth shape and most importantly its affinity towards gold surfaces, have produced directional rolling motions of the nanocars on the gold surface upon heating or electrostatic control.[6a] However, synthetic problems arise when using fullerenes. First, fullerenes and fullerene-containing molecules have very poor solubility. Long alkyl chains are incorporated to alleviate the solubility problems, but in return this addition increases the number of synthetic steps required to construct the nanocar. Second, because of their tendency to deactivate metal-catalyzed reactions, fullerenes have to be introduced onto the nanocar at the final step of the synthesis, resulting in a low yielding tetra-substitution reaction. Additionally, the electronic nature of fullerene makes

it unsuitable for the development of more complex nanomachines using light as the power input due to the rapid energy transfer to the fullerenes.[7]

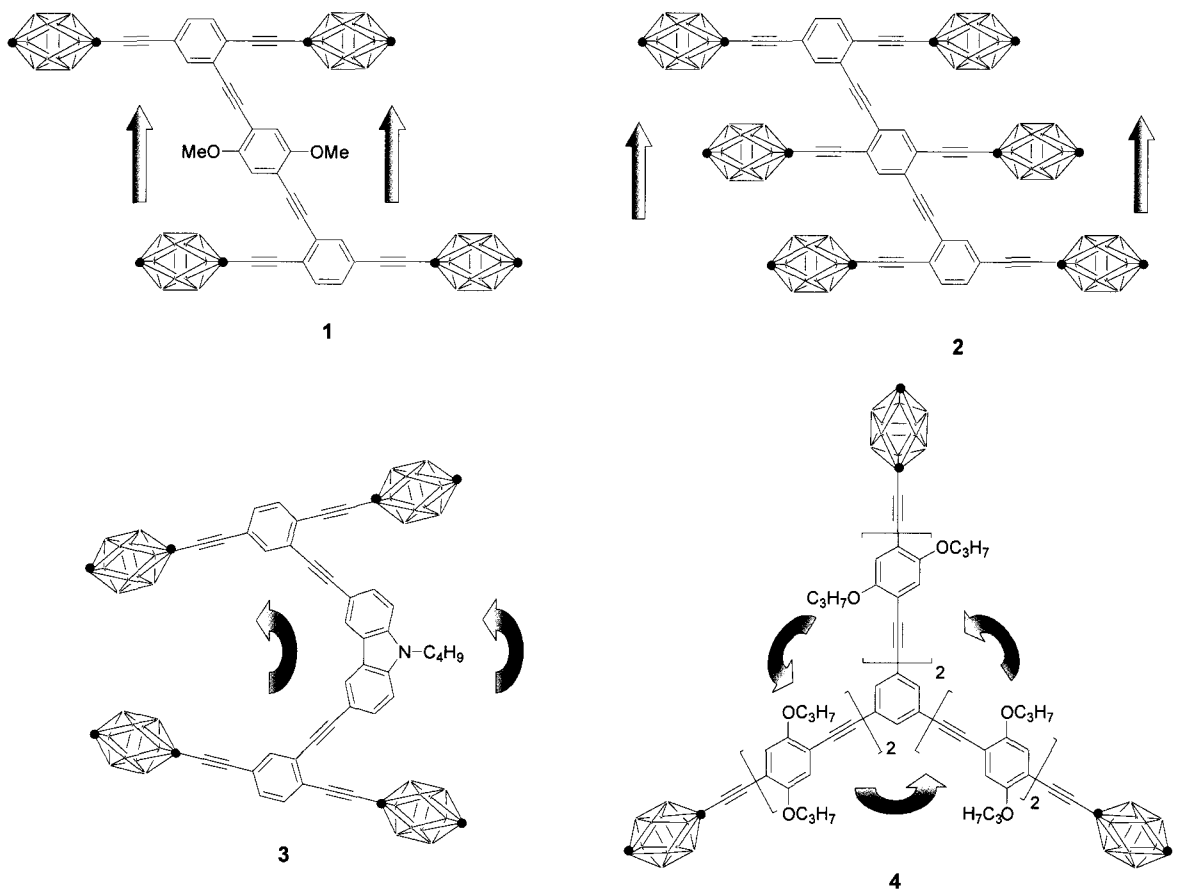

Figure 1. Molecular structures of **1-4** and the expected directionality of motion.

We report here the synthesis of four different nanovehicles: nanocars **1** and **3**, nanocaterpillar **2** and trimer molecule **4**, all bearing *p*-carboranes (Figure 1) as prepared by J. –F. Morin. Some synthetic intermediates as well as spectroscopic measurements were done by T. Sasaki. In completing the project, my work consisted of synthesizing some of the intermediates in route to various final products as well as spectroscopic measurements. *p*-Carborane was our choice for the potential development of rolling

molecules because of its spherical shape and its aromatic nature[8] that allow for easy substitution reactions at one or both of the carbon atoms positioned *para* to each other.[9] Moreover, they are robust, and unlike fullerenes, are very soluble in common organic solvents, thus allowing for the synthesis of smaller molecular machines in fewer synthetic steps. Lastly, carboranes can be introduced at any stage of the synthesis because they do not inhibit organometallic coupling reactions (unlike fullerenes). The work presented here is an extension of our previous work on the fullerene-containing nanocar[6] and the first step toward development of easily accessible functional nanomachines to address molecular rolling on surfaces. As shown in Figure 1, molecules **1-4** are designed to move in specific patterns on the surface. Nanocar **1** and nanocaterpillar **2** are expected to translate in a one-dimensional fashion since the axles are parallel to each other. The difference in the number of wheels will assist in the dimensional analysis of the molecules sliding or rolling on the surface by STM. Nanocar **3** was designed to make small circular motions on the surface. This movement could be useful for monitoring surface motion using the STM.[6a] Trimer **4** was designed to pivot on the surface with no translational movement, analogous to the pattern observed for the related fullerene trimers.[6]

Results and Discussions

Synthesis. Two different strategies were used to synthesize nanocar **1** and nanocaterpillar **2**. For **1**, the four wheels were introduced at the end of the synthetic pathway on the tetra(bromoalkyne) moiety. On the other hand, the wheels on **2** were

coupled to the axle prior to the synthesis of the central part of the chassis. This allowed us to compare both routes in terms of synthetic feasibility and efficiency.

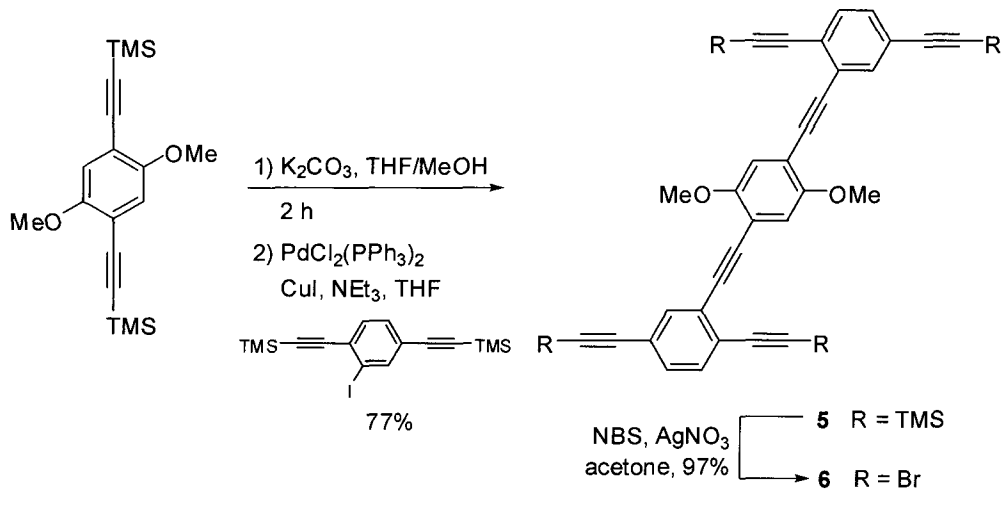

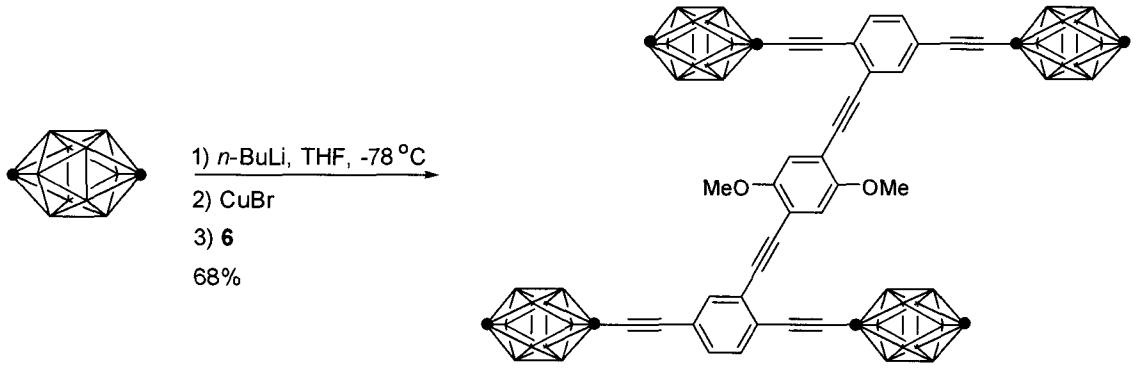

1

Scheme 1. Synthesis of the nanocar **1**. Every vertex on the starting carborane is BH except the darkened sites that are CH. The product nanocar, **1**, has the internal carborane carbon alkynyl-substituted.

In Scheme 1, the methoxy groups were installed to increase the polarity of the molecules, which was necessary in order to chromatographically separate the large excess

of non-polar unreacted *p*-carborane from the desired product. The starting compound 1,4-dimethoxy-2,5-bis(trimethylsilylacetylene)benzene was synthesized in two steps following known procedures.[10,11] The alkynes were then deprotected. Due to the unstable nature of the free alkyne intermediate, the deprotection step was carried out immediately prior to the coupling with the 1-iodo-2,5-bis(trimethylsilyacetylene)benzene that was previously synthesized.[7] The four TMS protecting groups were removed by desilyl bromination[12] to give **6** in good yield. Finally, the *p*-carborane moieties were introduced at the four bromoalkyne positions to give **1** in 68% yield. The nanocar **1** is quite soluble in common organic solvents such as chloroform, acetone, THF and toluene. Thermogravimetric analysis (TGA) was performed on **1** in order to obtain information on its thermal stability. At a scan rate of 20 °C/min (under N_2), Gradual decomposition of **1** from its original mass was observed around 390 °C. This result suggests that the alkyne-carborane bond is stronger and more stable than the alkyne-fullerene which showed decomposition around 300 °C upon heating, and this data will be essential as substrate heating[6] is used to propel the nanocars.

A CPK model of the planar conformation of **1** was generated using Spartan X. As shown in Figure 2, the wheel-to-wheel distance for **1** is approximately 14 Å in both directions (parallel and perpendicular to the axles), meaning that **1** is nearly a square molecule. Although **1** is one of the simplest nanocars we can synthesize, the square configuration limits its usefulness for STM studies. Since we can only image the wheels and not the inner chassis due to the relative differences in their density of states, we will not be able to distinguish the orientation of **1** on the surface. Thus addressing directionality will be even more difficult.

To bypass this problem, nanocaterpillar **2**, with three axles rather than two, was synthesized. The CPK model (Figure 2) of the planar conformation of **2** shows minimal spacing between the aligned carborane wheels. The UV data, explained in the latter section, confirms steric hindrance between the wheels that might lead to problems for surface rolling. The strategy used for the synthesis of **2** is depicted in Scheme 2.

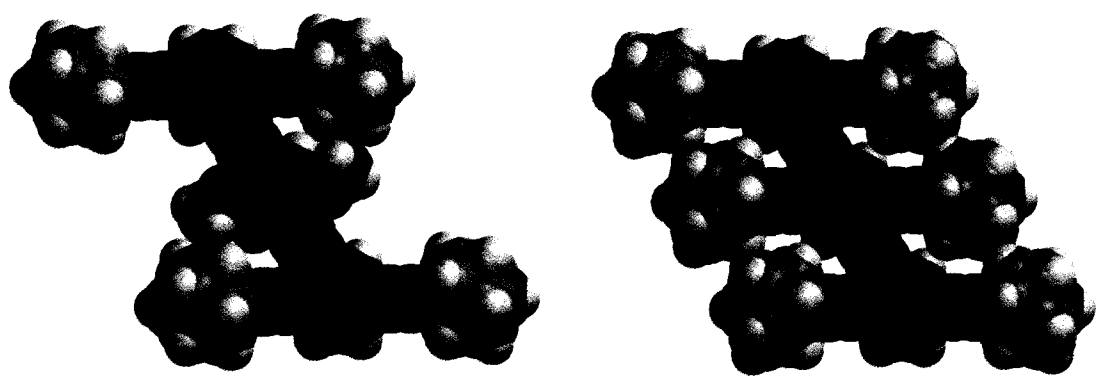

1 **2**

Figure 2. CPK models of planar conformations of **1** and **2.**

Following known procedures,[13,14] 1,4-dibromo-2,5-bis(trimethylsilylacetylene)benzene was synthesized in two steps from 1,4-dibromobenzene. The bromides were replaced by iodides using *tert*-butyllithium followed by 1,2-diiodoethane. This step was necessary in order to perform the Sonogashira coupling reaction between the iodide-containing axle and the central chassis.[15] The TIPS-acetylene groups were introduced on **7** by standard Sonogashira coupling to provide **8** in good yield. Selective desilyl bromination of the TMS-acetylene groups[12b] was achieved using NBS and $AgNO_3$ in acetone to give **9** in almost quantitative yield. The *p*-carborane wheels were introduced to give **10** followed by deprotection of the

TIPS-acetylene groups. The resulting **11** was then coupled with wheel/axle (1-iodo-2,5-bis(*p*-carboraneacetylene)benzene)[7] to give the nanocaterpillar **2**. As with **1**, **2** is also soluble in common organic solvents.

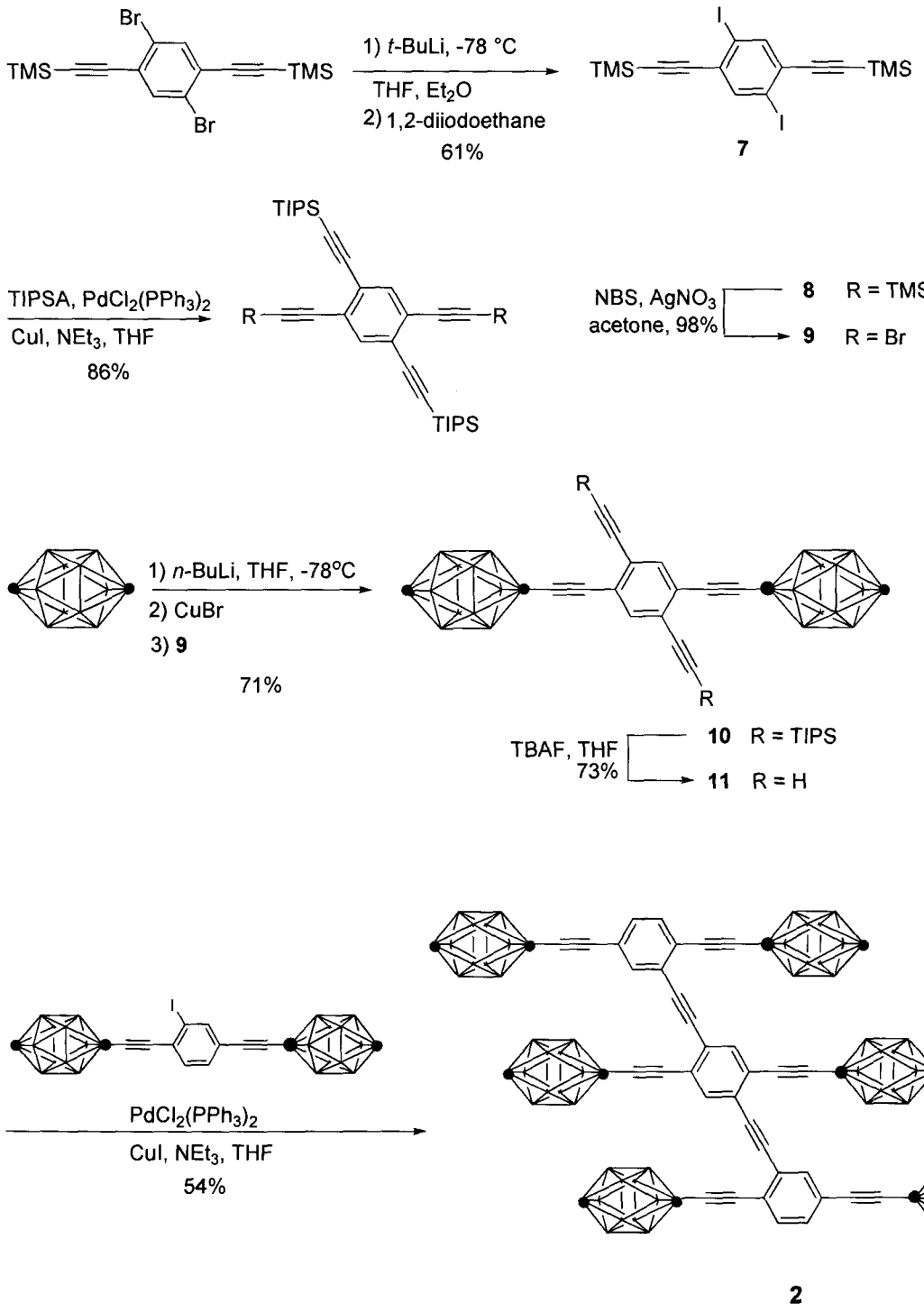

Scheme 2. Synthesis of the nanocaterpillar **2**.

The wheel/axle (1-iodo-2,5-bis(*p*-carboraneacetylene)benzene)[7] is a versatile tool and can be used in combination with several different chassis to create nanovehicles having specific conformations for accomplishing different tasks, hence Scheme 2 is preferable over Scheme 1. In this regard, we synthesized nanocar **3** (Scheme 3) which is expected to move in a circular motion due to its "curved" conformation (Figure 1). The chassis **13** of nanocar **3** bearing two terminal alkynes was synthesized in four straightforward steps.[16] Compound **13** was then coupled to the wheel/axle to give nanocar **3** in 67% yield.

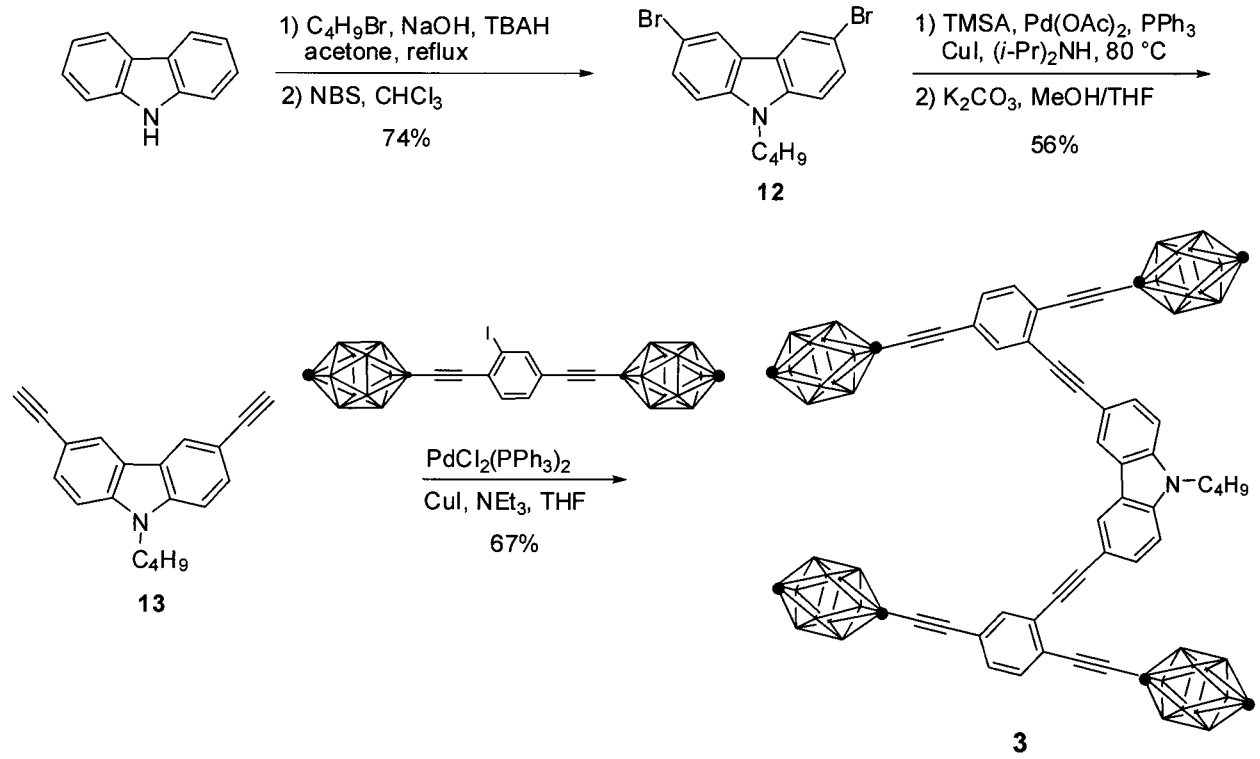

Scheme 3. Synthesis of the "curved" nanocar **3**.

The CPK model of **3** and **4** was modeled by Spartan X (Figure 3). Despite the "curved" feature of the inner chassis of **3**, the model shows no overlapping of the inner carborane wheels. Unlike **1**, the distances perpendicular and parallel to the axis are distinct. This will allow for an easier assessment of molecular orientation and movement on the surface. Trimer **4** was designed to rotate on the surface with the center of rotation coincident with the center of the molecule. A similar molecule, bearing fullerene wheels instead of *p*-carborane proved to be useful in studying the pivot-rolling mechanism using STM, since it did not show translational movement on a gold surface.[6a]

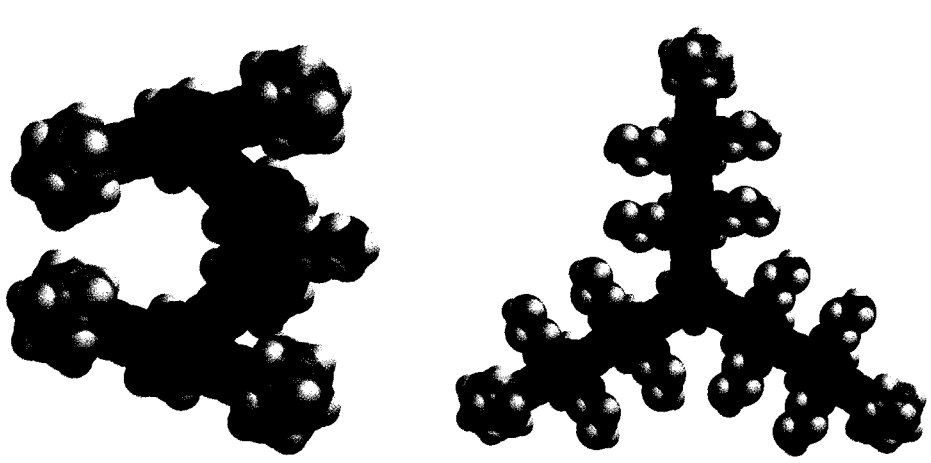

Figure 3. CPK models of planar conformations of **3** and **4.**

To synthesize **4** (Scheme 4), we first tried a linear strategy involving the successive addition of phenylacetylene moieties onto a 1,3,5-trisubstituted benzene ring followed by addition of the three carborane wheels. However, we found that desilyl bromination of the long oligo(phenylene ethynylene) (OPE) gave a low yield and led to various side products. Compound **4** was instead synthesized using a convergent strategy

involving a triangular central part and a carborane-containing substituted phenylacetylene moiety. Thus, the triangular core was synthesized in two steps from 1,3,5-dibromobenzene using a Sonogashira coupling reaction followed by a deprotection reaction to provide **18** in 79% overall yield.[17] Compound **18** was then coupled to **14**, synthesized in three steps from hydroquinone,[18] using the Sonogashira coupling reaction to afford **19** in 68% yield. The carborane-containing moiety was synthesized in two steps from 1,4-bis(propyloxy)-2,5-diiodobenzene[19] by desilyl bromination[12] followed by reaction with carborane-copper adduct as described above. In this case, the latter reaction proceeded slowly and 48 h were necessary for the reaction to be completed. This can be attributed to the electron-donating nature of the propyloxy groups present on the phenyl ring that partially deactivate the alkynyl bromide toward oxidative addition. Compound **20** was then coupled to **16** to give **4** in good yield.

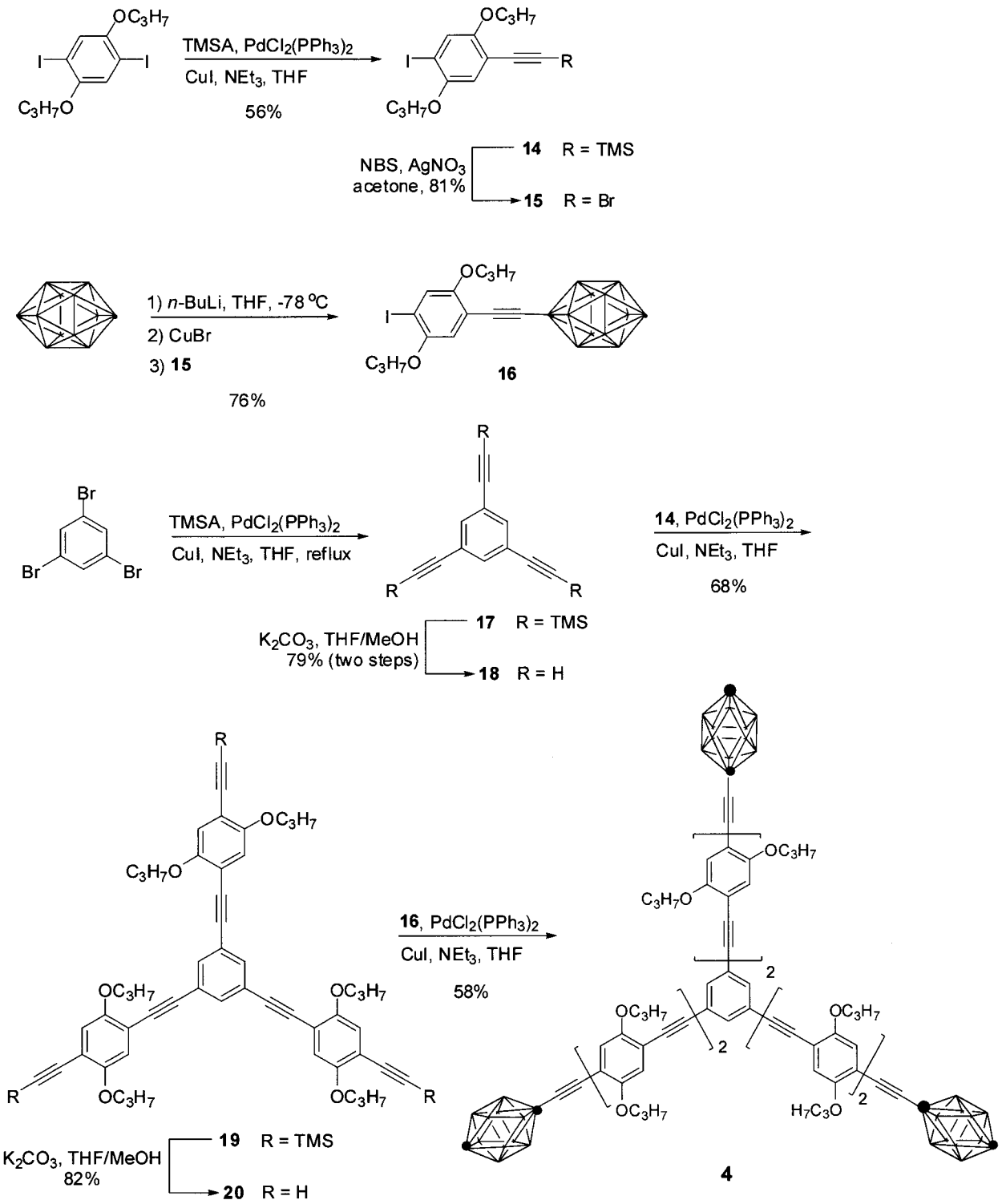

Scheme 4. Synthesis of the trimer **4**, designed to rotate about its center on the surface.

Optical Properties. There are few reports on the optical properties of carborane-containing conjugated molecules; therefore, the optical properties of molecules **1-4** were investigated using solution phase absorption and fluorescence spectroscopy. As an alternative to STM, it is possible that the optical properties could be exploited to image these molecules on a non-metallic surface using fluorescence, hence these studies are essential. As shown in Figure 4, **1-4** absorb light in the regions λ_{max} = 375–410 nm, as commonly observed for OPEs containing three phenyl rings.[20] Compound **4** absorbs light at the longest wavelength out of the four (λ_{max} = 410 nm), which can be attributed to the electron-donating nature of the four propyloxy groups and the increased conjugation length of the OPE. Electron donating substituents are known to increase the energy of the HOMO level and, consequently, the band gap of π-conjugated systems. A portion of this effect can be attributed to the aromatic character of carborane,[8] acting to extend the conjugated length of the molecule. Next, compound **1** (λ_{max} = 385 nm) is further red-shifted than **2** and **3** due to again the electron donating methoxy groups. However, lower conjugation of this molecule results in a shorter wavelength than that of compound **4**. Compound **3** contains no significant electron-withdrawing groups resulting in a shorter wavelength. The interesting feature is that the spectrum of **3** shows a slight absorbance at ~362 nm, that may indicate a rigid conformation.[21] On the other hand, the UV-visible spectrum of **2** is blue-shifted compared to **1**, **3** and **4**. This blue shift can be attributed to the steric hindrance between carborane wheels of different axles, which leads to a high dihedral angle between phenyl rings of the molecule's core, thereby possibly limiting its usefulness on a surface. However, the surface-carborane attraction might be sufficient to make the system planar; therefore we are waiting expectantly the surface analyses.

Additionally, the UV-visible spectrum of **2** shows two distinct maxima (353 and 375 nm) indicating that **2** adopts a rigid conformation in its ground state. This type of vibronic structure is frequently observed in cases of rigid ladder-shaped molecules.[21] The energy difference between the two maxima (about 0.20 eV) is consistent with a C=C stretching mode that would be expected to couple strongly to the electronic structure.[22] In comparison, **1**, **3** and **4** do not show significant vibronic structure, indicating that they have a fairly flexible conformation in the ground state.

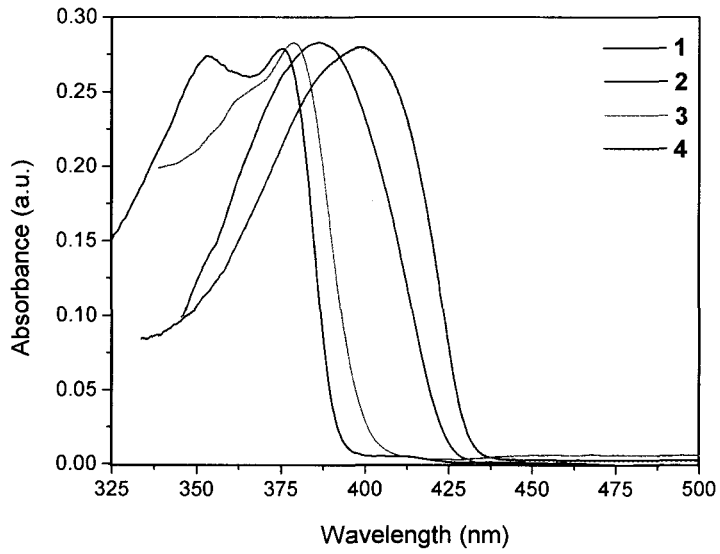

Figure 4. UV-visible absorption spectra of **1-4** (1.0×10^{-5} M) in chloroform.

To determine the specific effect of the carboranes on the optical properties of conjugated molecules, UV-visible spectra of **1** and its TMS-substituted precursor **5** were compared. As expected, the λ_{max} of **1** (386 nm) is red-shifted compared to its precursor **5** (379 nm). This can be attributed to an increase in the conjugation length of the molecule containing carborane, therefore underscoring the conjugation effect of the carboranes.

The electron-withdrawing nature of carborane can be part of an intramolecular charge-transfer complex with the 1,4-dimethoxy moiety of the core, decreasing the band gap. Furthermore, the introduction of carborane does not induce significant steric hindrance between the two axles since both spectra have a similar shape with no vibronic structure.

The fluorescence properties of **1-4** were investigated with the results summarized in Figure 5 and Table 1. As expected, all four compounds fluoresce in chloroform in the UV-blue region. The wavelength of the emission maxima increases in the order of **2** < **3** < **1** < **4** reflecting the extent of conjugation plus the influence of electron rich moieties of the propoxyl, methoxyl, and butyl carbazole groups. A reversed result is seen with the band gap (optical, Eg, from the lower energy onset of the absorption spectra) in the order of **4** < **1** < **3** < **2**, as expected. Interestingly, **2** and **4** show fine vibronic structure, generally associated with a rigid conformation in the excited state. The small Stoke shift observed for compound **2** (14 nm) is characteristic of a molecule having a rigid conformation.[23] Table 1 summarized the optical data.

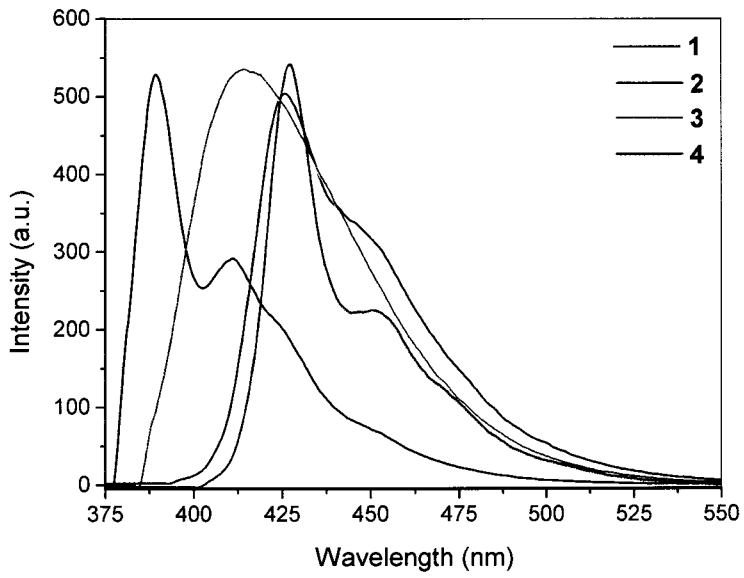

Figure 5. Fluorescence spectra of 1-4 (1.0×10^{-7} M) in chloroform.

Table 1. Optical properties of compound **1-4**

Compound	Abs(λ_{max})[a]	Emi (λ_{max})[a]	E_g (eV)[b]
1	386	426	2.89
2	375 (353)	389 (411)	3.14
3	379	414	3.05
4	399	427 (451)	2.85

[a] Spectra in chloroform.

[b] Band gap (optical), determined from the lower energy onset of the absorption spectra.

Conclusion

The design and the synthesis of four potential nanovehicles bearing *p*-carborane as wheels is reported. The use of *p*-carboranes overcomes several synthetic problems observed in fullerene-wheel nanovehicles: no long-chain alkyl groups are necessary to obtain soluble structures and addition of the wheels at different stages in the synthesis is possible. STM imaging analysis of the **1-4** is underway to investigate the movement of these nanovehicles on a metallic surface. The synthesis of more complex functional nanomachines is also underway.

Experimental Section

General Methods. ^{1}H NMR and ^{13}C NMR spectra were recorded at 400 and 100 MHz respectively. Proton chemical shifts (δ) are reported in ppm downfield from tetramethylsilane (TMS). Mass spectrometry was performed at the Rice University and University of South Carolina Mass Spectrometry Laboratory. Infrared spectra (IR) assignments have 2 cm^{-1} resolution. Reagent grade tetrahydrofuran (THF) and diethyl ether (Et_2O) were distilled from sodium and benzophenone under a N_2 atmosphere. Triethylamine (NEt_2) and CH_2Cl_2 were distilled from CaH_2 under N_2 atmosphere unless otherwise stated. THF and NEt_2 were degassed with a stream of argon for 1 h before being used in the Castro-Stephens-Sonogashira coupling. All other reagents were purchased from commercial suppliers and used without further purification. Trimethylsilylacetylene (TMSA) was donated by FAR Research Inc or Petra Research. *n*-BuLi 1.7 M in pentane, and *t*-BuLi 2.5 M in hexanes from Sigma-Aldrich Co. were used. Flash chromatography was carried out using silica gel (grade 60, mesh size 230-400, EM science). Thin layer chromatography (TLC) was performed using glass silica gel plates (40 F_{254} 0.25 mm layer thickness, Merck). Melting points were measured on a Mel-Temp instrument (uncorrected). All reactions were conducted under a dry oxygen-free atmosphere using oven-dried glassware unless otherwise stated. $PdCl_2(PPh_3)_2$,[1] 1,4-dimethoxy-2,5-diiodobenzene,[5] 1,4-dimethoxy-2,5-bis(trimethylsilylacetylene)benzene,[6] 1,4-dibromo-2,5-diiodobenzene,[7] 1,4-dibromo-2,5-bis(trimethylsilylacetylene)benzene[8] and 1,4-bis(propyloxy)-2,5-diiodobezene[9] were prepared using literature procedures. **1** – **6**, **8** – **11**, **19** and **20** were prepared as described by Morin and co-workers.[24]

General Procedure for Palladium-Catalyzed Coupling Reaction of Terminal Alkynes and Aryl Bromides or Aryl Iodides (Castro-Stephens-Sonogashira Coupling). An oven-dried round bottom flask equipped with a magnetic stir bar was charged with the terminal alkyne (1 equiv), aryl halide (1 equiv), $PdCl_2(PPh_3)_2$ (3-5 mol % per halide), CuI (6-10 mol % per halide), triethylamine (4 equiv per halide) and THF ([aryl halide] = 0.1 – 0.3 M). If the halide was an aryl iodide, the mixture was stirred at room temperature for 24 h. In case of an aryl bromide, PPh_3 (6-10 mol % per halide) was added and the mixture was stirred at 70 °C for the same period of time. After that period, saturated NH_4Cl was added and the mixture was extracted twice with dichloromethane. The combined organic layers were washed with water and dried over $MgSO_4$. The mixture was filtered and the solvent was removed and the desire product was isolated using column chromatography (silica gel as stationary phase) to provide the product.

General Procedure for Deprotection of Trimethylsilyl-Protected Alkynes. To a round bottom flask equipped with a magnetic stir bar, the protected alkyne was dissolved in a mixture of THF and MeOH ([protected alkyne] = 0.05 – 0.1 M). Then, K_2CO_3 (2 equiv per alkyne) was added. The mixture was stirred at room temperature for 2 h or until the reaction was complete (monitored by TLC). After that period, brine was added and the mixture was extracted twice with dichloromethane. The combined organic layers were washed with water and dried over $MgSO_4$. The solvent was removed and the desired product was isolated using column chromatography (silica gel as stationary phase) to provide the product.

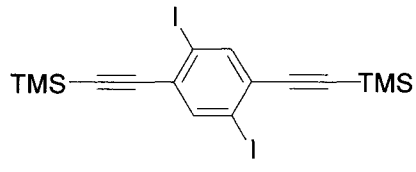

1,4-Diiodo-2,5-bis(trimethylsilylacetylene)benzene (7). An oven-dried 250 mL round bottom flask equipped with a magnetic stirrer was charged with 1,4-dibromo-2,5-bis(trimethylsilylacetylene)benzene[8] (2.59 g, 6.05 mmol), diethyl ether (60 mL) and THF (60 mL). The mixture was cooled -78 °C and *t*-BuLi (16.0 mL, 27.2 mmol) was added over 15 min. The resulting deep red solution was stirred for 1 h at -78 °C and 1,2-diiodoethane (5.45 g, 19.4 mmol) was added quickly. The solution was stirred 1 h at -78 °C and an additional 16 h at room temperature. The red solution was poured into water and extracted twice with dichloromethane. The combined organic layers were washed with 0.1 M sodium bisulfite, water and dried over $MgSO_4$. The solvent was removed under reduced pressure and the resulting orange solid was purified by column chromatography (silica gel, hexanes as eluent) to provide 1.93 g of the title product as a white waxy solid (61%): mp 129-131 °C; IR (KBr) 1453, 1248, 1048, 887, 860, 837, 796, 761 cm^{-1}; ^1H NMR (400 MHz, $CDCl_3$, ppm) δ 7.87 (s, 2H), 0.27 (s, 18H); ^{13}C NMR (100 MHz, $CDCl_3$, ppm) δ 141.8, 131.0, 104.8, 102.3, 99.7, -0.1; HRMS calcd for $C_{16}H_{20}I_2Si_2$ 521.9193, found 521.9191.

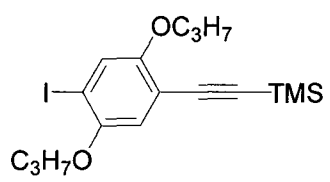

1,4-Bis(propyloxy)-2-iodo-5-trimethylsilylacetylenebenzene (14). See general procedure for Castro-Stephens-Sonogashira coupling. The compounds used were 1,4-

bis(propyloxy)-2,5-diiodobenzene[9] (3.35 g, 7.51 mmol), TMSA (1.06 mL, 7.51 mmol), CuI (86 mg, 0.45 mmol), $PdCl_2(PPh_3)_2$ (158 mg, 0.23 mmol), well-degassed triethylamine (5 mL) and THF (75 mL) at room temperature for 16 h. The resulting brown oil was purified by column chromatography (silica gel, 8% dichloromethane in hexanes as eluent) to provide 1.77 g of **14** as a yellow solid (56%): mp 34-36 °C; IR (KBr) 2149, 1495, 1464, 1376, 1248; 1216, 860, 845 cm^{-1}; ^1H NMR (400 MHz, $CDCl_3$, ppm) δ 7.26 (s, 1H); 6.84 (s, 1H); 3.90 (m, 4H); 1.81 (m, 4H); 1.07 (t, 6H, J = 7.4 Hz), 0.25 (9H); ^{13}C NMR (100 MHz, $CDCl_3$, ppm) δ 155.3, 152.1, 124.4, 116.7, 113.9, 101.2, 99.9, 88.3, 72.0, 71.8, 23.1, 23.0, 11.2, 10.9, 0.4; HRMS calcd for $C_{17}H_{25}IO_2Si$ 416.0669, found 416.0671.

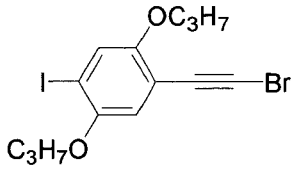

1,4-Bis(propyloxy)-2-iodo-5-bromoacetylenebenzene (15). A 25 mL round bottom flask equipped with a magnetic stir bar was charged with **14** (400 mg, 0.96 mmol) and acetone (12 mL). Then, freshly purified and dried *N*-bromosuccinimide (205 mg, 1.15 mmol) and silver(I) nitrate (16 mg, 96 μmol) were added. The mixture was stirred in the dark at room temperature for 2 h and poured into water (100 mL). The resulting slurry was extracted twice with dichloromethane and the combined organic layers were dried with $MgSO_4$. The solvent was removed under reduced pressure and the resulting orange-red oil solid was purified by column chromatography (silica gel, 10% dichloromethane in hexanes as eluent) to provide 330 mg of **15** as an orange oil (81%): IR (KBr) 2961, 2933, 2872, 2200, 1586, 1487, 1461, 1375, 1262, 1214, 1060, 1048, 1009, 974, 853, 837, 731

^{1}H NMR (400 MHz, $CDCl_3$, ppm) δ 7.27 (s, 1H), 6.82 (s, 1H), 3.90 (m, 4H), 1.82 (m, 4H), 1.06 (q, J = 7.5 Hz, 6H); ^{13}C NMR (100 MHz, $CDCl_3$, ppm) δ 155.1, 151.8, 124.1, 116.6, 113.1, 88.3, 76.4, 71.69, 71.63, 54.1, 22.7 (2C), 10.9, 10.6; HRMS calcd for $C_{14}H_{16}BrIO_2$ 421.9378, found 421.9374.

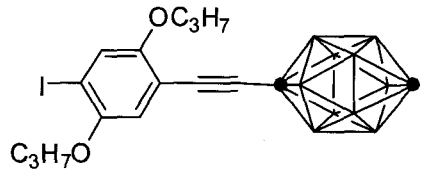

1,4-Bis(propyloxy)-2-iodo-5-(1',12'-dicarba-*closo*-dodecaborane)benzene (16). An oven-dried 50 mL round bottom flask equipped with a magnetic stir bar was charged with *p*-carborane (135 mg, 0.94 mmol) and THF (20 mL). The solution was cooled to -78 °C and *n*-BuLi (0.39 mL, 0.98 mmol, 2.5 M in hexanes) was added dropwise. The solution was allowed to warm to room temperature and stirred for 30 min before it was cooled again to -78 °C. Copper(I) bromide (146 mg, 1.02 mmol) was then added and the mixture was allowed to stir at room temperature for 30 min. A solution of **15** (330 mg, 0.78 mmol) in THF (10 mL) was then added and the resulting mixture was allowed to stir at room temperature for 48 h. A few drops of water were added and the mixture was filtered through a silica gel pad using dichloromethane as the eluent. The resulting greenish solid was purified by column chromatography (silica gel, 20% dichloromethane in hexanes as eluent) to provide 288 mg of **16** as a white powder (76%): mp 96-98 °C; IR (KBr) 2614, 1496, 1486, 1463, 1383, 1212, 1064, 1026, 979 cm^{-1}; ^{1}H NMR (400 MHz, $CDCl_3$, ppm) δ 7.19 (s, 1H), 6.63 (s, 1H), 3.83 (m, 4H), 3.39-1.39 (broad m, 15H), 1.05 (t, J = 7.4 Hz, 6H); ^{13}C NMR (100 MHz, $CDCl_3$, ppm) δ 155.2, 151.8, 124.0, 116.1, 111.8, 90.3, 88.9,

76.0, 71.9, 71.4, 60.18, 60.15, 22.94, 22.85, 11.0, 10.8. HRMS calcd for $C_{16}H_{27}B_{10}IO_2$ 488.1986, found 488.1984.

References and Notes

(1) (a) Soong, R.K.; Bachand, G. D.; Neves, H. P.; Olkhovets, A. G.; Craighead, H. G.; Montemagno, C. D; *Science* **2000**, *290*, 1555. (b) Bachand, G. D.; Soong, R. K.; Neves, H. P.; Olkhovets, A. G.; Craighead, H. G.; Montemagno, C. D. *Nano Lett.* **2001**, *1*, 42.

(2) For examples, see: Balzani, V.; Credi, A.; Venturi, M. *Molecular Devices and Machines: A Journey Into the Nanoworld* 2003, Wiley-Vch, Weinheim.

(3) (a) Shirai, Y.; Morin, J.-F.; Sasaki, T.; Guerrero, J.; Tour, J. M. *Chem. Soc. Rev.* **2006**, 35, 1043-1055. (b) Kay, E. R.; Leigh, D. A.; Zerbetto, F. *Ang. Chem. Int. Ed.* **2006**, *46*, 72-191.

(4) (a) Joachim, C.; Tang, H.; Moresco, F.; Rapenne, G.; Meyer, G. *Nanotechnology* **2002**, *13*, 330. (b) Jimenez-Bueno, G.; Rapenne, G; *Tetrahedron Lett.* **2003**, *44*, 6261. (c) Rapenne, G. *Org. Biomol. Chem.* **2005**, *7*, 1165.

(5) (a) Kwon, K.-Y.; Wong, K. L.; Pawin, G.; Bartels, L.; Stolbov, S.; Rahman, T. S. *Phys. Rev. Lett.* **2005**, 95, 166101/1-166101/4. (b) Wong, K. L.; Pawin, G.; Kwon, K. Y.; Lin, X.; Jiao, T.; Solanki, U.; Fawcett, R. H. J.; Bartels, L.; Stolbov, S.; Rahman, T. S. *Science* **2007**, *315*, 1391-1393.

(6) (a) Shirai, Y.; Osgood, A. J.; Zhao, Y., Kelly, K. F.; Tour, J. M. *Nano Lett.* **2005**, *5*, 2330. (b) Shirai, Y.; Osgood, A. J.; Zhao, Y.; Yao, Y.; Saudan, L.; Yang, H.; Yu-Hung, C.; Sasaki, T.; Morin, J.-F.; Guerrero, J. M.; Kelly, K. F.; Tour, J. T. *J. Am. Chem. Soc.* **2006**, *128*, 4854. (c) Shirai Y.; Morin, J. -F.; Sasaki, T.; Guerrero, J. M.; Tour, J. M. *Chem. Soc. Rev.* **2006**, *35*, 1043.

(7) Morin, J.-F.; Shirai, Y.; Tour, J. M. *Org. Lett.* **2006**, *8*, 1713.

(8) (a) King, R. B. *Chem. Rev.* **2001**, *101*, 1119. (b) Chen, Z.; King, R. B., *Chem. Rev.* **2005**, *105*, 3613.

(9) Valliant, J. F.; Guenter, K. J.; King, A. S.; Morel, P.; Schaffer, P.; Sogbein, O. O.; Stephenson, K. A. *Coord. Chem. Rev.* **2002**, *232*, 173.

(10) Wariishi, K.; Morishima, S.; Inagaki, Y. *Org. Process Res. Dev.* **2003**, *7*, 98.

(11) Dirk, S. M.; Price, D. W.; Chanteau, S.; Kosynkin, D. V.; Tour, J. M. *Tetrahedron* **2001**, *57*, 5109.

(12) (a) Nishikawa, T.; Shibuya, S.; Hosokawa, S.; Isobe, M. *Synlett* **1994**, 485. (b) Kim, S.; Kim, S.; Lee, T.; Ko, H.; Kim, D. *Org. Lett.* **2004**, *6*, 3601.

(13) Hart, H.; Harada, K.; Du, C. J. F. *J. Org. Chem.* **1985**, *50*, 3104.

(14) Tovar, J. D.; Swager, T. *J. Organomet. Chem.* **2002**, *653*, 215.

(15) *Caution: it is known that 1,2-dialkynyl benzene derivatives can decompose or explode violently upon heating.*

(16) Wong, W. -Y.; Lu, G. -L.; Choi, K. -H.; Shi, J. -X. *Macromolecules* **2002**, *35*, 3506.

(17) Weber, E.; Hecker, M.; Koepp, E.; Orlia, W.; Czugler, M.; Csoregh, I. *J. Chem. Soc., Perkin Trans. 2* **1988**, *7*, 1251.

(18) (a) Shirai, Y.; Zhao, Y.; Chen, L.; Tour, J. M. *Org. Lett.* **2004**, *6*, 2129. (b) Zhao, Y.; Shirai,Y.; Slepkov, D. A.; Cheng, L.; Alemany, L. B.; Sasaki, T.; Hegmann, F. A.; Tour, J. M. *Chem. Eur. J.* **2005**, *11*, 3643.

(19) Meier, H.; Ickenroth, D.; Stalmach, U.; Koynov, K.; Bahtiar, A.; Bubeck, C. *Eur. J. Org. Chem.* **2001**, *23*, 4431.

(20) (a) Crisp, G. T.; Bubner, T. P. *Tetrahedron* **1997,** *53*, 11899. (b) Yamaguchi, Y.; Ochi, T.; Miyamura, S.; Tanaka, T.; Kobayashi, S.; Wakamiya, T.; Matsubara, Y.; Yoshida, Z. -I. *J. Am. Chem. Soc.* **2006**, *128*, 4504.

(21) Wakim, S.; Bouchard, J.; Blouin, N.; Michaud, A.; Leclerc, M. *Org. Lett.* **2004**, *6*, 3413.

(22) (a) Dufresne, G.; Bouchard, J.; Belletête, M.; Durocher, G.; Leclerc, M. *Macromolecules* **2000**, *33*, 8252. (b) Setayesh, S.; Marsitzky, D.; Müllen, K. *Macromolecules* **2000**, *33*, 2016. (c) Xia, C.; Advincula, R. C. *Macromolecules* **2001**, *34*, 6922.

(23) Michels, J. J.; O'Connell, M. J.; Taylor, P. N.; Wilson, J. S.; Cacialli, F.; Anderson, H. L. *Chem. Eur. J.* **2003**, *9*, 6167.

(24) Morin, J.–F.; Sasaki, T.; Shirai. Y.; Guerrero J. M.; Tour, J. M. *J. Org. Chem.* **2007**, *72*, 9481-9490.

Supporting Information for Chapter 5.1

Compound 7

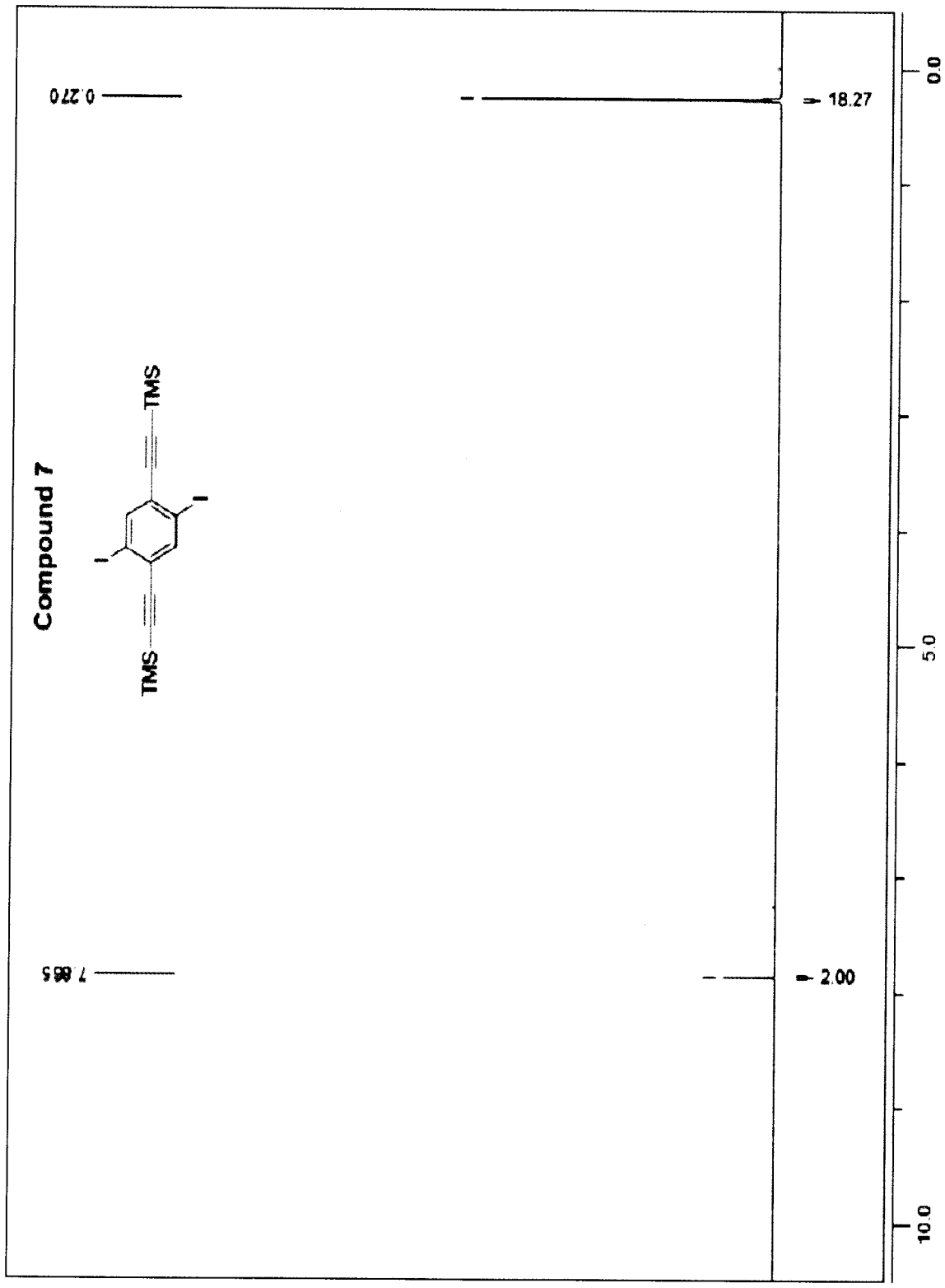

Figure S-5.1-1. ^{1}H NMR Spectrum of Compound **7.**

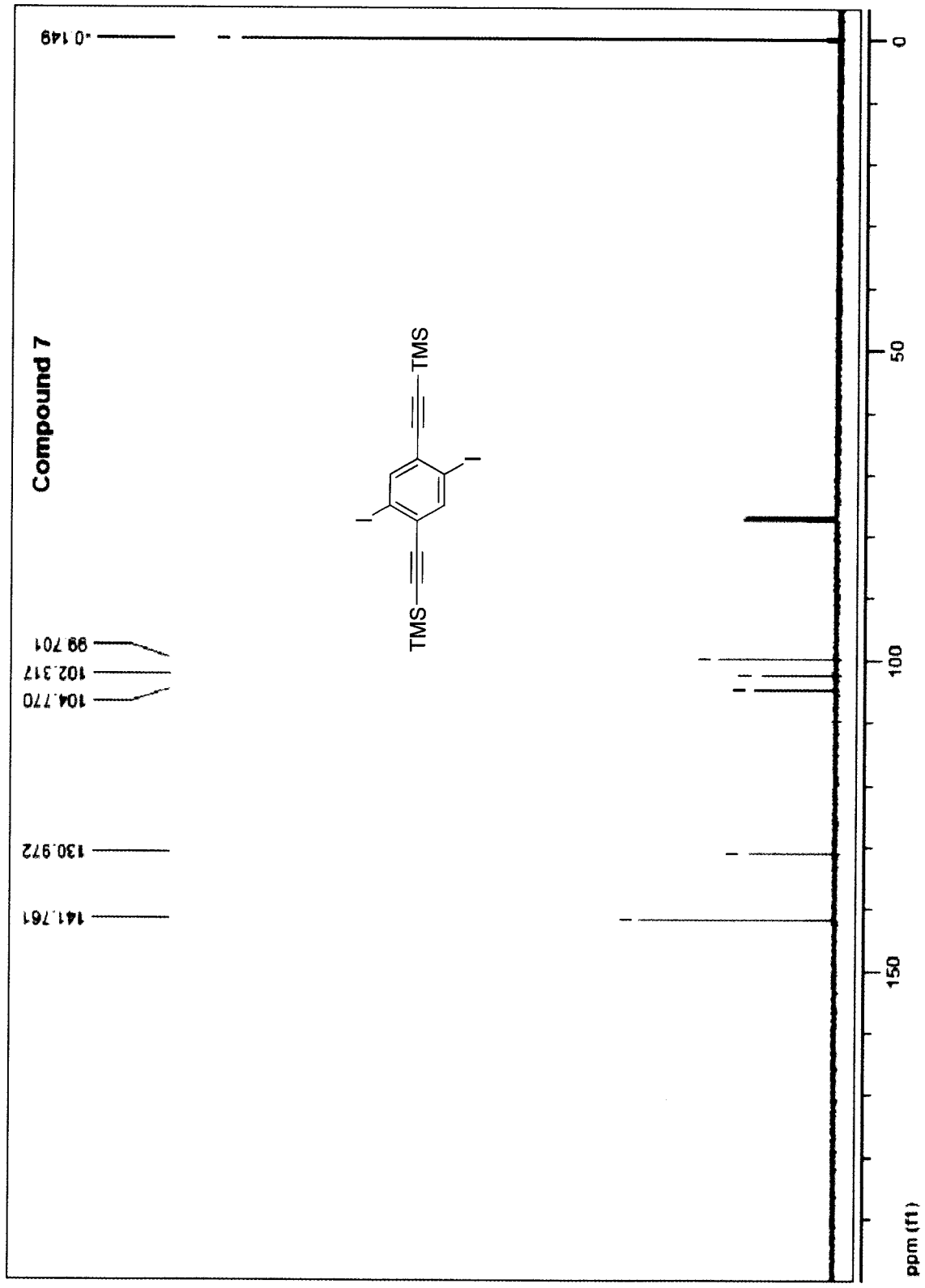

Figure S-5.1-2. ^{13}C NMR Spectrum of Compound **7**.

Compound 15

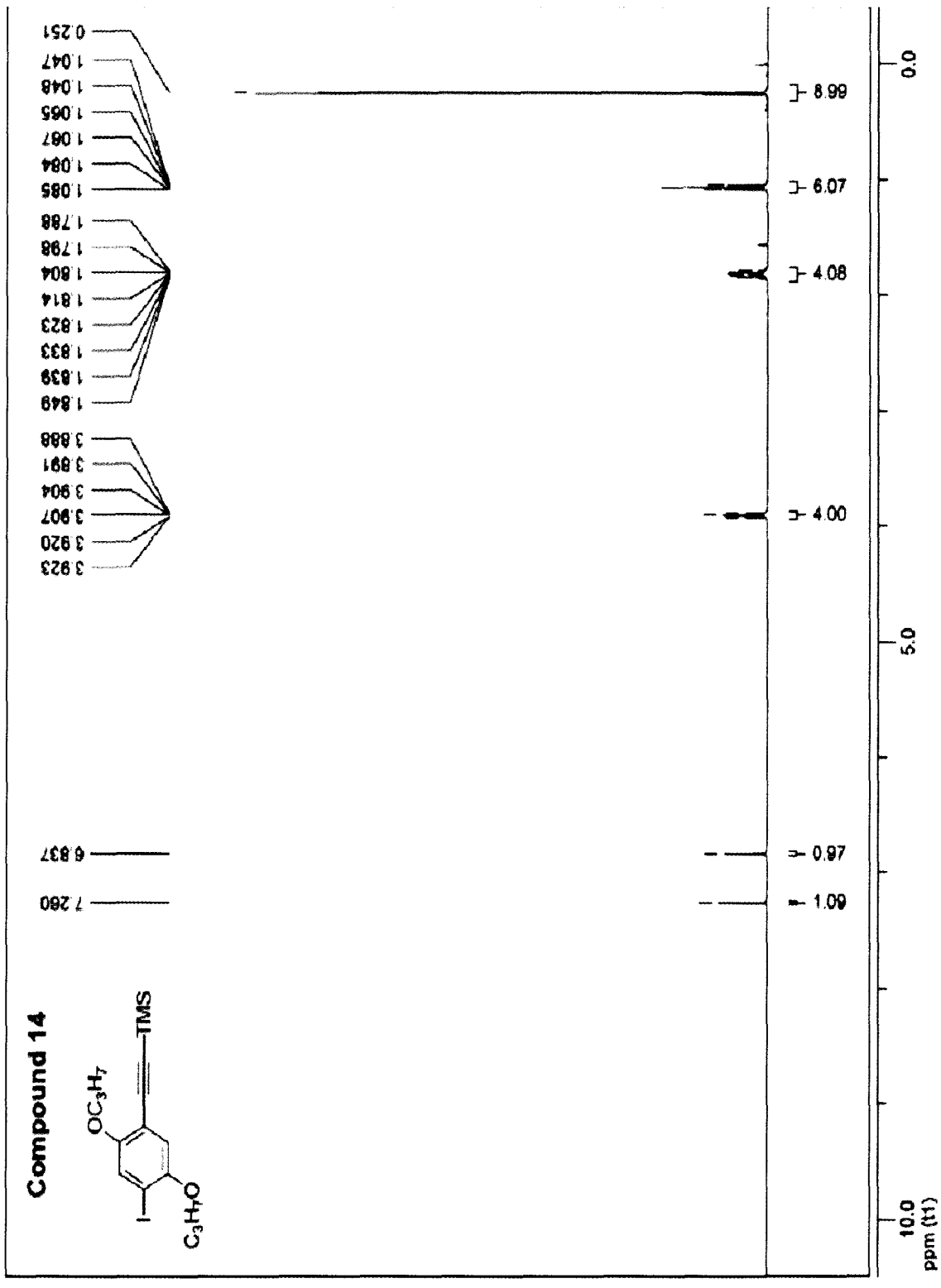

Figure S-5.1-3. ^{1}H NMR Spectrum of Compound **14**.

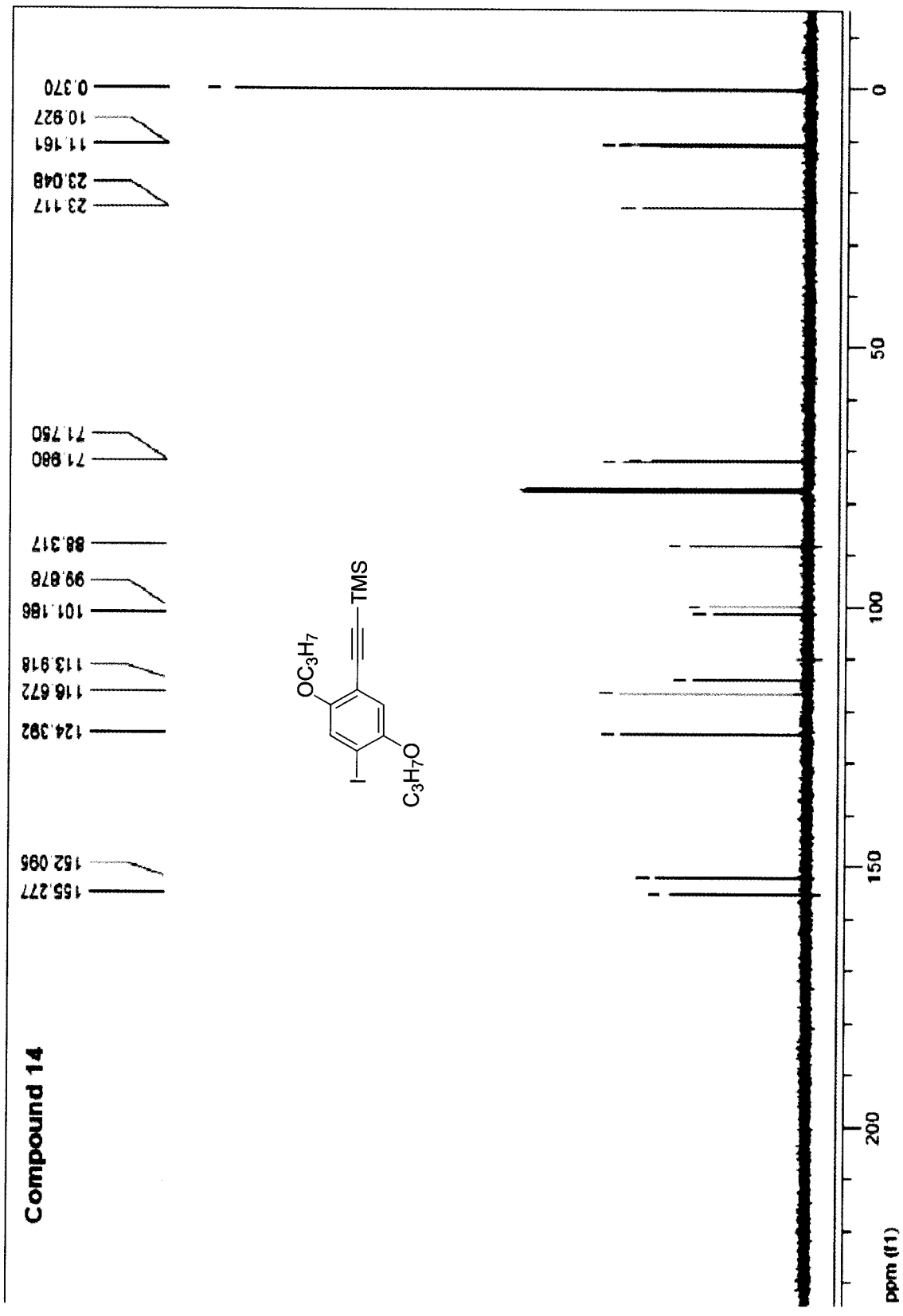

Figure S-5.1-4. ^{13}C NMR Spectrum of Compound **14**.

Compound 15

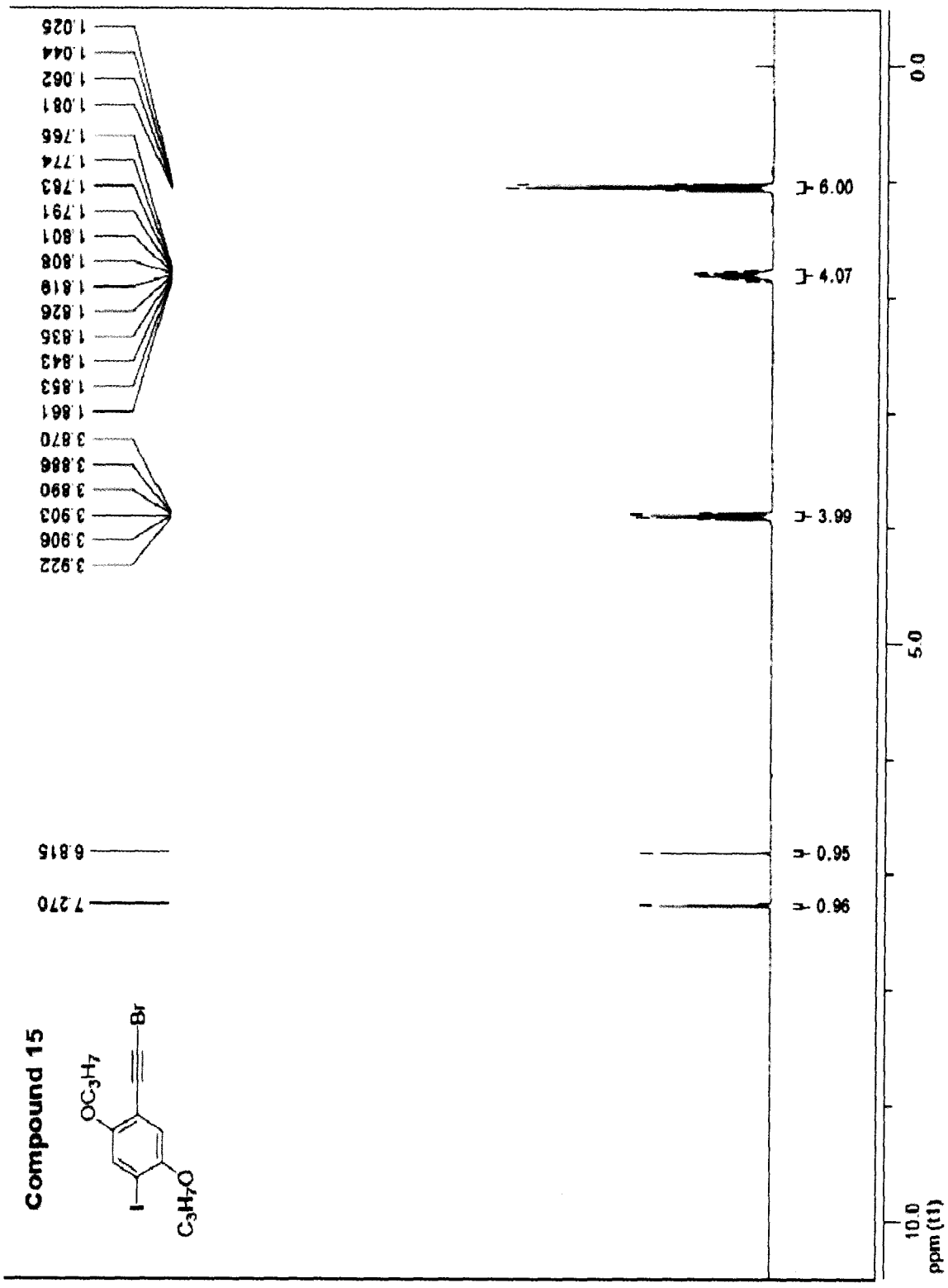

Figure S-5.1-5. ^{1}H NMR Spectrum of Compound **15**.

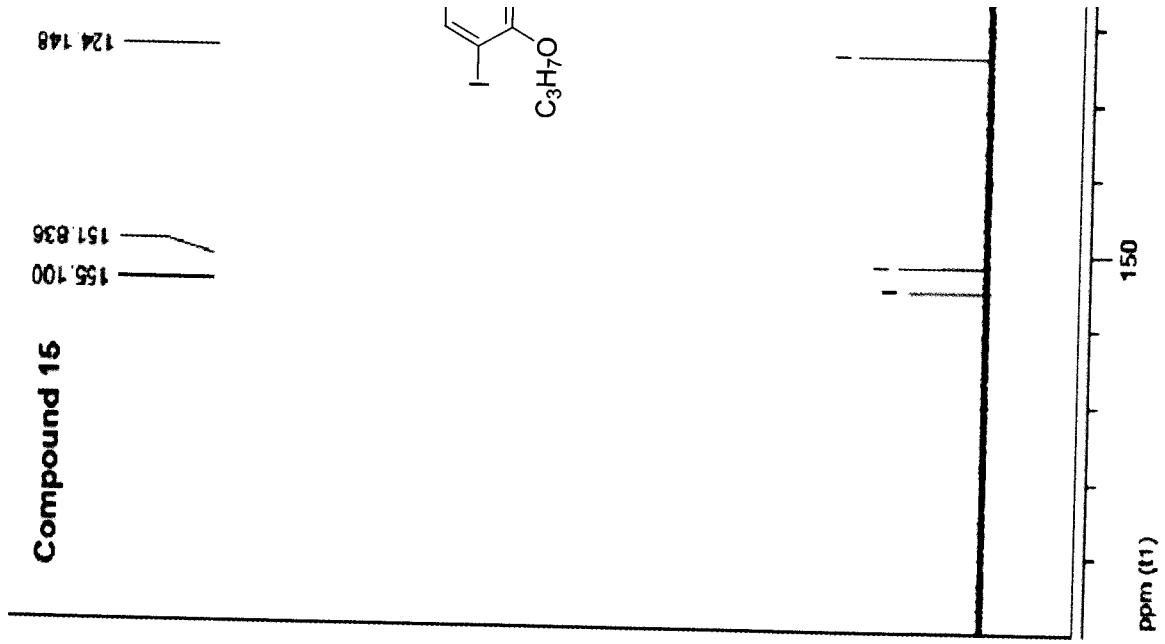

Figure S-5.1-6. ^{13}C NMR Spectrum of Compound **15.**

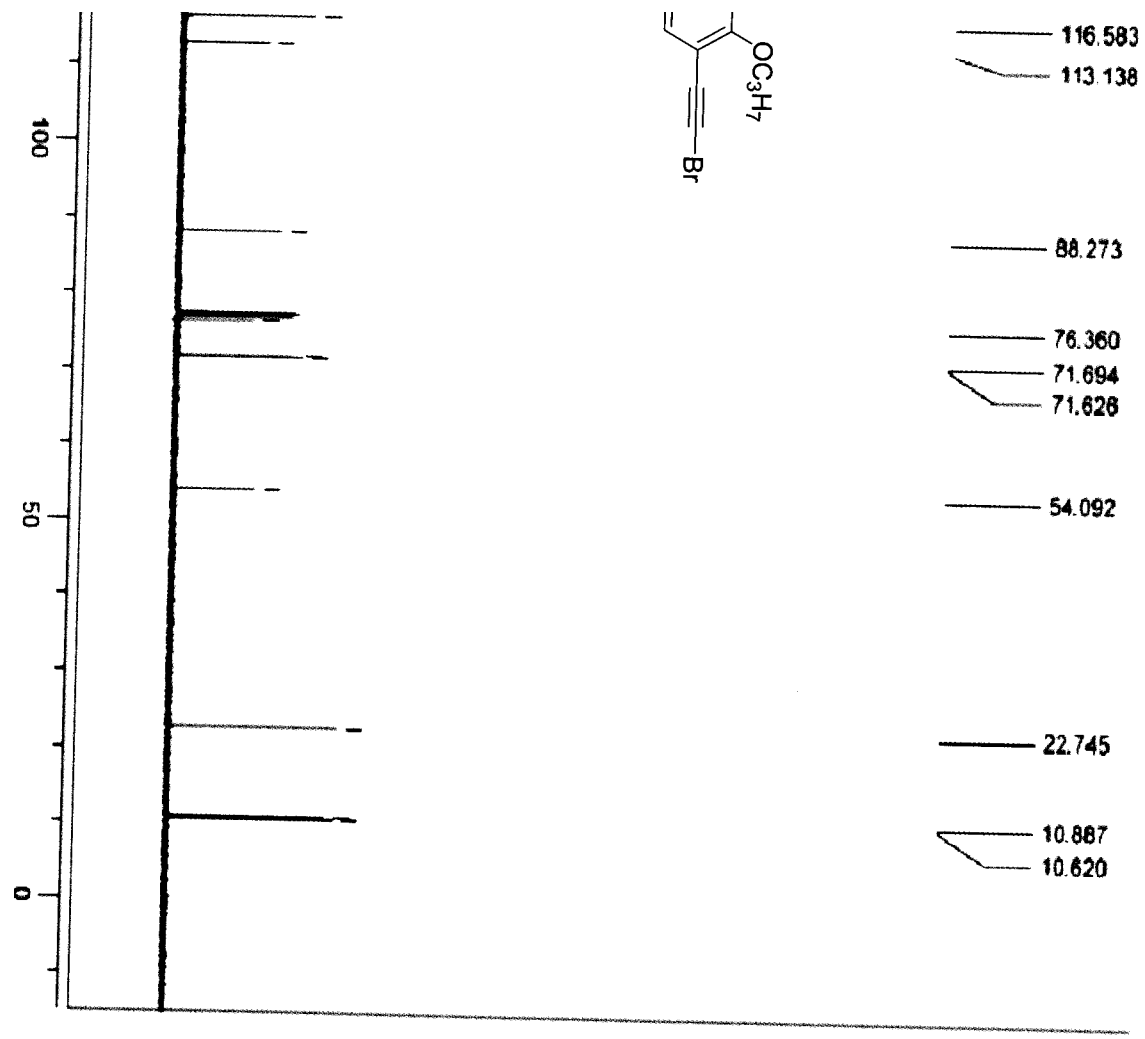
100
50
0
OC3H7
Br
116.583
113.138
88.273
76.360
71.694
71.626
54.092
22.745
10.887
10.620

Compound 16

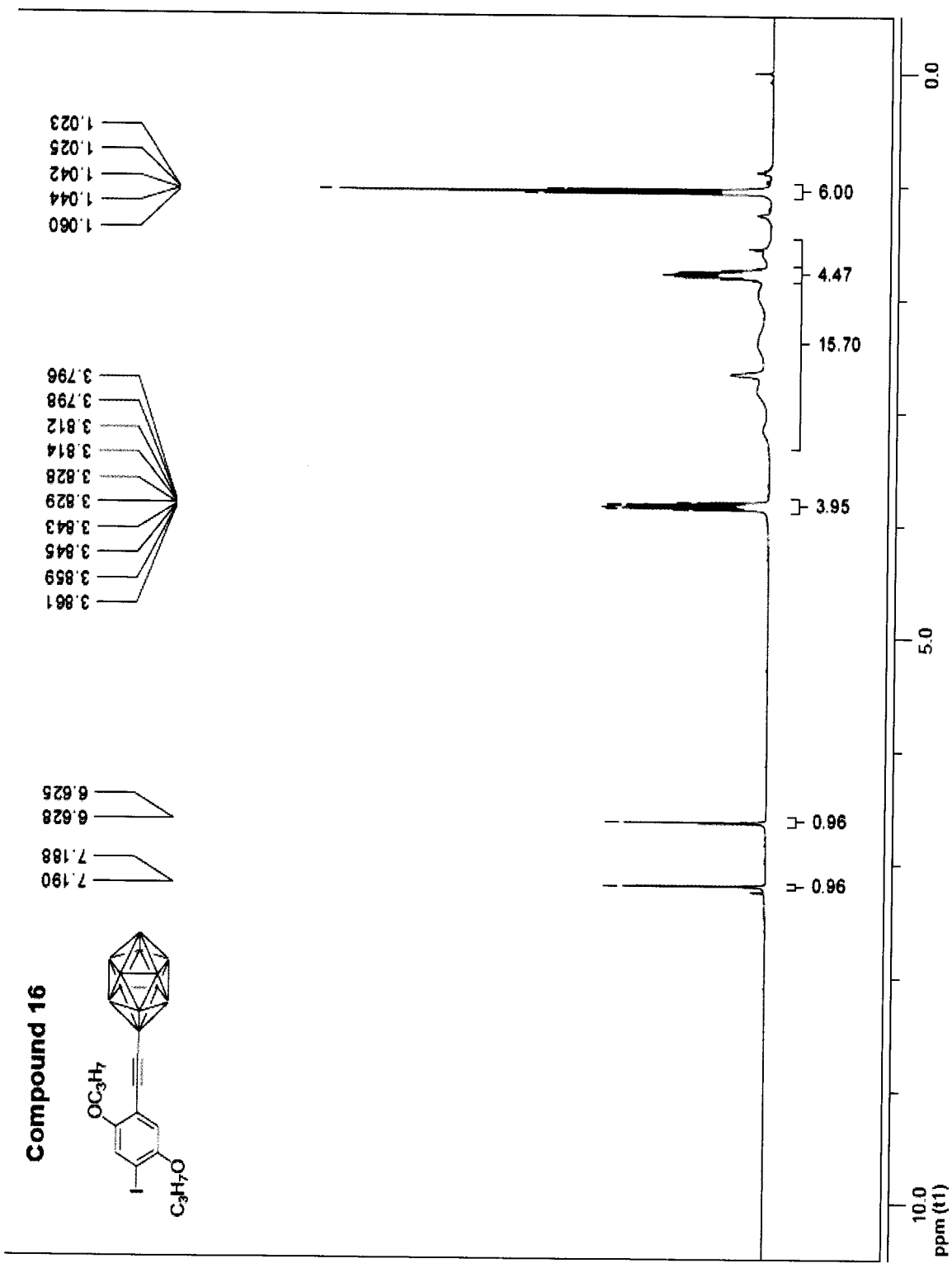

Figure S-5.1-7. ^{1}H NMR Spectrum of Compound **16**.

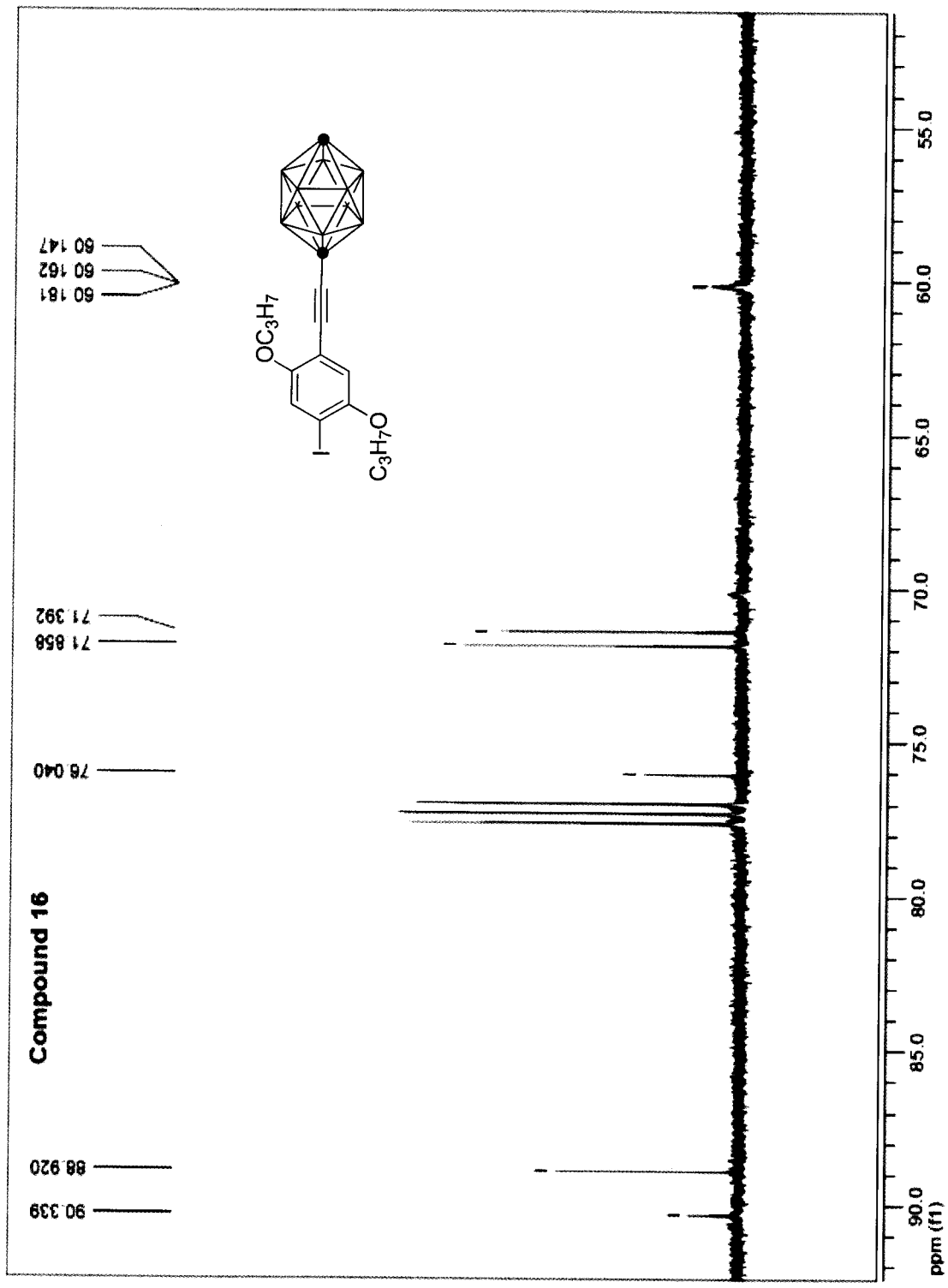

Figure S-5.1-8. ^{13}C NMR Spectrum of Compound **16**.

Chapter 6

Fullerene-Based Nanodevices

6.1

Synthesis and Photoisomerization of Fullerene – and Oligo(phenylene ethynylene) – Azobenzene Derivatives

Introduction

Advances in molecular science continue to facilitate the miniaturization of devices and the innovation of new molecule-based functional devices.[1-5] Of particular interest to our group is the design and synthesis of molecular machines that resemble macroscopic machinery; the ultimate goal of such work is the realization of useful nanomachines constructed using a "bottom-up" approach.[6,7] In the development of such molecular-sized devices and machines, the design scheme is quite different from that in the macroscopic world.[6-8] A strong understanding of both the functionality of molecular building blocks and the specific interactions between them is essential in the construction of devices and machines at the molecular scale.[9-11] Because the number of potential molecular building blocks continues to increase, we have focused on those that contain functionality such as electro- and photoactive components. The understanding of the interaction between these components has been gradually advanced.[12-14] In our previous study of the construction of a light-powered molecular vehicle, or a "motorized nanocar," we found that the motor unit was inoperative in the presence of fullerenes.[15] The result implied that rapid intramolecular energy transfer to the fullerene moiety quenched the photoexcited state of the motor moiety. Similar quenching of a photoexcited state with fullerenes have been reported.[16]

On the other hand, among the several photoisomerization processes studied previously, *cis-trans* photoisomerization of azobenzene chromophores have been extensively examined since their discovery in the late 1930s,[17] and widely used, even to the present, in photo responsive systems and devices.[18-21] The advantage of using

azobenzenes is based on the large geometrical change accompanying *cis-trans* isomerization and their photo-stability, enabling the development of variety of photo-responsive functional devices such as smart polymers,[18] liquid crystals,[19] and molecular switches[20] and machines.[21] Recently, a hybrid of the azobenzene chromophore and fullerene was reported as a dendrimer having a fullerene in its core, and photoisomerization of the azobenzene moiety was briefly demonstrated.[22] The unique combination of the two functional groups, azobenzene chromophores and fullerenes, may lead to advances in the field of molecular switching because of the novel functional synergy.[23-25] However, no report on the properties of such hybrid materials has been published except for the brief communication on the dendritic fullerene derivatives.[22] In particular, the effect of the fullerene moiety on the photoisomerization behavior of the azobenzene has been overlooked. In the present work it has been found that the presence of the fullerene can strongly affect the photoisomerization behavior of azobenzenes, and in some cases, quench photo excitation of azobenzenes so that no photoisomerization occurs. This is in concert with findings in our previous work on the light-powered molecular motor[15] and other's stilbene-fullerene derivatives.[16]

It has also been found that oligo(phenylene ethynylene)s (OPE)s attached to an azobenzene moiety have a strong impact on its photoisomerization behavior. OPEs are an important class of organic building blocks for molecular device scientists because their shape-persistent nature and the relatively simple synthetic access facilitate the design and construction of devices with well-defined order.[26-30] Recently, the combination of the shape-persistent nature of OPEs and large geometrical changes of the azobenzene

photoisomerization was used to generate dendrimers in which a large photo-modulation of hydrodynamic volumes was achieved.[31]

Here we report the effect of fullerenes and OPEs on the photoisomerization behavior of azobenzene moieties using a variety of fullerene-azobenzene hybrid molecules and azobenzene derivatives (Figure 1) designed for UV-vis and NMR spectroscopic studies. The *cis-trans* photo isomerization of azobenzenes in the presence of fullerenes and OPEs only proceeds under certain conditions, and these conditions are delineated here.

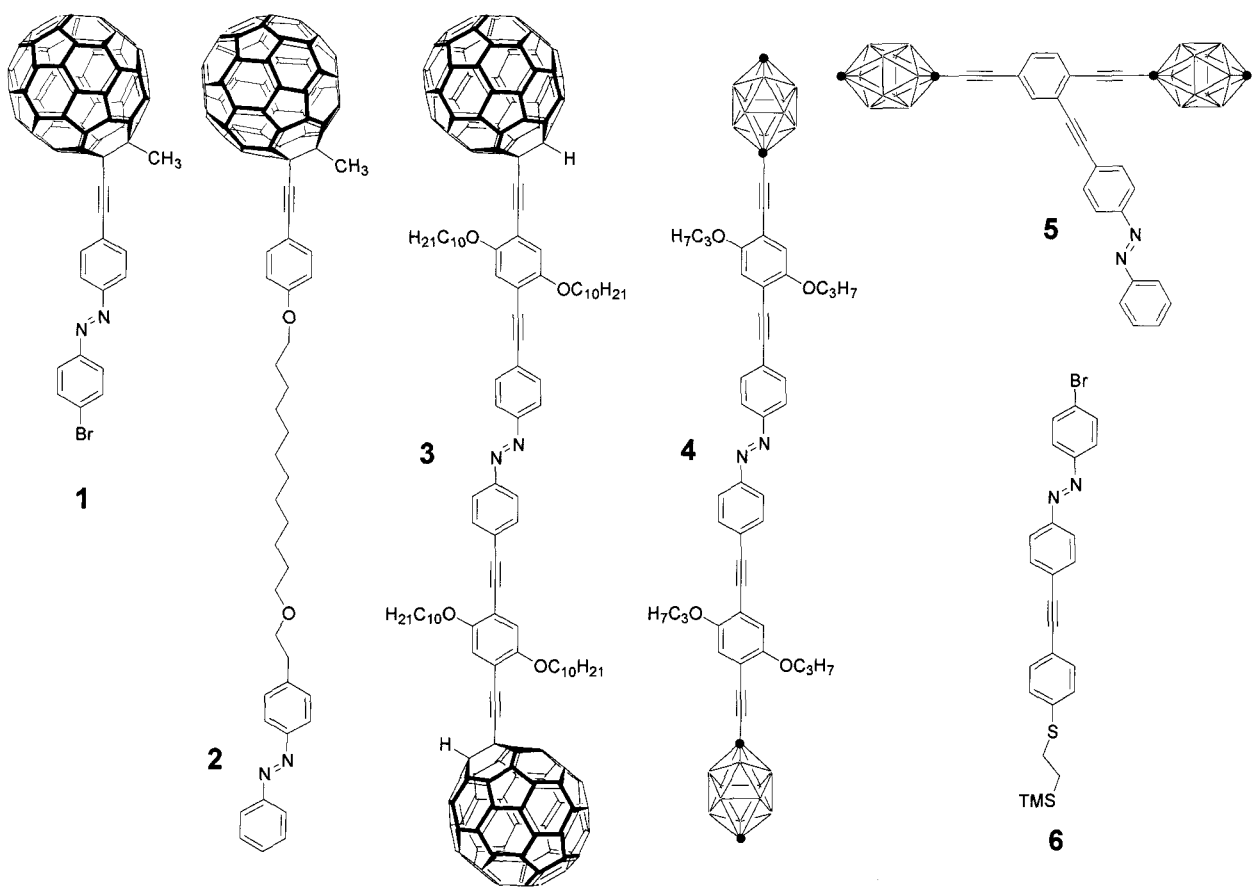

Figure 1. Fullerene-azobenzene hybrid and OPE-conjugated azobenzenes studied in this work. Compound **4** contains *p*-carborane termini where the two darkened vertices are C and CH, *ipso* and *para*, respectively, and all other vertices are BH.

Result and Discussion

Synthesis and testing of molecules **1**, **2**, and **6** was done by Y. Shirai. Molecules **3** and **4** were synthesized and tested by T. Sasaki. My research was the synthesis and testing of the carborane axle-functionalized **5** as well as the intermediates for **2** (Figure 1). Energy transfer between the fullerene and azobenzene moieties occurs via intra- or intermolecular interactions, or a combination of both. We examined intermolecular interactions between pristine C_{60} and simple diiodo-azobenene **17**[32] using NMR spectroscopy. Intramolecular interactions between the functionalities were studied in two different cases, wherein the separation of the two functional groups was small, as in **1**, or large, as in **2**. The effect due to the presence of multiple fullerenes was examined with **3**. Finally, the effect due to the presence of OPEs was examined with structures **4-6**).

Design and synthesis of azobenzene derivatives. (a) Fullerene-azobenzene hybrids. The details of the syntheses of fullerene-azobenzene hybrids **1-3** are given in Schemes 1-3. The structures were designed and synthesized to produce two extreme cases: where the fullerene and azobenzene moieties are close together as in structure **1**, and where they are farther apart as in structure **2**. The difullerene derivative **3** was also synthesized to determine the effects of multiple fullerenes. In Scheme 1, the azobenzene derivative **7**[33] was coupled with trimethylsilylacetylene (TMSA) to afford compound **8**,

and then it was attached to the fullerene via the in-situ ethynylation method[34] to afford **1**. For the isolation of the fullerene and the azobenzene moieties in **2**, we used a dodecyl alkyl chain for ease of synthesis and to produce a large isolation distance. Thus, in Scheme 2, **10**[33,35] was alkylated with dibromododecane using sodium hydride in DMF, and then the 4-iodophenol was alkylated to afford compound **12**. After the Pd-catalyzed coupling reaction with TMSA and the removal of the TMS group in TBAF, fullerene was attached using the in-situ ethynylation method[34] to obtain the product **2** in 49% yield. In Scheme 3, the difullerene-azobenzene hybrid **3** was synthesized in a similar manner. The diiodo-azobenzene (**14**) was coupled with compound **15**,[34,36] and then the fullerenes were attached via the in-situ ethynylation method.[34]

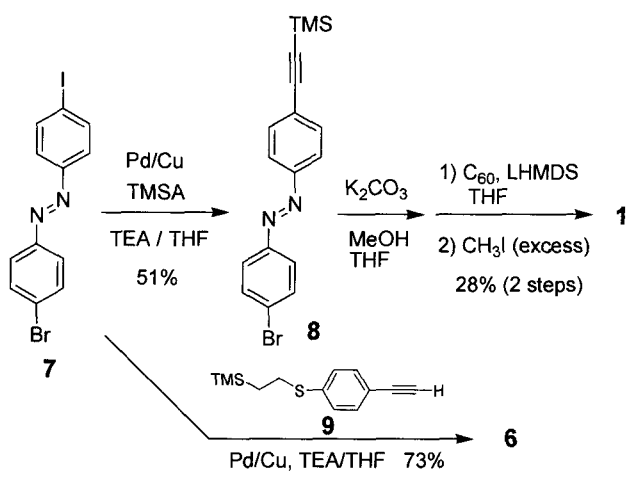

Scheme 1. Synthesis of the azobenzene derivatives **1** and **6.** Pd/Cu = $PdCl_2(PPh_3)_2$, CuI.

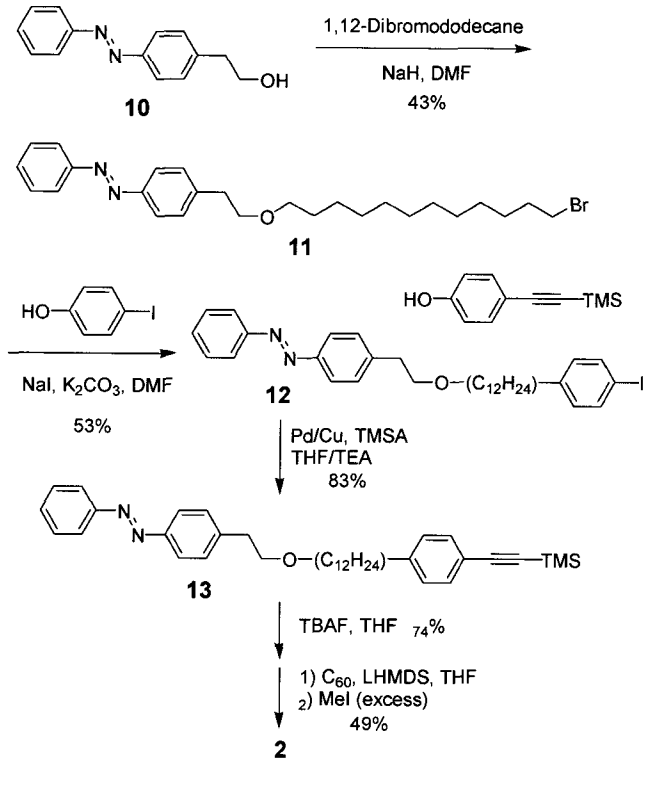

Scheme 2. Synthesis of the fullerene-azobenzene hybrid **2**. Pd/Cu = $PdCl_2(PPh_3)_2$, CuI.

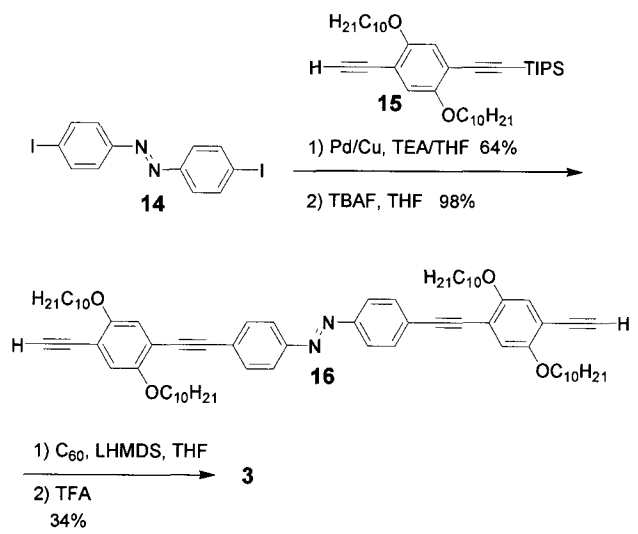

Scheme 3. Synthesis of the fullerene-azobenzene hybrid **3**. Pd/Cu = $PdCl_2(PPh_3)_2$, CuI.

(b) Azobenzene derivatives with conjugated OPEs. Addition of functional groups to the azobenzene moiety has various effects; it was thought that in addition to fullerenes, OPEs might also strongly affect their photoisomerization behavior. Because there are only a few reports on azobenzene-OPE conjugates[31-33] and there is no report on the photoisomerization yield of these azobenzene derivatives, it was decided to investigate this class of compounds. Schemes 4 and 5 outline the syntheses of the mono (**5**)- and di (**4**)-OPE substituted azobenzene derivatives. Another mono-OPE substituted azobenzene **6** was also prepared as an example of an OPE-azobenzene conjugate without carboranes (Scheme 1). The carboranes have no effect on the photoisomerization behavior of azobenzenes, and they were attached for other purposes in the later study of this class of compounds. It was found in previous work that the carborane will not interfere with the photoexcited state of a stilbene-like derivative, a molecular motor unit.[15] In Scheme 4, **19** was synthesized from 1,4-bis(propyloxy)-2,5-diiodobenzene (**17**)[37] by the Pd-catalyzed coupling reaction with TMSA followed by the in situ desilyl bromination.[38,39] The bromoalkyne **19** was then coupled with the *p*-carborane-copper adduct to afford the *p*-carborane-containing moiety **20**. The coupling reaction with **19** proceeded slowly and 48 h were necessary for the reaction to be completed. This can be attributed to the electron-donating nature of the propyloxy groups present on the aryl ring that partially deactivate the alkynyl bromide toward oxidative addition by the organocopper reagent. Compound **20** was then coupled to **21**[40] to give the final product **4** in good yield. The mono-OPE substituted azobenzene **5** (Scheme 5) was synthesized in three steps from the iodo-azobenzene **22**.[33] Following the Pd-catalyzed coupling reaction

with TMSA and the removal of the TMS group with TBAF, the dicarborane unit **25**[15] was coupled to afford the product **5**.

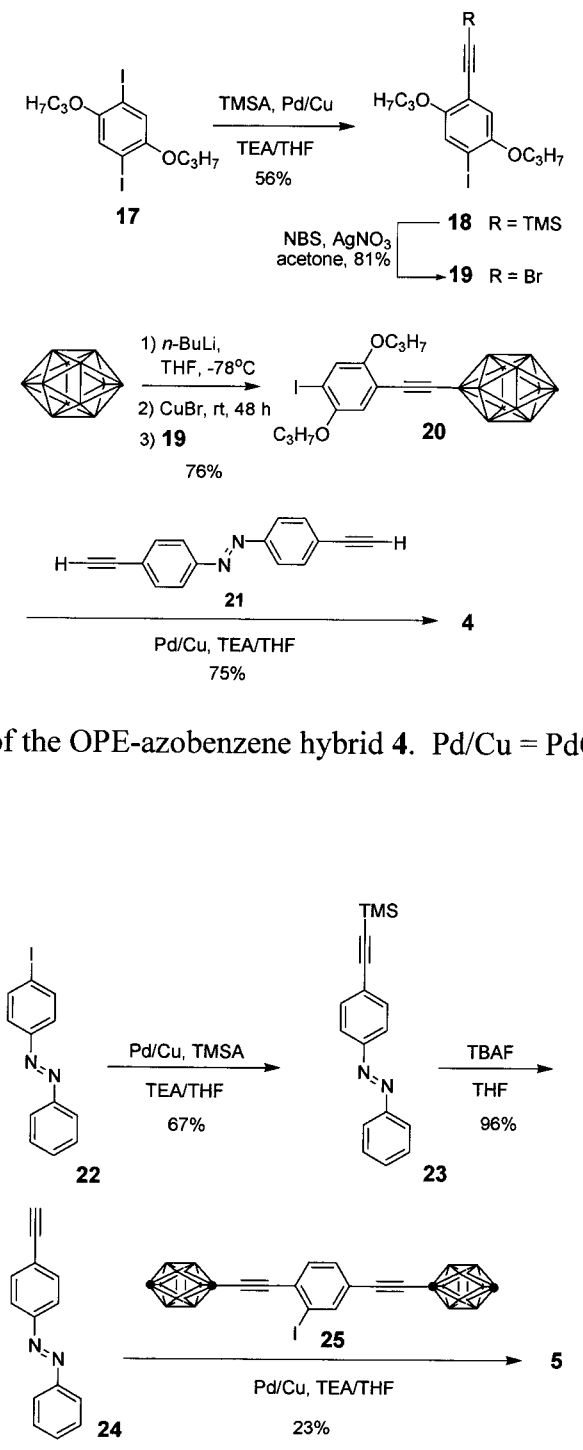

Scheme 4. Synthesis of the OPE-azobenzene hybrid **4**. Pd/Cu = $PdCl_2(PPh_3)_2$, CuI.

Scheme 5. Synthesis of the OPE-azobenzene hybrid **5**. Reagents: Pd/Cu = $PdCl_2(PPh_3)_2$, CuI.

Intermolecular energy transfer between C_{60} and azobenzenes. Intermolecular interactions between pristine C_{60} and the diiodo-azobenene **14** were studied using NMR spectroscopy (Figure 2). The interaction was monitored using three different mixtures; 1:1 molar mixture of C_{60} and **14**, 1:9 molar mixture, and **14** without C_{60}. Upon irradiation of these samples in a NMR tube with 365 nm light, the intensity of new peaks corresponding to the *cis* isomer of **14** increased with a concomitant decrease in the *trans* isomer peaks. Within 10 min of irradiation, a photo stationary state (PSS) was achieved in all three cases (Figure 2 inset). Almost complete conversation from *trans* to *cis* isomer was achieved without C_{60}, while the conversion was decreased severely when even a small amount of C_{60} was present. The relaxation process from the *cis* to *trans* isomer in dark conditions at room temperature was also monitored following the same NMR peaks. It is clear from Figure 2 that C_{60} has a dramatic impact both on the photoisomerization yield and the rate of the thermal relaxation process. The increase in the rate of conversion from the *cis* to *trans* isomer implies that the C_{60} catalyzes that isomerization. Catalytic activity of electron acceptors such as tetrachloroquinone on thermal isomerization of azobenzenes has been previously shown.[41] The decrease in the photoisomerization yield implies that the photo excited singlet state of the azobenzene moiety is quenched by fullerenes via intermolecular electronic energy transfer. With the excitation at 365 nm, the pristine C_{60} should also be excited along with azobenzenes. In the diffusion limited bimolecular process, however, only triplet-triplet energy transfer can take place because

of the very short lifetime of the fullerene singlet excited state. The triplet-excited energy level of the fullerenes (~35 kcal/mol)[42,43] is higher than that of the *cis* azobenzene derivatives (~29 kcal/mol) and comparable to that of the *trans* azobenzene derivatives (~35 kcal/mol).[44] Therefore, fullerenes could act as a triplet sensitizer rather than a quencher in the presence of the *cis* azobenzene derivatives. In fact, such bimolecular photo-induced energy transfer processes between pristine or functionalized fullerenes and many other compounds has been well studied.[42] It is also known that, in the triplet excited state, azobenzene derivatives favor *trans* isomers.[45-48] Therefore, as a quencher or a triplet sensitizer, fullerenes will always shift the isomerization equilibrium of azobenzenes at the PSS to the *trans* isomers. Because the bimolecular reaction can be diffusion limited, the intermolecular interactions should be suppressed under more diluted conditions. This was confirmed by the UV-vis spectroscopic study of the 1:1 molar mixture of **14** and C_{60} at 17 μM for both compounds, which is 100 times less concentrated than that of the NMR study. In this case, no decrease in the photoisomerization yield and no significant change in the rate of the thermal isomerization were observed over the time periods used in the former NMR study.

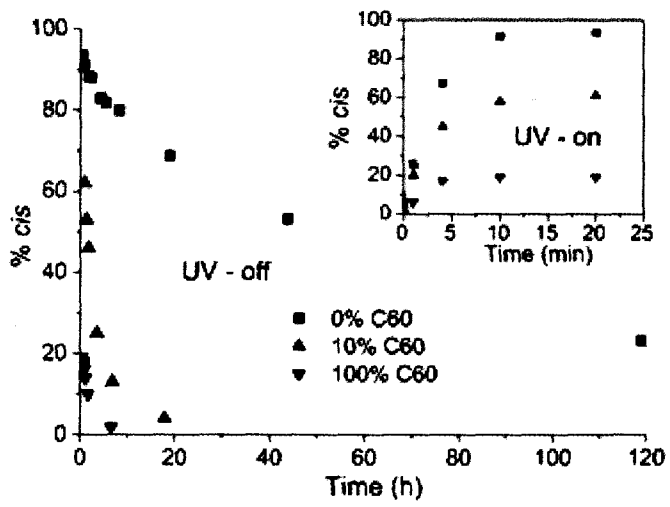

Figure 2. Changes in the amount of *cis* isomer of **14** in mixtures of **14** and C_{60} at three different ratios (1:1 (100% C_{60}) and 9:1 (10% C_{60}) molar ratios, and no C_{60} (0% C_{60})) in the dark after establishing a photo-stationary state using 365 nm light. Inset: *trans* to *cis* conversion in the same sample solutions during irradiation with light at 365 nm.

Intramolecular energy transfer in the fullerene-azobenzene hybrid. Photo-excited properties of fullerenes including both pristine C_{60} and functionalized fullerenes are generally known for their low-lying excited electronic levels (~1.7 eV for singlet and ~1.5 eV for triplet).[42,43] These electronic levels are smaller than that of the lowest excited state S_1 of azobenzene derivatives (~2.9 eV).[44] An exothermic energy transfer from the excited azobenzene to the covalently linked fullerene in the fullerene-azobenzene hybrid can be expected. We investigated such intramolecular energy transfer process using **1** and **2** (Figure 1). In **1**, the two functional moieties are isolated by a single triple bond, and one sp^3-hybridized carbon atom isolates the fullerene π system from the azobenzene moiety. However, there is experimental evidence suggesting that there is a weak electronic interaction called periconjugation[49] between the fullerene and attached moieties, thus **1** can be treated as an example of weakly conjugated fullerene-azobenzene hybrid. On the other hand, in **2**, the long saturated carbon chain between the azobenzene and the fullerene moieties should disrupt electronic communication between the two functional groups. These analyses can be experimentally supported by observing the electronic absorption spectra of the each functional moiety (Figures 3 and 4). In **1**, the electronic transition (Figure 3, red line) is different from the sum of original features of both functional groups (Figure 3, blue line), while the electronic transition of **2** (Figure 4, red

line) remains unchanged from the sum of each component (Figure 4, blue line). These results suggest that there is no electronic communication in the isolated fullerene-azobenzene hybrid **2** and there is a strong interaction in the conjugated fullerene-azobenzene hybrid **1**.

Upon irradiation of each solution (17 μM) at 365 nm (Figure 3) or 334 nm (Figure 4), the azobenzene moiety underwent photoisomerization from *trans* to *cis* with a characteristic decrease in the 320-370 nm band. However, the change in the absorption (Δabs) of **1** was extremely small. This may indicate an efficient electronic energy transfer between the azobenzene and fullerene moieties, as predicted from its conjugated structure. From the Δabs of **1** (0.03) and **8** (0.33) in Figure 3, the photoisomerization yield of **1** is estimated to be about 10% of that of **8** (no fullerene moiety). On the other hand, from the Δabs of **2** (0.025) and **13** (0.07) in Figure 4, the photoisomerization yield for **2** was about 35% of **13** (no fullerene moiety). The 1:1 molar mixture of the pristine C_{60} and the compounds without a fullerene moiety (**8** and **13**) showed no decrease in the photoisomerization yield (blue lines in the Figure 3 and 4), indicating that there is no significant intermolecular effect at the studied conditions. Although the length of separation between the two functional moieties in 2 is 3 nm when displayed as drawn in Figure 1, the actual distance is likely much closer in solution due to the flexibility of the alkyl chain. The decrease in the photoisomerization yield for **2** was much smaller than that of the conjugated azobenzene-fullerene hybrid **1**. The result clearly indicates that the isolation of the two functional groups has some effect. Nevertheless, the physical separation of the π-systems has a marked effect on the isomerization of the azobenzene.

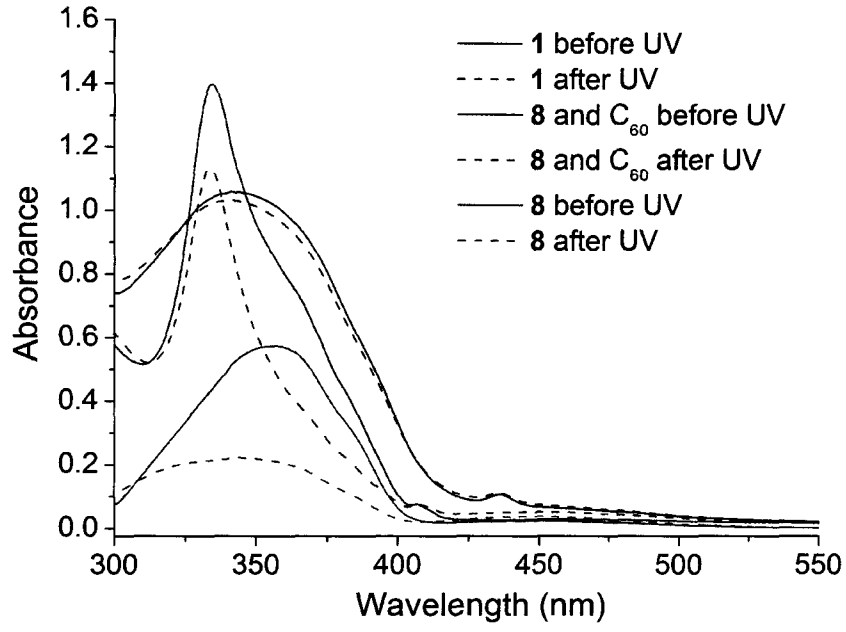

Figure 3. Absorption spectra of **1**, **8**, and 1:1 mixture of **8** and C_{60} (chloroform, ~17 μM). Upon irradiation with 365 nm light for 10 min, the electronic transitions at ~357 nm were decreased in all cases and the PSS was achieved (change in abs. at 357 nm: 0.05 (**1**), 0.33 (**8**), 0.33 (mixture of **8** and C_{60})). Due to the electronic communication between the fullerene and azobenzene moieties, the absorption spectrum of **1** (red line) is significantly different from the sum of the spectrum for **8** and C_{60} (blue line).

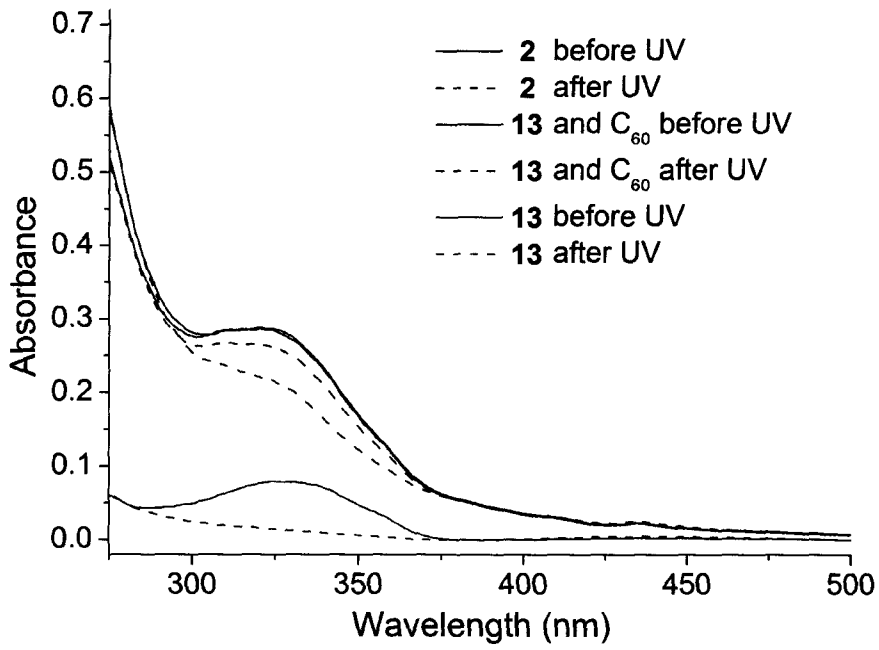

Figure 4. Absorption spectra of **2**, **13**, and 1:1 mixture of **13** and C_{60} (chloroform, ~4 μM). Upon the irradiation with 334 nm light for 5 min, the electronic transitions at ~330nm were decreased in all cases and the PSS was achieved (change in abs. at 330 nm: 0.025 (**2**), 0.07 (**13**), 0.07 (mixture of **13** and C_{60})). Absorption spectrum of **2** (red line) is almost identical to the sum of the spectrum for **13** and C_{60} (blue line), suggesting the no electronic communication between the two functional groups.

Effect of the conjugated OPEs attached to azobenzene moiety. Finally, we examined the effect of OPEs on the photoisomerization behavior of azobenzene chromophores. Because of the shape-persistent nature of OPEs and their simplicity of design and synthesis, many molecular devices and machines use OPEs in the molecular framework.[26-30] However, not many examples of the azobenzene derivatives incorporated into OPEs have been reported,[31-33] and there is no report on the effect of OPEs on the photoisomerization yield of azobenzene derivatives. The photoisomerization yield for

each OPE-azobenzene derivative **4-6** was determined using NMR, and the results are summarized in Table 1. In this work, the following trend was observed: as the number of OPEs attached to the azobenzene moiety was increased, a significant decrease in the photoisomerization yield at the PSS was observed. Thus, when only one OPE was attached to the azobenzene (**5** and **6**), the photoisomerization yield was reduced to ~50% of that of the azobenzene derivative without any OPEs (**8**), while the yield was further reduced to less than 25% when two OPEs were attached as in **4**. The other noticeable feature of the disubstituted azobenzene **4** was the red shift of the azobenzene absorption band due to the elongated conjugation along the OPE backbone (see Figure S-1 in the Supporting Information for the UV-vis spectrum of **4**). Visible light at ~ 436 nm was necessary to achieve the highest conversion to *cis* isomer in this case. As expected from the other fullerene-azobenzene hybrids, the difullerene and OPE substituted derivative **3** showed no photoisomerization. Because **4**, which is similar to **3** but with carboranes instead of fullerenes, showed a small but noticeable photoisomerization yield, the data suggests the severe deactivation of **3** is due, in large part, to the presence of the two fullerene moieties.

Table 1. Photoisomerization Yield at the PSS for Various Azobenzene Derivatives

Type	Compound	% *cis*	Excitation wavelength (nm)
Fullerene Azobenzene	**14**	> 90[a]	365

mixtures	**14** + C_{60} (10%)	58[a]	365
	14 + C_{60} (100%)	19[a]	365
Fullerene-azobenzene conjugated hybrid	**1**	< 10[b]	365
	8	> 90[a,b]	365
Fullerene-azobenzene isolated hybrid	**2**	~35[b]	334
	13	> 90[b]	334
Difullerene-azobenzene hybrid	**3**	~ 0[a,b]	365
Azobenzene-OPE hybrid	**4**	22[a]	436
	5	48[a]	365
	6	46[a]	365

[a] Photoisomerization yield was determined by NMR. [b]Photoisomerization yield was estimated by UV-vis.[50-52]

Conclusion

It has been shown that fullerenes and OPEs have a large effect on the photoisomerization behavior of azobenzene derivatives (Figure 1). Fullerenes can severely reduce the photoisomerization yield for *cis* isomers, while OPEs directly attached to the azobenzenes have a noticeable but smaller effect. These trends have not been previously considered for fullerene- and OPE-azobenzene derivatives but were clearly detected in this work using NMR and UV-vis spectroscopies. Fullerenes, OPEs, and azobenzenes are examples common molecular device building blocks; however,

when they are combined together to form more complex systems, the present work underscores that their synergistic effects must be considered.

Experimental Section

General Methods. All reactions were performed under an atmosphere of nitrogen unless stated otherwise. Precursors **7**,[33] **9**,[53] **10**,[33,35] **14**,[32] **15**,[34,36] **17**,[37] **18-20**,[54] **21**,[40] **22**[33] and **25**[15] were prepared according to literature procedures. Compounds **1- 4**, **6**, **11-13**, were prepared as described by Y. Shirai and co-workers.[55] Reagent grade diethyl ether and THF were distilled from sodium benzophenone ketyl. Triethylamine (TEA) and CH_2Cl_2 were distilled over CaH_2. Fullerene (99.5+% pure) was purchased from MTR Ltd. and used as received. LHMDS (1 M solution in THF) and TBAF (1 M solution in THF) were obtained from Sigma-Aldrich and used as received. Flash column chromatography was performed using 230-400 mesh silica gel from EM Science. Thin layer chromatography was performed using glass plates pre-coated with silica gel 40 F_{254} purchased from EM Science. Melting points were uncorrected. The ultrasonicated fullerene slurry in THF was prepared in general ultrasonic cleaners.

NMR and UV-vis spectroscopy irradiation experiments were performed in deoxygenated solutions at ~1.7 mM (NMR) or 4~17 μM (UV-vis) using a 100 W Hg arc light source (EFOS Acticure A4000 UV Light Source/Curing System) with appropriate wavelength Hg line filters (Andover) and band-pass filters. The light intensity after passing through the filters was monitored with a radiant power meter (Oriel). Typical light intensity for NMR experiments was 10~50 mW/cm^2, and up-to 10 mW/cm^2 for UV-

vis experiments. The rate of the thermal isomerization for all experiments was slow enough to allow the determination of the photoisomerization yields at the PSS without significant change using normal NMR and UV-vis operations (measured within 1~3 min after reaching the PSS). In all experiments, reversibility of the photoisomerization process was checked by irradiating the sample solutions with appropriate wavelength cut-on long-pass filters or by keeping the samples in the dark to induce *cis-trans* reverse isomerization. *ChemDraw* 9.0 was used in naming the compounds.

General Procedure for the Coupling of a Terminal Alkyne with an Aryl Halide Using a Palladium-Catalyzed Cross-Coupling (Sonogashira) Protocol. To an oven-dried round bottom flask equipped with a magnetic stir bar were added the aryl halide, the terminal alkyne, $PdCl_2(PPh_3)_2$ (ca. 2 mol% per aryl halide), and CuI (ca. 4 mol% per aryl halide). A solvent system of TEA and/or THF was added depending on the substrates. Upon completion, the reaction was quenched with a saturated solution of NH_4Cl. The organic layer was then diluted with hexanes, diethyl ether or CH_2Cl_2, and washed with water or saturated NH_4Cl (1×). The combined aqueous layers were extracted with hexanes, diethyl ether, or CH_2Cl_2 (2×). The combined organic layers were dried over $MgSO_4$, filtered, and the solvent was removed from the filtrate in vacuo to afford the crude product, which was purified by column chromatography (silica gel). Eluents and other slight modifications are described below for each compound.

General Procedure for the Addition of C_{60} to Terminal Alkynes Using LHMDS, in situ ethynylation method. To an oven-dried round bottom flask equipped with a magnetic stir bar was added the terminal alkyne and C_{60} (2 equiv per terminal alkyne H). After adding THF, the mixture was sonicated for at least 3 h. To the greenish-

brown suspension formed after the sonication was added LHMDS dropwise at room temperature over 0.5 to 1.5 h. As the reaction progressed, the mixture turned into a deep greenish-black solution. During the addition of the LHMDS, small aliquots from the reaction were extracted and quenched with trifluoroacetic acid (TFA), dried, and re-dissolved in CS_2 for TLC analysis (developed in a mixture of CS_2, CH_2Cl_2 and hexanes). Completion of the reaction was confirmed by the disappearance of the starting materials. The reaction was usually complete within 1.5 h from the beginning of the LHMDS addition. Upon completion, the reaction was quenched with TFA or MeI to give a brownish slurry. When MeI was used, the reaction was stirred at room temperature for at least 6 h. Excess TFA or MeI and solvent were then removed in vacuo to afford a crude product that was purified by flash column chromatography (silica gel). Eluents and other slight modifications are described in the following experiments for each compound. Compounds **1-4** and **6** were prepared as described by Shirai and co-workers.[55]

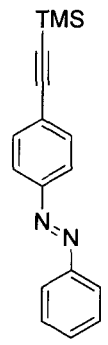

(E)-1-Phenyl-2-(4-((trimethylsilyl)ethynyl)phenyl)diazene (23). See the general procedure for the Pd/Cu coupling reaction. The materials used were **22** (0.2 g, 0.65 mmol), TMSA (0.28 mL, 1.95 mmol), $PdCl_2(PPh_3)_2$ (0.005 g, 0.006 mmol), CuI (0.0025 g, 0.012 mmol), TEA (0.8 mL), and THF (9 mL) at room temperature for 20 min. The dark brown solid was purified by flash column chromatography with 5% CH_2Cl_2 in

hexanes to give product **23** (0.12 g, 67%) as an orange powder. FTIR (KBr) 3057, 2962, 2898, 2154, 1594, 1492, 1250, 1223, 1152, 866, 843, 762, 588, 588 cm-1; ^{1}H NMR (400 MHz) δ 7.91 (dd, J_1 = 8.0 Hz, J_2 = 1.6 Hz, 2H), 7.86 (d, J = 8.8 Hz, 2H), 7.60 (d, J = 8.8 Hz, 2H), 7.49 (m, 3H), 0.27 (s, 9H); ^{13}C NMR ($CDCl_3$, 100 MHz) δ 152.9, 152.2, 133.1, 131.6, 129.4, 126.1, 123.3, 123.1, 104.9, 97.3, 0.27; EI-HRMS m/z calcd for $C_{17}H_{18}N_2Si$ 278.1239, found 278.1244.

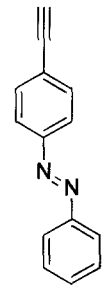

(E)-1-(4-Ethynylphenyl)-2-phenyldiazene (24). To a round-bottom flask equipped with a magnetic stirrer were added compound **23** (0.12 g, 0.43 mmol), THF (5 mL), and TBAF (0.8 mL, 0.8 mmol). The reaction mixture was stirred at room temperature for 20 min, then quenched with water and diluted with CH_2Cl_2. The aqueous layer was extracted with CH_2Cl_2 (×3). Combined organic layers were dried over $MgSO_4$, filtered, and concentrated under vacuum. Crude material was purified by flash column with 10% CH2Cl2 in hexanes to afford deprotected product **24** (0.086 g, 96%) as an orange-red solid. FTIR (KBr) 3290, 3260, 3196, 2924, 2564, 1515, 1493, 1483, 1265, 1154, 843 cm-1; ^{1}H NMR (CDCl3, 400 MHz) δ 7.93–7.87 (m, 4H), 7.63 (d, J = 8.4 Hz, 2H), 7.54–7.48(m, 3H), 3.22 (s, 1H); ^{13}C NMR ($CDCl_3$, 100 MHz) δ 152.6, 152.2, 133.0, 131.4, 129.2, 124.7, 123.0, 122.9, 83.3, 79.5; EI-HRMS m/z calcd for $C_{14}H_{10}N_2$ 206.0844, found 206.0842.

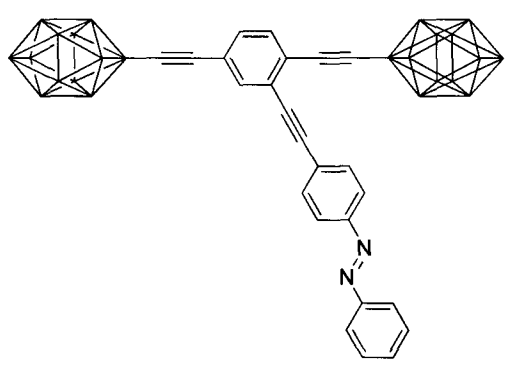

Compound 5. See the general procedure for the Pd/Cu coupling reaction. The materials used were 24 (0.054 g, 0.26 mmol), 25 (0.140 g, 0.26 mmol), $PdCl_2(PPh_3)_2$ (0.007 g, 0.0104 mmol), CuI (0.004 g, 0.0208 mmol), TEA (0.3 mL), and THF (3.7 mL) at room temperature overnight. The residue was purified by flash column chromatography with 10% CH_2Cl_2 in hexanes to give product 5 (0.037 g, 23%) as a red-orange oil. FTIR (KBr) 3066, 2919, 2849, 2610, 1605, 1497, 1057, 845, 758 cm^{-1}; ^1H NMR (500 MHz, $CDCl_3$) δ 7.98 (m, 4H), 7.71 (d, J = 9.0 Hz, 2H), 7.56 –7.50 (m, 3H), 7.46 (dd, J = 1.5, 0.5 Hz, 1H), 7.25 (dd, J = 8.0, 0.5 Hz, 1H), 7.16 (dd, J = 8.0, 1.5 Hz, 1H), 3.0 –1.9 (broad m, 22H); ^{13}C NMR (125 MHz, $CDCl_3$) δ 152.6, 152.1, 135.1, 132.6, 132.1, 131.3,131.1, 129.1, 126.2, 125.2, 124.0, 122.97, 122.96, 122.0, 94.0, 91.2, 88.7, 87.9, 77.8, 77.6, 69.3, 69.0, 60.4 (×2); EI-HRMS *m/z* calcd for $C_{28}H_{34}B_{20}N_2$ 615.4713, found 615.4708.

References and Notes

(1) Tour, J. M. *Molecular Electronics: Commercial Insights, Chemistry, Devices, Architecture and Programming*; World Scientific: River Edge, NJ, 2003.

(2). *Nanoelectronics and Information Technology: Advanced Electronic Materials and Novel Devices Information Technology*; Waser, R., Ed.; Wiley-VCH: Weinheim, 2003.

(3) Timp, G. L. *Nanotechnology*; AIP Press: Springer: New York, 1999.

(4) Joachim, C.; Gimzewski, J. K.; Aviram, A. *Nature* **2000**, *408*, 541–548.

(5) Forrest, S. R. *Nature* **2004**, *428*, 911–918.

(6) Shirai, Y.; Morin, J. -F.; Sasaki, T.; Guerrero, J. M.; Tour, J. M. *Chem. Soc. Rev.* **2006**, *35*, 1043-1055.

(7) Kay, E. R.; Leigh, D. A.; Zerbetto, F. *Angew. Chem., Int. Ed.* **2007**, *46*, 72-191.

(8) Porto, M.; Urbakh, M.; Klafter, J. *Phys. Rev. Lett.*, **2000**, *84*, 6058–6061

(9) Balzani, V.; Credi, A.; Venturi, M. *Molecular Devices and Machines – A Journey into the Nano World*; Wiley-VCH: Weinheim, 2004.

(10) Feringa, B. E. *Molecular Switches*; Wiley-VCH: Weinheim, 2001.

(11) Kelly, T. R. *Topics in Current Chemistry 262*; Springer: Heidelberg, 2005.

(12) *Stimulating Concepts in Chemistry*; Shibaski, M.; Stoddart, J. F.; Vogtle, F. Eds.; Wiley-VCH: Weinheim, 2000.

(13) Raymo, F. M.; Tomasulo, M. *Chem. Soc. Rev.* **2005**, *34*, 327-336.

(14) Browne, W. R.; O'Boyle, N. M.; McGarvey, J. J.; Vos, J. G. *Chem. Soc. Rev.* **2005**, *34*, 641-663.

(15) Morin, J.; Shirai, Y.; Tour, J. M. *Org. Lett.* **2006**, *8*, 1713-1716.

(16) Schuster, D. I.; Nuber, B.; Vail, S. A.; ManMahon, S.; Lin, C.; Wilson, S. R.; Khong, A. *Photochem. Photobiol. Sci.* **2003**, *2*, 315-321.

(17) Hartley, G. S. *Nature* **1937**, *140*, 281–282.

(18) Shimoboji, T.; Larenas, E.; Fowler, T.; Kulkarni, S.; Hoffman, A. S.; Stayton, P. S. *Proc. Natl. Acad. Sci. USA* **2002**, *99*, 16592-16596.

(19) Yu Y.; Nakano, M.; Ikeda, T. *Nature* **2003**, *425*, 145–156.

(20) Yasuda, S.; Nakamura, T.; Matsumoto, M.; Shigekawa, H. *J. Am. Chem. Soc.* **2003**, *125*, 16430-16433.

(21) Ichimura, K.; Oh, S. -K.; Nakagawa, M. *Science* **2000**, *288*, 1624-1626.

(22) Kay, K.-Y.; Han, K.-J.; Yu, Y.-J.; Park, Y. D. *Tetrahedron Lett.* **2002**, *43*, 5053-5056.

(23) Prato, M. *Top. Curr. Chem.* **1999**, *199*, 173-187.

(24) Konishi, T.; Ikeda, A.; Shinkai, S. *Tetrahedron* **2005**, *61*, 4881-4899.

(25) Segura, J. L.; Martín, N.; Guldi, D. M. *Chem. Soc. Rev.* **2005**, *34*, 31-47.

(26) Bunz, U. H. F. *Chem. Rev.* **2000**, *100*, 1605-1644.

(27) Schwab, P. F. H.; Levin, M. D.; Michl, J. *Chem. Rev.* **1999**, *99*, 1863-1933.

(28) Shirai, Y.; Osgood, A. J.; Zhao, Y.; Kelly, K. F.; Tour, J. M. *Nano Lett.* **2005**, *5*, 2330-2334.

(29) Shirai, Y.; Osgood, A. J.; Zhao, Y.; Yao, Y.; Saudan, L.; Yang, H.; Yu-Hung, C.; Sasaki, T.; Morin, J.-F.; Guerrero, J. M. *J. Am. Chem. Soc.* **2006**, *128*, 4854-4864.

(30) Tour, J. M.; Rawlett, A. M.; Kozaki, M.; Yao, Y.; Jagessar, R. C.; Dirk, S. M.; Price, D. W.; Reed, M. A.; Zhou, C.-W.; Chen, J. *Chem. Eur. J.* **2001**, *7*, 5118-5134.

(31) Liao, L.-X.; Stellacci, F.; McGrath, D. V. *J. Am. Chem. Soc.* **2004**, *126*, 2181-2185.

(32) Flatt, A. K.; Dirk, S. M.; Henderson, J. C.; Shen, D. E.; Su, J.; Reed, M. A.; Tour, J. M. *Tetrahedron* **2003**, *59*, 8555-8570.

(33) Yu, B.-C.; Shirai, Y.; Tour, J. M. *Tetrahedron* **2006**, *62*, 10303-10310.

(34) Shirai, Y.; Zhao, Y.; Cheng, L.; Tour, J. M. *Org. Lett.* **2004**, *6*, 2129-2132.

(35) Ueno, A.; Takahashi, K.; Anzai, J.-I.; Osa, T. *Bull. Chem. Soc. Jpn.* **1980**, *53*, 1988-1992.

(36) Zhao, Y.; Shirai, Y.; Slepkov, A. D.; Cheng, L.; Alemany, L. B.; Sasaki, T.; Hegmann, F. A.; Tour, J. M. *Chem.-Eur. J.* **2005**, *11*, 3643-3658.

(37) Meier, H.; Ickenroth, D.; Stalmach, U.; Koynov, K.; Bahtiar, A.; Bubeck, C. *Eur. J. Org. Chem.* **2001**, 4431-4444.

(38) Nishikawa, T.; Shibuya, S.; Hosokawa, S.; Isobe, M. *Synlett* **1994**, 485-486.

(39) Kim, S.; Kim, S.; Lee, T.; Ko, H.; Kim, D. *Org. Lett.* **2004**, *6*, 3601-3604.

(40) Grebel-Koehler, D.; Liu, D. J.; De Feyter, S.; Enkelmann, V.; Weil, T.; Engels, C.; Samyn, C.; Mu¨llen, K.; De Schryver, F. C. *Macromolecules* **2003**, *36*, 578-590.

(41) Schulte-Frohlinde, D *Ann.* **1957**, *612*, 131-138.

(42) *Fullerenes: From Synthesis to Optoelectronic Properties*; Guldi, D. M., Martin, N., Eds.; Kluwer Academic Publishers: Dordrecht, The Netherlands, 2002.

(43) Guldi, D. M.; Prato, M. *Acc. Chem. Res.* **2000**, *33*, 695-703.

(44) Åstrand, P. -O.; Ramanujam, P. S.; Hvilsted, S.; Bak, K. L.; Sauer, S. P. A. *J. Am. Chem. Soc.* **2000**, *122*, 3482-3487 and references therein.

(45) Fischer, E. *J. Am. Chem. Soc.* **1968**, *90*, 796-797.

(46) Yamamura, T.; Momotake, A.; Arai, T. *Tetrahedron. Lett.* **2004**, *45*, 9219-9223.

(47) Jones, L. B.; Hammond, G. S. *J. Am. Chem. Soc.* **1965**, *87*, 4219-4220.

(48) Bortolus, P.; Monti, S. *J. Phys. Chem.* **1979**, *83*, 648-652.

(49) Hamasaki, R.; Ito, M.; Lamrani, M.; Mitsuishi, M.; Miyashita, T.; Yamamoto, Y. *J. Mater. Chem.* **2003**, *13*, 21-26 and references therein.

(50) Change in absorption (Δabs.) for the main absorption band of the *trans* isomer (π,π^*) transition band (λ_{max} ~ 330-400 nm) reflects the minimum concentration of *cis* isomer at the photostationary state; see 51 and 52.

(51) King, N. R.; Whale, E. A.; Davis, F. J.; Gilbert A.; Mitchell, G. R. *J. Mater. Chem.* **1997**, *7*, 625-630.

(52) Brode, W. R.; Gould, J. H.; Wyman, G. M. *J. Am. Chem. Soc.* **1952**, *74*, 4641-4646.

(53) Yu, C. J.; Chong, Y.; Kayyem, J. F.; Gozin, M. *J. Org. Chem.* **1999**, *64*, 2070-2079.

(54) Morin, J. –F.; Sasaki, T.; Shirai. Y.; Guerrero J. M.; Tour, J. M. *J. Org. Chem.* **2007**, *72*, 9481-9490.

(55) Shirai. Y.; Sasaki, T.; Guerrero, J. M.; Yu B. -Y.; Hodge, P.; Tour, J, M. *ACS Nano* **2008**, *2*, 97-106.

6.2

Fullerene Terminated Molecular Wires

Introduction

Our approaches to molecular electronics using oligo(phenylene ethynylene) OPE devices[1-4] have gained considerable attention since the successful demonstration of switching effects using this class of compounds.[5-7] To further advance the development of OPE based devices for molecular electronic applications, we have investigated fullerene-OPE hybrid devices (Figure 1). These fullerene-terminated molecular wires with thiol and protected thiol alligator clips can be easily prepared using our in situ ethynylation method[8] (Scheme 1-6). Moreover, this class of fullerene-derivatized OPEs is unique in that one can expect periconjugation[9,10] effects due to the close proximity between the fullerene cage and the OPE π systems. Fullerenes have gained considerable attention since their discovery due to their unusual structure and optical and electrical properties, and there has been a tremendous amount of research aimed at developing new fullerene-based materials with novel and potentially useful applications.[11,12] The combination of self-assembled monolayer (SAM) formation[13] with the advantageous properties of fullerene derivatives could lead to advances in this field.[14,15] To that end, we have demonstrated the self-assembly of fullerene-OPE hybrid devices on Au surfaces, and delineated the specific mechanisms associated with self-assembly of fullerene-OPE hybrids.[16] Here we expand the series of fullerene-terminated molecular wires by introducing a variety of functional groups, and describe their electronic properties with the aid of theoretical calculations. Ultraviolet photoelectron spectroscopy (UPS) and inverse photoemission spectroscopy (IPES) studies were also done to further examine the electronic properties of the fullerene-terminated OPEson gold surfaces.

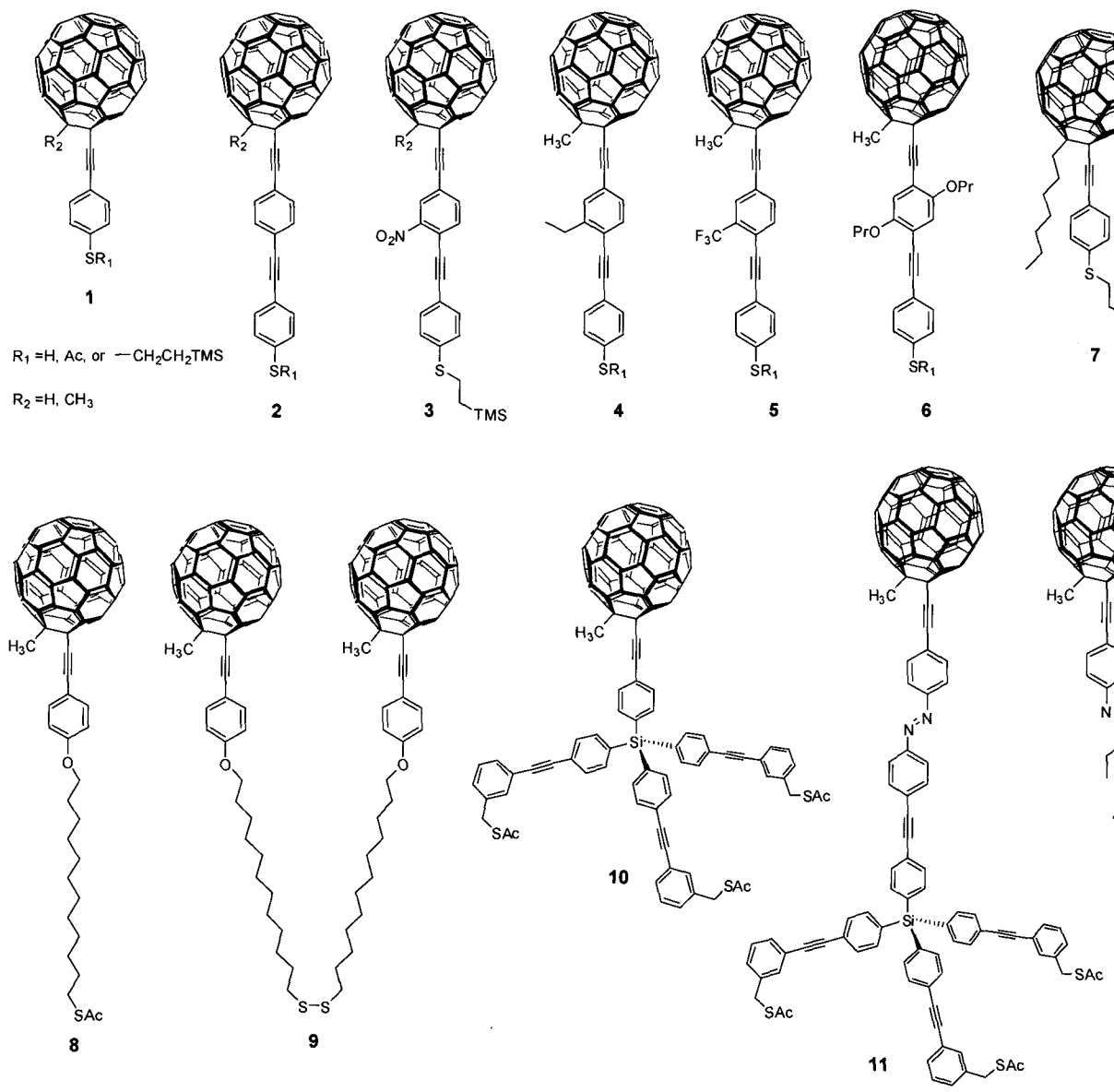

Figure 1. Fullerene-terminated molecular wires presented in this work.

Results and Discussion

Synthesis of fullerene-terminated OPEs 1 and 7.Compounds **1**, **2** and **7-12** were prepared by Y. Shirai. Compound **5** was prepared by T. Sasaki. Compound **6** was prepared by G. Vives. My research consisted of the preparation of compounds **3** and **4** as well as intermediates for **5** and **6**. The fullerene-OPE hybrids **1** and **7** can be synthesized in a single step from the known compound **13**[17] using the in situ ethynylation method[8]

with moderate yields (Scheme 1). The ethyl-TMS group (–CH_2CH_2TMS) was employed as the protecting group for the sulfur atom because it can tolerate the in situ ethynylation reaction using lithium hexamethyldisylazide (LHMDS). Once the fullerene moiety is attached, the ethyl-TMS protecting group can be easily removed using tetrabutylammonium fluoride (TBAF) in THF (**1-Me-SH**) or converted to the acetyl group (**1-Me-SAc**) using $AgBF_4$ and acetyl chloride (AcCl).[18] The in situ deprotection and self-assembly of the ethyl-TMS protected derivatives have been shown previously,[19] however, in our hands, it was difficult to obtain consistent assembly results.[20] We also found in our previous work that the thiol esters (-SAc) were more convenient and reliable.[16] The functional group attached on the fullerene cage can be modified in the ethynylation step by quenching the fullerene anions with the appropriate alkyl iodide or a proton. In the synthesis of **7**, 1-iodoheptane was used to introduce a bulky group at the fullerene site to reduce the cross-sectional mismatch that was one of the causes for the head-to-tail assemblies in fullerene SAMs.[16] Unfortunately, this synthesis approach proved to be difficult, with a low yield presumably because of the lower reactivity of the 1-iodoheptane toward the fullerene anions.

Synthesis of fullerene-terminated OPEs 2-6. A series of fullerene-terminated molecular wires **2-6** were synthesized via Pd-catalyzed coupling reactions and removal of the TMS groups followed by the fullerene coupling reaction (Scheme 2). With this synthesis scheme, simple modification of the functional groups in the compound **14** can result in the rapid generation of the wide variety of the fullerene-terminated molecular wires. We have previously demonstrated the combinatorial synthesis of OPE tetramers on a solid support.[21] In this work, we were able to synthesize –H (neutral), –Et (electron

rich), $-CF_3$ (electron deficient), –OMe (electron rich), and $-NO_2$ (electron deficient) derivatives of the fullerene-terminated molecular wires **2-6**. The ethyl-TMS protecting groups for the sulfur atom were removed as before, except for the nitro derivative **3**, that was found to undergo side reactions to form insoluble materials during the deprotection step.

Synthesis of fullerene-terminated alkyl thiol 8 and disulfide 9. Fullerene-terminated molecular wires incorporating a long alkyl chain were prepared as thiol ester **8** and disulfide **9** (Scheme 3). The 4-iodophenol was alkylated with 1,12-dibromododecane, and the mono-functionalized bromododecane **17** was isolated using chromatography. The ethyl-TMS protected sulfur atom was introduced by the lithiation of 2-(trimethylsilyl)ethanethiol followed by a condensation reaction with bromododecane **17**, giving the product **18**. After the introduction of the terminal alkyne via Pd-catalyzed reaction with TMSA and the removal of the TMS group, the fullerene moiety was coupled to give the fullerene-terminated alkyl thiol **21**. The sulfur atom protecting group was converted from ethyl-TMS to the thiol ester with the same strategy as in previous reactions to give the product **8**. Basic deprotection of the thiol ester **8** and oxidative coupling of the resulting thiol in air can easily generate the disulfide **9**.

Synthesis of fullerene-tripods 10 and 11. Fullerene-terminated molecular devices incorporating a tripod base were also synthesized (Schemes 5 and 6). The ethyl-TMS protected sulfur atom was introduced by the lithiation of 2-(trimethylsilyl)ethanethiol followed by a condensation reaction with 3-iodobenzyl bromide (**22**) affording the product **23**. Each leg of the tripod base (**25**) was obtained by a Pd-catalyzed reaction with trimethylsilylacetylene (TMSA) followed by the removal of the TMS group, and then the

legs (**25**) were coupled to the center part (**26**) to give the ethoxyl-terminated tripod **27**. The aryl lithium generated from the bromide **28** displaces the ethoxyl group of **27** to give the product **29**. Finally, the tripod **30** was obtained after deprotection of the terminal alkyne. The fullerene tripod **10** was obtained after the in situ ethynylation of fullerenes and the conversion of the sulfur protecting groups using the same strategies with $AgBF_4$. The fullerene tripod with azobenzene functionality (**11**) was also synthesized from the tripod **30** by introducing the azobenzene moiety **31**[22] before the fullerene coupling and the protecting group exchange reaction (Scheme 6).

Synthesis of the fullerene-triazene hybrid 12. The fullerene-triazene hybrid **12** can be easily synthesized from the triazene **35** with a terminal alkyne using the in situ ethynylation method (Scheme 7). This strategy can be useful to assemble fullerene-terminated molecular wires on silicon surfaces.[23]

Scheme 1. Synthesis of the Fullerene-Terminated Devices **1** and **7**.

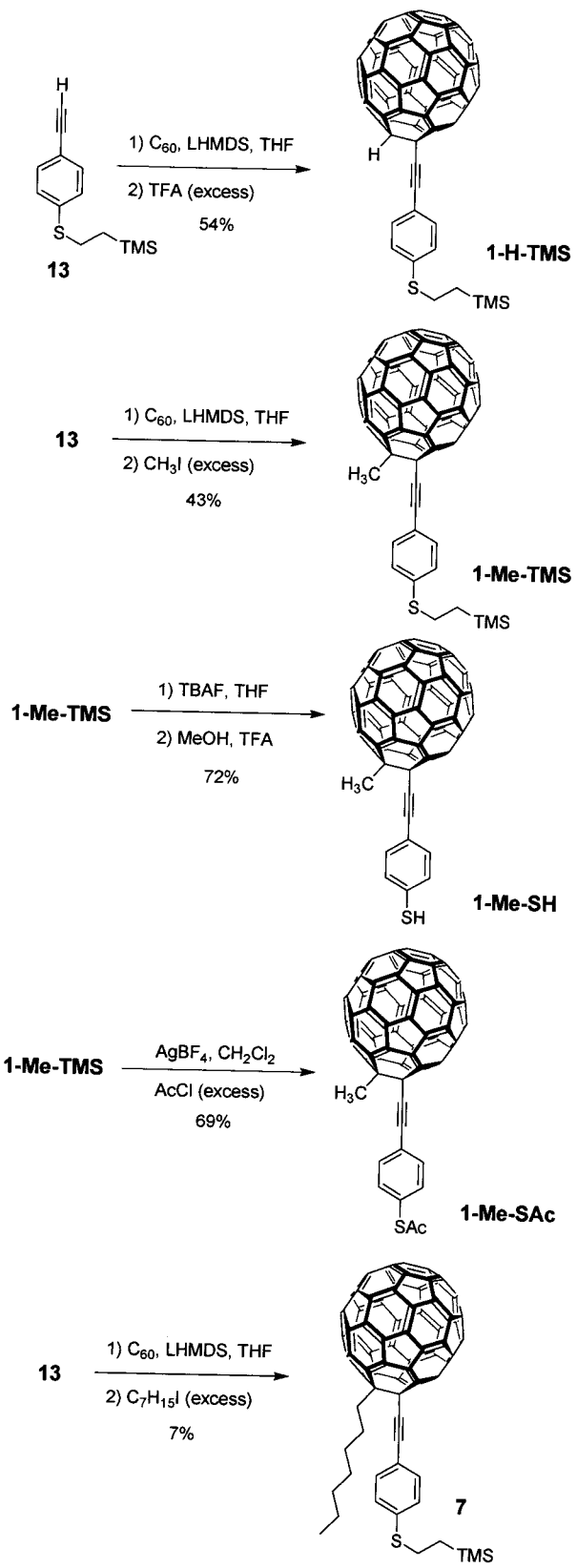
H
1) C_{60}, LHMDS, THF
2) TFA (excess)
54%
S
TMS
13
H
S
TMS
1-H-TMS
13
1) C_{60}, LHMDS, THF
2) CH_3I (excess)
43%
H_3C
S
TMS
1-Me-TMS
1-Me-TMS
1) TBAF, THF
2) MeOH, TFA
72%
H_3C
SH
1-Me-SH
1-Me-TMS
$AgBF_4$, CH_2Cl_2
AcCl (excess)
69%
H_3C
SAc
1-Me-SAc
13
1) C_{60}, LHMDS, THF
2) $C_7H_{15}I$ (excess)
7%
7
S
TMS

Scheme 2. Synthesis of the Fullerene-Terminated Molecular Wires **2-6**.

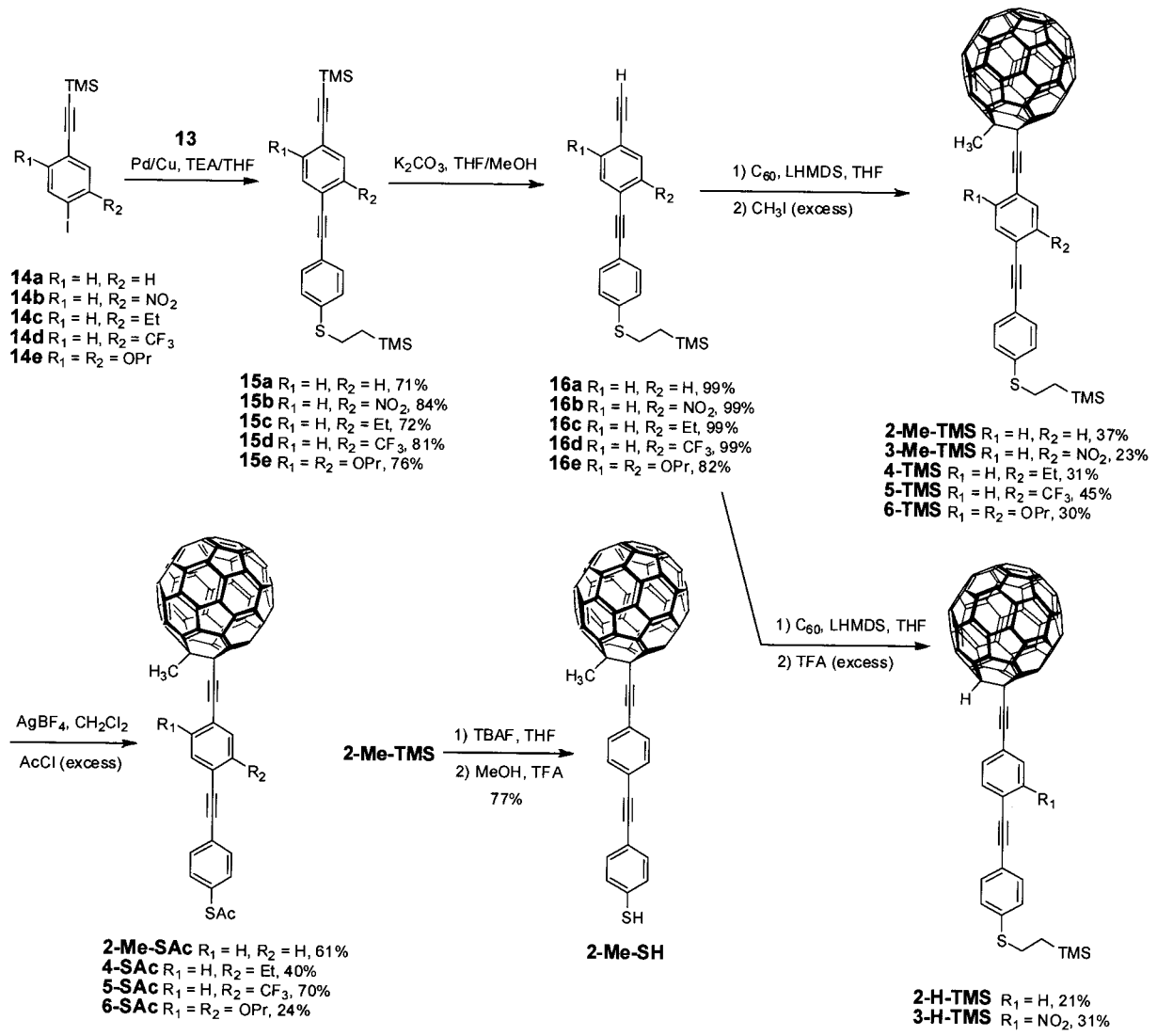

Scheme 3. Synthesis of the Fullerene Terminated Alkyl Thiol **8** and Disulfide **9**.

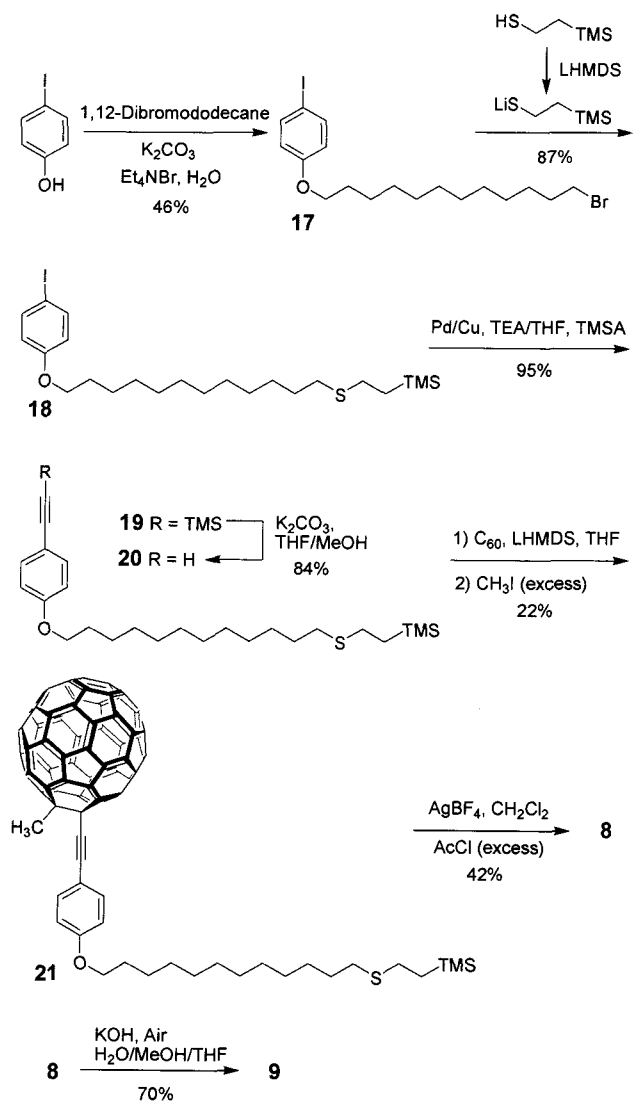

Scheme 4. Synthesis of the Fullerene Tripod **10**.

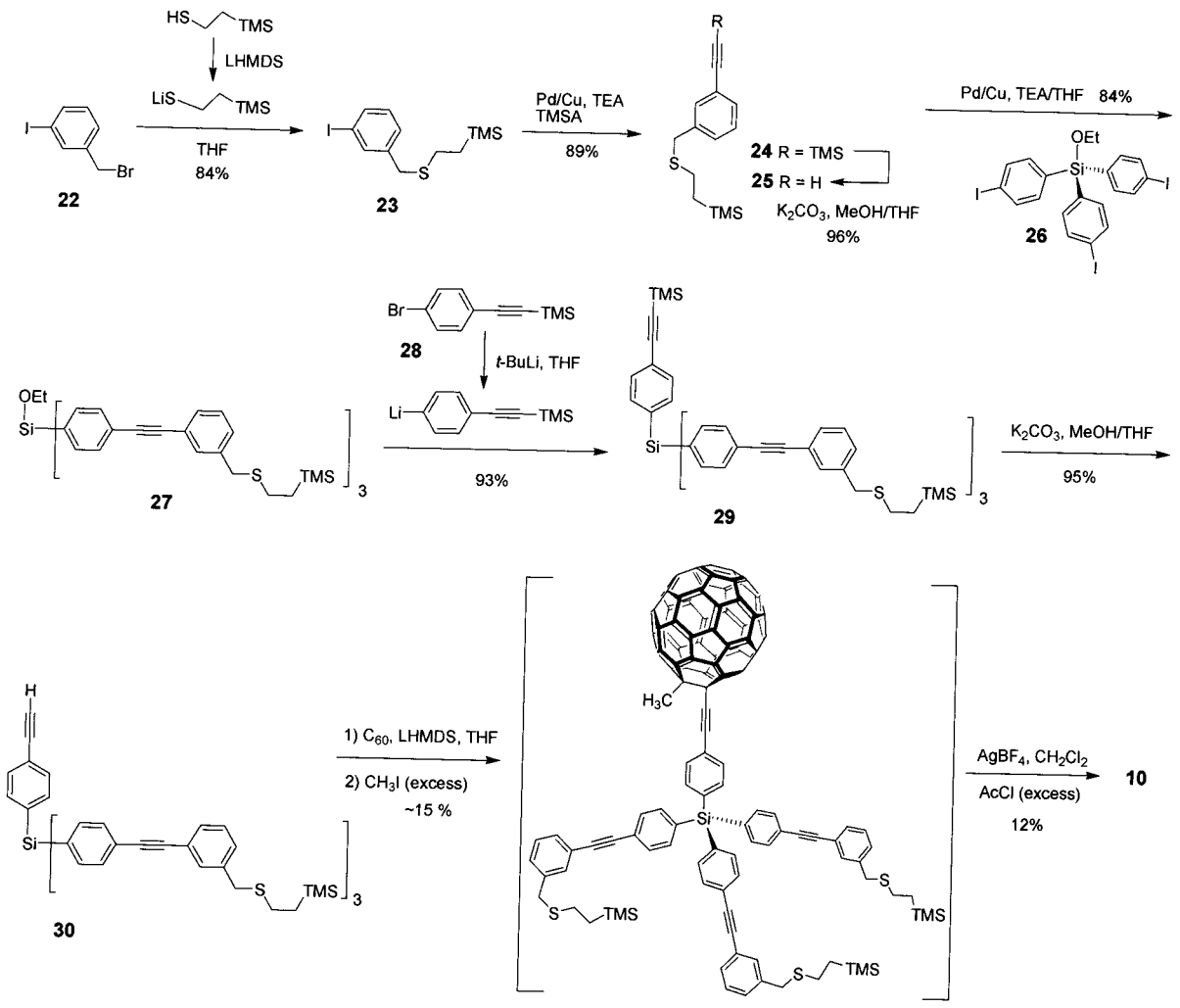

Scheme 5. Synthesis of the Fullerene Tripod **11**.

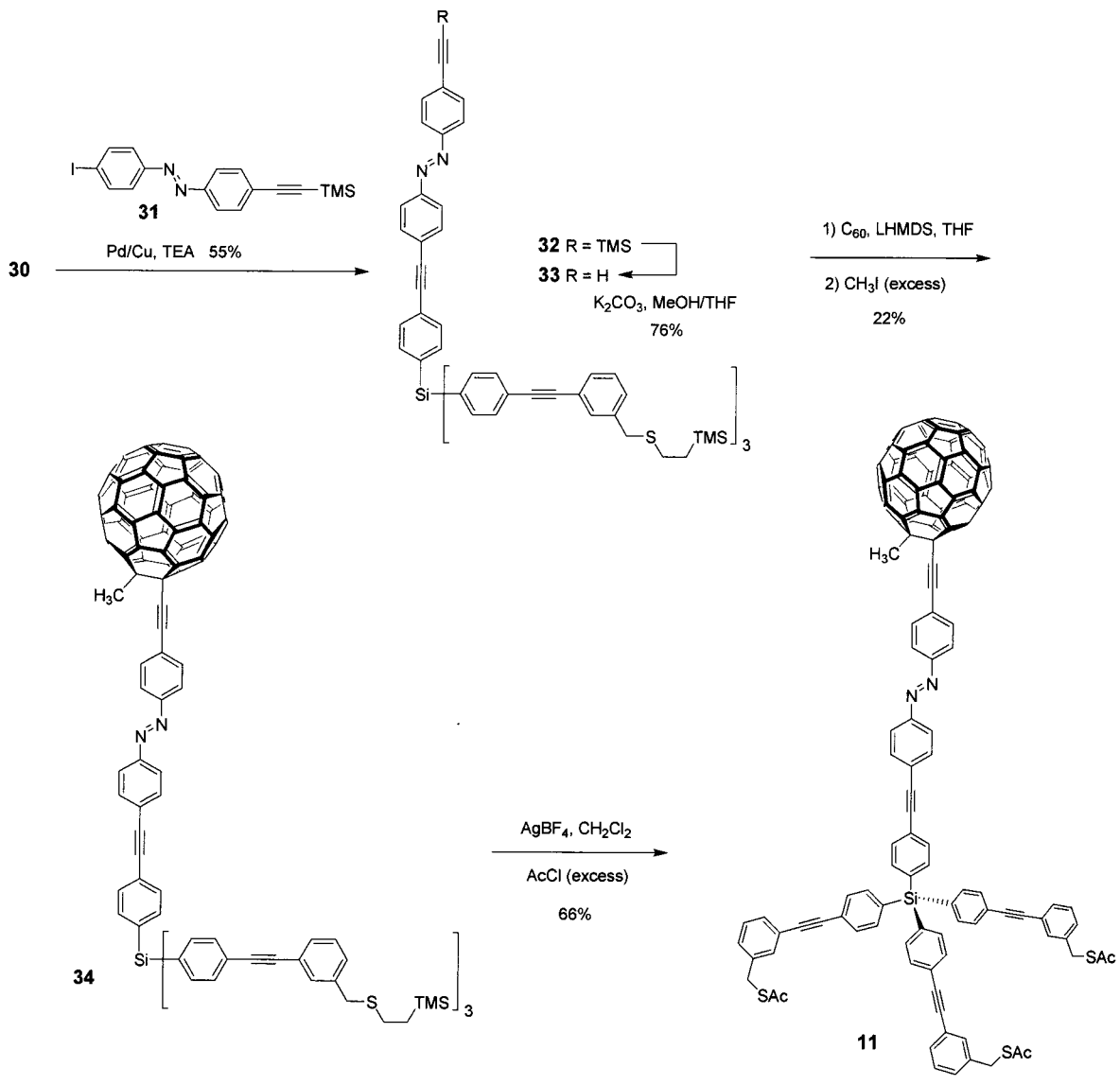

Scheme 6. Synthesis of the Fullerene-Terminated Device **12**.

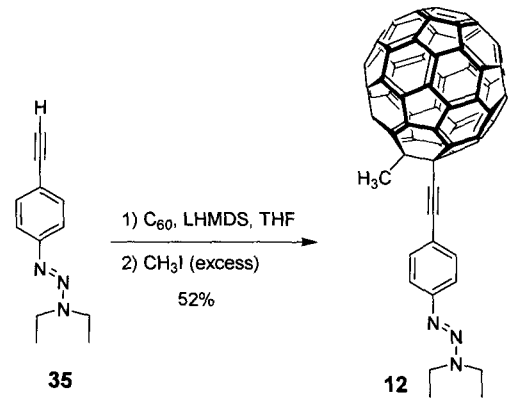

35 12

Theoretical study on fullerene-terminated OPEs.

The molecular orbital (MO) level is an important concept in explaining the fundamental behaviors of molecules, such as reactivity and kinetics. Furthermore, MO theory has been utilized as a powerful tool in the field of molecular electronics to describe charge transfer processes on molecules. Electron transfer through molecules can be influenced by several factors such as molecular length, conformation, and various functional groups present within the molecule, and these factors eventually determine the frontier MOs such as the highest occupied MO (HOMO), lowest unoccupied MO (LUMO), and HOMO-LUMO gap energies.[24] Thus, it is quite common to extract trends in molecular behavior based on the MOs. For example, a smaller HOMO-LUMO gap can generally provide higher charge transport efficiency.[25] Molecules with deep-lying HOMO and LUMO levels can possibly result in better candidates for n-type organic semiconductors. The spatial distribution or extent of these MOs within the molecule is also important because the rectifying behaviors of molecules can be predicted.[26,27] Unfortunately, although MO theory is of immense utility, popular computational methods such as the B3LYP/6-31G(d) protocol cannot provide accurate (absolute) MO energy values. Nevertheless, the method is quite reliable for predicting molecular geometry and

total energies.[28] We calculated total energies using B3LYP/6-31G(d) implemented in the Gaussian03 program, and geometry optimizations were done using the HF/3-21G* level of theory. The calculated frontier MO energies (HOMO and LUMO eigenvalues in the total energy calculation) for our fullerene-terminated OPEs **1-6** are tabulated along with the similar OPEs without C_{60} for comparison (Figure 2 and Table 1). In order to minimize calculation time, the propoxyl groups of **6** were replaced by methoxyl substituents for the calculation. The frontier MOs for the pristine C_{60} was also calculated to compare with our devices. It is clear from Table 1 that the HOMO-LUMO gaps (HLG)s of our fullerene-terminated molecular wires **1-5** (2.75~2.77 eV) are almost identical to that of pristine C_{60} (2.76 eV) even though our devices contain various functional groups with different electron-donating (–Et for **4**), -accepting (–NO_2 and –CF_3 for **3** and **5**, respectively) characters, or length of OPEs (one benzene ring for **1** and two rings for **2**). This is unusual compared with common OPE-based devices (**2_{Ph}**, **3_{Ph}**, **6_{Ph}**, see Figure 2 for structures), whose HLGs vary depending on the functional groups attached to the OPE backbone. Only the molecule with -OMe groups (**6**) gave a unique HLG (2.53 eV), which was the smallest of all. On the other hand, reasonable correlations between these electron-donating or -accepting characters of functional groups and HOMO/LUMO energy levels are clearly observed (Figure 2). Both HOMO and LUMO levels are aligned in the order of increasing electron-donating characters, –NO_2 < –CF_3 < –H < –Et < –OMe groups. The molecule with the nitro group (**3**) has the lowest HOMO and LUMO levels, and the molecule with methoxyl groups (**6**) gives the highest energy levels for both HOMO and LUMO. The size of the OPE backbone has almost no effect because compound **1** and **2** share almost identical HOMO and LUMO levels. The HOMO and

LUMO levels of pristine C_{60} are deeper than that of our devices by ~0.2 eV, and this calculation result suggests that electron-accepting power of fullerene is reduced when it is functionalized. This is a physically observable phenomenon, which we and other groups have previously reported in the study of fullerene-OPE hybrid devices using cyclic voltammetry.[16] The redox waves for fullerene derivatives always shift toward more negative potentials relative to pristine C_{60}, possibly due to the decrease of π-delocalization on the fullerene cage after the introduction of two sp^3 carbon atoms. The examination of the spatial distribution of these MOs suggests that the frontier MOs in these fullerene-terminated molecular wires are dominated by the fullerene-related MOs. This can be demonstrated when these frontier MOs are plotted on molecules (Figure 3). Except for compound **6**, all frontier MOs reside predominantly on the fullerene cage, giving a narrow distribution of HLGs for fullerene-terminated OPEs.

Table 1. Molecular Orbital Energies Calculated Using B3LYP/6-31G(d) Theory[a]

Compound	Energies (eV)		
	HOMO	LUMO	HOMO-LUMO gap
C_{60}	-5.99	-3.23	2.76
1	-5.76	-3.00	2.76
2 (-H)	-5.74	-2.99	2.76
3 ($-NO_2$)	-5.84	-3.07	2.77
4 (-Et)	-5.72	-2.97	2.75
5 ($-CF_3$)	-5.80	-3.03	2.76
6 (-OMe)	-5.46	-2.93	2.53
2_{Ph}	-5.64	-1.72	3.92
3_{Ph}	-6.00	-2.70	3.30
6_{Ph}	-5.20	-1.59	3.61

[a]For the structures of 1-6, see Figure 1. The stuctures of 2_{Ph}, 3_{Ph} and 6_{Ph} are shown in Figure 2.

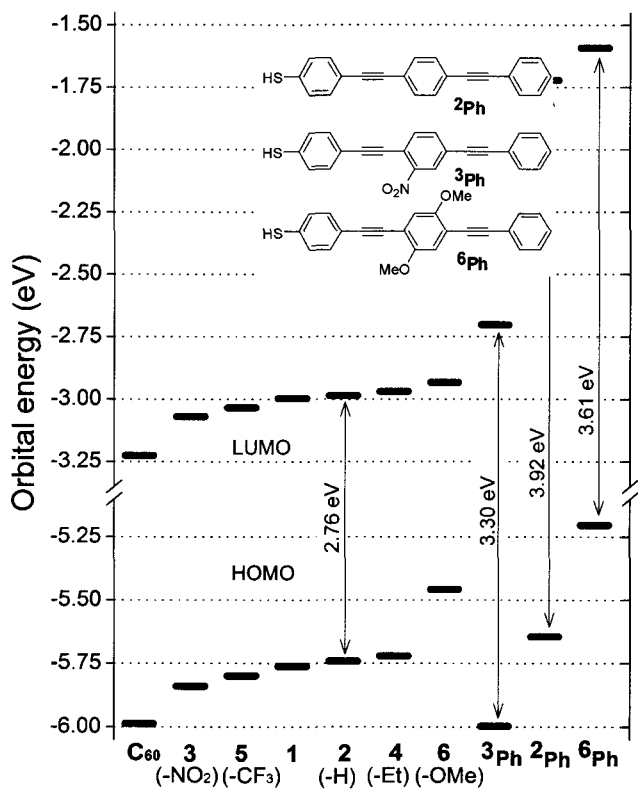

Figure 2. Calculated MO energy levels. The inset shows chemical structures for $\mathbf{2_{Ph}}$, $\mathbf{3_{Ph}}$, and $\mathbf{6_{Ph}}$. The structures of **1-6** are shown in Figure 1.

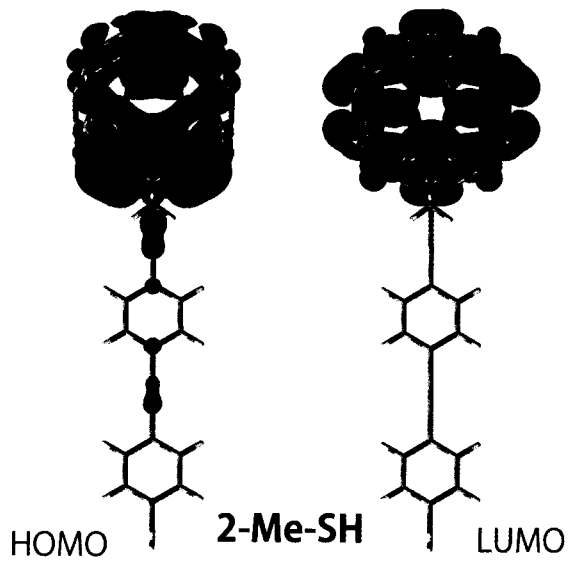
HOMO
2-Me-SH
LUMO

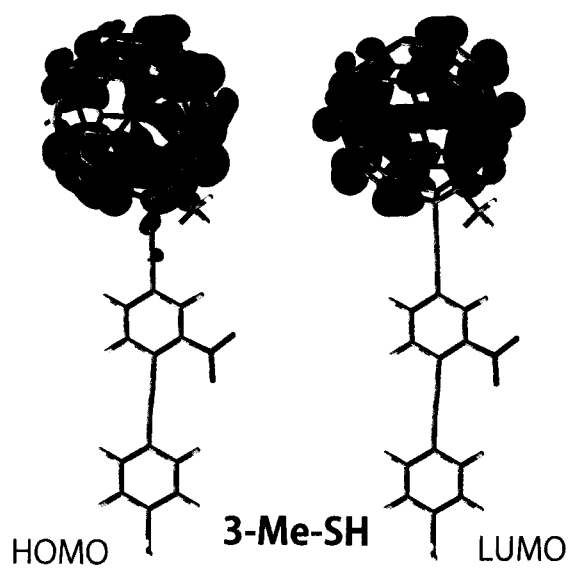
HOMO
3-Me-SH
LUMO

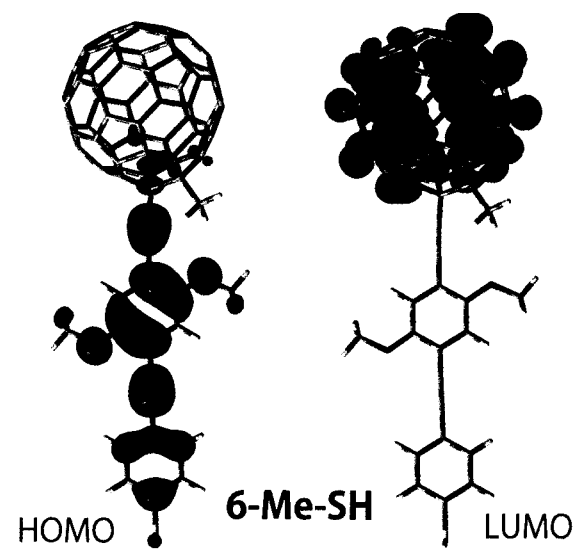
HOMO
6-Me-SH
LUMO

Figure 3. The HOMO and LUMO molecular orbitals of representative fullerene-terminated OPEs.

Ultraviolet Photoelectron Spectroscopy and Inverse Photoemission Spectroscopy results on Fullerene-Terminated OPE.

The electronic structure of the fullerene-terminated OPE monolayer on the Au surface was examined. Figure 4 shows the distribution of the occupied and empty electronic states determined by the UPS and IPES, respectively. The simulated density of states (DOS) of the model compound (inset of Figure 4) was also plotted along with the experimental spectra. The simulated DOS was shifted for the best fit with the experimental spectra, and the vertical bars along with the DOS spectrum show the positions of the calculated MOs. The convolution of the MOs was performed using a Gaussian function with FWHM of 0.5 eV. The MO calculation was performed by applying B3LYP/LanL2DZ theory to the compound **2-Me-S** adsorbed at the three-fold hollow site of the Au cluster (inset of Figure 4). The small Au cluster containing three gold atoms was used as the Au surface for the calculation because we are interested in the qualitative picture of MOs on surfaces. The strength of the small cluster approach has been justified with theoretical studies of self-assembled monolayers on metal surfaces.[29-32] During the structure optimization using the HF/LanL2DZ method, the Au–Au bond distances were fixed at 2.884 Å and equivalent S–Au distances were maintained. All other parameters were allowed to relax during the structure optimization. The optimized molecular structure is shown in the inset of Figure 4.

The work function of the clean Au substrate was 5.2 eV in our work, and it was decreased to 4.4 eV after the SAM formation. The decrease of the work function by ~0.8 eV is in accord with previous studies of self-assembled monolayers on metal surfaces.[25,32] The ionization potential (IP), electron affinity (EA), and bandgap (Eg) energies were estimated to be 5.2 eV, 3.7 eV, and 1.5 eV, respectively, from these photoelectron spectra. The observed UPS spectrum was broad comparing to that of the simulated DOS spectrum. The broadening can be a result of the strong intermolecular interactions in the SAM. Our previous study on fullerene SAMs revealed the existence of mixed species such as head-to-tail assemblies due to the strong fullerene-Au and/or fullerene-fullerene interactions.[16] Thus, the observed UPS spectrum can be the sum of the signals from these mixed species in slightly different electronic and/or chemical environments, resulting in the rather broad spectrum. The observed small bandgap (1.5 eV) is noticeable, and it is presumably due to the unique structure of our fullerene-terminated OPEs, in which the C_{60} moiety can be connected to the Au surface through the conjugated OPE backbone.

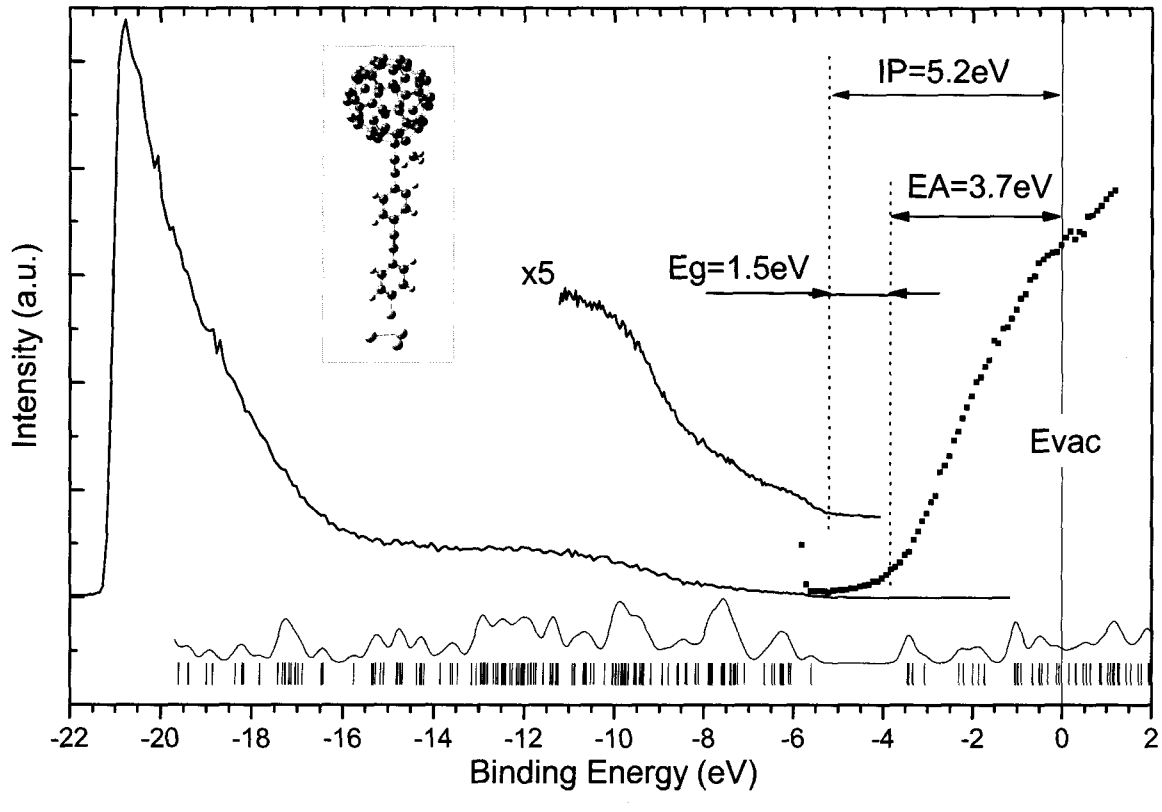

Figure 4. UPS and IPES spectra of **3-Me-SAc** assembled on Au surface. The inset shows the molecular conformation of **3-Me-S** on Au cluster that was used for the simulation of DOS.

Conclusions

In this chapter, we have reported efficient synthesis routes for the generation of a variety of fullerene-terminated molecular wires (Figure 1). Theoretical studies using DFT calculations have been performed to reveal the electronic nature of those fullerene-terminated OPEs. The calculation indicates that the frontier MOs of fullerene-terminated OPEs reside mainly on the fullerene cage and give the narrow distribution of HLG values regardless of the functional groups of the OPE moiety. The electronic structures of

fullerene-terminated OPEs on Au surfaces have also studied using UPS and IPES methods. The broad nature of the UPS and IPES spectra can be an indication of strong intermolecular interactions, a result which agrees with our previous findings on the self-assembly of these fullerene-terminated molecular wires on Au surfaces.[16] The observed small bandgap (1.5 eV) shows the unique nature of our fullerene-terminated OPEs, in which the C_{60} moiety can be coupled to the Au surface through the conjugated OPE backbone.

Experimental Section

Materials. The synthesis of compounds **1-Me-xxx**, **2-Me-xxx**, **8-10,** and **13** have been detailed in the literature.[16] Precursors **14a-e**,[21] **15a**,[33] **15e**,[33] **16a**,[33] **16e**,[33] **31**,[22] and **35**[34] were prepared according to literature procedures. Compounds **1**, **2**, **5-7**, **11** and **12** were prepared as described by Y. Shirai and co-workers.[38] All reactions were performed under an atmosphere of nitrogen unless stated otherwise. Reagent grade diethyl ether and tetrahydrofuran (THF) were distilled from sodium benzophenone ketyl. Triethylamine (TEA) and CH_2Cl_2 were distilled over CaH_2. Fullerene (99.5+% pure) was purchased from MTR Ltd. and used as received. LHMDS (1 M solution in THF) and TBAF (1 M solution in THF) were obtained from Aldrich and used as received. Flash column chromatography was performed using 230-400 mesh silica gel from EM Science. Thin layer chromatography was performed using glass plates pre-coated with silica gel 40 F_{254} purchased from EM Science. Melting points were uncorrected. Ultra-sonicated fullerene slurry in THF was prepared in general ultrasonic cleaners.

Ultraviolet Photoelectron Spectroscopy (UPS) and Inverse Photoemission Spectroscopy (IPES). Photoemission spectroscopy of occupied and unoccupied states of the system was performed using a VG ESCA Lab system equipped with both UPS and IPES.[35-37] The spectrometer chamber of the UHV system had a base pressure of 8×10^{-11} Torr. Occupied states spectra were obtained by UPS using the unfiltered He I line (21.2 eV) of a discharge lamp with the samples biased at –5.0 V to avoid the influence of the detector work function and to observe the true low-energy secondary cut-off. The typical instrumental resolution for UPS measurements ranges from ~ 0.03-0.1 eV with photon energy dispersion of less than 20 meV. Unoccupied states were measured by IPES using a custom-made spectrometer composed of a commercial Kimball Physics ELG-2 electron gun and a bandpass photon detector. IPES was done in the isochromat mode using a photon detector centered at a fixed energy of 9.8 eV. The combined resolution (electron + photon) of the IPES spectrometer was determined to be ~ 0.6 eV from the width of the Fermi edge measured on a clean polycrystalline Au film. The UPS and IPES energy scales were aligned by measuring the position of the Fermi level on a freshly evaporated Au film. The position of the vacuum level, E_{vac}, was measured for each surface using the onset of the secondary cut-off in the UPS spectra. The HOMO/LUMO level was determined directly using the onset edge in the UPS/IPES spectra instead of the peak value. All the measurements were done at room temperature.

Synthesis details for all new compounds.

General Procedure for the Coupling of a Terminal Alkyne with an Aryl Halide Using a Palladium-Catalyzed Cross-Coupling (Sonogashira) Protocol. To an oven-

dried round bottom flask equipped with a magnetic stir bar were added the aryl halide, the terminal alkyne, $PdCl_2(PPh_3)_2$ (ca. 2 mol% per aryl halide), and CuI (ca. 4 mol% per aryl halide). A solvent system of TEA and/or THF was added depending on the substrates. Upon completion, the reaction was quenched with a saturated solution of NH_4Cl. The organic layer was then diluted with hexanes, diethyl ether or CH_2Cl_2, and washed with water or saturated NH_4Cl (1×). The combined aqueous layers were extracted with hexanes, diethyl ether, or CH_2Cl_2 (2×). The combined organic layers were dried over $MgSO_4$, filtered, and the solvent was removed from the filtrate in vacuo to afford the crude product, which was purified by column chromatography (silica gel). Eluents and other slight modifications are described below for each compound.

General Procedure for the Addition of C_{60} to Terminal Alkynes Using LHMDS, in situ ethynylation method. To an oven-dried round bottom flask equipped with a magnetic stir bar was added the terminal alkyne and C_{60} (2 equiv per terminal alkyne H). After adding THF, the mixture was bath-sonicated for at least 3 h. To the greenish-brown suspension formed after the sonication was added LHMDS dropwise at room temperature over 0.5 to 1.5 h. As the reaction progressed, the mixture turned into a deep greenish-black solution. During and after the addition of the LHMDS, small aliquots from the reaction were extracted and quenched with trifluoroacetic acid (TFA) or methyl iodide (MeI), dried, and re-dissolved in CS_2 for TLC analysis (developed in a mixture of CS_2, CH_2Cl_2 and hexanes). Completion of the reaction was confirmed by the disappearance of the starting materials. The reaction usually completed within 1.5 h from the beginning of LHMDS addition. Upon completion, the reaction was quenched with TFA or MeI to give a brownish slurry. When MeI was used, the reaction was stirred at room temperature for

at least 6 h. Excess TFA or MeI and solvent were then removed in vacuo to afford a crude product that was purified by flash column chromatography (silica gel). Eluents and other slight modifications are described below for each compound.

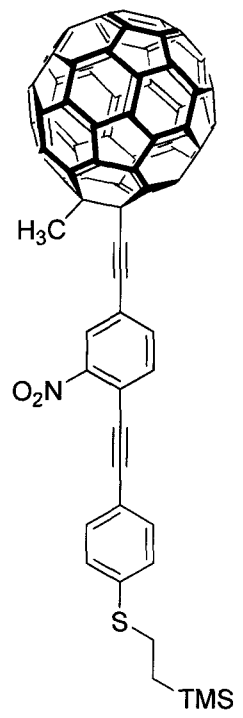

Compound (3-Me-TMS). The compound **16b** (0.15 g, 0.40 mmol) was subjected to the general in situ ethynylation procedure with C_{60} (0.22 g, 0.31 mmol), THF (120 mL), LHMDS (1.0 mL, 1.0 mmol), and MeI (5 mL, 80 mmol). Crude products were dissolved in CS_2 and directly loaded onto flash column, and eluted with 100% CS_2 in hexanes. The product was further purified using another flash column with graduated elution of 5–75% CS_2 in hexanes then CS_2: CH_2Cl_2 :hexanes (4: 1: 5) to afford the product (0.079 g, 23%) as a brown solid. FTIR (KBr) 2950, 2922, 2208, 1713, 1606, 1588, 1541, 1514, 1344, 1248 cm^{-1} (drop cast); ^1H NMR (CS_2:$CDCl_3$, 1:5, 500 MHz) δ 8.47 (d, J = 1.5Hz, 1H), 7.95 (dd, J = 1.5, 8.3 Hz, 1H), 7.78 (d, J = 8.3 Hz, 1H), 7.51 (d, J = 8.6 Hz, 2H), 7.26 (d, J = 8.6 Hz, 2H), 3.52 (s, 3H), 3.03–2.99 (m, 2H), 0.99–0.96 (m, 2H), 0.08 (s, 9H); ^{13}C

NMR (CS_2:$CDCl_3$, 1:5, 125 MHz) δ 156.6, 152.6, 149.4 (Ar), 148.0, 147.8, 146.6, 146.5, 146.4, 146.3, 145.9, 145.7, 145.6, 145.5, 145.4, 145.01, 144.98, 144.8, 144.6, 143.2, 142.71, 142.66, 142.21, 142.16, 142.1, 142.0, 141.7, 141.6, 140.7 (Ar), 140.4, 140.2, 135.7, 134.7 (30 signals from sp^2-C in the C_{60} core), 134.5, 134.2, 132.4, 128.2, 127.3, 123.1, 119.1, 118.5, 99.8, 92.6, 85.2, 82.8, 61.7 (CCH_3 in the C_{60} core), 59.7 (quaternary sp^3-C in the C_{60} core), 33.0, 28.6, 16.6, -1.7; MALDI-TOF MS *m/z* (sulfur as the matrix) calcd for $C_{82}H_{23}NO_2SSi$ 1114.2, found 1114.2 (M^+).

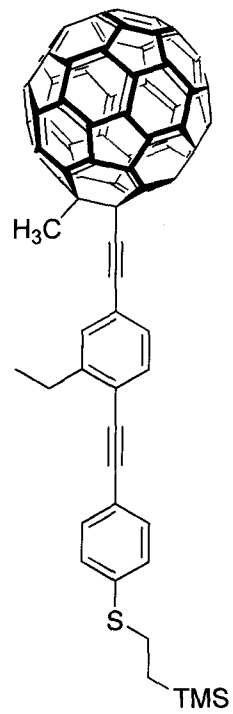

Compound (4- TMS). The compound **16c** (0.100 g, 0.275 mmol) was subjected to the general in situ ethynylation procedure with C_{60} (0.297 g, 0.413 mmol), THF (125 mL), LHMDS (0.600 mL, 0.600 mmol), and MeI (6 mL). Crude products were dissolved in CS_2 and directly loaded onto flash column, and eluted with 1–40% CS_2 in hexanes. The product was further purified using another flash column with graduated elution from hexanes to CS_2:CH_2Cl_2:hexanes (1:3:6) to afford the product (0.093 g, 31 %) as a brown

solid. FTIR (KBr) 2960, 1496, 1429, 1248 cm^{-1}; ^1H NMR (CS_2:$CDCl_3$, 1:5, 400 MHz) δ 7.65 (s, 1H), 7.59 (m, 2H), 7.46 (d, J = 8.1 Hz, 2H), 7.28 (s, 1H), 3.53 (s, 3H), 2.99 (m, 4H), 1.39 (t, J = 7.5 Hz, 3H), 0.97 (m, 2H), 0.07 (s, 9H); ^{13}C NMR (CS_2:$CDCl_3$, 1:5, 100 MHz) δ 157.5, 153.6, 148.4, 148.0, 147.8, 146.6, 146.5, 146.4, 146.3, 146.0, 145.6, 145.5, 142.6, 142.2, 142.1, 142.0, 141.8, 141.7, 141.6, 141.5, 140.3, 140.2, 138.7, 134.6, 134.4, 132.2, 131.8, 131.5, 129.4, 128.0, 123.2, 122.4, 120.0, 94.9, 89.5, 88.0, 85.4, 61.8, 59.9, 33.0, 31.6, 29.0, 27.8, 22.7, 16.7, 14.7, -1.7 ; MALDI-TOF MS *m/z* (sulfur as the matrix) calcd for $C_{84}H_{28}SSi$ 1096, found 1096 (M^+).

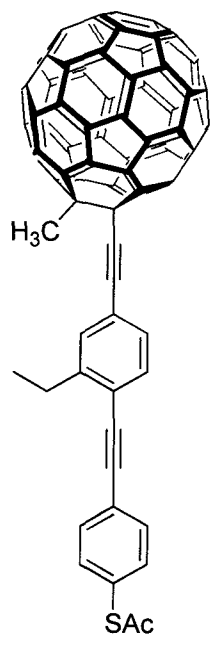

Compound (4-SAc). To a round bottom flask equipped with a magnetic stirrer was added compound **4-TMS** (32 mg, 0. 029 mmol), excess AcCl (1 mL), CH_2Cl_2 (20 mL), and $AgBF_4$ (17 mg, 0.08 mmol). The reaction mixture was stirred for 1 h at room temperature, and then quenched with saturated $NaHCO_3$, diluted with CH_2Cl_2 and water. The aqueous layer was extracted with CH_2Cl_2 (×1). The combined organic layers were dried over $MgSO_4$, filtered, and concentrated under vacuum. Crude material was loaded

onto flash column using pure CS_2, and eluted with hexane, CS_2:CH_2Cl_2:hexane (1:1:3), and then CS_2:CH_2Cl_2:hexane (5:2:3) to give the product **4-SAc** as a brown powder (12.0 mg, 40%). FTIR (KBr) 2963, 2923, 1709, 1495 cm^{-1}; ^1H NMR (CS_2:$CDCl_3$, 1:1, 400 MHz) δ 7.64 (m, 1H), 7.57 (m, 4H), 7.41 (d, J = 8 Hz, 2H), 3.53 (s, 3H), 2.96 (q, J = 8 Hz, 2H), 2.45 (s, 3H), 1.39 (t, J = 8 Hz); ^{13}C NMR (CS_2:$CDCl_3$, 1:1, 100 MHz) δ 157.0, 153.2, 147.9, 147.7, 146.52, 146.51, 146.4, 146.3, 146.2, 146.0, 145.6, 145.5, 145.4, 145.3, 145.2, 145.0, 144.8, 144.7, 143.2, 142.7, 142.6, 142.2, 142.13, 142.12, 142.0, 141.7, 141.5, 140.3, 140.2, 134.5, 134.4, 134.2, 132.3, 132.0, 131.6, 129.4, 128.4, 124.4, 122.8, 122.7, 94.2, 89.7, 89.6, 85.3, 61.7, 59.8, 33.0, 30.2, 29.9, 27.9, 14.8; MALDI-TOF MS *m/z* (sulfur as the matrix) calcd for $C_{81}H_{18}OS$ 1038, found 1038 (M^+).

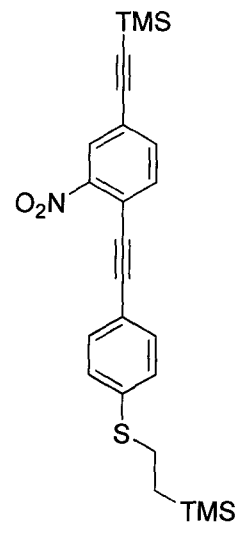

Compound (15b). See the general procedure for the Pd/Cu coupling reaction. The materials used were **14b** (1.03 g, 2.98 mmol), **13** (0.615 g, 2.62 mmol), $PdCl_2(PPh_3)_2$ (0.033 g, 0.047 mmol), CuI (0.014 g, 0.074 mmol), TEA (10 mL), and THF (20 mL) at room temperature overnight. The residue was purified by flash column chromatography with 10–20% CH_2Cl_2 in hexanes to give product **15b** (0.99 g, 84%) as a yellow solid.

FTIR (KBr) 2954, 2211, 2163, 1588, 1542, 1499, 1346, 1249, 1089 cm^{-1}; ^1H NMR (500 MHz, $CDCl_3$) δ 8.16 (s, 1H), 7.63 (s, 2H), 7.49 (d, J = 8.5 Hz, 2H), 7.26 (d, J = 8.5 Hz, 2H), 3.03–2.98 (m, 2H), 0.99–0.94 (m, 2H), 0.28 (s, 9H), 0.07 (s, 9H); ^{13}C NMR (125 MHz, $CDCl_3$) δ 149.4, 140.6, 135.8, 134.5, 132.5, 128.3, 127.6, 123.9, 118.9, 118.7, 102.2, 99.6, 99.3, 85.3, 28.8, 16.8, -0.1, -1.5; EI-MS m/z calcd for $C_{24}H_{29}NO_2SSi_2$ 451.14, found 452.15 ($[M+H]^+$).

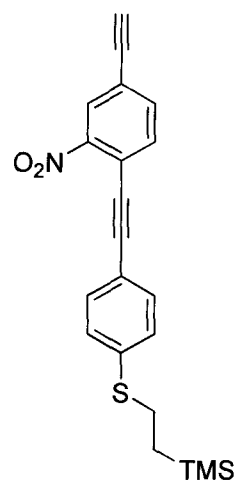

Compound (16b). To a round bottom flask equipped with a magnetic stirrer was added **15b** (0.36 g, 0.8 mmol), THF/MeOH (1:1) (30 mL), and K_2CO_3 (0.16 g, 1.2 mmol). The reaction mixture was stirred for 1 h at room temperature, then quenched with water and diluted with hexanes. The aqueous layer was extracted with CH_2Cl_2 (×2). Combined organic layers were dried over $MgSO_4$, filtered, and concentrated under vacuum. Crude material was filtered through a plug of silica gel using CH_2Cl_2/hexanes mixture to give the product **16b** as reddish-brown solid (0.30 g, 99%). FTIR (KBr) 3288, 2951, 2209, 1588, 1498 cm^{-1}; ^1H NMR (400 MHz, $CDCl_3$) δ 8.19(s, 1H), 7.66 (s, 2H), 7.50 (d, J = 6.7 Hz, 2H), 7.26 (d, J = 6.7 Hz, 2H), 3.30 (s, 1H), 3.03–2.99 (m, 2H), 0.99–0.94 (m, 2H), 0.08 (s, 9H); ^{13}C NMR (100 MHz, $CDCl_3$) δ 149.4, 140.7, 136.0, 134.6, 132.6, 128.5,

127.6, 122.8, 119.2, 118.8, 99.5, 85.1, 81.5, 81.2, 28.8, 16.8, -1.5; EI-HRMS *m/z* calcd for $C_{21}H_{21}NO_2SSi$ 379.1062, found 380.1136 ($[M+H]^+$).

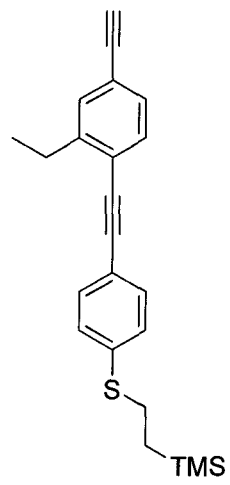

Compound (16c). See the general procedure for the Pd/Cu coupling reaction. The materials used were **14c** (0.353 g, 1.506 mmol), **13** (0.498 g, 1.506 mmol), $PdCl_2(PPh_3)_2$ (0.025 g, 0.036 mmol), CuI (0.010 g, 0.053 mmol), TEA (10 mL), and THF (20 mL) at room temperature overnight. The residue was purified by flash column chromatography with 1–5% CH_2Cl_2 in hexanes to give product **15c** (0.471 g, 72%) as a yellow oil. The solid was then transferred to a round bottom flask equipped with a magnetic stirrer dissolved in THF:MeOH (1:1) (30 mL), and K_2CO_3 (0.312 g, 2.26 mmol). The reaction mixture was stirred for 1 h at room temperature, then quenched with water and diluted with hexanes. The aqueous layer was extracted with CH_2Cl_2 (×1). Combined organic layers were dried over $MgSO_4$, filtered, and concentrated under vacuum. Crude material was filtered through a plug of silica gel using CH_2Cl_2/hexanes (20%) mixture to give the product **16c** as yellow/orange oil (0.372 g, 99%). FTIR (KBr) 3294, 2952, 1590, 1496, 1248 cm^{-1}; ^1H NMR (400 MHz, $CDCl_3$) δ 7.37 (m, 3H), 7.32 (d, J = 1 Hz, 1H), 7.24 (dd, J_1 = 8 Hz, J_2 = 1.5 Hz, 1H), 7.19 (d, J = 8.5 Hz, 2H), 3.09 (s, 1H), 2.95 (m, 2H), 2.8 (q, J

= 7.5 Hz, 2H), 1.23 (t, J = 7.5 Hz, 3H), 0.88 (m, 2H); ^{13}C NMR (100 MHz, $CDCl_3$) δ 146.2, 138.8, 132.1, 132.0, 131.8, 129.5, 128.0, 123.3, 122.0, 120.1, 94.8, 88.1, 83.8, 78.6, 29.1, 27.7, 16.8, 14.7, -1.6; EI-HRMS m/z calcd for $C_{23}H_{26}SSi$ 362.1524, found 362.1525.

Acknowledgement. The Welch Foundation, DARPA/AFOSR, and the NSF Penn State MRSEC funded this work. We thank Drs. I. Chester of FAR Research Inc. and R. Awartani of Petra Research Inc. for providing TMSA. This work was supported in part by World Premier International Research Center (WPI) Initiative on Materials Nanoarchitectonics, MEXT, Japan. Y. Shirai thanks Iketani Science and Technology Foundation for funding.

References

1. Tour, J. M.; Rawlett, A. M.; Kozaki, M.; Yao, Y. X.; Jagessar, R. C.; Dirk, S. M.; Price, D. W.; Reed, M. A.; Zhou, C. W.; Chen, J.; Wang, W. Y.; Campbell, I., *Chem.-Eur. J.* **2001**, *7*, 5118-5134.

2. James, D. K.; Tour, J. M., *Aldrichimica Acta* **2006**, *39*, 47-56.

3. James, D. K.; Tour, J. M., *Molecular Wires: From Design to Properties* **2005**, *257*, 33-62.

4. Tour, J. M., *Molecular Electronics: Commercial Insights, Chemistry, Devices, Architecture and Programming*. World Scientific: River Edge, NJ, 2003.

5. Chen, J.; Reed, M. A.; Rawlett, A. M.; Tour, J. M., *Science* **1999**, *286*, 1550-1552.

6. Chen, J.; Wang, W.; Reed, M. A.; Rawlett, A. M.; Price, D. W.; Tour, J. M., *App. Phys. Lett.* **2000**, *77*, 1224-1226.

7. Tour, J. M.; Cheng, L.; Nackashi, D. P.; Yao, Y. X.; Flatt, A. K.; St Angelo, S. K.; Mallouk, T. E.; Franzon, P. D., *J. Am. Chem. Soc.* **2003**, *125*, 13279-13283.

8. Shirai, Y.; Zhao, Y. M.; Cheng, L.; Tour, J. M., *Org. Lett.* **2004**, *6*, 2129-2132.

9. Hamasaki, R.; Ito, M.; Lamrani, M.; Mitsuishi, M.; Miyashita, T.; Yamamoto, Y., *J. Mater. Chem.* **2003**, *13*, 21-26.

10. Zhao, Y. M.; Shirai, Y.; Slepkov, A. D.; Cheng, L.; Alemany, L. B.; Sasaki, T.; Hegmann, F. A.; Tour, J. M., *Chem.- Eur. J.* **2005**, *11*, 3643-3658.

11. Prato, M., Fullerene materials. In *Fullerenes and Related Structures*, Springer-Verlag Berlin: Berlin, 1999; Vol. 199, pp 173-187.

12. Konishi, T.; Ikeda, A.; Shinkai, S., *Tetrahedron* **2005**, *61*, 4881-4899.

13. Love, J. C.; Estroff, L. A.; Kriebel, J. K.; Nuzzo, R. G.; Whitesides, G. M., *Chem. Rev.* **2005**, *105*, 1103-1169.

14. Mirkin, C. A.; Caldwell, W. B., *Tetrahedron* **1996**, *52*, 5113-5130.

15. Zeng, C. G.; Wang, H. Q.; Wang, B.; Yang, J. L.; Hou, J. G., *App. Phys. Lett.* **2000**, *77*, 3595-3597.

16. Shirai, Y.; Cheng, L.; Chen, B.; Tour, J. M., *J. Am. Chem. Soc.* **2006**, *128*, 13479-13489.

17. Yu, C. J.; Chong, Y. C.; Kayyem, J. F.; Gozin, M., *J. Org. Chem.* **1999**, *64*, 2070-2079.

18. Grundberg, H.; Andergran, M.; Nilsson, U. J., *Tetrahedron Lett.* **1999**, *40*, 1811-1814.

19. Creager, S.; Yu, C. J.; Bamdad, C.; O'Connor, S.; MacLean, T.; Lam, E.; Chong, Y.; Olsen, G. T.; Luo, J. Y.; Gozin, M.; Kayyem, J. F., *J. Am. Chem. Soc.* **1999**, *121*, 1059-1064.

20. Dirk, S. M.; Price, D. W.; Chanteau, S.; Kosynkin, D. V.; Tour, J. M., *Tetrahedron* **2001**, *57*, 5109-5121.

21. Hwang, J. J.; Tour, J. M., *Tetrahedron* **2002**, *58*, 10387-10405.

22. Yu, B. C.; Shirai, Y.; Tour, J. M., *Tetrahedron* **2006**, *62*, 10303-10310.

23. Chen, B.; Flatt, A. K.; Jian, H. H.; Hudson, J. L.; Tour, J. M., *Chem. Mater.* **2005**, *17*, 4832-4836.

24. Zhang, G.; Musgrave, C. B., *J. Phys. Chem. A* **2007**, *111*, 1554-1561.

25. Ishii, H.; Sugiyama, K.; Ito, E.; Seki, K., *Adv. Mater.* **1999**, *11*, 605-+.

26. Mizuseki, H.; Niimura, K.; Majumder, C.; Kawazoe, Y., *Computational Materials Science* **2003**, *27*, 161-165.

27. Majumder, C.; Mizuseki, H.; Kawazoe, Y., *J. Phys. Chem. A* **2001**, *105*, 9454-9459.

28. Zhan, C. G.; Nichols, J. A.; Dixon, D. A., *J. Phys. Chem. A* **2003**, *107*, 4184-4195.

29. Johansson, A.; Stafstrom, S., *Chem. Phys. Lett.* **2000**, *322*, 301-306.

30. Seminario, J. M.; Zacarias, A. G.; Tour, J. M., *J. Am. Chem. Soc.* **1999**, *121*, 411-416.

31. Vondrak, T.; Wang, H.; Winget, P.; Cramer, C. J.; Zhu, X. Y., *J. Am. Chem. Soc.* **2000**, *122*, 4700-4707.

32. Patnaik, A.; Setoyama, H.; Ueno, N., *J. Chem. Phys.* **2004**, *120*, 6214-6221.

33. Ying, J. W.; Ren, T., *J. Organomet. Chem.* **2006**, *691*, 4021-4027.

34. Flatt, A. K.; Chen, B.; Taylor, P. G.; Chen, M. X.; Tour, J. M., *Chem. Mater.* **2006**, *18*, 4513-4518.

35. He, T.; Ding, H. J.; Peor, N.; Lu, M.; Corley, D. A.; Chen, B.; Ofir, Y.; Gao, Y. L.; Yitzchaik, S.; Tour, J. M., *J. Am. Chem. Soc.* **2008**, *130*, 1699-1710.

36. Yan, L.; Watkins, N. J.; Zorba, S.; Gao, Y. L.; Tang, C. W., *App. Phys. Lett.* **2001**, *79*, 4148-4150.

37. Ding, H. J.; Zorba, S.; Gao, Y. L.; Ma, L. P.; Yang, Y., *J. App. Phys.* **2006**, *100*, 113706.

38. Shirai, Y.; Guerrero, J. M.; Sasaki, T.; He, T.; Ding, H.; Vives, G.; Yu, B. -C.; Cheng, L.; Flatt, A. K.; Taylor, P.; Gao, Y.; Tour, J. M. *J. Am. Chem. Soc.*, manuscript in preparation.

Supporting Information for Chapter 6.1

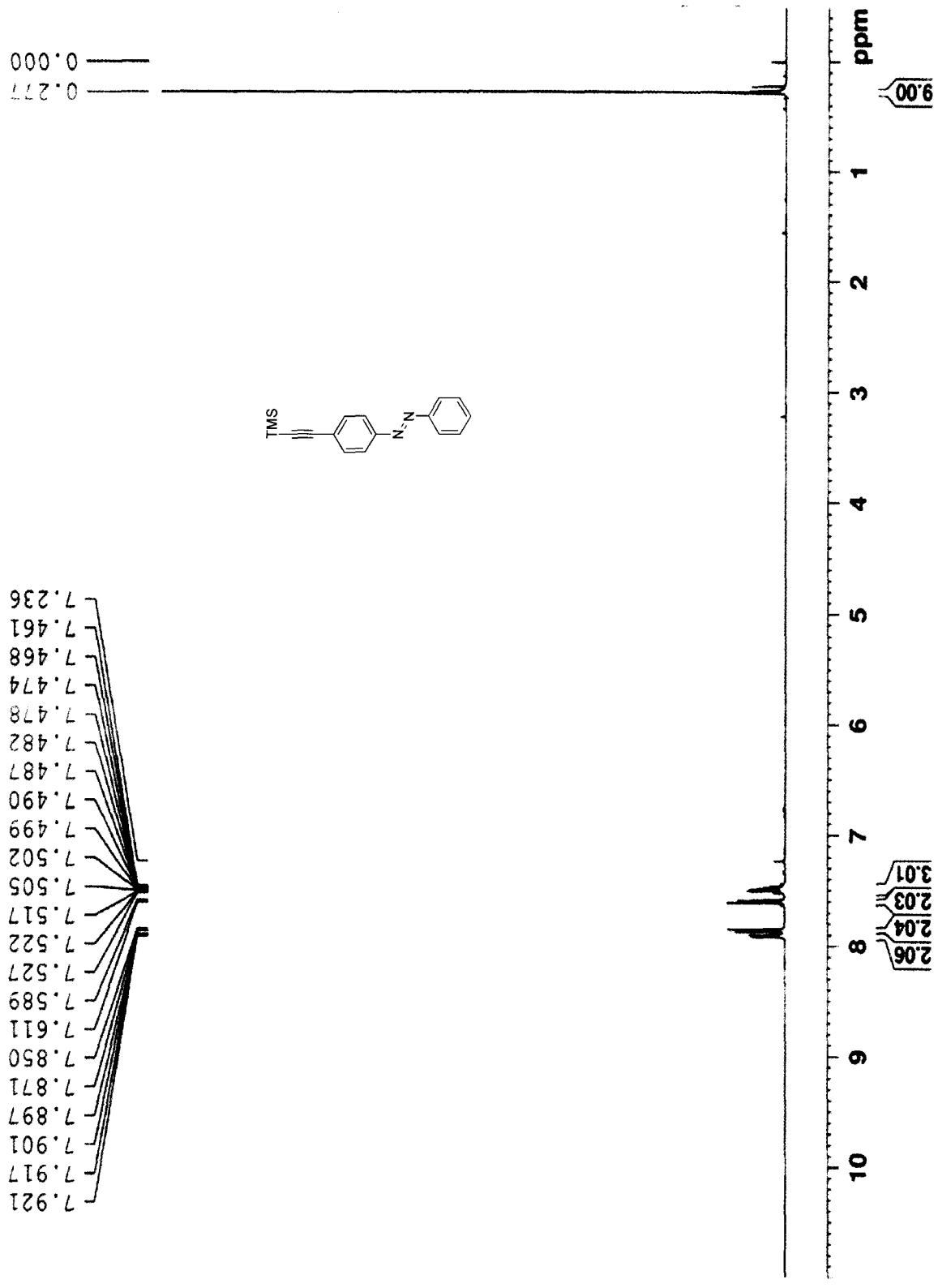

Figure S-6.1-1. ^{1}H NMR Spectrum of Compound 23.

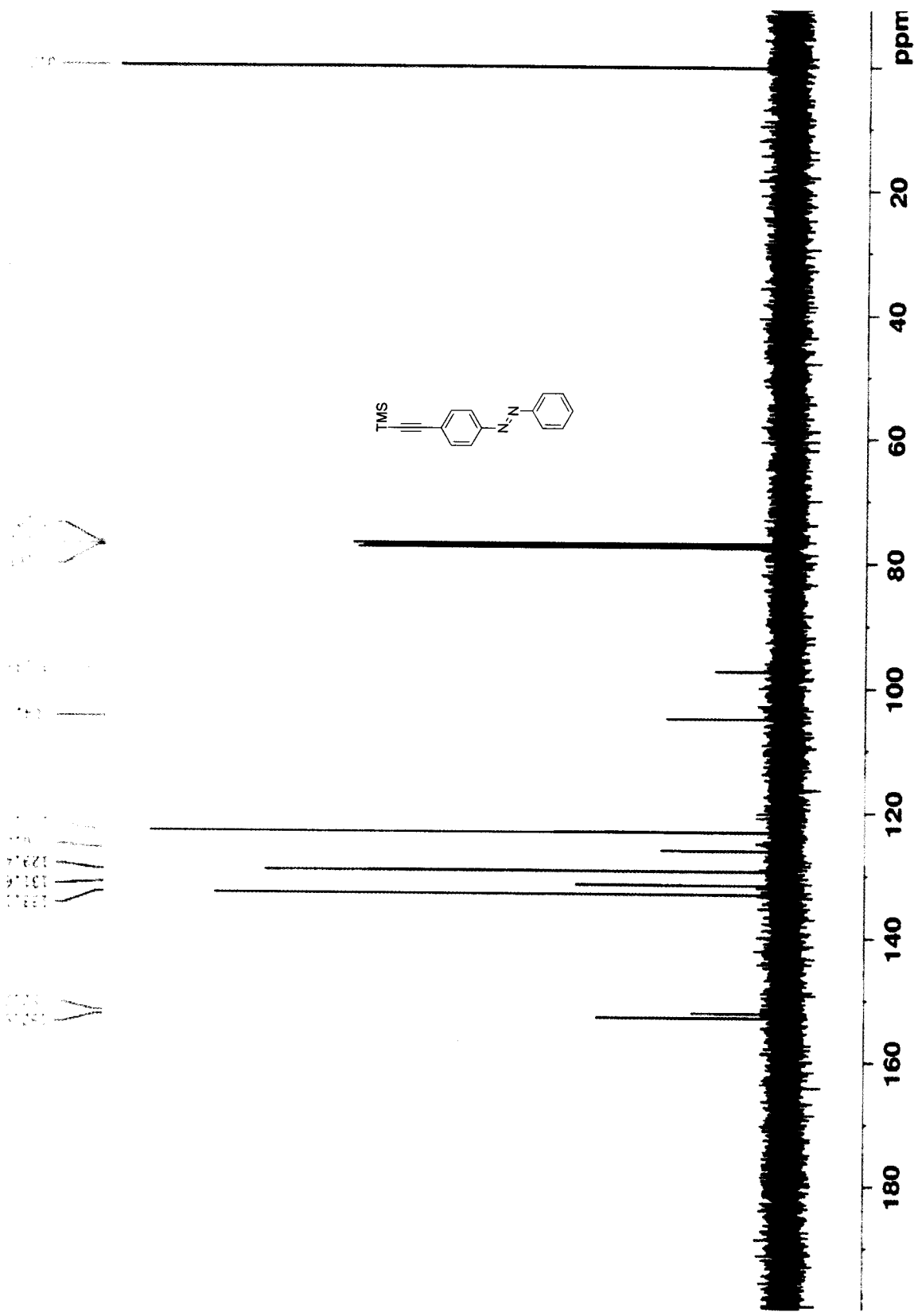

Figure S-6.1-2. ^{13}C NMR Spectrum of Compound 23.

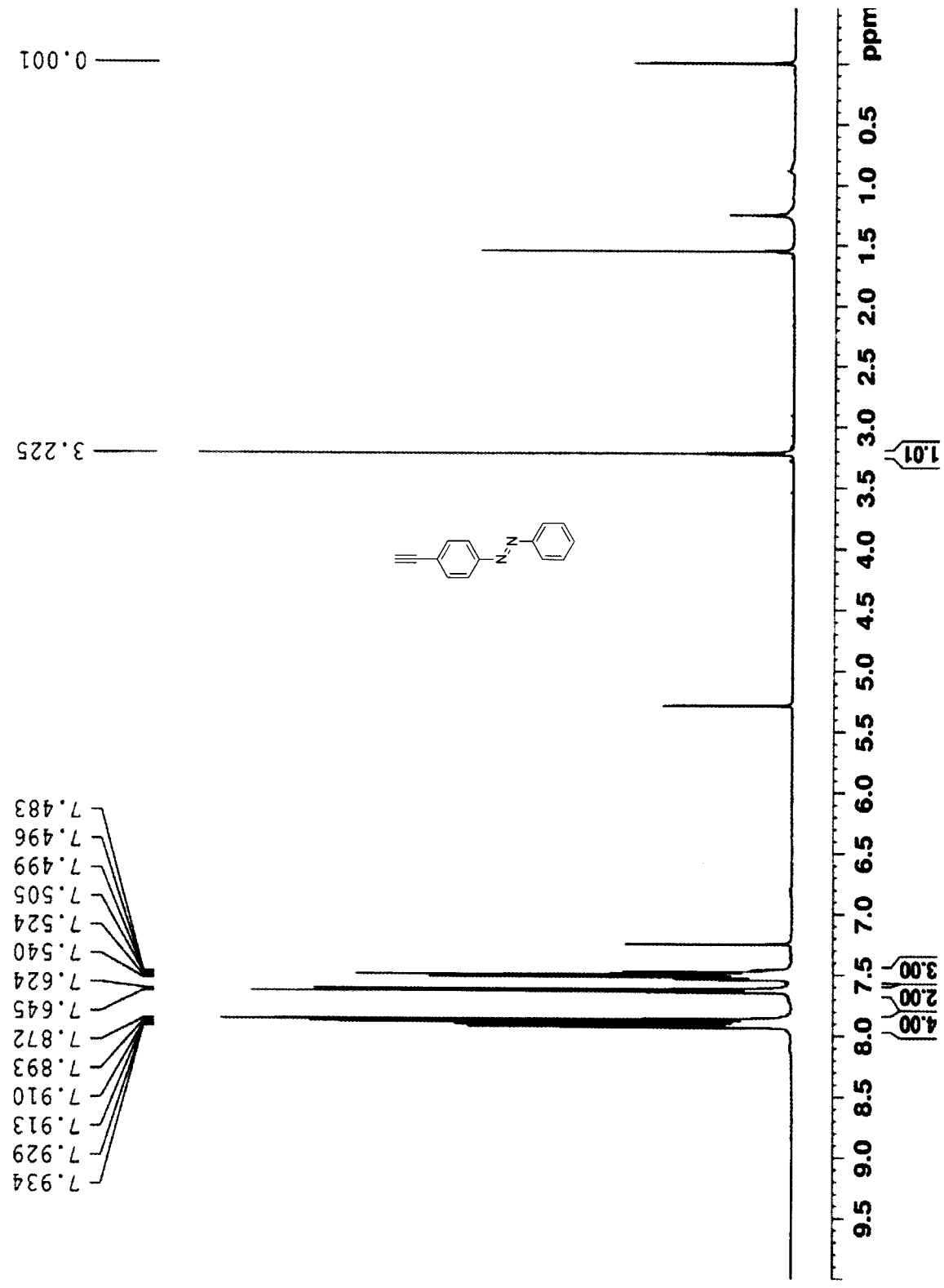

Figure S-6.1-3. ^{1}H NMR Spectrum of Compound 24.

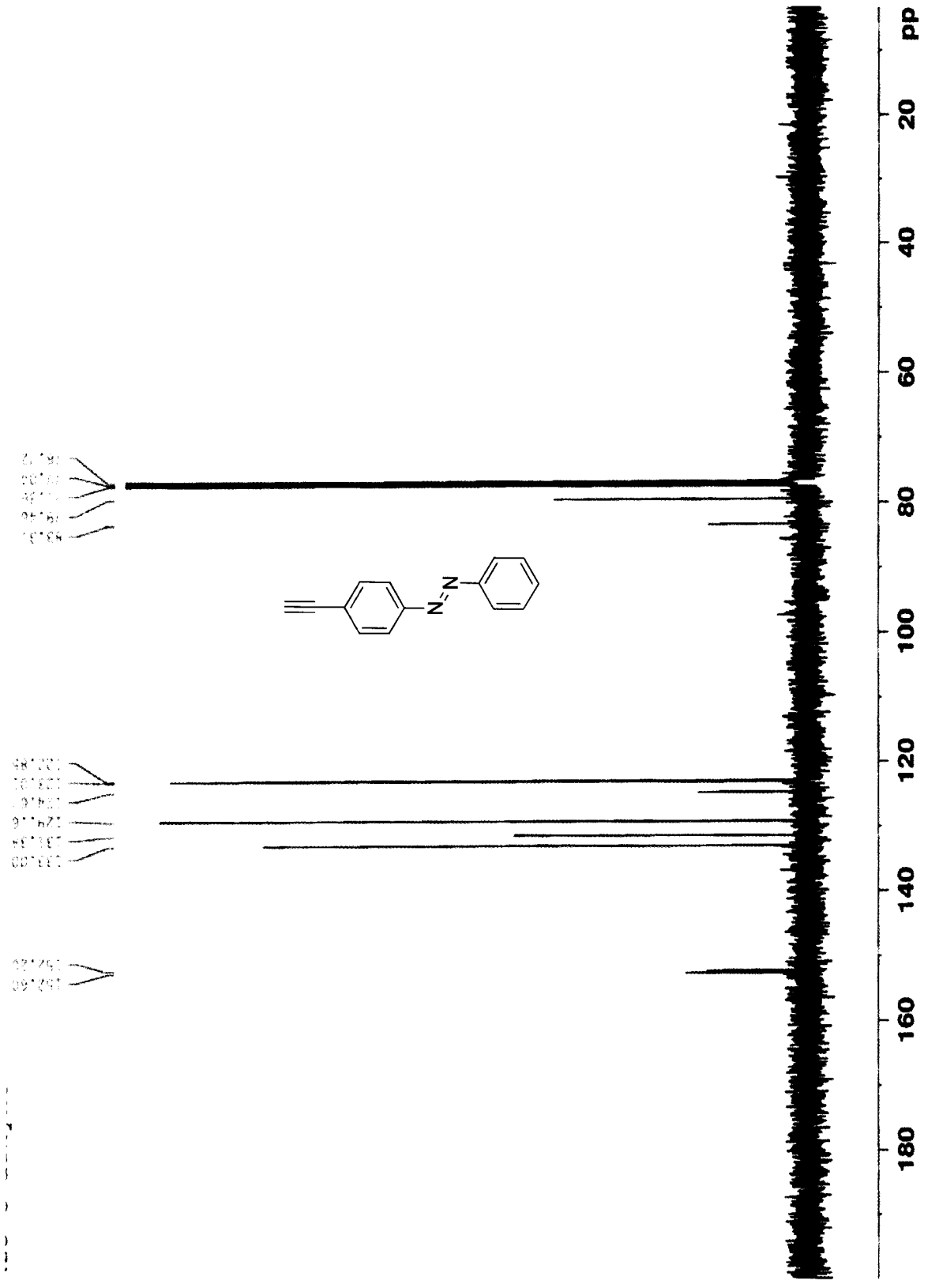

Figure S-6.1-4. ^{13}C NMR Spectrum of Compound 24.

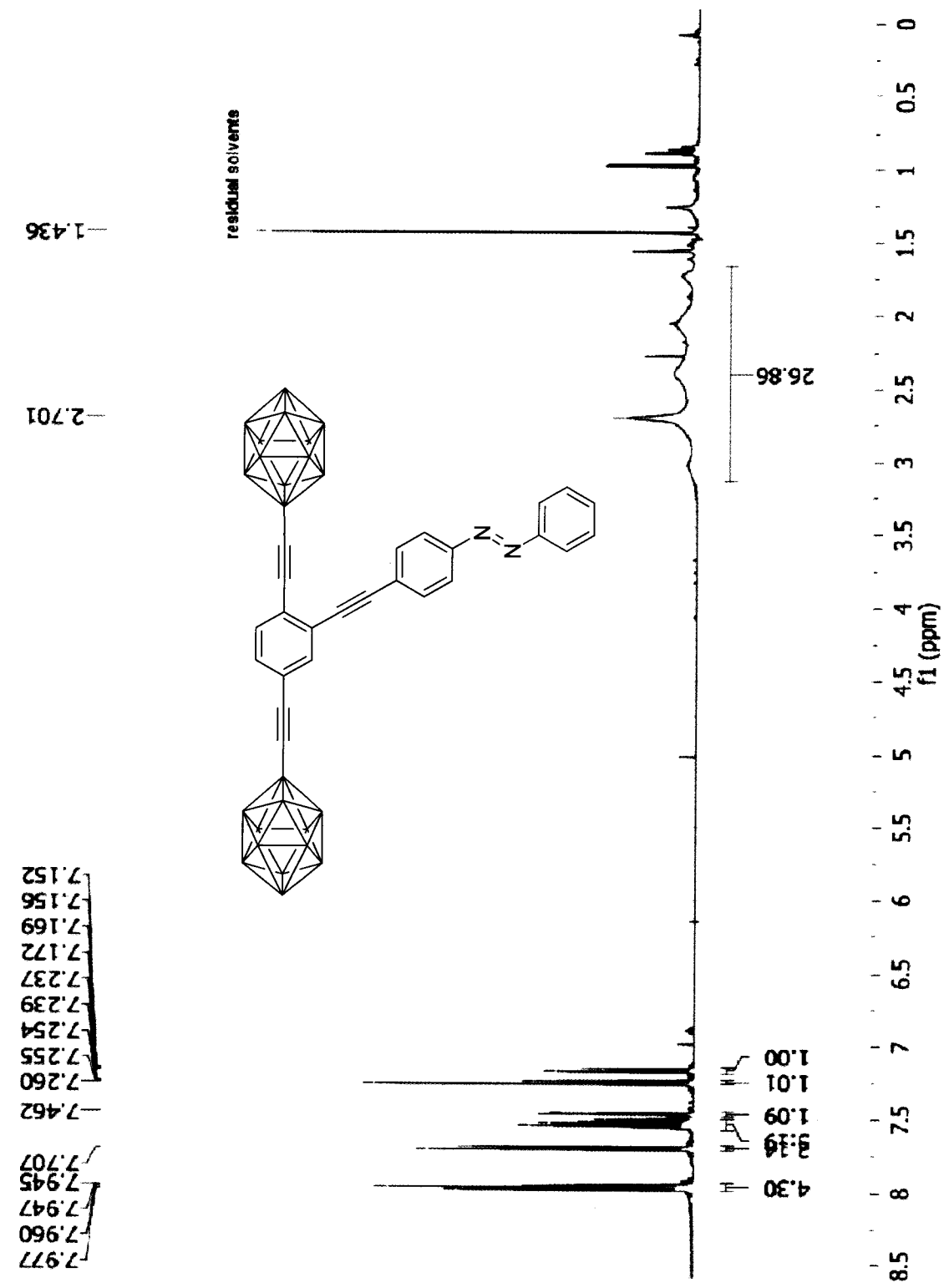

Figure S-6.1-4. ^{1}H NMR Spectrum of Compound 5.

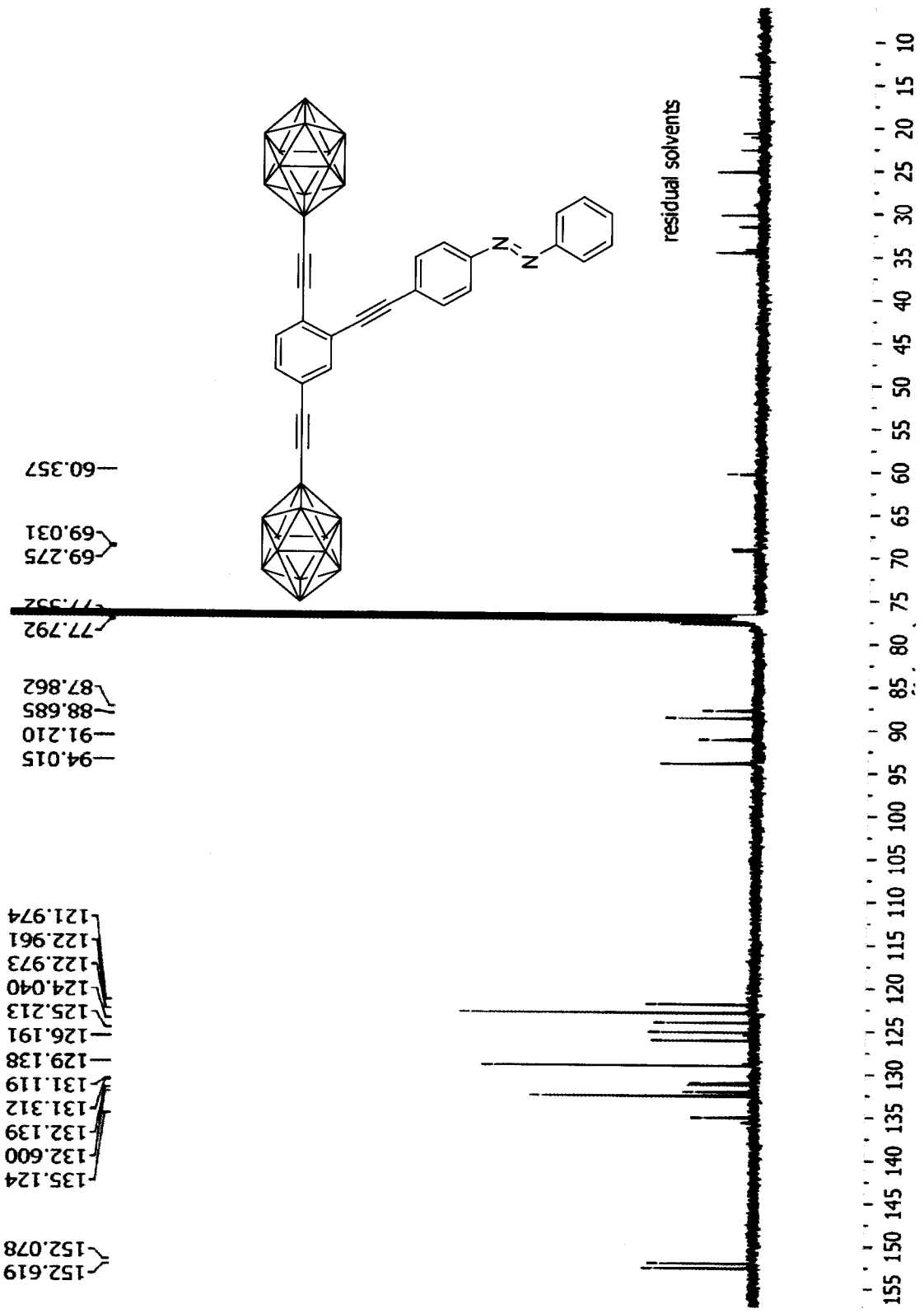

Figure S-6.1-6. ^{13}C NMR Spectrum of Compound 5.

Supporting Information for Chapter 6.2

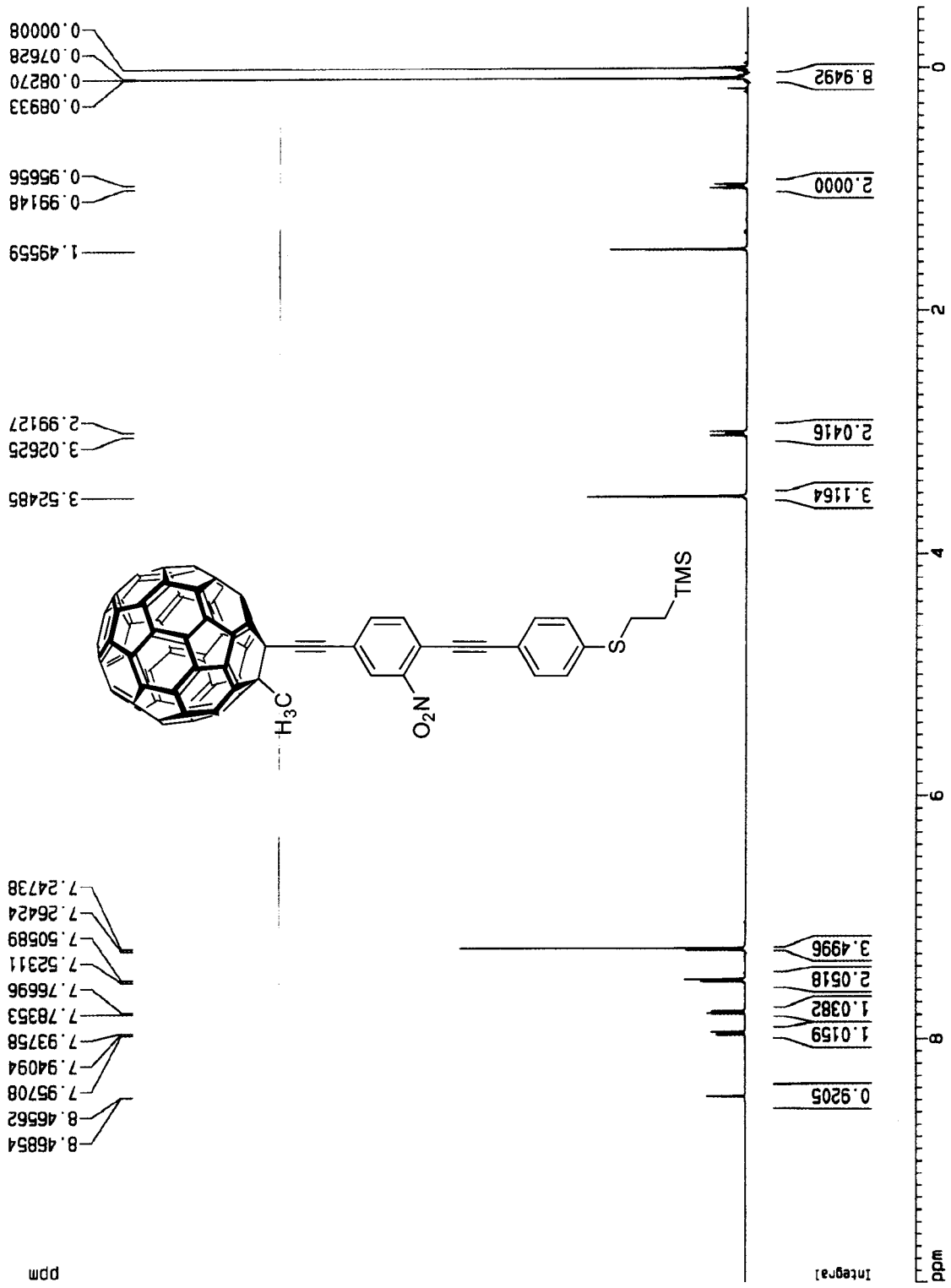

Figure S-6.2-1. ^{1}H NMR Spectrum of Compound **3-Me-TMS**.

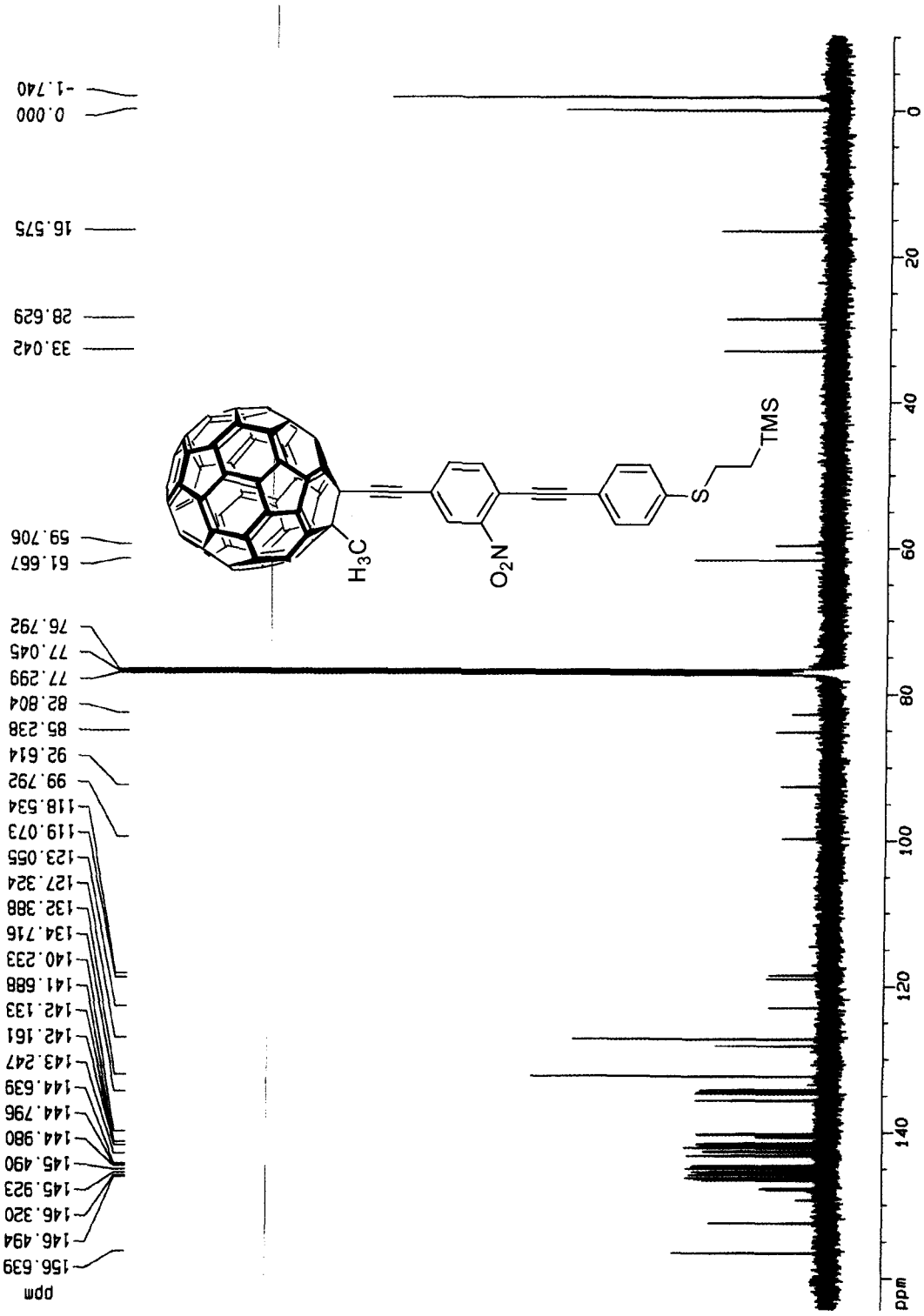

Figure S-6.2-2. ^{13}C NMR Spectrum of Compound **3-Me-TMS**.

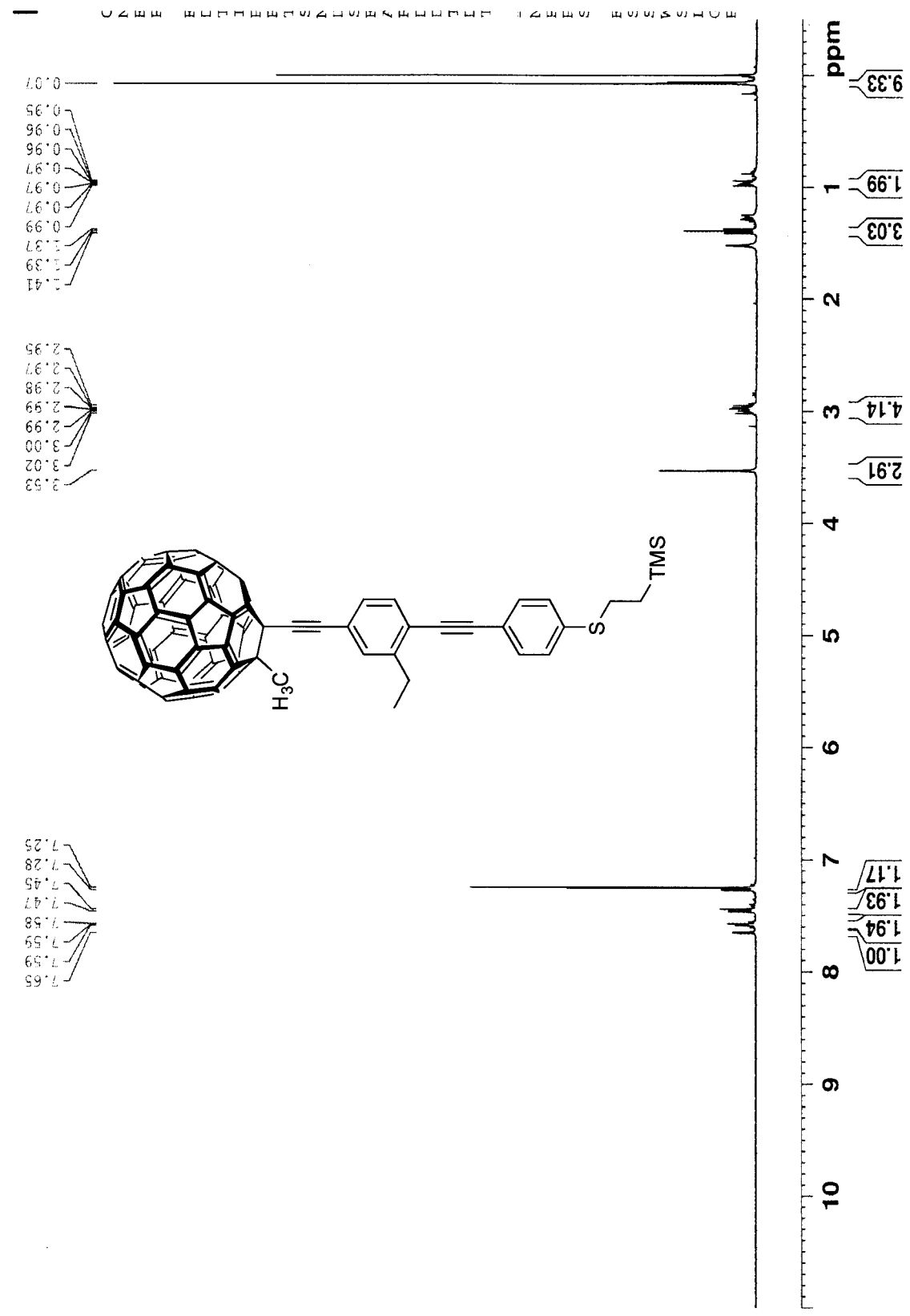

Figure S-6.2-3. ^{1}H NMR Spectrum of Compound **4-TMS**.

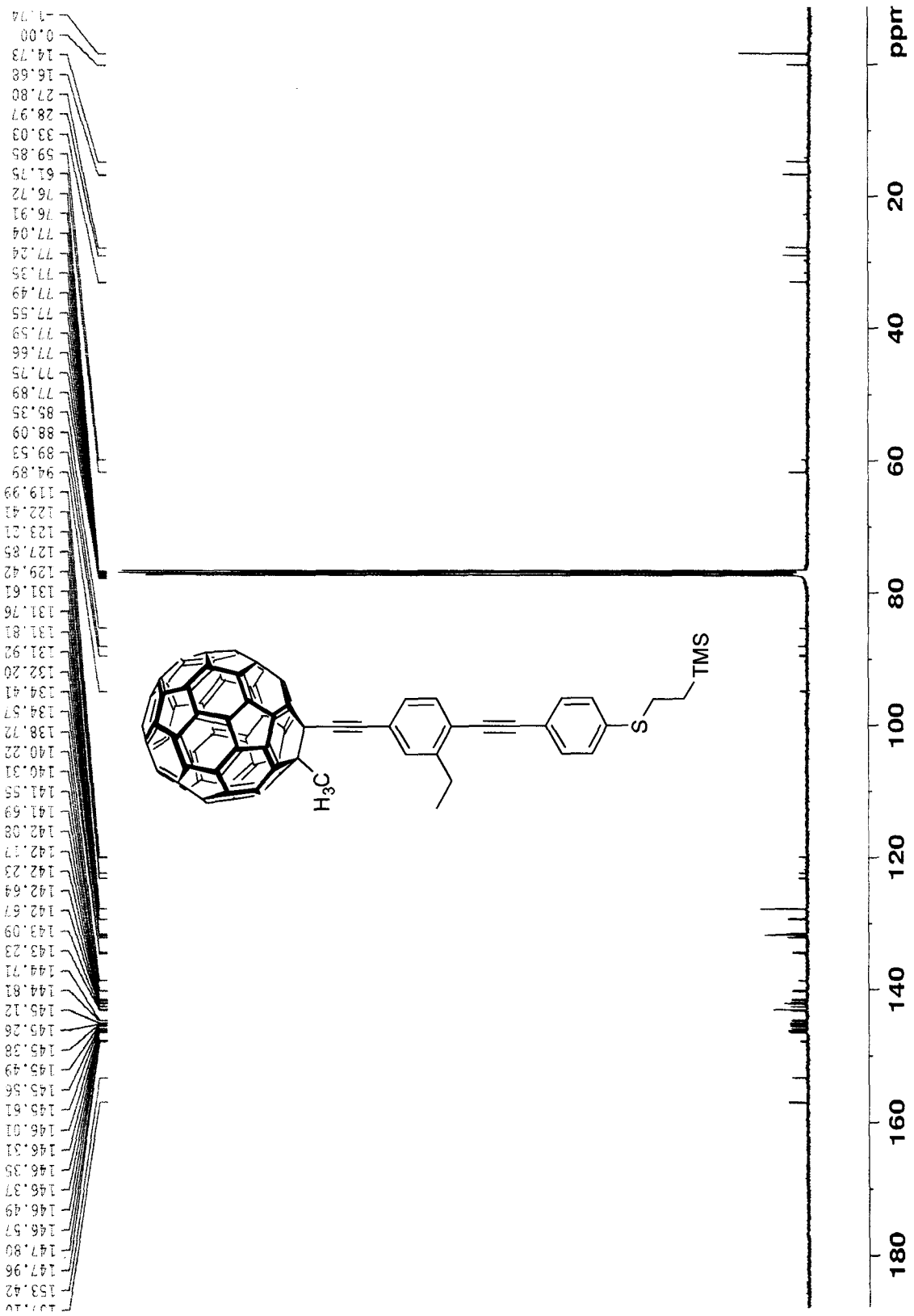

Figure S-6.2-4. ^{13}C NMR Spectrum of Compound **4-TMS**.

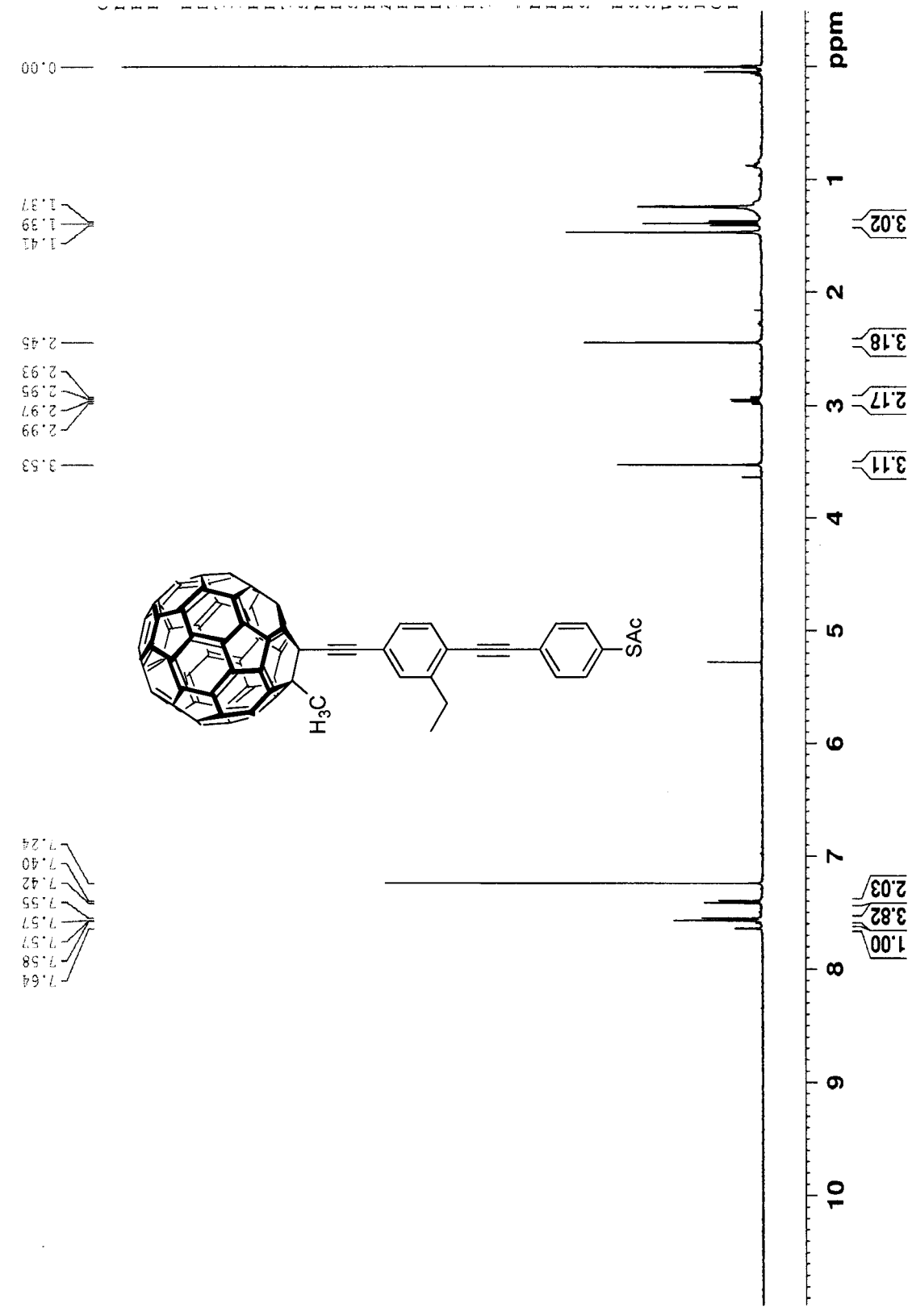

Figure S-6.2-5. ^{1}H NMR Spectrum of Compound **4-SAc**.

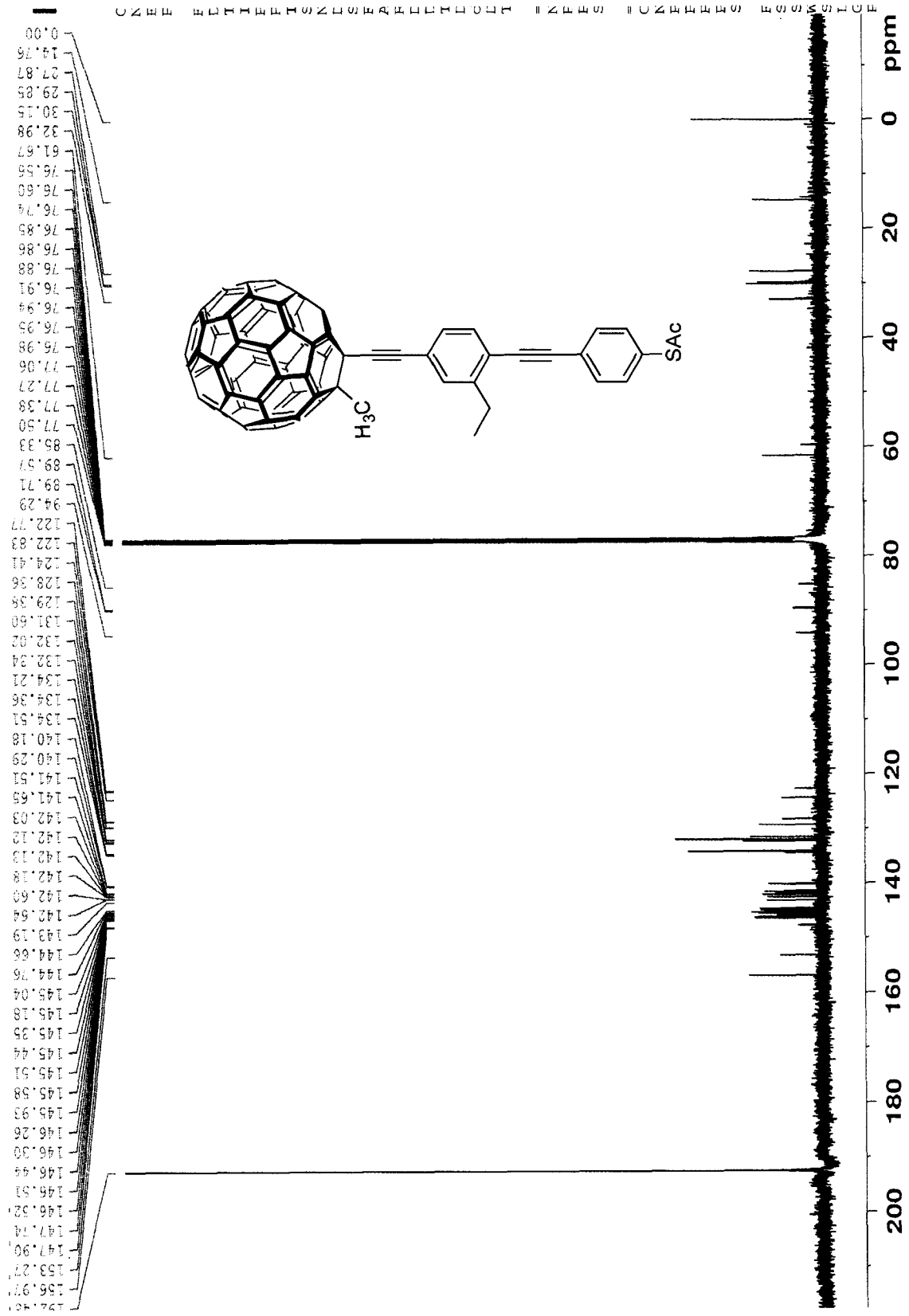

Figure S-6.2-6. ^{13}C NMR Spectrum of Compound **4-SAc**.

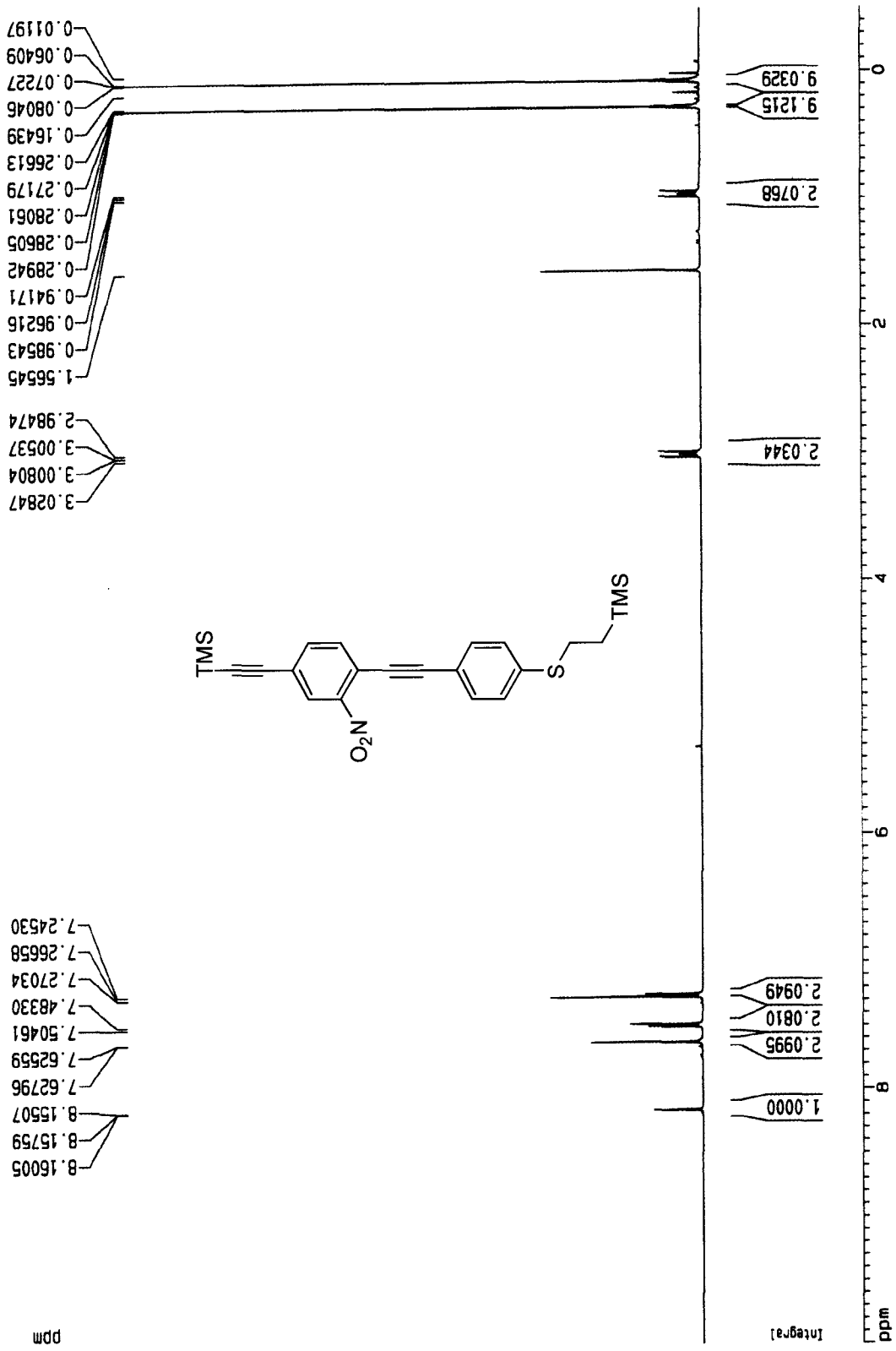

Figure S-6.2-7. ^{1}H NMR Spectrum of Compound **15b**.

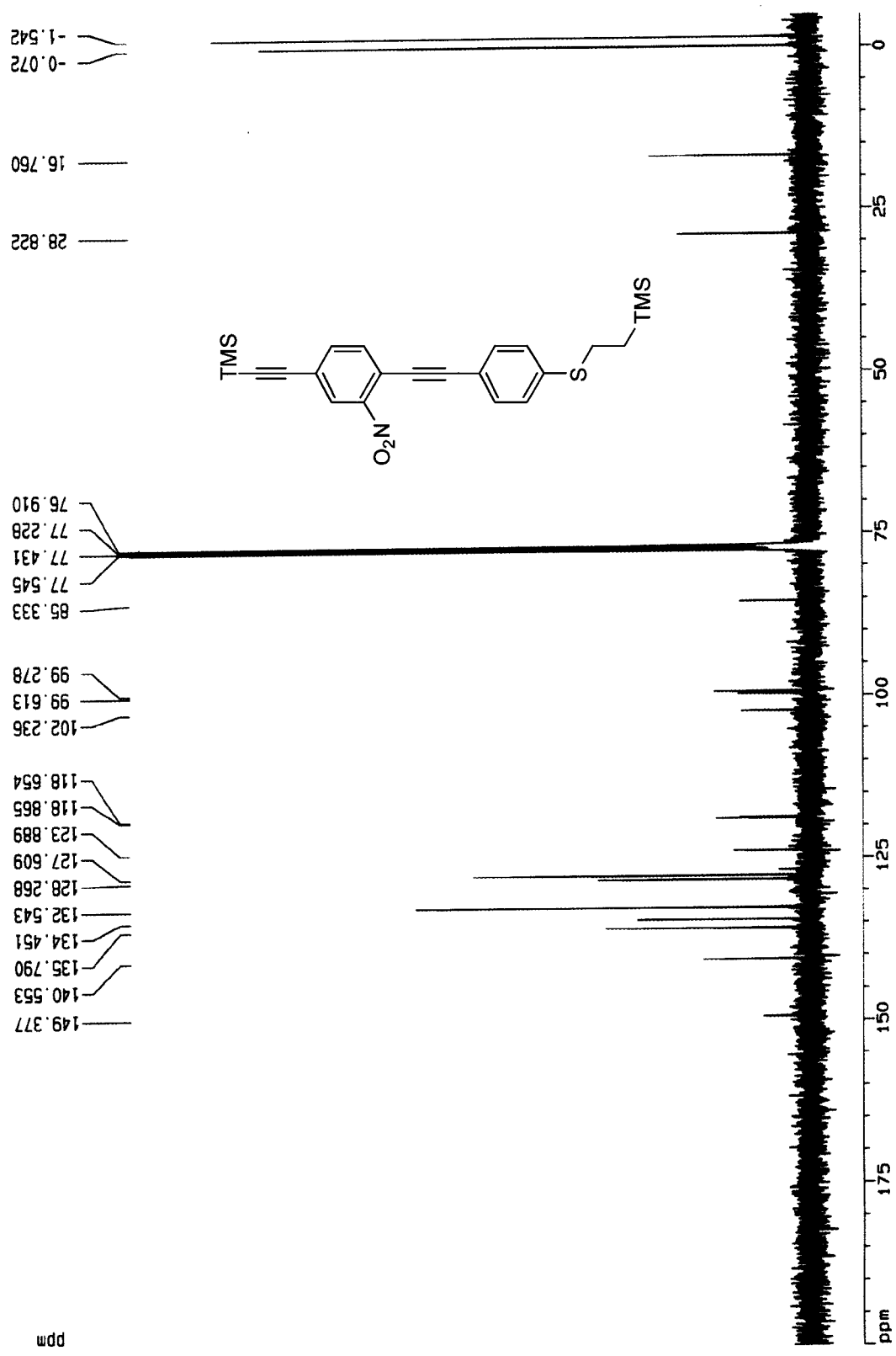

Figure S-6.2-8. ^{13}C NMR Spectrum of Compound **15b**.

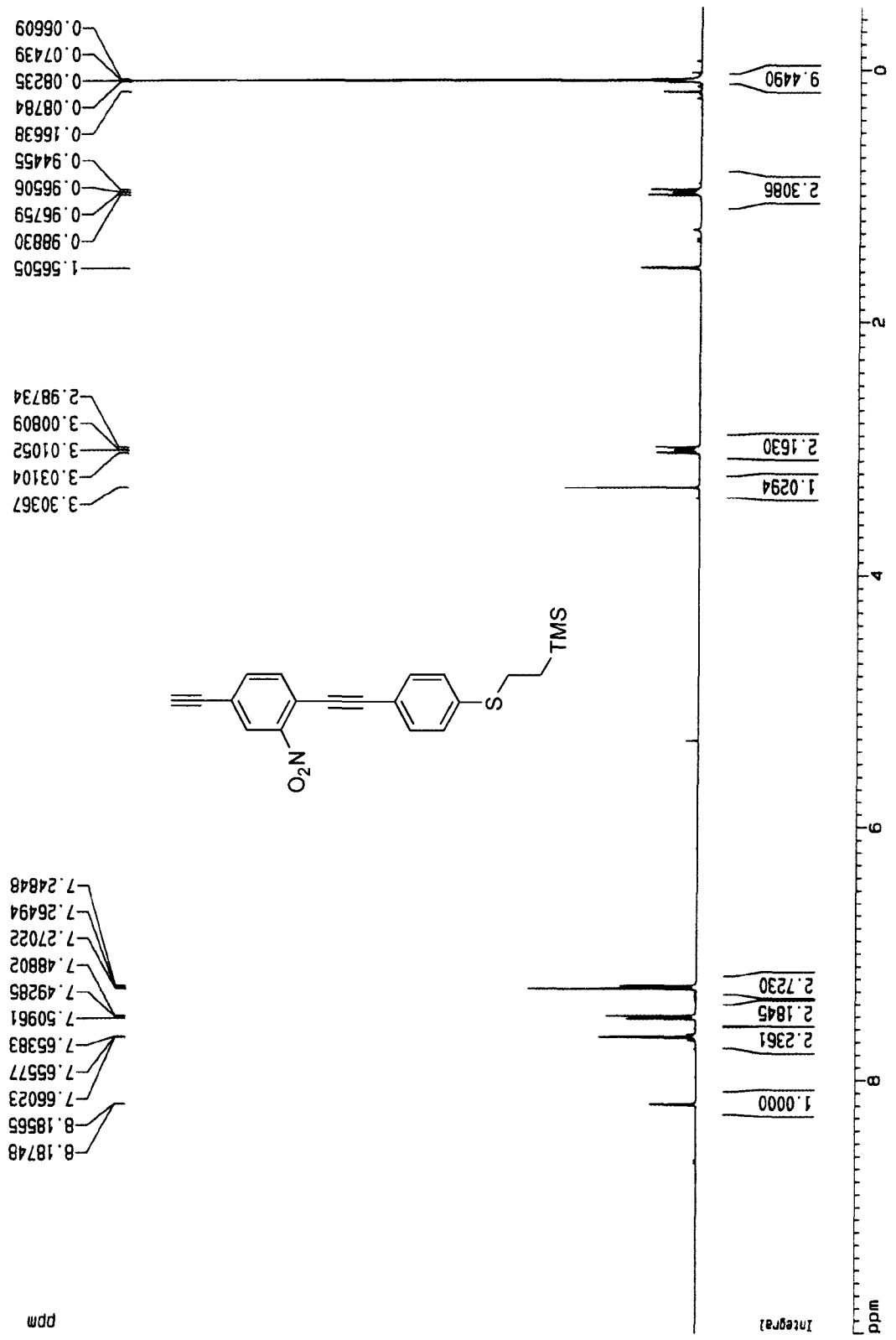

Figure S-6.2-9. ^{1}H NMR Spectrum of Compound **16b**.

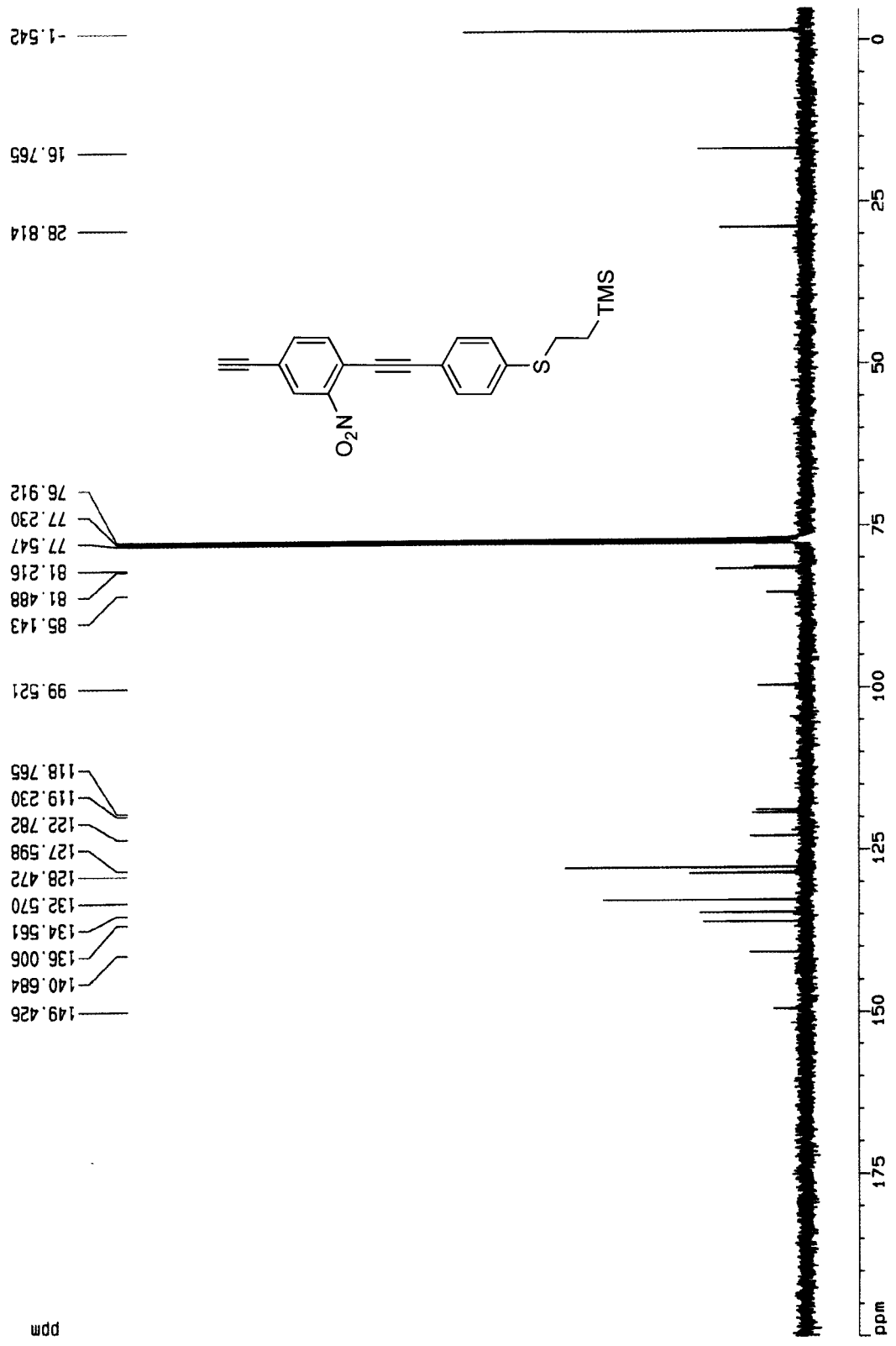

Figure S-6.2-10. ^{13}C NMR Spectrum of Compound **16b**.

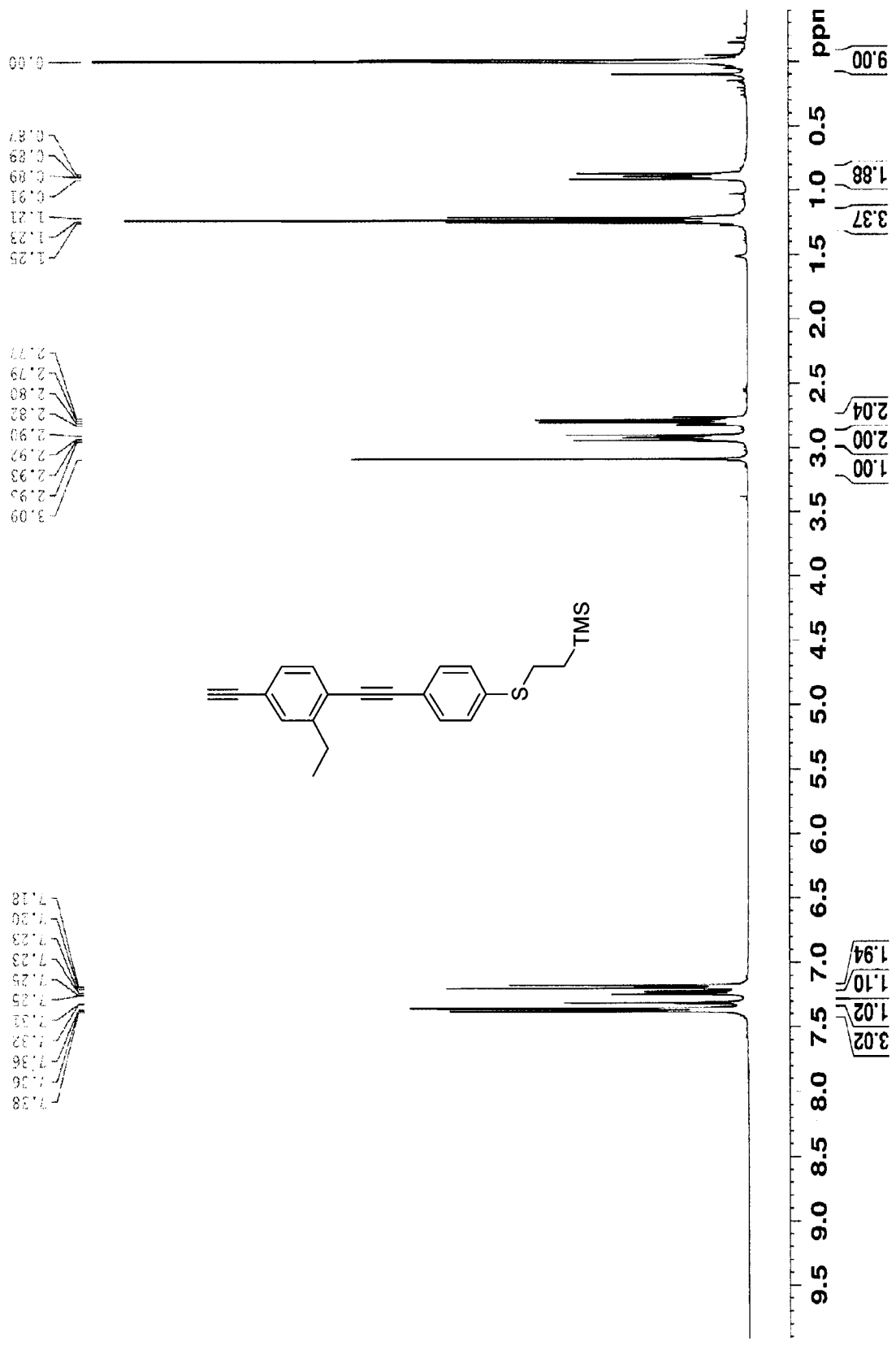

Figure S-6.2-11. ^{1}H NMR Spectrum of Compound **16c**.

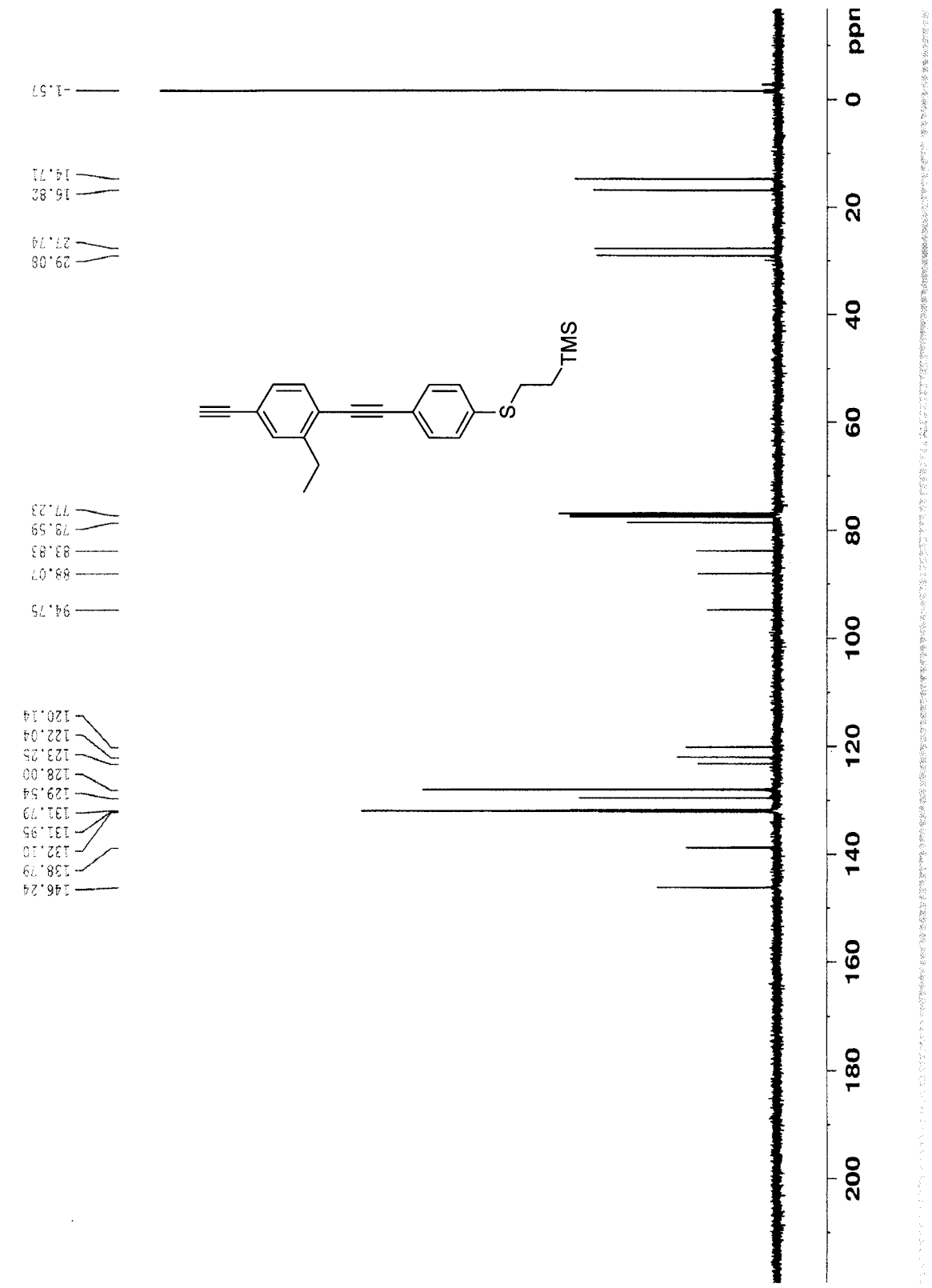

Figure S-6.2-11. ^{13}C NMR Spectrum of Compound **16c**.